

AD-A073 930

MCDONNELL DOUGLAS RESEARCH LABS ST LOUIS MO

F/G 11/9

THE RELATION BETWEEN THE CHEMICAL AND PHYSICAL STRUCTURE AND TH--ETC(U)

JUN 79 R J MORGAN, J E O'NEAL

F44620-76-C-0075

MDC-Q0653

NL

UNCLASSIFIED

1 OF 2

AD
A073930

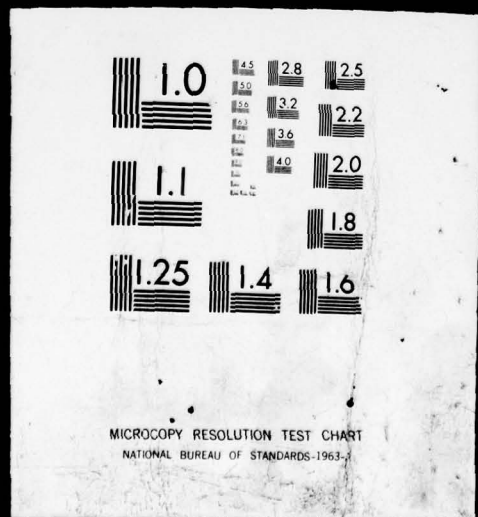


120

1 OF 2

AD

A0 73930



73 930
MCDONNELL DOUGLAS

MDC 0665
Contract No. F49620-78-D-0076

LEVEL 1 2

THE RELATION BETWEEN THE CHEMICAL AND PHYSICAL STRUCTURE AND THE MECHANICAL RESPONSE OF POLYMERS

R.L. Morgan
J.E. O'Reil

McDonnell Douglas Research Laboratories
St. Louis, Missouri 63169

D D C
RECEIVED
SEP 16 1978

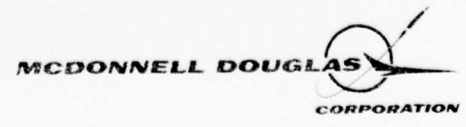
1978
Scientific Report for Period 1 April 1978 - 30 June 1978

Approved for public release; distribution unlimited

FOR THE
UNITED STATES AIR FORCE
Air Force Office of Scientific Research/AFSC
Wright Air Force Base, DC 20332

DDC FILE COPY

MCDONNELL DOUGLAS RESEARCH LABORATORIES



79 09 16 010

UNCLASSIFIED

SECURITY CLASSIFICATION OF THIS PAGE (When Data Entered)

REPORT DOCUMENTATION PAGE		READ INSTRUCTIONS BEFORE COMPLETING FORM
1. REPORT NUMBER	2. GOVT ACCESSION NO.	3. RECIPIENT'S CATALOG NUMBER
4. TITLE (and Subtitle) THE RELATION BETWEEN THE CHEMICAL AND PHYSICAL STRUCTURE AND THE MECHANICAL RESPONSE OF POLYMERS		5. TYPE OF REPORT & PERIOD COVERED Final Scientific Report 1 Apr 76 - 30 June 78
7. AUTHOR(s) Roger J. Morgan James E. O'Neal		6. PERFORMING ORG. REPORT NUMBER MDC-Q0653
9. PERFORMING ORGANIZATION NAME AND ADDRESS McDonnell Douglas Research Laboratories McDonnell Douglas Corporation St. Louis, MO 63166		8. CONTRACT OR GRANT NUMBER(s) F44620-76-C-0075
11. CONTROLLING OFFICE NAME AND ADDRESS Air Force Office of Scientific Research/NC Bolling Air Force Base, DC 20332		10. PROGRAM ELEMENT, PROJECT, TASK AREA & WORK UNIT NUMBERS 2303/A3, 61102F
14. MONITORING AGENCY NAME & ADDRESS (if different from Controlling Office) 12 155p.		11. REPORT DATE 30 June 79
		12. NUMBER OF PAGES 154
		15. SECURITY CLASS. (of this report) Unclassified
		15a. DECLASSIFICATION/DOWNGRADING SCHEDULE
16. DISTRIBUTION STATEMENT (of this Report) Approved for public release; distribution unlimited		
17. DISTRIBUTION STATEMENT (of the abstract entered in Block 20, if different from Report)		
18. SUPPLEMENTARY NOTES		
19. KEY WORDS (Continue on reverse side if necessary and identify by block number) Epoxies Failure modes Swelling Durability Crazing Fabrication stresses Network structure Sorbed moisture Environmental stresses Microvoids Glass transition Deformation modes Diffusion		
20. ABSTRACT (Continue on reverse side if necessary and identify by block number) The structure/failure-process/mechanical-property relations of epoxies, polycarbonate and polybenzoxazole and the effect of fabrication and environmental factors on these relations were studied. Diethylene triamine cured bisphenol-A-diglycidyl ether (DGEBA-DETA) epoxies consist of intramolecularly crosslinked molecular domains interconnected by less highly crosslinked regions. These DGEBA-DETA epoxies are relatively ductile and deform and fail by a crazing process. Diaminodiphenyl		

DD FORM 1473 1 JAN 73

EDITION OF 1 NOV 65 IS OBSOLETE

UNCLASSIFIED

SECURITY CLASSIFICATION OF THIS PAGE (When Data Entered)

405 315

9/17/79

20. Abstract (Continued)

sulfone cured tetraglycidyl 4,4'diaminodiphenyl methane (TGDDM-DDS) epoxies exhibit homogeneous crosslink densities. These epoxies are not highly cross-linked despite the tetrafunctionality of the TGDDM molecule because steric and diffusional restrictions inhibit the cure reactions. The TGDDM-DDS epoxies can microscopically deform by both crazing and shear banding.

The pertinent basic physical phenomena induced and/or modified by sorbed moisture that affect the durability of epoxies are reviewed. Sorbed moisture acts as a plasticizer and a swelling and solvent crazing agent to epoxies. The physical and mechanical integrity of the epoxies are deteriorated by certain thermal-moisture exposure combinations.

Factors controlling the toughness of polycarbonate are reported. In tension the toughness of polycarbonate is controlled by the ease of shear-band deformation and the resultant strain-hardening characteristics of the cold-drawn material together with the characteristics of surface crazes which form prior to macroscopic necking. The effects of strain-rate and environmental factors such as handling on the surface craze characteristics are reported.

Polybenzoxazole (PBO) is relatively ductile at room temperature. The presence of sulfuric acid in PBO, which is eliminated only on decomposition of the polymer near 500°C, suggests that this acid is strongly associated with the rod-like macromolecules, and may affect their aggregation characteristics.

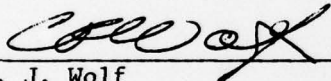
Accession For	<input checked="" type="checkbox"/>
NTIS GRA&I	
DDC TAB	
Unannounced	
Justification	
By	
Distribution/	
Availability Codes	
Dist	
Avail and/or special	
A	

PREFACE

This final report contains a summary of a research program performed by the McDonnell Douglas Research Laboratories, St. Louis, Missouri, on the relation between the chemical and physical structure and the mechanical response of polymers. The research was conducted under Contract No. F44620-76-C-0075 for the Air Force Office of Scientific Research. The performance period was 1 April 1976-30 June 1978. This report was submitted in June 1978.

The principal investigator was Dr. Roger J. Morgan; Mr. James E. O'Neal was coinvestigator. The program managers were Dr. Donald R. Ulrich and Lt. Col. Richard Haffner, Directorate of Chemical Science, Bolling Air Force Base, Washington, DC.

This report has been reviewed and is approved.



C. J. Wolf
Chief Scientist, Chemical Physics
McDonnell Douglas Research Laboratories



D. P. Ames
Staff Vice President
McDonnell Douglas Research Laboratories

TABLE OF CONTENTS

	<u>Page</u>
1. INTRODUCTION	1
2. OBJECTIVES	2
3. PROGRESS	3
3.1 Structure-Property Studies of Epoxies	3
3.2 The Durability of Epoxies	5
3.3 The Modes of Deformation and Failure of Polycarbonate	6
3.4 Polybenzoxazole	7
4. PUBLICATIONS AND PRESENTATIONS	8
APPENDIX A: Microscopic Flow and Failure Processes in Polymer Glasses, Org. Plast. Coat. Preprints (ACS) <u>37</u> , No. 2, 480	10
(1977).	10
APPENDIX B: The Microscopic Failure Processes and their Relation to the Structure of Amine-Cured Bisphenol-A-Diglycidyl Ether	17
Epoxies, J. Mater. Sci. <u>12</u> , 1966 (1977)	17
APPENDIX C: The Durability of Epoxies, Polym. Plast. Tech. and Eng. <u>10(1)</u> , 49 (1978)	33
APPENDIX D: Epoxies as Composite Matrices, Org. Plast. Coat. Preprints (ACS) <u>38</u> , 485 (1978)	102
APPENDIX E: The Structure, Modes of Deformation and Failure and Mechanical Properties of Diaminodiphenyl Sulfone Cured Tetraglycidyl 4,4'Diaminodiphenyl Methane Epoxy, J. Mater. Sci. <u>14</u> , 109 (1979)	109
APPENDIX F: The Modes of Deformation and Failure of Polycarbonate, Polymer <u>20</u> , 375 (1979)	126
APPENDIX G: The Effect of Thermal History and Strain-Rate on the Mechanical Properties of Diethylene Triamine-Cured Bisphenol-A-Diglycidyl Ether Epoxies, J. Appl. Polym. Sci. <u>23</u> , 2711 (1979)	140
DISTRIBUTION LIST	148

1. INTRODUCTION

The aerospace industry utilizes polymers in numerous applications which include matrices for composite materials, adhesives, transparencies, and sealants and insulators for heat, sound, and electricity. In many of these applications the polymeric materials are exposed to extreme service environments. The need to predict the durability of these materials over long periods without resorting to empiricism requires a detailed understanding of the structure-property relations of polymers and how such relations are modified by fabrication and environmental factors.

In this program our studies were concentrated on three classes of polymer glasses utilized in the aerospace industry:

- 1) Epoxies, crosslinked thermosetting polymers, which are the primary materials utilized in adhesives and high-performance polymer-fiber composite matrices.
- 2) Polycarbonate, an amorphous but crystallizable thermoplastic which is utilized as a high-impact-strength transparency.
- 3) Aromatic heterocyclic polymers, which possess good flame resistance and the ability to withstand high temperatures. These glasses have been utilized in aircraft wire insulation and have acquired limited usage as adhesives and composite matrices.

The overall aims of this program were to study 1) the chemical structure and physical arrangement of the macromolecules in the bulk, 2) the modes of deformation and failure, 3) the structural parameters that control the modes of deformation and failure, 4) the effect of the modes of deformation and failure on the mechanical properties, and 5) how these structure-property relations are modified by fabrication procedures and the service environment. A thorough understanding of these interrelationships is required for any durability predictions of these polymeric materials.

2. OBJECTIVES

The specific objectives of this research program were to:

- determine 1) the network structure and microvoid characteristics of epoxies, 2) the microscopic modes of deformation and failure of epoxies and their relation to the structure and mechanical properties, and 3) the effect of environmental factors such as sorbed moisture and elevated-temperature exposure on the structure/failure-process/mechanical-property relations of epoxies.
- investigate the structural and environmental factors affecting the modes of deformation and failure and embrittlement of polycarbonate.
- initiate structure-property studies on aromatic heterocyclic polybenzoxazole.

3. PROGRESS

The progress in this research program has been reported in detail in Publications and Presentations 1-11 (Section 4). Publications 4-10 are included as appendices A-G of this report. A comprehensive summary of the major findings of this research program is documented in this section.

3.1 Structure-Property Studies of Epoxies

Two epoxy systems were studied: 1) diethylene triamine (Eastman)-cured bisphenol-A-diglycidyl ether (Dow, DER 332) epoxy (DGEBA-DETA) and 2) diamino-diphenyl sulfone (Ciba-Geigy, Eporal)-cured tetraglycidyl 4,4'-diaminodiphenyl methane (Ciba-Geigy, MY 720) epoxy (TGDDM-DDS).

The DGEBA-DETA Epoxy System - DGEBA-DETA epoxies exhibit considerable microscopic flow during the failure processes and 15-20% extension to break 25°C below their T_g 's. Reversible thermal annealing cycles, above and below T_g , produce reversible changes in the macroscopic yield stress of DGEBA-DETA epoxies. These changes in the yield stress are a result of free-volume changes. These epoxies, however, exhibited little swelling in organic solvents. The lack of swelling, the ductility, and the free-volume dependence of the mechanical properties of the DGEBA-DETA epoxies can be explained if these glasses possess a heterogeneous crosslink density distribution. It is suggested that these glasses consist of regions of high-crosslink density interconnected by free-volume-dependent, low-crosslinked or non-crosslinked material with the latter material controlling the flow properties. This morphological model is consistent with our bright-field transmission electron microscope observations. Films strained directly in the electron microscope revealed a network of interconnected 6-9 nm diameter particles. These particles remain intact and flow past one another during the flow processes. It is suggested that these particles are molecular domains that are intramolecularly crosslinked and form during the initial stages of polymerization.

The DGEBA-DETA epoxies fail by a crazing process. The failure processes of DGEBA-DETA epoxies were monitored by optical and electron microscopy of a) the fracture topographies and edges of epoxy specimens fractured in tension as a function of temperature and strain-rate and b) thin epoxy films deformed on a metal substrate. In addition, the epoxy films were strained directly in the electron microscopy, and failure processes were monitored by bright-field transmission electron microscopy.

The fracture topographies of the DGEBA-DETA epoxies can be interpreted in terms of a crazing failure process. The coarse initiation region of the fracture topography of these epoxies, which has a mica-like appearance, is at the center of a cavity and is surrounded by a smooth, mirror-like, slow crack-growth region. The mica-like structure results from void growth and coalescence through the center of a simultaneously growing, poorly developed craze, which consists of coarse fibrils. The diameters of the broken fibrils depend on the relative rates of craze and void propagation. The smooth, mirror-like region results from crack propagation either through the center or along the craze-matrix boundary interface of a thick, well-developed craze consisting of fine fibrils.

The TGDDM-DDS Epoxy System - The TGDDM-DDS epoxies are not highly cross-linked systems, despite the tetrafunctionality of the TGDDM molecule, and exhibit 15-20% extension to break 25°C below their T_g 's. Steric and diffusional restrictions inhibit the cure reactions for glasses prepared from ~ 30 wt% DDS. (For all the epoxide groups to react with primary amines requires 54 wt% DDS.) For glasses with ~ 30 wt% DDS, unreacted DDS molecules act as plasticizers and lower the T_g . Aggregates of these unreacted molecules recrystallize in the epoxy glass and have been identified by electron diffraction and X-ray emission spectroscopy. The elimination of unreacted molecules during the later stages of the cure produces stress-raising microvoids in these glasses.

No evidence was found for heterogeneous crosslink-density distributions in TGDDM-DDS (15-35 wt% DDS) epoxies on straining films in the electron microscope. However, transmission electron microscopy reveals that the poor network produced for lower DDS concentrations (10-15 wt% DDS) breaks into ~ 2.5 nm particles which are approximately the size of the TGDDM epoxide molecule.

TGDDM-DDS (12-35 wt% DDS) epoxies predominantly deform and fail in tension by a crazing process as indicated by fracture topography studies. These glasses also deform to a limited extent by shear banding as indicated by unique, regular, right-angle steps in the fracture topography initiation region. The shear-band mode of deformation becomes more predominant with increasing temperature and is the primary mode of deformation during the initial stages of fracture just below T_g . Fracture topographical features

also indicate that mixed modes of deformation that involve both shear banding and crazing can occur in these epoxies. The shear-band mode of deformation enhances the high-temperature ductility of these TGDDM-DDS epoxies.

3.2 The Durability of Epoxies

The pertinent basic physical phenomena induced and/or modified by sorbed moisture that affect the durability of epoxies have been investigated and reviewed (Publications 6,7, and 11). Our primary findings and conclusions are as follows:

(1) Epoxies are plasticized by sorbed moisture, and their T_g 's are lowered to a greater extent than predicted from free-volume considerations. Strong hydrogen bonding or the preferential accumulation of moisture in regions of low-crosslink density could explain the anomalous plasticization.

(2) Moisture diffusion in epoxies can be adequately described by Fick's laws of diffusion. Non-Fickian diffusion with accelerated moisture sorption will occur, however, in environments that cause microvoid or crack formation in the epoxies. For example, TGDDM-DDS (27 wt% DDS) epoxies exposed to stresses of > 40 MPa at room temperature exhibit a significant change in moisture sorption and diffusion characteristics.

(3) Local swelling stresses generated by the sorption of moisture in epoxies cannot be predicted accurately without detailed knowledge of the epoxy network structure and the moisture distribution within the network.

(4) Sorbed moisture enhances the craze cavitation and propagation processes in the epoxies by plasticization. The craze cavitation stress is more susceptible to sorbed moisture than T_g , particularly when microscopic regions of high-moisture concentration are present in the epoxy. Therefore, modification of T_g by sorbed moisture alone cannot be utilized as a sensitive guide to predict deterioration in the mechanical response and durability of epoxies.

(5) Combined thermal-moisture exposure can deteriorate the physical and mechanical integrity of epoxies. For certain conditions, moisture clusters form in epoxies which on subsequent elimination produce stress-raising microvoids in the glass that reduce the tensile strength by $\sim 25\%$. Thermal spiking causes enhanced moisture sorption because of the breaking of crosslinks and further growth of fabrication-induced surface micro-cracks.

3.3 The Modes of Deformation and Failure of Polycarbonate

Polycarbonate embrittles as a result of premature failure by a crazing mechanism. In addition to free-volume changes, the embrittlement processes are a result of either surface crystallization and/or solvent-induced relaxation of fabrication stresses.

In these studies we investigated the effect of strain-rate and organics (finger-grease) on the surface crazing of polycarbonate. Also, polycarbonate films were strained directly in the electron microscope to achieve a greater understanding of the microscopic deformation and failure modes. This work is described in detail in Publication 9.

Our major findings and conclusions in these studies are as follows:

(1) The flow processes and toughness of glassy polycarbonate in tension are controlled by the ease of shear-band deformation and the resultant strain-hardening characteristics of the cold-drawn material together with the characteristics of surface crazes which form prior to macroscopic necking. The geometry and physical structure of the surface crazes together with the crack resistance of the oriented polymer can directly control the stage at which deformation fracture occurs and, hence, the toughness of the polymer. The characteristics of these surface crazes varied as a function of strain-rate in 1 mm thick polycarbonate specimens deformed in tension at room temperature. In the 10^{-2} - 10^{+2} min^{-1} strain-rate region, the polycarbonate specimens deformed predominantly by shear-band deformation and cold-drawing. However, surface crazes that form prior to macroscopic necking and cold-drawing serve as sites for ultimate fracture. In the 10^{-2} - 1 min^{-1} strain-rate region, the crazes grow to ~ 5 - 10 μm in length prior to macroscopic shear-band deformation. Subsequent cold-drawing leads to the growth of these craze sites by plastic tearing. In the 1 - 10^{+2} min^{-1} strain-rate region, larger surface crazes up to ~ 100 μm in length develop prior to macroscopic shear-band deformation. These crazes, however, do not significantly grow in area prior to catastrophic crack propagation through the oriented, cold-drawn material. In the $\sim 10^{+2}$ min^{-1} strain-rate region, specimens with low free-volumes, as a result of annealing at 125°C , ceased to cold-draw and either deformed and failed by crazing or by a neck rupture process. Such specimens are embrittled because of a corresponding decrease in molecular flow and energy to failure.

(2) Surface crazing is enhanced in polycarbonate by environmental factors such as handling. The regions of the polycarbonate surface that have come into contact with finger-grease are plasticized, and fabrication stresses in such regions relax near T_g at a faster rate than those in the unplasticized surroundings. The plasticized, relaxed regions separate from their surroundings producing microcracks which serve as sites for craze initiation and growth and possible embrittlement of the polymer.

(3) Crazes initiated and propagated in the polycarbonate films that were deformed directly in the electron microscope. Nodular regions, ~ 10 nm in size, which did not break up during the craze flow processes were observed in these films.

3.4 Polybenzoxazole

Structure-property studies were initiated on polybenzoxazole (PBO) which was supplied by AFML. Fracture topography studies reveal that PBO is relatively ductile at room temperature on a microscopic level. This aromatic heterocyclic polymer is soluble only in inorganic solvents such as concentrated sulfuric acid. Fabrication of the solid involves precipitation from the solvent and/or evaporation of the solvent. X-ray emission scanning spectroscopy studies of PBO fibers revealed the presence of sulfur which indicates that sulfuric acid remains in the solid-state polymer after fabrication. The sulfuric acid is eliminated from the solid polymer only after annealing in the PBO decomposition range, $\sim 500^\circ\text{C}$. These observations suggest that sulfuric acid strongly associates with the rod-like macromolecules and may affect their solid-state aggregation characteristics. A completely solvent-free polymer may be difficult to obtain.

4. PUBLICATIONS AND PRESENTATIONS

The following publications and presentations were based on research performed under this contract.

1. R. J. Morgan, Relationship of Structure, Fracture Processes and Mechanical Response of Polymer Glasses, presented at Gordon Research Conference on Deformation and Failure Mechanisms in Polymers and Composites, Santa Barbara, CA, January 1977.
2. R. J. Morgan, The Morphology and Failure Processes of Epoxies, Educational Seminar Presented for the Society of Plastics Engineers, held in conjunction with Pittsburgh Conference on Analytical Chemistry and Applied Spectroscopy, Cleveland, OH, March 1977.
3. R. J. Morgan and J. E. O'Neal, The Network Structure and Microscopic Failure Processes of Epoxies, presented at the American Physical Society Meeting, San Diego, CA, March 1977; Bull. Am. Phys. Soc. 22, 368 (1977).
4. R. J. Morgan and J. E. O'Neal, Microscopic Flow and Failure Processes in Polymer Glasses, presented at the Non-linear Viscoelastic Behavior of Molten and Solid Polymers Symposium of the American Chemical Society Meeting, Chicago, IL, 1977; Org. Plast. Coat. Preprints (ACS) 37, (No. 2), 480 (1977); also Polym. Sci. and Eng. 18, 1081 (1978).
5. R. J. Morgan and J. E. O'Neal, The Microscopic Failure Processes and their Relation to the Structure of Amine-Cured Bisphenol-A-Diglycidyl Ether Epoxies, J. Mater. Sci. 12, 1966 (1977).
6. R. J. Morgan and J. E. O'Neal, The Durability of Epoxies, Polym. Plast. Tech. and Eng. 10(1), 49 (1978); also McDonnell Douglas Report MDC Q0631, (August 1977).
7. R. J. Morgan and J. E. O'Neal, Epoxies as Composite Matrices, presented at the High-Performance Composites - Chemical Aspects Symposium of the American Chemical Society Meeting, Anaheim, CA, 1978; Org. Plast. Coat. Preprints (ACS) 38, 485 (1978).
8. R. J. Morgan, J. E. O'Neal, and D. B. Miller, The Structure, Modes of Deformation and Failure and Mechanical Properties of Diaminodiphenyl Sulfone Cured Tetraglycidyl 4,4'-Diaminodiphenyl Methane Epoxy, J. Mater. Sci. 14, 109 (1979).

9. R. J. Morgan and J. E. O'Neal, The Modes of Deformation and Failure of Polycarbonate, *Polymer* 20, 375 (1979).
10. R. J. Morgan, The Effect of Thermal History and Strain-Rate on the Mechanical Properties of Diethylene Triamine-Cured Bisphenol-A-Diglycidyl Ether Epoxies, *J. Appl. Polym. Sci.* 23, 2711 (1979).
11. R. J. Morgan, J. E. O'Neal, and D. L. Fanter, The Effect of Moisture on the Physical and Mechanical Integrity of Epoxies, *J. Mater. Sci.* (submitted).

APPENDIX A: Microscopic Flow and Failure Processes
in Polymer Glasses, Org. Plast. Coat.
Preprints (ACS) 37, No. 2, 480 (1977)

Microscopic Flow and Failure Processes in Polymer Glasses*

Roger J. Morgan and James E. O'Neal
McDonnell Douglas Research Laboratories
McDonnell Douglas Corp., St. Louis, Missouri 63166

Introduction

In the aerospace industry, polymeric glasses are utilized in extreme service environments. The need to predict the durability of these materials over long periods without resorting to empiricism requires a detailed understanding of the microscopic flow and failure processes in these glasses and how these processes are modified by the service environment. Flow occurs in polymer glasses either microscopically via crazing or shear banding or macroscopically via necking. This flow absorbs energy during the failure process and enhances the toughness of a polymer glass. The strains in shear bands and crazes are similar [1], and it is uncertain which structural parameters determine if one mode of deformation predominates in a given set of stress-time-temperature conditions.

In this paper we present studies on (i) the microscopic flow and failure processes, (ii) the structural parameters controlling these processes, and (iii) how such processes are modified by the service environment. Our studies cover three different classes of polymer glasses utilized in the aerospace industry, namely:

(1) Polycarbonate, an amorphous but crystallizable thermoplastic which is utilized as a high-impact-strength transparency.

(2) Polyimides, the most widely used of the aromatic heterocyclic polymers, possess good flame resistance and the ability to withstand high temperatures. These glasses have been utilized in aircraft wire insulation and have acquired limited usage as adhesives and composite matrices.

(3) Epoxies, crosslinked thermosetting polymers, are the primary materials utilized in adhesives and high-performance polymer-fiber composites.

Experimental

Material

The bisphenol A polycarbonate (poly-4,4'-dioxydiphenyl 2,2-propane carbonate) (Lexan, General Electric) used in this study had a viscosity-average molecular weight of 30 000 and contained no significant additives. The polyimides studied were (1) (poly 4,4'-oxydiphenylene) pyromellitimide (Vespel, duPont) (PODPPMI) and (2) a solution-soluble copolyimide based on 3,3',4,4'-benzophenone tetracarboxylic acid anhydride (Upjohn, Polyimide 2080), which is designated here as BTAD-polyimide. Two epoxy systems were studied: (1) diethylene triamine (Eastman)-cured bisphenol-A-diglycidyl ether (Dow, DER 332) epoxy (DGEBE-DETA) and (2) diaminodiphenyl sulfone (Ciba Geigy, Eporal)-cured tetraglycidyl 4,4'-diaminodiphenyl methane (Ciba Geigy, MY720) epoxy (TGDDM-DDS).

Experiments

The failure processes were monitored by optical and electron microscopy (1) of the fracture topographies and edges of specimens fractured in tension as a function of temperature and strain-rate and (2) of thin films deformed on a metal substrate. In addition, films were strained directly in the electron microscope, and the failure processes were monitored by bright-field microscopy.

*Research sponsored in part by the McDonnell Douglas Independent Research and Development Program and in part by the Air Force Office of Scientific Research/AFSC, United States Air Force, under Contract No. F44620-76-C-0075. The United States Government is authorized to reproduce and distribute reprints for governmental purposes notwithstanding any copyright notation hereon.

For fracture topography and mechanical property studies, dogbone-shaped specimens were fractured in tension in a table-model tensile tester (Instron TM-S-1130). A scanning reflection electron microscope (JEOL model JEM-100B) and optical microscope (Zeiss UltraphotII) were used for fracture topography studies. Transmission electron microscopy was used for thin-film and carbon-platinum surface replica studies.

Results and Discussion

Polycarbonate

Polycarbonate can embrittle, particularly at high strain-rates and for specimens < 5 mm thick, on annealing in the 80-130°C range ($T_g \approx 150^\circ\text{C}$) [2-11]. In tension, this embrittlement is a result of the cessation of shear yielding and macroscopic necking and a reversion to crazing as the predominant deformation and failure mode [5, 10, 12]. This transition is accompanied by a corresponding decrease in molecular flow and energy to failure. The inhibition of molecular flow is a direct result of free-volume decreases produced in bulk specimens on annealing in the glassy state.

Crazing still occurs, however, and plays a predominant role in the failure process when shear yielding is the primary mode of deformation. In Fig. 1, ductile crazes are illustrated along the edges of the necked portion of a polycarbonate glass. We observed from fracture topography studies that failure in the oriented neck often originates from a well-formed craze. Crazes can originate from surface flaws which can be generated by surface crystallization. The ability of polycarbonate to crystallize at and immediately above T_g allows precrystalline and/or crystalline entities to grow below the bulk T_g on free surfaces where mobility restrictions are less severe than in the bulk [10]. Surface crystallization causes surface stresses which can produce microcracking. We have directly observed microcracks along the edges of prespherulitic arms. Surface crystallization is enhanced by finger grease and subsequent exposure to $\sim 100^\circ\text{C}$ [13]. Caird [14] has shown that handling the surface of polycarbonate followed by exposure to 130°C seriously deteriorates the mechanical properties relative to untouched glasses exposed to the same temperatures.

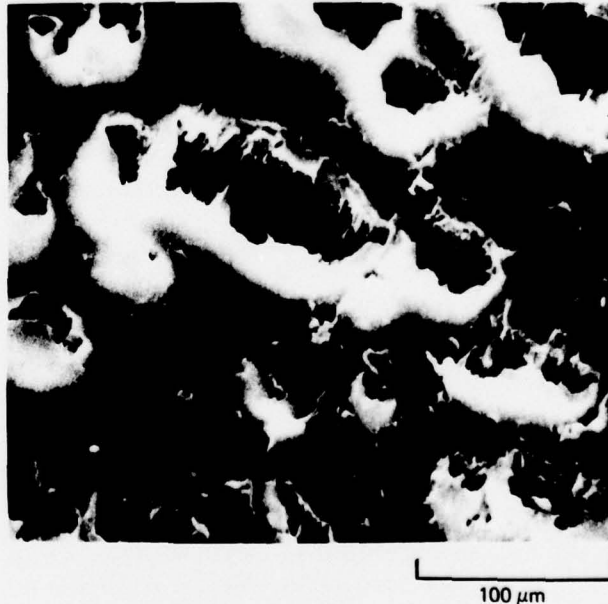


Figure 1 Ductile crazes in the edge of necked portion of polycarbonate.

Hence, the flow properties and toughness at a specified strain-rate and thickness of polycarbonate are controlled by (1) the ease of shear-band deformation which depends on free volume and previous thermal history and (2) surface crazes whose characteristics depend on exposure to organics, thermal history, and surface crystallization and fabrication stresses. Therefore, the

desirable toughness of polycarbonate cannot be fully utilized when this glass is exposed to temperatures above 80°C. For many applications, the polycarbonate surface has to be protected by a hard coating to protect this soft glass from the environment. In aerospace transparency service environments, it is often difficult to keep the coating adhered to the polycarbonate.

Polyimides

In the bulk, both the PODPPMI and BTAD polyimides deform and fail by a crazing process with extensive fibrillation; e.g., all tensile fracture topographies of PODPPMI polyimide fractured from 20-300°C in the 10^{-2} to 10^{+2} /min strain-rate range exhibited features characteristic of a craze-viscous-rupture process.

However, BTAD polyimide films strained directly in the electron microscope exhibited three microscopic modes of deformation: crazing, fine shear-band propagation, and an edge-yielding phenomenon [15]. Edge-yielding, which has some of characteristics of both crazing and shear banding, results in a thinning of the film at the specimen edge. This yielding phenomenon occurred in $\sim 1 \mu\text{m}$ wide bands which are at an angle of 20-30° to the tensile stress direction. Shear-band deformation occurs in fine bands $\sim 100 \text{ nm}$ wide. Wu and Li [16] have characterized two shear band deformation processes in polystyrene: one appears as fine shear bands, similar to those we observe in BTAD polyimide, and the other as diffuse shear zones. The fine shear bands in BTAD polyimide exhibit a sharp boundary between themselves and the surrounding undeformed material. From the lack of any contrast differences within the shear bands in bright-field transmission electron microscopy, we conclude that there is uniform shear strain within these bands. Microscopic shear-bands, some of which were $\sim 1 \text{ nm}$ wide, were found to initiate from 1.5-15 nm diameter microvoids. The length of these shear bands increases with increasing microvoid diameter as shown in Fig. 2. The data scatter in this figure arises from the modification of the shear-band length by the proximity of other microvoids and the $\sim 100 \text{ nm}$ wide shear bands. The microscopic shear band width increases by a tearing of the microvoid initiation sites. These shear bands cease to widen or thicken and become only longer when their width approaches $\sim 100 \text{ nm}$. This phenomenon may be related to unique stress-field conditions at the shear-band initiation regions. The dimensions of the microscopic shear bands suggest that only polymer chain segments of a few monomer units rather than any larger morphological entities are the basic units involved in the flow processes in this polymer.

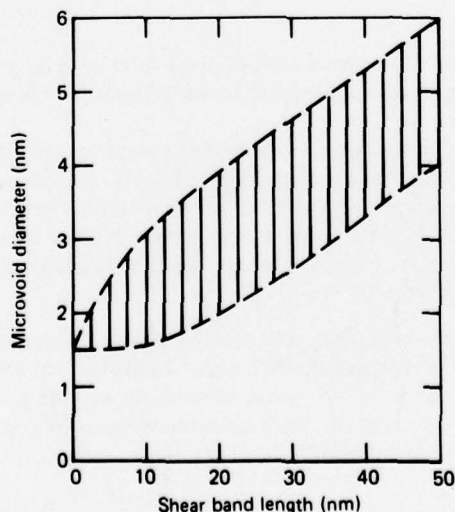


Figure 2 Diameter of microvoid shear-band initiation site as a function of shear-band length for BTAD-polyimide.

The ability of polyimides to fibrillate increases the wear resistance of these material as aircraft wire insulation. The in-service polymer-polymer wear processes involve shearing off platelets which protrude above the general contour of the polymer surfaces. Electron microscope studies of the wear processes reveal that fibrils often hold the platlets onto the surface which enhances the wear resistance. Such fibrillation is not affected by service environment conditions.

Epoxies

Both DGEBA-DETA and TGDDM-DDS epoxies deform and fail by a crazing process [17]. (These glasses are not highly crosslinked because of the steric and diffusional restrictions during polymerization and network formation.) Crazes were observed in films either strained directly in the electron microscope or strained on a metal substrate. The fracture topographies of these epoxies fractured as a function of temperature and strain-rate are interpreted in terms of a crazing process. A coarse fracture topography initiation region results from void growth and coalescence through the center of a simultaneously growing, poorly developed craze which consists of coarse fibrils. A surrounding, smooth, slow-crack-growth mirror region results from crack propagation either through the center or along the craze-matrix boundary interface of a thick, well-developed craze consisting of fine fibrils.

From straining films directly in the electron microscope, DGEBA-DETA epoxies were found to consist of 6-9 nm diameter particles which remain intact when flow occurs within craze fibrils. It is suggested that these particles are intramolecularly crosslinked, molecular domains which form during the initial stages of polymerization and later interconnect to form larger network morphological entities. A network of these particles within a craze fibril is illustrated in the bright-field transmission electron micrograph in Fig. 3. The TGDDM-DDS epoxies possess larger $\sim 1 \mu\text{m}$ regions of high crosslink density.

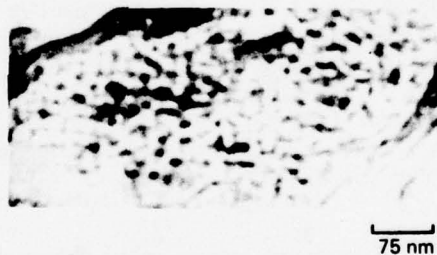


Figure 3 Bright-field transmission electron micrograph of strained network structure of 6-9 nm particles in DGEBA-DETA epoxy.

The TGDDM-DDS epoxies also deform to a limited extent by shear banding. Regular right-angle steps were observed in the fracture topography initiation region, as illustrated in Fig. 4. This topography was observed in $\sim 20\%$ of all room-temperature fractures and $\sim 40\%$ of all fractures at 150°C ($T_g \approx 250^\circ\text{C}$). Shear band propagation in these crosslinked glasses produces structurally weak planes because of bond cleavage caused by molecular flow. The craze or crack jumps into these structurally weak planes.

The crazing process in these epoxies is enhanced by absorbed moisture. The absorbed water lowers the craze cavitation stress and allows crazes to propagate at lower stresses. The cavities formed at the craze tip serve as a sink for water absorption, and the porous craze structure allows rapid diffusion of water to the craze tip. Such phenomena must be considered in any durability predictions of these glasses in high humidity environments.

Conclusions

(1) The flow characteristics of polycarbonate are controlled by (1) the ease of shear band deformation which depends on free-volume and previous thermal history and (2) surface crazes whose characteristics depend on exposure to organics, thermal history, and surface crystallization and fabrication stresses.

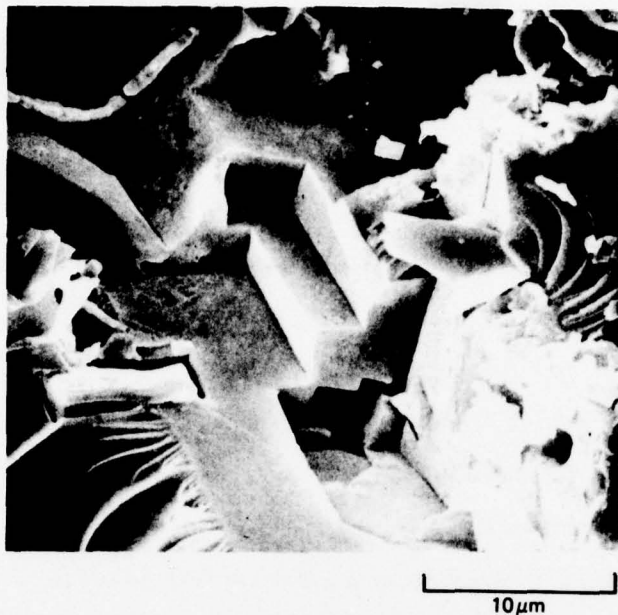


Figure 4 Scanning electron micrograph illustrating right-angle steps in the fracture topography initiation region of TGDDMS-DDS epoxies.

(2) PODPPMI and BTAD polyimides deform and fail in the bulk by crazing with extensive fibrillation. Polymer chain segments of only a few monomer units are the basic units involved in the shear-band flow processes in BTAD-polyimide.

(3) DGEBA-DETA and TGDDM-DDS epoxies predominantly deform and fail by crazing with regions of high crosslink density remaining intact during the flow processes. Right-angle steps in the fracture topography initiation region of the TGDDM-DDS epoxy suggest that shear-band deformation also occurs in this glass. Craze cavitation and growth are enhanced in these epoxies by the presence of absorbed water.

Acknowledgements

We wish to acknowledge Dr. D. Ulrich of Air Force Office of Scientific Research and Drs. D.P. Ames and C.J. Wolf of McDonnell Douglas Research Laboratories for their support and encouragement of this work.

References

1. S. Rabinowitz and P. Beardmore, in *Critical Reviews in Macromolecular Science*, Vol. 1, Chem. Rubber Co., Cleveland, (1972) p.1.
2. G. Peilstocker, *Kunststoffe* 51, 509 (1961).
3. G. Peilstocker, *Brit. Plastics* 35, 365 (1962).
4. J.H. Golden, B.L. Hammant, and E.A. Hazell, *J. Appl. Polym. Sci.* 11, 1571 (1967).
5. D.G. LeGrand, *J. Appl. Polym. Sci.* 13, 2129 (1969).
6. D.G. LeGrand, *J. Appl. Polym. Sci.* 16, 1367 (1972).
7. R.E. Robertson and C.W. Joynson, *J. Appl. Polym. Sci.* 16, 773 (1972).
8. G. Allen, D.C.W. Morley, and T. Williams, *J. Mater. Sci.* 8, 1449 (1973).
9. G.A. Adam, A. Cross, and R.N. Haward, *J. Mater. Sci.* 10, 1582 (1975).
10. R.J. Morgan and J.E. O'Neal, *J. Polym. Sci. (Polymer Phys. Ed.)* 14, 1053 (1976).
11. N.J. Mills, *J. Mater. Sci.* 11, 363 (1976).
12. D. Hull and T.W. Owen, *J. Polym. Sci. (Polymer Phys. Ed.)* 11, 2039 (1973).
13. K. Neki and P.H. Geil, *J. Macromol. Sci. - Phys.* B8 (1-2), 295 (1973).
14. D.W. Caird, *Proc. of Air Force Conference on Aerospace Transparent Materials and Enclosures*, AFML-TR-76-54 (1976) p. 367.
15. R.J. Morgan and J.E. O'Neal, *J. Mater. Sci.* (in press).
16. J.B.C. Wu and J.C.M. Li, *J. Mater. Sci.* 11, 434 (1976).
17. R.J. Morgan and J.E. O'Neal, *J. Mater. Sci.* (in press).

APPENDIX B: The Microscopic Failure Processes and their
Relation to the Structure of Amine-Cured
Bisphenol-A-Diglycidyl Ether Epoxies, J.
Mater. Sci. 12, 1966 (1977)

The microscopic failure processes and their relation to the structure of amine-cured bisphenol-A-diglycidyl ether epoxies

ROGER J. MORGAN, JAMES E. O'NEAL

McDonnell Douglas Research Laboratories, McDonnell Douglas Corporation, St. Louis, Missouri, USA

Electron and optical microscopy are used to study the relation between the structure and the microscopic flow and failure processes of diethylene triamine-cured bisphenol-A-diglycidyl ether epoxies. By straining films directly in the electron microscope, these epoxies are found to consist of 6 to 9 nm diameter particles which remain intact when flow occurs. It is suggested that these particles are intramolecularly crosslinked molecular domains which can interconnect to form larger network morphological entities. Epoxy films, either strained directly in the electron microscope or strained on a metal substrate, deform and fail by a crazing process. The flow processes that occur during deformation are dependent on the network morphology in which regions of either high or low cross-link density are the continuous phase. The fracture topographies of the epoxies are interpreted in terms of a crazing process. The coarse fracture topography initiation regions result from void growth and coalescence through the centre of a simultaneously growing poorly developed craze which consists of coarse fibrils. The surrounding smooth slow-crack growth mirror-like region results from crack propagation either through the centre or along the craze-matrix boundary interface of a thick, well developed craze consisting of fine fibrils.

1. Introduction

Epoxies are utilized by the aerospace industry in the form of matrices for composite materials and in adhesive joints. The increasing use of epoxies in extreme service environments requires a knowledge of their lifetime in such environments. To predict the lifetime of these glasses in a service environment requires knowledge of (1) the chemical structure and the physical arrangement of the crosslinked network in the bulk, (2) how such structural parameters affect the failure processes, (3) the effect of the failure processes on the mechanical properties, and (4) how these structural parameters are modified by fabrication procedures and the service environment. Such information is necessary before durability predictions about the

mechanical integrity of epoxy-adhesive joints and epoxy-composites can be made with any degree of confidence. The structure-property relationships of epoxy glasses, however, have received little attention compared with other commonly utilized polymer glasses.

The mechanical response of a polymer glass depends on the amount of flow occurring during the failure process, either microscopically via crazing and/or shear banding or macroscopically via necking [1-13]. The major parameters controlling the flow processes in non-crosslinked polymer glasses are the free volume [14-19] and the stress-raising microvoid characteristics of the glass [17, 20, 21].

In the case of crosslinked glasses such as epoxies,

the presence of crosslinking is an additional structural parameter affecting the flow processes. Generally, the cure process and final network structure of epoxies have been estimated from the chemistry of the system, if the curing reactions were known and assumed to go to completion, and from experimental techniques such as infrared spectra, swelling, dynamic mechanical, thermal conductivity and differential scanning calorimetry measurements. [22–37]. There have, however, been no systematic studies relating the chemical and physical structure of epoxies to their mechanical response.

The network structure and microvoid characteristics, which play a major role in the mechanical response, vary with cure conditions. For certain cure conditions, high crosslink-density regions from 6 to 10^4 nm in diameter have been observed in crosslinked resins [17, 24, 38–56]. The conditions for formation of a heterogeneous rather than a homogeneous system depend on polymerization conditions (i.e., temperature, solvent and/or chemical composition). These regions have been described as agglomerates of colloidal particles [43, 44] or floccules [46] in a lower molecular-weight interstitial fluid. Solomon *et al.* [45] suggested that a two-phase system is produced by microgelation prior to the formation of a macrogel. Kenyon and Nielsen [24] suggested that the highly crosslinked microgel regions are loosely connected during the latter stages of the curing process. More recently, Karyakina *et al.* [54] suggested that microgel regions originate in the initial stages of polymerization from the formation of micro-regions of aggregates of primary polymer chains. The high crosslink-density regions have been reported to be only weakly attached to the surrounding matrix [43, 44, 46], and their size varies with cure conditions [43], proximity of surfaces [46, 53] and the presence of solvents [24, 45].

The relation between the network structure, microvoid characteristics and failure processes of epoxies has received little attention. Localized plastic flow has been reported to occur during the failure processes of epoxies [49, 51, 57–65], and in a number of cases, the fracture energies have been reported to be a factor of 2 to 3 times greater than the expected theoretical estimate for purely brittle fracture [57, 58, 62, 64, 66–72].

No systematic studies, however, have been made to elucidate the microscopic flow processes

that occur during the deformation of epoxies and the relation of such flow processes to the network structure. Fracture topography studies on the effect of monomer crystallization and cure conditions on the physical structure and tensile mechanical response of polyamide-cured bisphenol-A-diglycidyl (DGEBA) epoxies led us to conclude that these glasses fail by void growth and coalescence through a simultaneously growing craze [65].

In this study, our objective was to elucidate the microscopic failure processes of amine-cured DGEBA epoxies and to determine how the network structure contributes to these processes. Bright-field transmission electron microscopy of thin films and carbon-platinum surface replicas was used to study the network morphology of these glasses. The failure processes were monitored by optical and electron microscopy of the fracture topographies and edges of epoxy specimens fractured in tension as a function of temperature and strain-rate, and of thin epoxy films deformed on a metal substrate. In addition, epoxy films were strained directly in the electron microscope, and the failure processes were monitored by bright-field microscopy.

2. Experimental

2.1. Materials and sample preparation

DER 332 (Dow) pure bisphenol-A-diglycidyl ether epoxide monomer (DGEBA) was used in this study. An aliphatic amine, diethylene triamine DETA (Eastman), containing both primary and secondary amines, was used as the curing agent.

Prior to mixing, both the DGEBA and DETA monomers were exposed to vacuum to remove absorbed water. The DGEBA epoxy monomer was also heated to 60°C to melt any crystals present [65] and then was immediately mixed with the curing agent at room temperature. Each type of epoxy specimen was cured at room temperature for 24 h and then in a vacuum at 150°C for 24 h. Epoxies with three different epoxy: amine ratios were prepared; namely 9, 11 and 13 parts per hundred by weight (phr) DETA. (The stoichiometric mixture for the DGEBA–DETA system is ~ 11 phr DETA [73]. This composition was determined by assuming that all amine hydrogens react with epoxide groups in absence of side reactions.)

For the fracture topography specimens, a 0.75 mm thick sheet of each epoxy mixture was prepared between glass plates separated by Teflon

spacers. A release agent (Crown 3070) was used to facilitate the removal of the partially cured epoxy sheets from the glass plates. Dogbone-shaped specimens, suitable for tensile fracture, were machined to a 2.5 cm gauge length and a width of 0.3 cm within the gauge length from the cured sheets; the edges were polished along the gauge length.

Epoxy films 0.1 mm thick for deformation on a brass substrate were prepared by pouring the initial unreacted epoxy-amine mixture directly on to a brass substrate. After post-curing, a rectangular specimen, suitable for straining in a tensile tester, was cut from the sheet.

Epoxy films $\sim 1 \mu\text{m}$ thick, suitable for straining directly in the electron microscope were cast between salt crystals. After post-curing, the crystals were dissolved in water and the film was washed with distilled water. Specimens 2 mm square were cut from the epoxy film. Thinner, $\sim 100 \text{ nm}$ thick films were prepared by a similar procedure for morphology studies.

2.2. Experimental

For the fracture topography studies, dogbone-shaped specimens were fractured in tension in a tensile tester (Instron TM-S-1130) in the crosshead speed range of 0.05 to 5.0 cm min^{-1} from 23 to 110°C. A scanning reflection electron microscope (JEOL model JEM-100B) and optical microscope (Zeiss Ultraphot II) were used for fracture topography studies. For the SEM studies, the fracture surfaces were coated with gold while the sample was rotated in vacuum.

The epoxy films that adhered to the metal substrate were strained on the tensile tester at a

strain-rate of $\sim 3 \times 10^{-2} \text{ min}^{-1}$. After removal of the stress, the deformation processes in the epoxy film were monitored by dark-field reflection optical microscopy and bright-field transmission electron microscopy of one-stage carbon-platinum surface replicas.

Bright-field transmission electron microscopy was used to monitor the failure processes of the $\sim 1 \mu\text{m}$ thick films that were strained directly in the electron microscope. The 2 mm square epoxy specimens were fastened to standard cartridge specimen holders with Duco Cement (E.I. duPont). The specimen holder was attached to an EM-SEH specimen elongation holder which was introduced into the microscope through the side entry goniometer. The specimens were deformed in the microscope at a strain-rate of $\sim 10^{-2} \text{ min}^{-1}$.

The network morphology of the epoxies was monitored by (1) one-stage carbon-platinum surface replicas of leached (3 h in acetone) and non-leached surfaces of the epoxy films fastened to a brass substrate and (2) bright-field transmission electron microscopy of $\sim 100 \text{ nm}$ thick films.

3. Results and discussion

3.1. Morphology

Structural heterogeneity was observed in the DGEBA-DETA epoxy systems. The carbon-platinum surface replica of a free epoxy surface shown in Fig. 1a reveals 20 to 35 nm diameter particles and aggregates of these particles protruding above the general surface contour, but such structures occurred only in patches and did not cover the entire surface of the DGEBA-DETA epoxies.

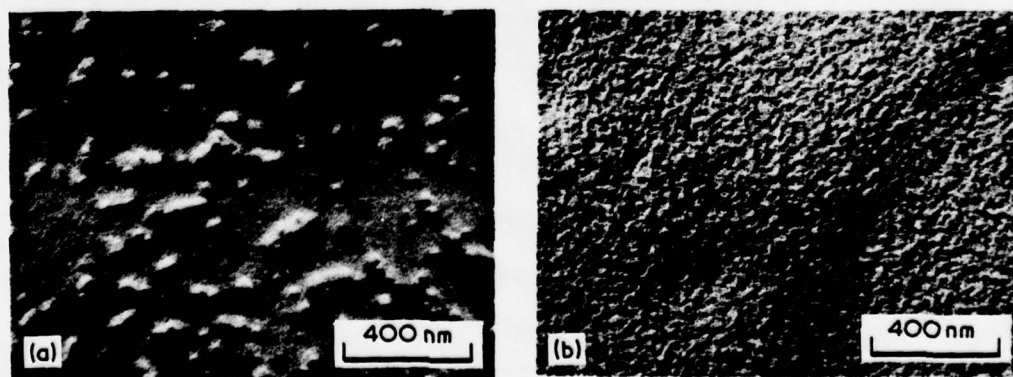


Figure 1 Carbon-platinum surface replica of (a) DGEBA-DETA (11 phr DETA) epoxy surface and (b) DGEBA-DETA (11 phr DETA) epoxy surface that was leached with acetone for 3 h.

1968

In an attempt to reveal regions of high crosslink density, epoxy surfaces were leached with acetone for 3 h. The organic solvent preferentially dissolves low molecular weight non-crosslinked material present on the surface. A carbon-platinum surface replica of such an acetone-leached epoxy surface is shown in Fig. 1b. The general surface roughness could be interpreted either in terms of indistinct 20 to 35 nm particles, or a surface wrinkling caused by solvent-induced relaxation of surface fabrication stresses.

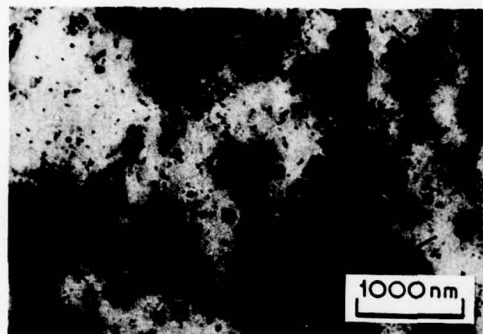


Figure 2 Bright-field transmission electron micrograph illustrating regions of ~ 30 nm diameter particles in DGEBA-DETA (13 phr DETA) epoxy film.

Bright-field transmission electron microscopy revealed regions consisting of spherical particles of ~ 30 nm diameter. These particles, which appear dark in the micrograph, are shown in Fig. 2. We suggest that the clarity of these particles in bright-field TEM results from surface emission phenomena. These surface effects have allowed the clear detection of surface microvoids 1 to 2 nm in diameter (which appear white in the micrograph) and their associated 1 to 2 nm wide dark shear bands in a strained polyimide film [17]. We suggest that the surface emission effects result from a charge accumulating on the top surface of the film [17], which may preferentially allow detection of any particles protruding above the general surface contour. The particles illustrated in Fig. 2 occur only in patches and were not observed in all the epoxy specimens investigated. The structure of these particles is discussed in Section 3.3.

3.2. Failure processes of films strained on a metal substrate

To elucidate the epoxy failure processes, 0.1 mm thick films were adhered to a brass substrate and strained $\sim 10\%$ in tension. After removal of the

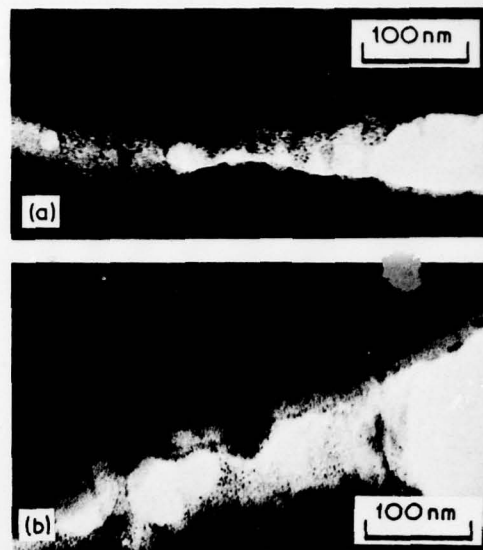


Figure 3 Carbon-platinum surface replicas of craze structure in DGEBA-DETA (11 phr DETA) epoxy films that were strained on a metal substrate.

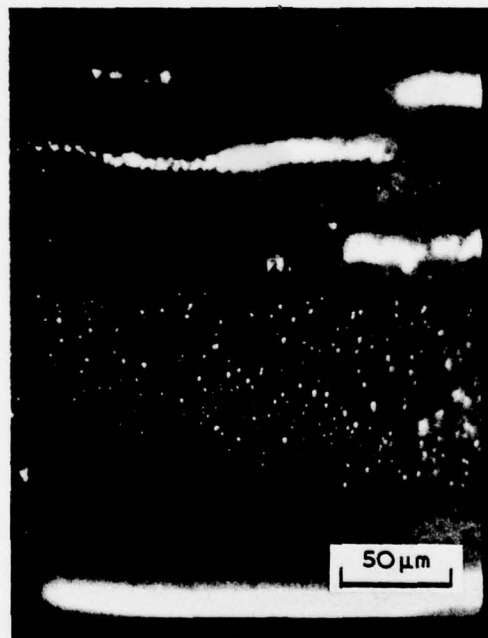


Figure 4 Dark-field reflection optical micrograph of voids and crazes in DGEBA-DETA (11 phr DETA) epoxy film that was strained on a metal substrate.

stress, one-stage carbon-platinum surface replicas of the epoxy film revealed the presence of crazes. The replicas in Figs. 3a and b illustrate the craze structure. The absence of any carbon-platinum

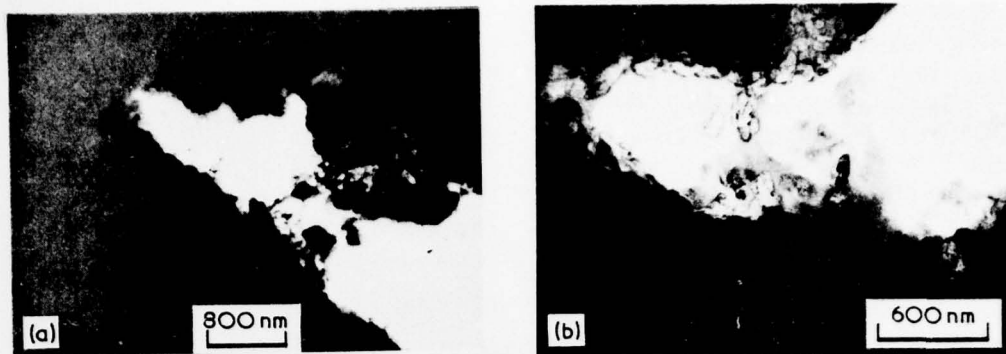


Figure 5 Bright-field transmission electron micrographs of (a) an overall craze and (b) a craze tip in DGEBA-DETA (13 phr DETA) epoxy.

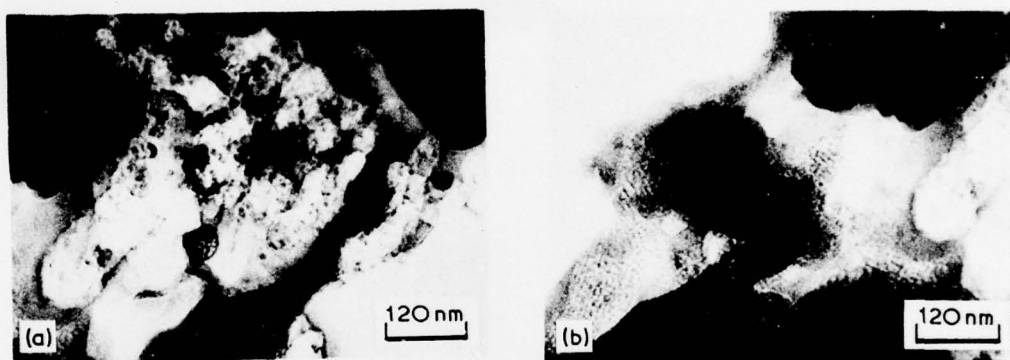


Figure 6 Bright-field transmission electron micrographs of craze fibril structure in DGEBA-DETA (13 phr DETA) epoxy.

particles within regions of the craze fibrils indicates a thin epoxy layer adhered to the replica. At the craze tip, ~ 10 nm diameter voids are produced by the tensile dilatational stress fields (Fig. 3a). These voids coalesce to form larger voids $\leq \sim 100$ nm diameter separated by 20 to 100 nm diameter fibrils. Further from the craze tip, the fibrils fracture as their length approaches ~ 100 nm. The latter phenomena may be a consequence of the poor structural integrity of the replica.

The crazes present in the epoxy film can also be detected by dark-field reflection optical microscopy. In Fig. 4 the optical micrograph illustrates voids and crazes in the epoxy film.

3.3. Failure processes and structure of epoxy films strained directly in the electron microscope

Significant information on the failure processes and structure of DGEBA-DETA epoxies was found from bright-field transmission electron

micrographs of $\sim 1 \mu\text{m}$ thick epoxy films strained directly in the microscope. An overall view of a craze consisting of coarse 100 to 1000 nm wide fibrils, produced by straining a film in the electron microscope, is shown in the bright-field TEM in Fig. 5a. The region near the craze tip is shown in more detail in Fig. 5b. The structure of the coarse ~ 1000 nm wide craze fibril in Fig. 5a is illustrated in more detail in Figs. 6a and b. These micrographs reveal that the epoxy deforms inhomogeneously within the craze fibril (Fig. 6a) and breaks up into 6 to 9 nm diameter particles. A network structure of interconnected 6 to 9 nm particles within the region of the craze fibril is illustrated in Fig. 6b. Bright-field TEMs of the epoxy network structure are shown in more detail at higher magnifications in Figs. 7a, b and c.

From studies on a number of DGEBA-DETA epoxy films, further evidence was found that these glasses deform inhomogeneously on a microscopic scale and that 6 to 9 nm particles remain intact

and flow past one another. Prior to deformation, the deformed film illustrated in Fig. 8a exhibited a uniform contrast in bright-field microscopy, however, on deformation, this film broke up inhomogeneously. Fig. 8b illustrates a region that

has flowed near the edge of an epoxy film. Particles 6 to 9 nm in diameter are evident throughout this deformed region.

The basic 6 to 9 nm diameter particles shown in Figs. 6 to 8 are in the size range associated with molecular domains. For crystallizable polymers, Wunderlich and Mehta [74] and Aharoni [75] presented theories in which the initial step of crystallization from the melt and solution occurs by formation of ordered molecular domains. Ordered nodules, 5 to 6 nm in diameter, the size of molecular domains, have been observed in thin films and on the surfaces of polycarbonate [19, 76]. We suggest that the 6 to 9 nm diameter particles illustrated in Figs. 7a, b and c are molecular domains which are intramolecularly crosslinked and which form during the initial stages of polymerization. In certain regions of the epoxies, these domains are interconnected to form a network during the later stages of the cure process. This hypothesis assumes that intramolecular crosslinking occurs in the early polymerization stages. For solution-phase condensation crosslinking, Flory [77] considered intramolecular crosslinking insignificant prior to gelation. Other workers, however, caution that in many thermoset systems, intramolecular crosslinking could occur to a significant extent prior to gelation [78-80]. The ability of the suggested 6 to 9 nm diameter molecular domains to remain intact during the flow processes suggests that intramolecular crosslinking has occurred within the domains. Particles the size of molecular domains were not observed when non-crosslinked polyimide films were deformed directly in the electron microscope [81]. The formation of the intramolecularly crosslinked domains could be explained by the inability of

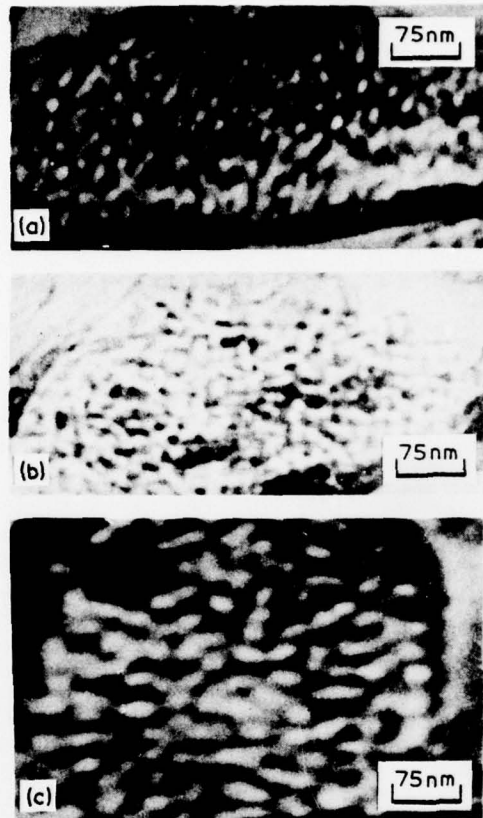


Figure 7 Bright-field transmission electron micrographs of network structure in deformed DGEBA-DETA (13 phr DETA) epoxies.

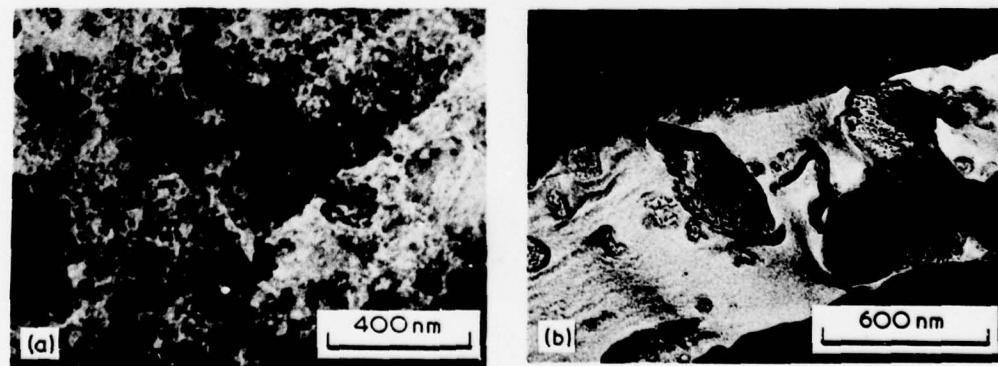


Figure 8 Bright-field transmission electron micrographs of deformed regions within DGEBA-DETA (13 phr DETA) epoxy films.

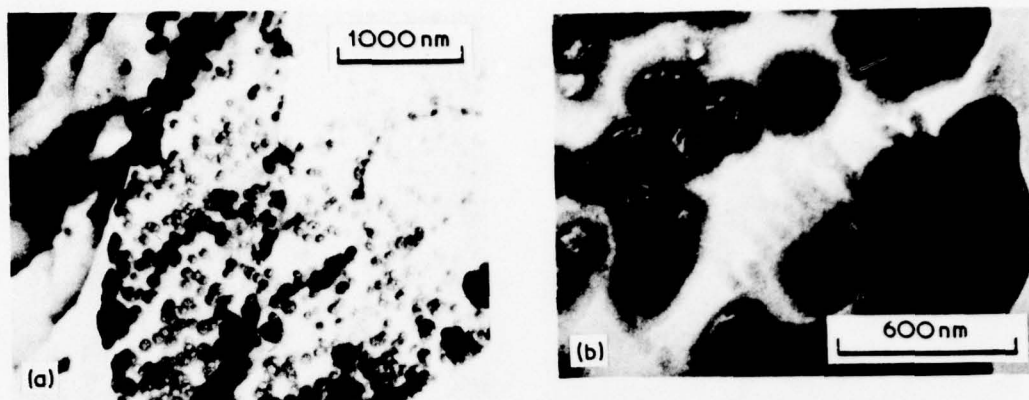


Figure 9 Bright-field transmission electron micrographs of strained DGEBA-DETA (9 phr DETA) epoxy illustrating (a) aggregates of 6 to 9 nm particles and (b) the presence of these aggregates at the craze-matrix boundary interface.

unreacted epoxy and amine species attached to a growing domain to diffuse to active species attached to neighbouring domains. These species would, therefore, only be able to react with active species in their immediate location. Chompff [82] has recently noted that configurational restrictions could lead to excessive intramolecular crosslinking.

Aggregates, 20 to 35 nm in diameter, of the 6 to 9 nm particles were observed by bright-field TEM studies of strained ~ 100 nm thick epoxy films. Such aggregates are shown in Fig. 9a: their size is similar to that of structures found on epoxy surfaces and in thin films (see Section 3.1). We, therefore, suggest that structures larger than ~ 10 nm found in epoxies could be aggregates of smaller particles.

The craze present in the bottom left of Fig. 9a is illustrated in more detail in Fig. 9b. This micrograph shows that 20 to 35 nm diameter aggregates are present at the craze-matrix boundary interface, which suggests that the craze fibrillation process may be inhibited by these aggregates. The inhibition of the drawing of new material across the craze-matrix boundary interface increases the possibility of strain-hardening and fracture of the fibrils and would, therefore, enhance crack propagation.

The interconnection of molecular domains by regions of either low or high crosslink density allows the possibility of two types of network structure: (1) regions of high crosslink density embedded in a low- or non-crosslinked matrix or (2) non-crosslinked or low crosslink density regions embedded in a high crosslink density matrix. From straining films in the electron

microscope, we observed both types of network morphology; the second type was more prevalent. An example of the first type of morphology is illustrated in Fig. 9a where aggregates of high crosslink density particles are embedded in a deformable low crosslink density matrix. Deformation of this type of network involves preferential deformation of the regions of low crosslink density without causing cleavage of the highly crosslinked regions, as apparently occurs in the craze in Fig. 9b. The deformation process is more complex for the second type of network. Local affine deformation requires network cleavage and flow to occur in the high crosslink density region simultaneously as flow with little network cleavage occurs in the neighbouring low crosslink density regions. This deformation process results in

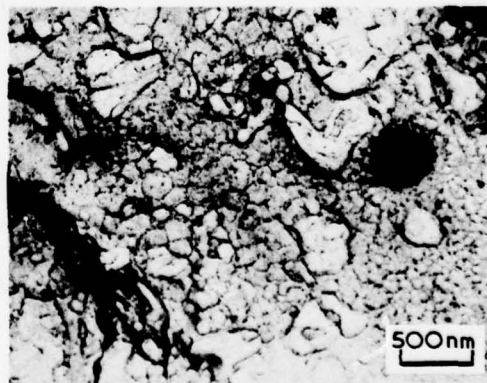


Figure 10 Bright-field transmission electron micrograph illustrating strained network of DGEBA-DETA (13 phr DETA) epoxy in which the high crosslink density regions form the continuous phase in the network.

progressively larger regions that are poorly cross-linked. Such a deformed network structure is illustrated in the bright-field TEM of a strained DGEBA-DETA epoxy film in Fig. 10. The dark network structure in Fig. 10 consists of 6 to 9 nm diameter interconnected domains separated by low crosslinked and/or thinned regions of the network which appear light in the micrograph. The network is more dense in the bottom right of the micrograph than in the upper portion which suggests that more deformation has occurred in the latter region.

It is surprising that the DGEBA-DETA epoxies

exhibit considerable microscopic flow because these glasses are prepared from approximately stoichiometric epoxy-amine mixtures which should produce highly crosslinked glasses. This suggests that many reactive groups remain unreacted within these epoxies because of diffusion and steric restrictions imposed during polymerization and network formation.

3.4. Edge deformation

The failures of the majority of the 0.75 mm thick epoxy dogbones, that were fractured in tension as a function of strain-rate and temperature, initiated

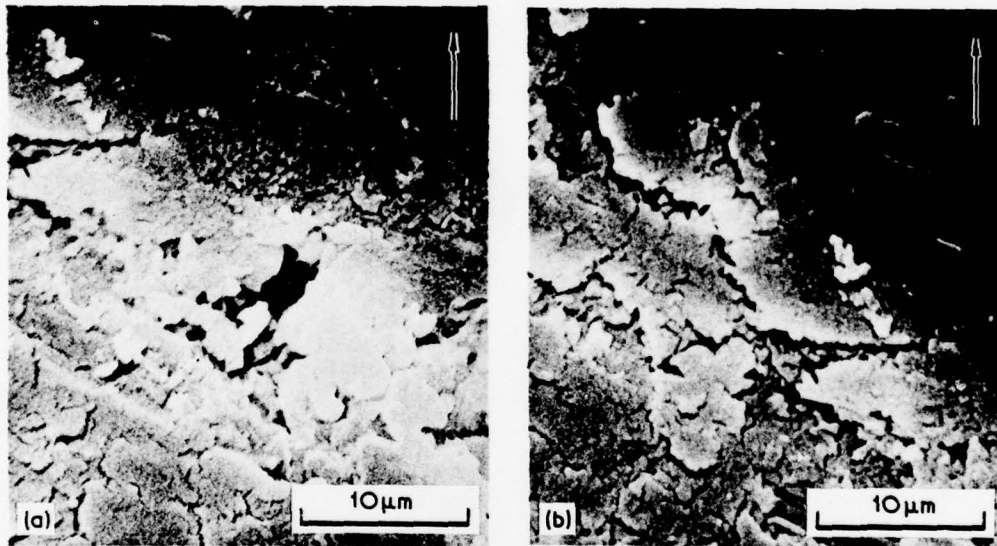


Figure 11 Scanning electron micrographs of edge microcracking in DGEBA-DETA (13 phr DETA) epoxy that was fractured at 77° C at a strain-rate of 10^{-2} min^{-1} . (Applied tensile stress direction indicated by the arrow.)

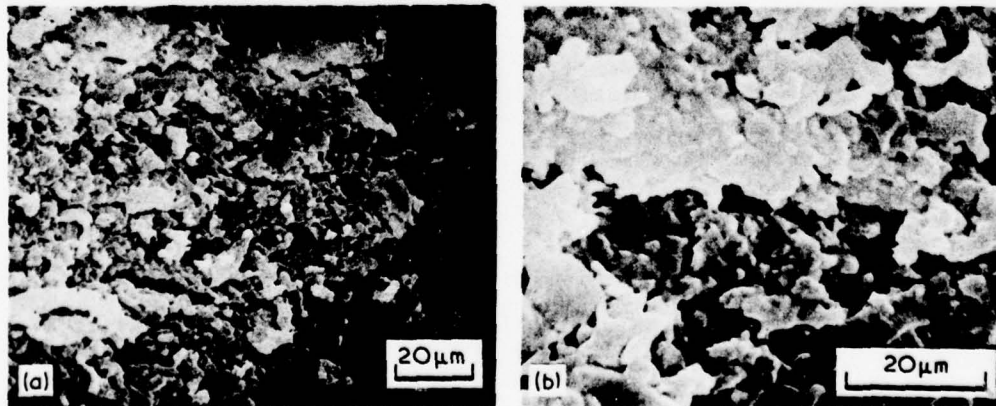


Figure 12 Scanning electron micrographs illustrating platelet structure at the edge of DGEBA-DETA (13 phr DETA) epoxy that was fractured at 77° C at a strain rate of $\sim 10^{-2} \text{ min}^{-1}$. (Applied tensile stress direction indicated by the arrow.)

at the specimen edge. The edges of the fractured specimens were investigated by scanning electron microscopy. The SEMs in Figs. 11a and b exhibit many irregular fine cracks which were not necessarily perpendicular to the applied tensile stress whose direction is indicated by the arrow. The irregularity of these cracks suggests that their growth is affected either by heterogeneities in the epoxy structure, which allow preferential paths for crack propagation, or by surface fabrication stresses. We suggest that the cavity in the centre of Fig. 11a could be a coarse craze in its initial stages. No well-defined crazes were found, however, at the specimen edges. In a number of the edges of fractured specimens, we observed a platelet-like structure in the vicinity of a poorly developed crack or craze as shown in Figs. 12a and b. Such structures are probably formed by the tearing and shearing past one another of regions originally interconnected by structurally weak planes. These observations also indicate the heterogeneous structure of these glasses.

3.5. Fracture topographies

The fracture topographies of DGEBA-DETA epoxies fractured as a function of temperature and strain rate were studied by optical and scanning electron microscopy. An optical micrograph, shown in Fig. 13, illustrates the three characteristic topography regions observed in these epoxies: (1) a coarse initiation region (dark area in centre of smooth region), (2) a slow crack-growth, smooth, mirror-like region and (3) a fast crack-growth, rough, parabola region. The topographies vary with temperature and strain-rate, with the mirror-like region covering a larger portion of the fracture surface with increasing temperature and/or decreasing strain rate.

The coarse initiation region is often found within a cavity as indicated by a cusp in the fracture topography which separates this region from the surrounding smooth mirror-like region. The coarse structure can cover a relatively small region in the centre of the initiation cavity, or it can cover the entire cavity or irregularly cover parts of the cavity. The SEM in Fig. 14 illustrates a portion of the cavity cusp and coarse regions irregularly covering parts of the cavity.

The structure of the coarse topography in the initiation region exhibited little consistency among samples or with varying temperatures and strain-rates. A typical range of topographies observed in

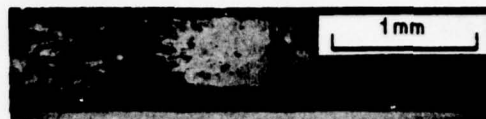


Figure 13 Optical micrograph of overall fracture topography of DGEBA-DETA (11 phr DETA) epoxy fractured at room-temperature at a strain rate of $\sim 10^{-2} \text{ min}^{-1}$.

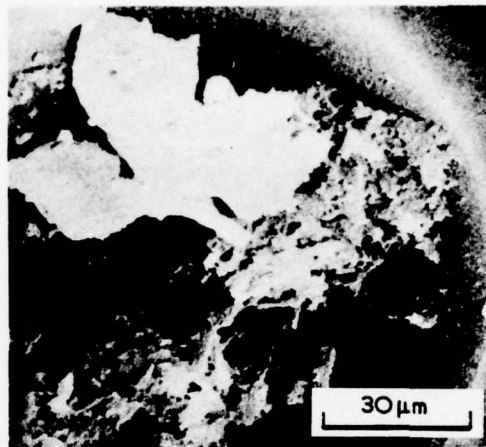


Figure 14 Scanning electron micrograph of fracture topography initiation cavity irregularly covered with a coarse topography of DGEBA-DETA (11 phr DETA) epoxy fractured at room temperature at a strain rate of $\sim 10^{-2} \text{ min}^{-1}$.

the initiation region is illustrated by SEM in Figs. 15 to 19. The mica-like structure illustrated in Fig. 15 becomes progressively more nodular in character in Figs. 16 and 17. A collapsed fibrillar topography was also observed in the initiation region as illustrated in Fig. 18. At temperatures near T_g (i.e., at $T_g - 25^\circ \text{C}$), the fracture initiation region in the DGEBA-DETA epoxies is non-existent and/or much smoother than at lower fracture temperatures, as illustrated in Fig. 19.

The fracture topography initiation region characteristics can be explained in terms of a crazing failure process. Murray and Hull [83] have reported that void growth and coalescence within a craze produce a planar cavity whose thickness is that of the craze. A mica-like structure in the slow crack-growth fracture topography of polymer glasses is generally associated with crack propagation through pre-existing craze material [84]. Murray and Hull [83] and Cornes and Haward [85] have observed irregularly furrowed or rumpled surfaces within

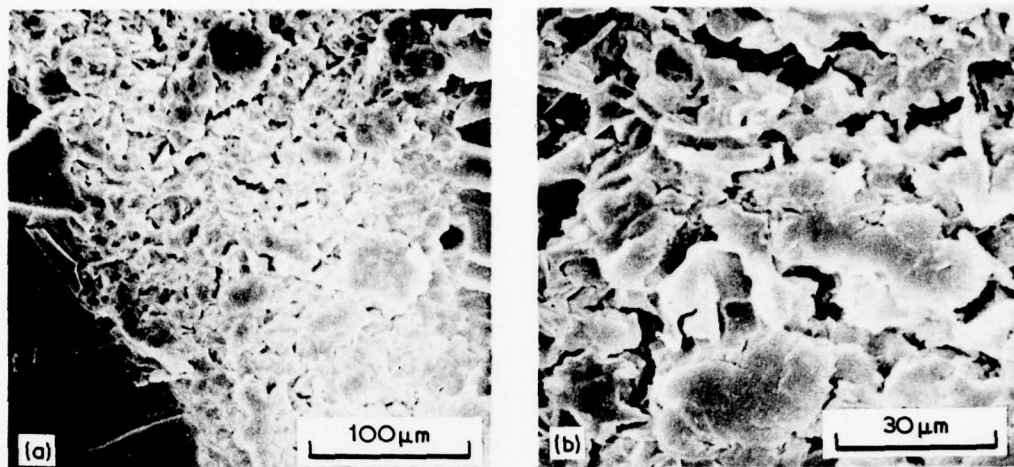


Figure 15 Scanning electron micrograph of mica-like structure in the fracture topography initiation region of DGEBA-DETA (9 phr DETA) epoxy fractured at 56° C at a strain rate of $\sim 10^{-2} \text{ min}^{-1}$.

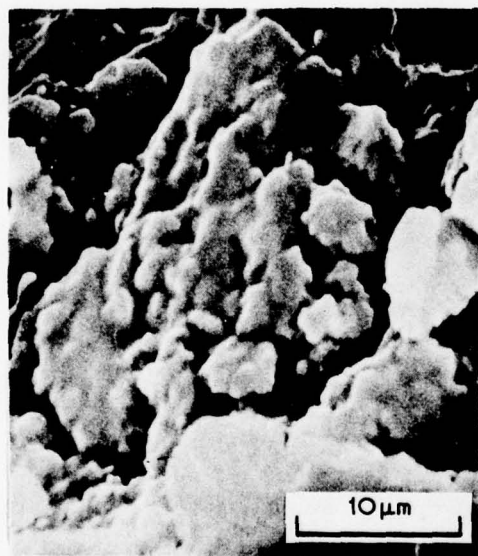


Figure 16 Scanning electron micrograph of nodular-mica-like structure in the fracture topography initiation region of DGEBA-DETA (11 phr DETA) epoxy fractured at 71° C at a strain rate of $\sim 10^{-1} \text{ min}^{-1}$.

initiation cavities in polystyrene and poly(vinyl chloride) respectively. Furthermore, there is evidence from studies on polystyrene that the initial stages of void growth and coalescence within a craze involve fracture through the centre of the craze [86, 87]. In addition, the coarseness of the craze fibrils has been reported to decrease with increasing craze width and thickness [87]. These facts suggest that the coarse initiation

region in epoxies results from void growth and coalescence through the centre of a simultaneously growing, poorly developed craze, which consists of coarse fibrils. The diameter of the broken fibrils depends on the relative rates of craze and void growth. The 200 to 500 nm diameter nodular particles illustrated in Fig. 17 and fibrillar structures that lie parallel to the fracture surface in Fig. 18 are associated with fractured craze fibrils. Doyle [88, 89] and Hoare and Hull [90] have reported broken fibrils that lie parallel to the fracture surface in polystyrene and have suggested that these fibrils are swept down on to the fracture surface as the crack passes through the craze. We cannot preclude, however, that the mica-like structure such as that observed in Fig. 15, results from the coalescence of a bundle of parallel microcrazes situated in slightly different planes rather than directly from the fracture of poorly formed coarse craze fibrils. Skibo *et al.* [91] suggested that the mica-like structure they observed in the non-initiation region of the fatigue-fracture topography of polystyrene is a result of the intersection of the crack plane with craze bundles. The more nodular-like topographies shown in Figs. 16 and 17 are similar to those observed in the fracture topographies of certain multiphase metals [92] and poly(vinyl chloride) [93-95]. In poly(vinyl chloride), this structure has been associated with the particulate nature of the polymer as a result of imperfect melting of resin particles [93-95]. Hence, we also cannot preclude that any heterogeneity in the epoxy

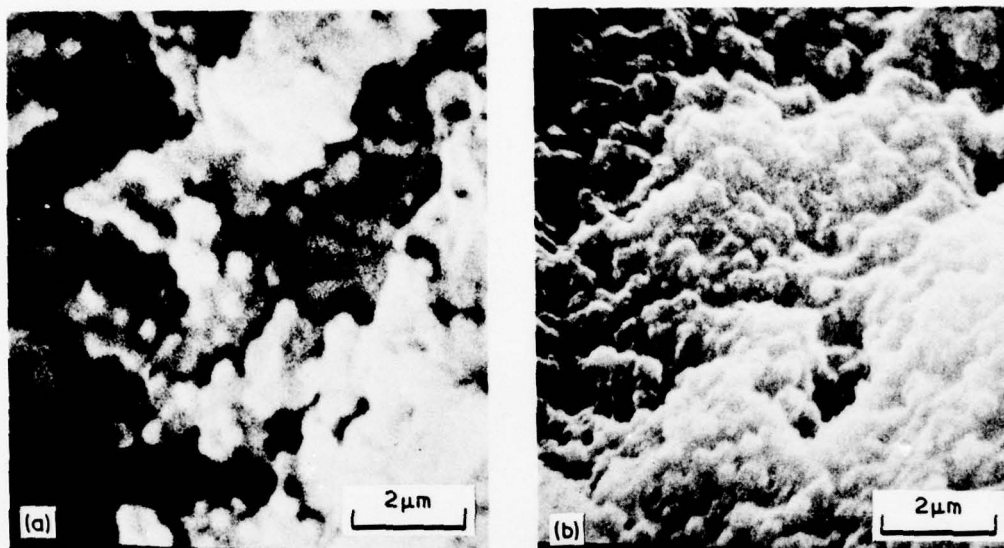


Figure 17 Scanning electron micrographs of nodular structure in the fracture topography initiation regions of (a) DGEBA-DETA (11 phr DETA) epoxy fractured at room temperature at a strain-rate of $\sim 10^{-2} \text{ min}^{-1}$ and (b) DGEBA-DETA (13 phr DETA) epoxy fractured at 77° C at a strain rate of $\sim 1 \text{ min}^{-1}$.

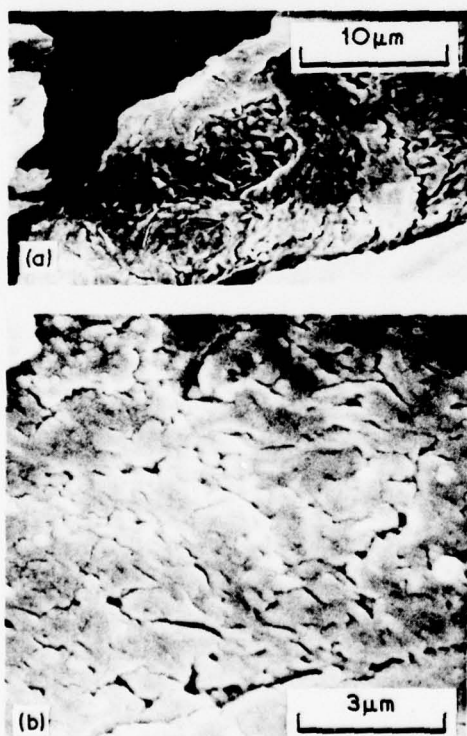


Figure 18 Scanning electron micrographs of collapsed fibrillar structure in the fracture topography initiation region of DGEBA-DETA (9 phr DETA) epoxy fractured at 56° C at a strain rate of $\sim 10^{-2} \text{ min}^{-1}$.

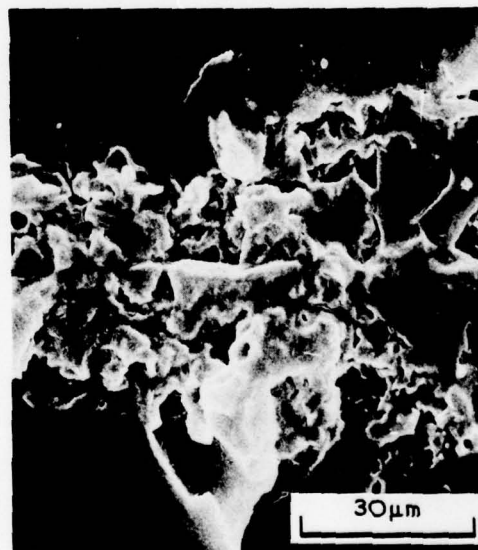


Figure 19 Scanning electron micrograph of relatively smooth fracture topography initiation region of DGEBA-DETA (13 phr DETA) epoxy fractured at 102° C at a strain rate of $\sim 10^{-1} \text{ min}^{-1}$.

structure could be partially responsible for the topographies observed in Figs. 15 to 19.

The variation in the fracture topography initiation region which did not exhibit consistent trends with strain-rate and temperature, except for the disappearance or smoothening of the coarse

topographies in those specimens fractured near T_g , is a result of a number of factors: (1) the relative rates of crack and craze propagation, (2) the craze structure immediately prior to crack propagation through the craze, (3) the modification of the craze structure by crack propagation, (4) the collapsing and relaxation of the craze remnants after crack propagation and (5) the variation in the local stress fields in the vicinity of a growing craze or crack which depends on the microvoid characteristics of the epoxy.

The smooth mirror-like region of the fracture topography of DGEBA-DETA epoxies, whose area increases with increasing temperature and decreasing strain-rate, can be attributed to a crazing process. For other polymers, this region has been associated with slow crack-growth, and its size varies with temperature, molecular weight and strain-rate [96-99]. In studies on polyester resins, Owen and Rose [100] report that the mirror-like area increases with resin flexibility. A number of workers have associated this smooth fracture topography region with slow crack-propagation through the median of the craze with subsequent relaxation of craze remnants [83, 84, 89, 90, 101, 102]. El-Hakeem *et al.* [102] directly observed the masking of the microfeatures of this fracture topography region by the subsequent relaxation processes. The smoothness of the fracture topography region surrounding the coarse initiation region in DGEBA-DETA epoxies results from crack propagation either through the centre or along the craze-matrix boundary interface of a thick, well-developed craze consisting of fine fibrils. The presence of fine fibrils would produce a smoother fracture topography than in the coarse initiation region, irrespective of any subsequent relaxation of craze remnants. One-stage carbon-platinum surface replicas of the mirror-like region reveal areas consisting of 15 to 30 nm diameter particles, as illustrated in Fig. 20. The granular appearance of the replica could be the result of fractured fine fibrils aligned normal to the surface. However, it is also possible that such structures are indeed regions of high crosslink density. The extent of the mirror-like region is a measure of the area in which crack propagation occurs through a preformed craze [83]. For a fracture surface completely covered by the mirror-like region, crazes have grown completely across the specimen prior to any significant crack propagation [90]. Hoare and Hull [90] have suggested that this area



Figure 20 Carbon-platinum surface replica illustrating granular appearance of mirror-like fracture topography region of DGEBA-DETA (9 phr DETA) epoxy which was fractured at 56° C at a strain rate of $\sim 10^{-2} \text{ min}^{-1}$.

depends on the ease of cavitation and crack propagation within the craze, the rate of craze nucleation and growth and the concentration of crazes. The decrease in the crazing stress with increasing temperature and/or decreasing strain-rate favours simultaneous craze and crack growth which results in a larger mirror-like region.

River markings which radiate from the fracture initiation site are also observed in the mirror-like region as illustrated in Fig. 13. These markings, which vary from one epoxy specimen to another, are steps formed by the subdivision of the main crack into segments running on parallel planes. This subdivision could result from the interaction of the crack front with the craze structure. Owen and Rose [100] found that the river markings become more ordered and regular as the flexibility, and therefore the ability to undergo crazing in polyester resins, is enhanced.

Interference colours, often observed in the mirror-like region of non-crosslinked polymer glasses [4], were not evident in the fracture topography of DGEBA-DETA epoxies. Broutman and McGarry [57] also found that interference colours are absent in the fracture surfaces of

crosslinked polymethylmethacrylates. They suggested that the thickness of the craze or craze remnants in the mirror-like regions of these crosslinked glasses is not large enough to cause interference with visible light. A similar explanation could be advanced for epoxies where the presence of crosslinking presumably inhibits the development of thick crazes.

4. Conclusions

(1) From electron microscopy studies, DGEBA-DETA epoxies were found to consist of 6 to 9 nm diameter particles which remain intact when flow occurs in these glasses. It is suggested that these particles are intramolecularly crosslinked molecular domains. The 6 to 9 nm diameter particles interconnect to form larger 20 to 35 nm diameter aggregates which are observed in patches on surfaces and in thin films of DGEBA-DETA epoxies. Two types of network structures were observed from straining thin DGEBA-DETA epoxy films in the electron microscope: (a) regions of high crosslink density embedded in a low- or non-crosslinked matrix and (b) low- or non-crosslink density regions embedded in a high crosslinked density matrix.

(2) The mode of deformation and failure in DGEBA-DETA epoxy films, either when strained directly in the electron microscope or on a metal substrate, was a crazing process.

(3) The flow processes that occur during deformation of DGEBA-DETA epoxy films strained in the electron microscope depend on the network structure. Deformation of a network consisting of high crosslink density particles embedded in a deformable low crosslink density matrix occurs by preferential deformation of the low crosslink density regions without causing cleavage of the high crosslink density regions. However, deformation of a network consisting of low crosslink density regions embedded in a high crosslink density matrix must involve network cleavage and flow in the high crosslink density regions simultaneously as flow with little network cleavage occurs in the neighbouring low crosslink density regions.

(4) The fracture topographies of bulk DGEBA-DETA epoxy glasses fractured as a function of temperature and strain rate can be interpreted in terms of a crazing failure process. The coarse structures observed in the fracture topography initiation regions result from void growth and

coalescence through the centre of a simultaneously growing poorly developed craze consisting of coarse fibrils. The surrounding smooth slow crack-growth mirror-like region results from crack propagation either through the centre or along the craze-matrix boundary interface of a thick, well-developed craze consisting of fine fibrils.

Acknowledgements

We wish to acknowledge Dr D. Ulrich of Air Force Office of Scientific Research and Dr D. P. Ames and Dr C. J. Wolf of McDonnell Douglas Research Laboratories for their support and encouragement of this work. The research was sponsored by the Air Force Office of Scientific Research/AFSC, United States Air Force, under Contract No. F44620-76-C-0075. The United States Government is authorized to reproduce and distribute reprints for governmental purposes notwithstanding any copyright notation hereon.

References

1. J. P. BERRY, *J. Polym. Sci.* **50** (1961) 107.
2. *Idem, ibid* **50** (1961) 313.
3. R. F. BOYER, *Rubber Chem. Technol.* **36** (1963) 1301.
4. R. P. KAMBOUR, *J. Polym. Sci.* **A3** (1965) 1713.
5. *Idem, Polym. Eng. Sci.* **8** (1968) 281.
6. *Idem, Appl. Polymer Symposia* **7** (1968) 215.
7. J. HEIJBOER, in "Macromolecular Chemistry", Prague, 1965, edited by O. Wichterle and B. Sedlacek (Interscience, New York, 1968) p. 3755.
8. E. H. ANDREWS, "Fracture in Polymers", (Elsevier, New York, 1968).
9. S. M. AHARONI, *J. Appl. Polym. Sci.* **16** (1972) 3275.
10. S. RABINOWITZ and P. BEARDMORE, in "Critical Reviews in Macromolecular Science", Vol. 1, (Chem. Rubber Co., Cleveland, 1972) p. 1.
11. R. J. MORGAN, *J. Polym. Sci. A-2* **11** (1973) 1271.
12. J. R. KASTELIC and E. BAER, *J. Macromol. Sci.-Phys.*, **B7(4)** (1973) 679.
13. R. J. MORGAN and L. E. NIELSEN, *ibid* **B9(2)** (1974) 239.
14. A. J. KOVACS, *Adv. Polym. Sci.* **3** (1964) 394.
15. M. H. LITT and A. V. TOBOLSKY, *J. Macromol. Sci.-Phys.* **B1(3)** (1967) 433.
16. R. F. BOYER, *Polym. Eng. Sci.* **8** (1968) 161.
17. R. J. MORGAN and J. E. O'NEAL, *Polym. and Plast. Tech and Eng.* **5(2)** (1975) 173.
18. S. E. B. PETRIE, in "Polymeric Materials: Relationships Between Structure and Mechanical Behaviour", edited by E. Baer and S. V. Radcliffe, (A.S.M., 1975) p. 55.
19. R. J. MORGAN and J. E. O'NEAL, *J. Polym. Sci. A-2* **14** (1976) 1053.
20. A. N. GENT, *J. Mater. Sci.* **5** (1970) 925.

21. E. H. ANDREWS, in "The Physics of Glassy Polymers", edited by R. N. Haward, (Applied Science Publishers Ltd., Barking 1973) Chapter 7.
22. D. KATZ and A. V. TOBOLSKY, *Polymer* **4** (1963) 417.
23. T. K. KWEI, *J. Polym. Sci.* **A1** (1963) 2977.
24. A. S. KENYON and L. E. NIELSEN, *J. Macromol. Sci.-Chem.*, **A3(2)** (1969) 275.
25. R. P. KREHLING and D. E. KLINE, *J. Appl. Polym. Sci.* **13** (1969) 2411.
26. J. P. BELL, *J. Polym. Sci. A2*, **8** (1970) 417.
27. T. MURAYAMA and J. P. BELL, *ibid* **8** (1970) 437.
28. M. A. ACITELLI, R. B. PRIME and E. SACHER, *Polymer* **12** (1971) 335.
29. R. G. C. ARRIDGE and J. H. SPEAKE, *ibid* **12** (1972) 443, 450.
30. P. V. SIDYAKIN, *Vysokomol. soyed.* **A14** (1972) 979.
31. T. HIRAI and D. E. KLINE, *J. Appl. Polym. Sci.* **16** (1972) 3145.
32. R. B. PRIME and E. SACHER, *Polymer* **13** (1972) 455.
33. P. G. BABAYEVSKY and J. K. GILLHAM, *J. Appl. Polym. Sci.* **17** (1973) 2067.
34. T. HIRAI and D. E. KLINE, *ibid* **17** (1973) 31.
35. E. SACHER, *Polymer* **14** (1973) 91.
36. D. A. WHITING and D. E. KLINE, *J. Appl. Polym. Sci.* **18** (1974) 1043.
37. J. K. GILLHAM, J. A. BENCI and A. NOSHAY, *ibid* **18** (1974) 951.
38. T. S. CARSWELL, "Phenoplasts", (Interscience, New York, 1947).
39. T. G. ROCHOW and F. G. ROWE, *Anal. Chem.* **21** (1949) 261.
40. R. A. SPURR, E. H. ERATH, H. MYERS and D. C. PEASE, *Ind. Eng. Chem.* **49** (1957) 1839.
41. E. H. ERATH and R. A. SPURR, *J. Polym. Sci.* **35** (1959) 391.
42. T. G. ROCHOW, *Anal. Chem.* **33** (1961) 1810.
43. E. H. ERATH and M. ROBINSON, *J. Polym. Sci. C* **3** (1963) 65.
44. H. P. WOHNSIEDLER, *J. Polym. Sci. C* **3** (1963) 77.
45. D. H. SOLOMON, B. C. LOFT and J. D. SWIFT, *J. Appl. Polym. Sci.* **11** (1967) 1593.
46. R. E. CUTHRELL *ibid* **11** (1967) 949.
47. A. N. NEVEROV, N. A. BIRKINA, Yu. V. ZHERDEV and V. A. KOZLOV, *Vysokomol. soyed.* **A10** (1968) 463.
48. G. NENKOV and M. MIKHAILOV, *Makromol. Chem.* **129** (1969) 137.
49. B. E. NELSON and D. T. TURNER, *J. Polym. Sci. A-2* **10** (1972) 2461.
50. L. G. BOZVELIEV and M. G. MIHAJLOV, *J. Appl. Polym. Sci.* **17** (1973) 1963, 1973.
51. R. J. MORGAN and J. E. O'NEAL, *Polymer Preprints* **16**, **2** (1975) 610.
52. K. SELBY and L. E. MILLER, *J. Mater. Sci.* **10** (1975) 12.
53. J. L. RACICH and J. A. KOUTSKY, *Bull. Am. Phys. Soc.* **20** (1975) 456.
54. M. I. KARYAKINA, M. M. MOGILEVICH, N. V. MAIOROVA and A. V. UDALOVA, *Vysokomol. soyed.* **A17** (1975) 466.
55. M. V. MAIOROVA, M. M. MOGILEVICH, M. I. KARYAKINA and A. V. UDALOVA, *ibid* **A17** (1975) 471.
56. V. M. SMARTSEV, A. Ye. CHALYKH, S. A. NENAKHOV and A. T. SANZHAROVSKII, *ibid* **A17** (1975) 836.
57. L. J. BROUTMAN and F. J. MCGARRY, *J. Appl. Polym. Sci.* **9** (1965) 609.
58. R. GRIFFITHS and D. G. HOLLOWAY, *J. Mater. Sci.* **5** (1970) 302.
59. R. L. PATRICK, W. G. GEHMAN, L. DUNBAR and J. A. BROWN, *J. Adhesion* **3** (1971) 165.
60. P. B. BOWDEN and J. A. DUKES, *J. Mater. Sci.* **7** (1972) 52.
61. R. L. PATRICK, in "Treatise on Adhesion and Adhesives", Vol. 3, edited by R. L. Patrick, (Dekker, New York, 1973) p. 163.
62. R. J. YOUNG, P. W. R. BEAUMONT, *J. Mater. Sci.* **10** (1975) 1343.
63. R. J. MORGAN and J. E. O'NEAL, *Amer. Chem. Soc. Div. Org. Coat. Plast. Preprints* **36** **2** (1976) 689.
64. A. CHRISTIANSEN and J. B. SHORTALL, *J. Mater. Sci.* **11** (1976) 1113.
65. R. J. MORGAN and J. E. O'NEAL, *J. Macromol. Sci.-Phys.* (in press).
66. S. MOSTOVOY and E. J. RIPLING, *J. Appl. Polym. Sci.* **10** (1966) 1351.
67. *Idem*, *ibid* **15** (1971) 611.
68. A. T. DIBENNEDETTO and A. D. WAMBACH, *Int. J. Polym. Mater.* **1** (1972) 159.
69. A. D. S. DIGGWA, *Polymer* **15** (1974) 101.
70. W. D. BASCOM, R. L. COTTINGTON, R. L. JONES and P. PEYSER, *J. Appl. Polym. Sci.* **19** (1975) 2545.
71. P. G. BABAYEVSKII and Ye. B. TROSTYAN-SKAYA, *Vysokomol. soyed.* **A17** (1975) 906.
72. R. A. GLEDHILL and A. J. KINLOCH, *J. Mater. Sci.* **10** (1975) 1263.
73. H. LEE and K. NEVILLE, "Handbook of Epoxy Resins", (McGraw-Hill, New York, 1967) Chapter 5.
74. B. WUNDERLICH and A. MEHTA, *J. Polym. Sci. A-2* **12** (1974) 255.
75. S. M. AHARONI, *J. Appl. Polym. Sci.* **19** (1975) 1103.
76. K. NEKI and P. H. GEIL, *J. Macromol. Sci.-Phys.*, **B8(1-2)** (1973) 295.
77. P. J. FLORY, "Principles of Polymer Chemistry", (Cornell University Press, Ithaca, 1953) Chapter 9.
78. E. G. K. PRITCHETT, *Chem. and Ind.* (1949) 295.
79. N. J. L. MEGSON, "Phenolic Resin Chemistry", (Academic Press, New York, 1958).
80. D. H. SOLOMON, *J. Macromol. Sci. C1* (1967) 179.
81. R. J. MORGAN and J. E. O'NEAL, *J. Mater. Sci.* **12** (1977) 1338.
82. A. J. CHOMPFF, *Amer. Chem. Soc. Div. Org. Coat. Plast. Preprints*, **36** **2** (1976) 529.
83. J. MURRAY and D. HULL, *Polymer* **10** (1969) 451.
84. S. RABINOWITZ, A. R. KRAUSE and P. BEADMORE, *J. Mater. Sci.* **8** (1973) 11.
85. P. L. CORNES and R. N. HAWARD, *Polymer* **15** (1974) 149.

86. J. MURRAY and D. HULL, *J. Polym. Sci. A-2* **8** (1970) 1521.
87. P. BEAHAN, M. BEVIS and D. HULL, *J. Mater. Sci.* **8** (1972) 162.
88. M. J. DOYLE, *J. Polym. Sci. A-2* **13** (1975) 127.
89. *Idem*, *J. Mater. Sci.* **10** (1975) 300.
90. J. HOARE and D. HULL, *ibid* **10** (1975) 1861.
91. M. D. SKIBO, R. W. HERTZBERG and J. A. MANSON, *ibid* **11** (1976) 479.
92. J. E. O'NEAL, unpublished work on titanium alloys (1975).
93. G. PEZZIN, G. AJROLDI, T. CASIRAGHI, C. GARBUGLIO and G. VITTADINI, *J. Appl. Polym. Sci.* **16** (1972) 1839.
94. R. G. FAULKNER, *J. Macromol. Sci.-Phys.* **B11(2)** (1975) 251.
95. R. P. CHARTOFF, *Polymer* **16** (1975) 470.
96. F. ZANDEMAN, *Publs. Scient. Tech. Minist. Air, Paris No. 291* (1954) Ch. 1V.
97. S. B. NEWMAN and I. WOLOCK, *J. Appl. Phys.* **29** (1958) 49.
98. I. WOLOCK and S. B. NEWMAN in "Fracture Processes in Polymeric Solids", edited by B. Rosen (Interscience, 1964) Ch. II c.
99. R. J. BIRD, J. MANN, G. POGANY and G. ROONEY, *Polymer* **7** (1966) 307.
100. M. J. OWEN and R. G. ROSE, *J. Mater. Sci.* **10** (1975) 1711.
101. M. J. DOYLE, *ibid* **10** (1975) 159.
102. H. EL-HAKEEM, G. P. MARSHALL, E. I. ZICHY and L. E. CULVER, *J. Appl. Polym. Sci.* **19** (1975) 3093.

Received 7 January and accepted 2 February 1977.

APPENDIX C: The Durability of Epoxies, Polym. Plast. Tech.
and Eng. 10(1), 49 (1978)

THE DURABILITY OF EPOXIES

ROGER J. MORGAN and JAMES E. O'NEAL

*McDonnell Douglas Research Laboratories
McDonnell Douglas Corporation
St. Louis, Missouri 63166*

I. INTRODUCTION	50
II. STRUCTURE OF EPOXIES	51
A. Network Structure	51
B. Microvoid Characteristics	65
III. DEFORMATION AND FAILURE MODES OF EPOXIES	71
A. The DGEBA-DETA Epoxy System	71
B. The TGDDM-DDS Epoxy System	81
IV. EFFECTS OF SORBED MOISTURE ON DURABILITY OF EPOXIES	85
A. The Glass Transition	85
B. Diffusion	88
C. Swelling	99
D. Modes of Deformation and Failure and Mechanical Response	91
V. FACTORS THAT CONTROL THE DURABILITY OF EPOXIES	99
VI. CONCLUSIONS	104
A. Structure-Property Relations	104
B. Sorbed Moisture	105
C. Durability	105
References	106

I. INTRODUCTION

Epoxies are utilized by the aerospace industry primarily in the form of matrices for composite materials and as adhesives. The increasing use of epoxies requires a knowledge of their lifetimes in extreme service environments. When epoxy adhesives and composites are utilized in primary structural components of airframes, it is vital that the durability of such components be known during design development. A number of laboratory and field studies have indicated that the combined effects of sorbed moisture and thermal environment can cause significant changes in the mechanical response of these materials [1, 2]. However, the long-term, in-service durability of epoxy adhesives and composites in primary structural airframe components is unknown primarily because (1) long-term, in-service aging characteristics are difficult to simulate by short-term laboratory and/or field tests, and (2) the basic phenomena responsible for the changes in the mechanical response in laboratory-simulated service environments have not been identified and/or understood.

To predict the durability of epoxies in a service environment with confidence requires knowledge of (1) the chemical structure and the physical arrangement of the cross-linked network structure in the bulk, (2) the molecular nature of the flow and failure processes, (3) the structural parameters which control the flow and failure processes, (4) the effect of the flow and failure processes on the mechanical properties, and (5) how these structural

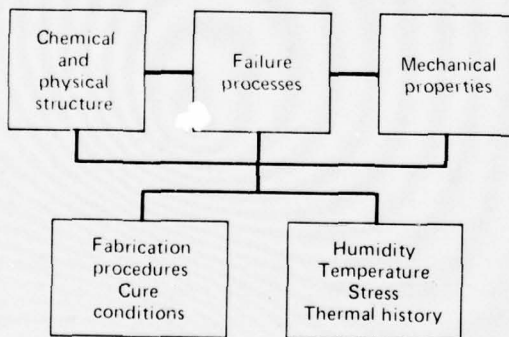


Fig. 1. The basic epoxy interrelationships necessary for durability predictions.

parameters are modified by fabrication procedures and the service environment. These basic relationships are illustrated in Fig. 1. To predict the durability of an epoxy in a specific environment requires identification of the primary failure mode, if any, and the structural phenomena controlling the initiation and growth characteristics of this mode. Identification of the primary failure mode, which may be difficult, and subsequent durability predictions require a thorough understanding of the relationships illustrated in Fig. 1.

In this report we review the basic areas necessary for meaningful durability predictions: (1) the structure of epoxies; (2) their modes of deformation and failure and the structural parameters controlling these modes; (3) the effects of sorbed moisture on the epoxy structure, properties, and modes of deformation and failure; and (4) the complex fabrication and environmental phenomena affecting the durability in service environments.

II. STRUCTURE OF EPOXIES

The mechanical response of a polymer glass depends on the amount of flow occurring during the failure process, either microscopically via crazing and/or shear banding or macroscopically via necking [2-15]. Hence it is important to identify the major structural parameters controlling the flow processes that occur during deformation and failure. The major parameters controlling the flow processes in uncross-linked polymer glasses are the free volume [16-21] and the stress-raising microvoid characteristics of the glass [19, 22, 23]. For cross-linked glasses, such as epoxies, the cross-linked network structure is an additional structural parameter affecting the flow processes.

A. Network Structure

Generally, the cure process and final network structure of epoxies have been estimated from (1) the chemistry of the system, if the curing reactions are known and assumed to go to completion; and (2) experimental techniques such as IR spectra, swelling, dynamic mechanical, thermal conductivity, and differential scanning calorimetry measurements [24-39]. However, in many epoxy systems the chemical reactions are diffusion controlled and incomplete, and a heterogeneous distribution in the cross-link density occurs. Both of these factors significantly modify the network structure. Figure 2

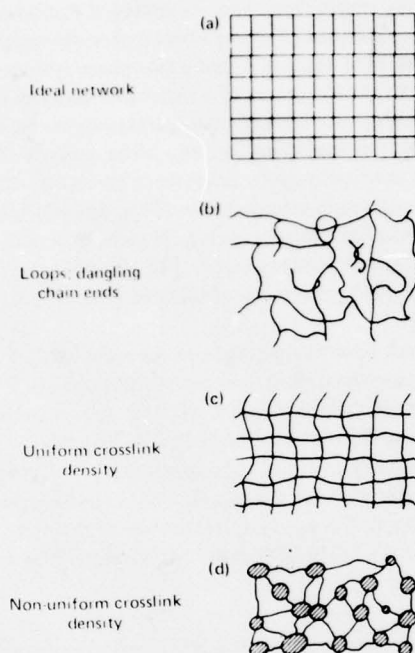


Fig. 2. Epoxy network morphologies [62].

schematically illustrates possible network topographies of epoxies [40, 41, 62]. An ideal uniform cross-linked network structure is illustrated in Fig. 2(a). In reality, however, networks contain loops and dangling chain-ends as illustrated in Fig. 2(b). Such networks can exhibit essentially a uniform cross-link density in a low-molecular-weight or cross-link density matrix [Fig. 2(c)]. Also, nonuniform cross-link density networks in which regions of high cross-link density form either a continuous (Fig. 2d) or a discontinuous phase in a low-molecular-weight or cross-link density matrix are other possible network morphologies.

High cross-link density regions from 6 to 10^4 nm in diameter have been observed in cross-linked resins [19, 26, 42-60]. The conditions for formation of a heterogeneous rather than a homogeneous system depend on polymeriza-

tion conditions (i.e., temperature, solvent, and/or chemical composition). The high cross-link density regions have been described as agglomerates of colloidal particles [47, 48] or floccules [50] in a lower-molecular-weight interstitial fluid. Solomon et al. [49] suggested that a two-phase system is produced by microgelation prior to the formation of a macrogel. Kenyon and Nielson [26] suggested that the highly cross-linked microgel regions are loosely connected during the latter stages of the curing process. More recently, Karyakina et al. [58] suggested that microgel regions originate in the initial stages of polymerization from the formation of microregions of aggregates of primary polymer chains. The high cross-link density regions have been reported to be only weakly attached to the surrounding matrix [47, 48, 50], and their size varies with cure conditions [47], proximity of surfaces [50, 57], and the presence of solvents [28, 49].

The epoxy network structure depends on the chemistry of the system, the initial epoxy:curing agent ratio, and cure conditions. In this report we consider two chemically different epoxy systems: (1) an amine (diethylene triamine, DETA)-cured difunctional bisphenol-A-diglycidyl ether epoxy (DGEBA) (Fig. 3) and (2) an amine (diaminodiphenyl sulfone, DDS)-cured tetrafunctional tetraglycidyl-4,4'-diaminodiphenyl methane epoxy (TGDDM) (Fig. 4). The DGEBA-DETA epoxy system is one of the more common epoxy systems, whereas the TGDDM-DDS system is currently the main constituent

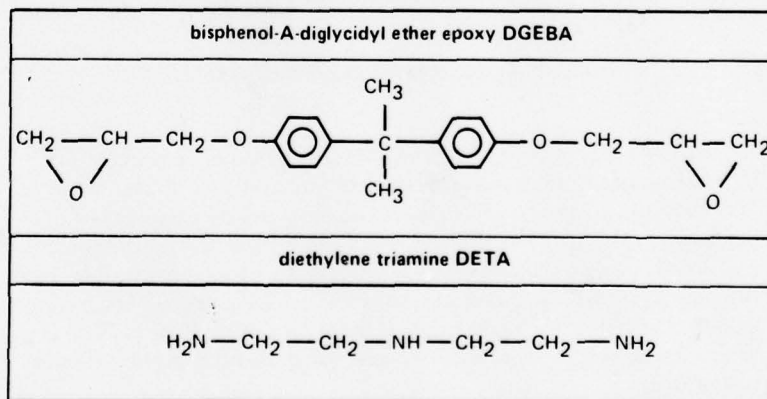


Fig. 3. The DGEBA-DETA epoxy system.

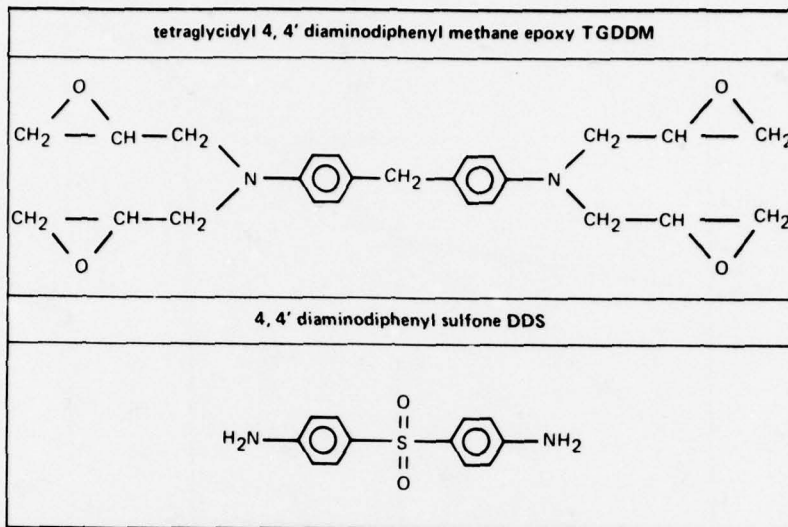


Fig. 4. The TGDDM-DDS epoxy system.

of many adhesives and composite matrices utilized by the Air Force and its contractors.

1. The DGEBA-DETA Epoxy System

The stoichiometric mixture for the DGEBA-DETA epoxy system is ~11 wt% DETA [61]. This composition was determined by assuming that all primary and secondary amine hydrogens react with epoxide groups in the absence of side reactions. However, DGEBA-DETA epoxies, despite being prepared from stoichiometric mixtures of epoxy and amine, are not highly cross-linked glasses because they exhibit 15 to 20% extension to break 25°C below their T_g 's. Also, considerable molecular flow occurs during the deformation and failure of these glasses.

Furthermore, the mechanical properties of these epoxies exhibit a free-volume dependence as a function of thermal history which indicates that these glasses consist of regions of lightly or noncross-linked material. A typical volume-temperature plot for a polymer is shown in Fig. 5. Changes in free volume, or local order, in the glassy state can occur as a result of extension to

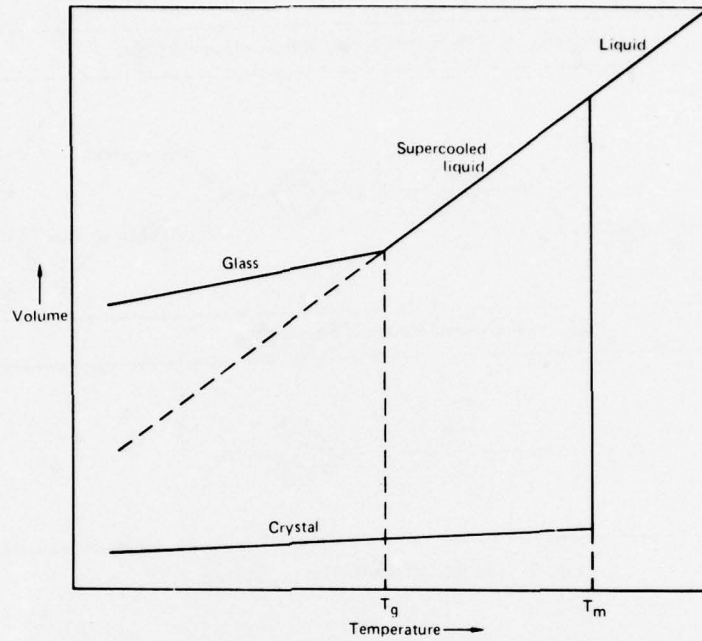


Fig. 5. A schematic volume-temperature plot for a polymer.

temperatures below T_g of packing changes associated with the liquid state. The liquid-volume temperature plot extrapolated to below T_g in Fig. 5 represents the lower free-volume, equilibrium state of the glass. The time necessary to achieve the equilibrium state at a given temperature below T_g depends on the glassy-state mobility. Below a certain temperature, the glassy-state mobility is too small to allow any changes in free volume. A decrease in free volume that occurs in the glassy state results in inhibition of the flow processes that take place during deformation and a more brittle mechanical response. Rapidly cooling from above T_g , however, produces a glass with a larger free volume.

Table 1 shows the effect of thermal history on the room-temperature tensile yield stress and ultimate elongation of a DGEBA-DETA (13 wt% DETA) epoxy glass ($T_g \sim 107^\circ\text{C}$). Annealing 5°C below T_g (Specimens 1 to 5 in Table 1) causes an increase in the macroscopic yield stress and a decrease in the extension to break as the equilibrium state of the glass at this temperature

TABLE I
Effect of Thermal History on the Room-Temperature Tensile Mechanical Properties (Strain Rate $\sim 10^{-2}$ /min) of DETA (13 wt%)-Cured DGEBA Epoxy

Thermal history	Yield stress, kPa $\times 10^4$	Ultimate elongation, %
1. Cured 24 hr, 23°C; 24 hr, 150°C; cooled 2°C/min to room temperature	7.9 \pm 0.1	14 \pm 1
2. 102°C, 1 day	8.2 \pm 0.1	14 \pm 1
3. 102°C, 3 days	8.2 \pm 0.1	13 \pm 1
4. 102°C, 6 days	8.2 \pm 0.1	12 \pm 1
5. 102°C, 17 days	8.2 \pm 0.1	11 \pm 1
6. 162°C, 10 min; quenched in ice water	7.3 \pm 0.1	15 \pm 1
7. 102°C, 1 day	8.3 \pm 0.1	13 \pm 1
8. 162°C, 10 min; quenched in ice water	7.3 \pm 0.1	17 \pm 1

is approached. Prior to testing, Samples 6, 7, and 8 in Table 1 were exposed to the same thermal history as preceding samples in this 6 to 8 series. Quenching from 55°C above T_g (Specimen 6 in Table 1) produces a low macroscopic yield stress because of the high free-volume frozen into the glass. Subsequent annealing of the quenched specimen in the glassy state 5°C below T_g (102°C) (Specimen 7 in Table 1) followed by a further quench from 55°C above T_g (Specimen 8 in Table 1) produces essentially reversible changes in the macroscopic yield stress. These modifications of the macroscopic yield stress and ultimate elongation with thermal history indicate that the flow processes in DGEBA-DETA epoxies are controlled by the free volume of the regions of lightly or noncross-linked material.

Figure 6 illustrates the effect of annealing [5°C below T_g (125°C)] on the temperature and strain-rate dependence of the macroscopic yield stress of DGEBA-DETA (11 wt% DETA) epoxy relative to the unannealed epoxy. The general increase in the yield stress at all temperatures and strain rates on annealing below T_g further illustrates the free-volume dependence of these epoxies.

The DGEBA-DETA epoxies did not significantly swell (maximum swell ratio achieved $\approx 1.5\%$) after 15 days exposure to the favorable swelling agents reported for similar materials [25]. The literature also suggests that swelling is not a valid technique to determine cross-link density of resins prepared from

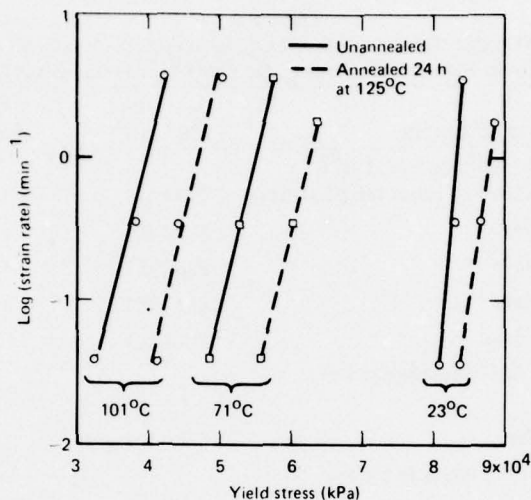


Fig. 6. Log (strain rate) versus yield stress of a DGEBA-DETA (11 wt% DETA) epoxy as a function of temperature and thermal history.

approximately stoichiometric quantities of epoxy and amine [26, 28, 62]. The lack of swelling does suggest, however, that these glasses are highly cross-linked.

The lack of swelling, the high-temperature ductility, and the free-volume dependence of the mechanical properties of DGEBA-DETA epoxies can be understood if these glasses possess a heterogeneous cross-link density distribution. We suggest that these glasses consist of regions of high cross-link density interconnected by free-volume dependent, low cross-linked or noncross-linked material. The latter control the flow properties of these epoxies.

This morphological model is consistent with bright-field transmission electron microscope observations. The bright-field transmission electron micrographs in Fig. 7 show the network structure of interconnected 6 to 9 nm diameter particles observed in a strained DGEBA-DETA epoxy film. By straining the epoxy films directly in the electron microscope, we observed that the 6 to 9 nm diameter particles remain intact and flow past one another during the flow processes. The basic 6 to 9 nm diameter particles shown in Fig. 7 are in the size range associated with molecular domains. For crystallizable polymers, Wunderlich and Mehta [63] and Aharoni [64] have presented

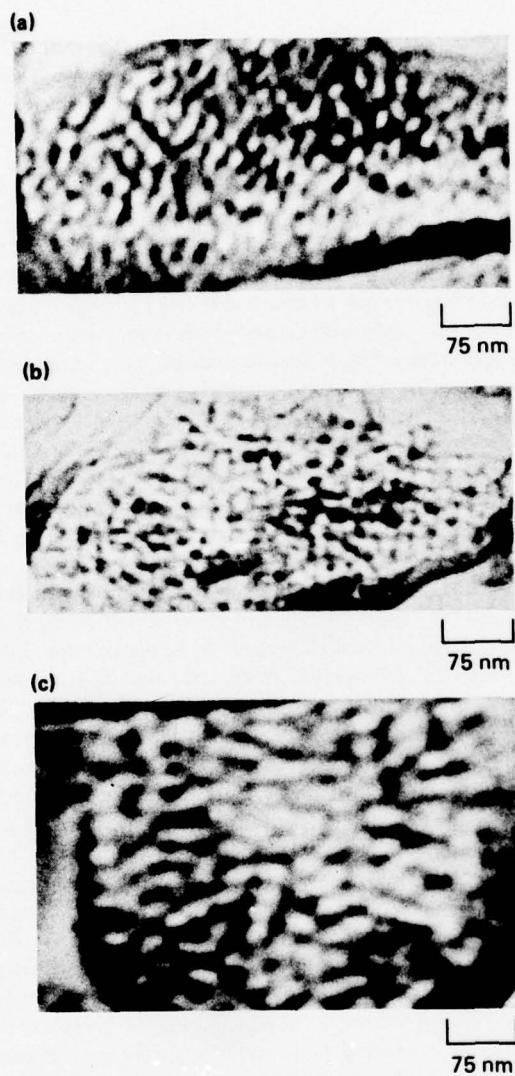


Fig. 7. Bright-field transmission electron micrographs of network structure in deformed DGEBA-DETA (13 wt% DETA) epoxies.

theories in which the initial step of crystallization from the melt and solution occurs by formation of ordered molecular domains. Ordered nodules the size of molecular domains (5 to 6 nm in diameter) have been observed in thin films and on the surfaces of polycarbonate [21, 65]. We suggest that the 6 to 9 nm diameter particles are molecular domains which are intramolecularly cross-linked and which form during the initial stages of polymerization. Chomppf [66] has recently noted that configurational restrictions favor excessive intramolecular cross-linking. Intramolecular cross-linking is also favored by the inability of many unreacted epoxy and amine species attached to a growing domain to diffuse to reactive species attached to neighboring domains. These species therefore can react only with active species in their immediate location. The intramolecularly cross-linked molecular domains are interconnected by either low or high cross-link density regions during the latter stages of the cure to form the final network structure. This hypothesis assumes that intramolecular cross-linking occurs in the early polymerization stages. For solution-phase condensation cross-linking, Flory [67] considered intramolecular cross-linking insignificant prior to gelation. Other workers, however, caution that in many thermoset systems, intramolecular cross-linking could occur to a significant extent prior to gelation [68-70]. The ability of the suggested 6 to 9 nm diameter molecular domains to remain intact during the flow processes does, however, suggest that intramolecular cross-linking occurred within the domains.

The interconnection of molecular domains by regions of either low or high cross-link density allows two types of network structure: (1) regions of high cross-link density embedded in a low or noncross-linked matrix or (2) noncross-linked or low cross-link density regions embedded in a high cross-link density matrix. From straining films in the electron microscope, we have observed both types of network morphology, with the second type more prevalent. An example of the first type of morphology is illustrated in Fig. 8(a) where aggregates of 6 to 9 particles are embedded in a deformable, low cross-link density matrix. Deformation of this type of network involves preferential deformation of the regions of low cross-link density without causing cleavage of the high cross-link regions. For the second type of network, the deformation process is more complex. Local affine deformation requires network cleavage and flow to occur simultaneously in the high cross-link density regions as flow with little network cleavage occurs in the neighboring low cross-link density regions. This deformation process results in progressively larger regions that are poorly cross-linked. Such a deformed network structure is illustrated in the bright-field transmission electron micrograph of a strained DGEBA-DETA epoxy film in Fig. 8(b). The dark network structure consists of 6 to 9 nm diameter interconnected domains separated by low cross-linked and/or thinned

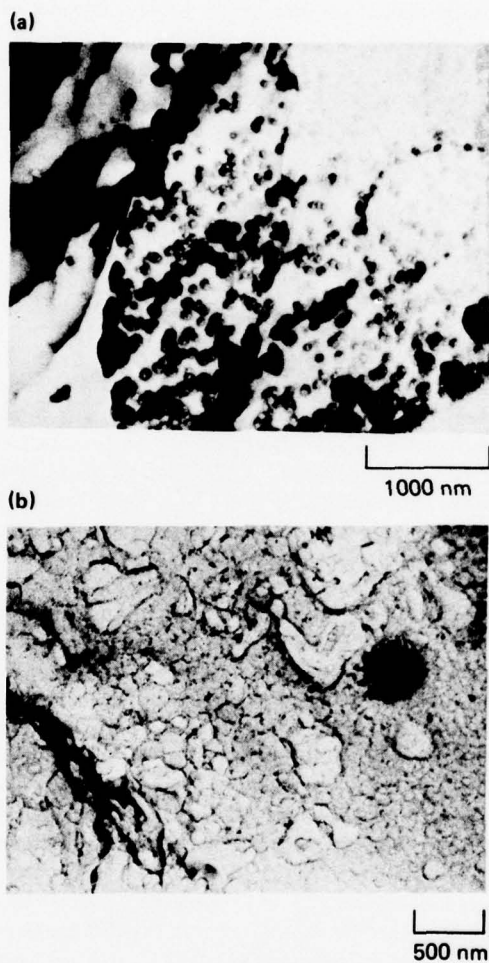


Fig. 8. Bright-field transmission electron micrographs of strained DGEBA-DETA epoxies illustrating (a) aggregates of 6 to 9 nm particles in a low cross-link density matrix and (b) a network in which high cross-link density regions form the continuous phase.

regions of the network which appear light in the micrograph. The network is tighter in the bottom right of the micrograph than in the upper portion which suggests that more deformation has occurred there.

The presence of regions of low cross-link density in the DGEBA-DETA epoxies suggests that many reactive groups remain unreacted within these glasses because of diffusion and steric restrictions imposed during polymerization and network formation.

Studies have not yet been performed on the effect of different cure conditions on the network structure. The room-temperature mechanical properties of DGEBA-DETA epoxies, however, do not vary as a function of postcure temperature when postcured for 24 hr in vacuum at 80 to 190°C [71]. Despite the presence of regions of low cross-link density containing unreacted groups, diffusion and steric restrictions inhibit additional cross-linking in this temperature range. However, exposure to temperatures above 180°C for 24 hr, where diffusional and steric restrictions may be partially overcome, causes the epoxies to embrittle because of the onset of complex oxidative cross-linking reactions. Differential IR analysis of an epoxy postcured above 180°C relative to a standard epoxy postcured at 150°C reveals an additional broad sorption band in the 700-1800 cm^{-1} region [71]. The intensity of this sorption increased with exposure time and increasing temperature, from 180 to 300°C, and increased more rapidly in air than in vacuum. A strong IR sorption at 1725 cm^{-1} appears during the initial stages of the degradation process, which indicates the formation of carbonyl groups. Such groups could result from oxidation of unreacted epoxide rings to form α -hydroxy aldehyde and carboxylic acid [72]. Degradation causes the epoxies to change from colorless to brown to cherry red with an accompanying increase in free-radical formation as monitored by electron paramagnetic resonance spectrometry [71]. Jain [73] first detected free-radical formation during thermooxidative degradation of epoxies. Ovenall [74], in more detailed studies of epoxies, concluded that at 180°C in air the formation and decay of radicals occur by oxidative scission and molecular diffusion interaction between radicals, respectively. Later studies have suggested that resonance-stabilized free radicals occur in the thermal degradation of epoxies [75, 76]. These data indicate that complex oxidative degradation reactions start to occur in DGEBA epoxies near 180°C and cause detectable embrittlement above $\sim 200^\circ\text{C}$. (Sorbed oxygen present in the epoxies allows such reactions to occur even when postcuring under vacuum.)

2. The TGDDM-DDS Epoxy System

Table 2 illustrates the percentage by weight of DDS required for (1) all primary and secondary amines in the DDS to react and (2) only primary amines

TABLE 2
Theoretical Reaction Mixtures for TGDDM-DDS Epoxy System

	100% TGDDM epoxide groups react	50% TGDDM epoxide groups react
100% DDS primary and secondary amines react	37 wt% DDS	23 wt% DDS
100% DDS primary amines react	54 wt% DDS	37 wt% DDS

to react with either 50 or 100% of the epoxide groups in the tetrafunctional TGDDM molecules.

Examination of molecular models indicates that considerable steric restrictions are present in the vicinity of the epoxide groups. Hence, because of this interference, it is unlikely that many secondary amines react in this system. Our studies indicate that steric and diffusional restrictions also limit the number of primary amines that react in the TGDDM-DDS system. Our cure conditions were 1 hr at 150°C and 5 hr at 177°C. The DDS is crystalline with a melting point of 162°C.

We have monitored the tensile mechanical properties of the TGDDM-DDS epoxy system as a function of composition (10 to 35 wt% DDS) and test temperature (23 to 250°C). Figure 9 plots tensile strength, ultimate elongation, and Young's modulus from 23 to 250°C for a TGDDM-DDS (35 wt% DDS) epoxy. The gradual decrease in tensile strength and modulus and the increase in ultimate elongation from 200 to 250°C suggests that a broad glass transition exists in this temperature range. Ultimate extension of $\geq 15\%$ near T_g for epoxies with 15 to 35 wt% DDS suggests these glasses are not highly cross-linked.

A plot of T_g versus initial DDS concentration, shown in Fig. 10, confirms that these epoxies are not highly cross-linked. [The temperatures representative of these broad T_g 's were taken as those temperatures at which the room-temperature modulus (E_{RT}) decreased by half (i.e., $E_{RT}/2$)]. From 10 to 25 wt% DDS, the T_g rises with increasing DDS concentration because of corresponding increases in molecular weight and/or cross-link density. The T_g exhibits a maximum of $\sim 250^\circ\text{C}$ at ~ 30 wt% DDS and subsequently decreases for higher DDS concentrations. For epoxies prepared from >25 wt% DDS, steric and diffusional restrictions evidently inhibit additional epoxy-amine reactions. Above ~ 30 wt% DDS concentrations, unreacted DDS molecules

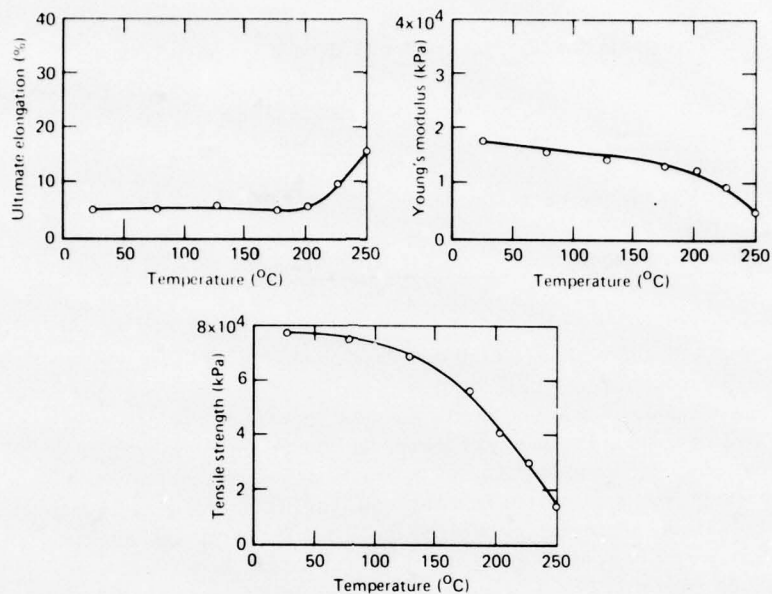


Fig. 9. Tensile strength, ultimate elongation, and Young's modulus versus temperature for TGDDM-DDS (35 wt% DDS) epoxy that was deformed at a strain rate of $\sim 10^{-2}$ /min.

plasticize the epoxy system and decrease the T_g . However, 37 wt% DDS is required to consume half the TGDDM epoxide groups when only epoxide-primary amine reactions occur (Table 2). Hence the maximum in T_g at 30 wt% DDS suggests that less than half the TGDDM epoxide groups have reacted when 100% of the DDS is consumed. These observations illustrate that the 5 hr, 177°C cured TGDDM-DDS epoxy systems are not highly cross-linked because of steric and diffusional restrictions during cure. After gelation, unreacted groups have difficulty approaching one another because of mobility restrictions.

After cure, aggregates of unreacted DDS molecules have been detected in TGDDM-DDS (≤ 25 wt% DDS) epoxies by both electron diffraction and x-ray emission spectroscopy studies. Electron diffraction patterns were obtained from thin films prepared from ≥ 25 wt% DDS that were similar to those ob-

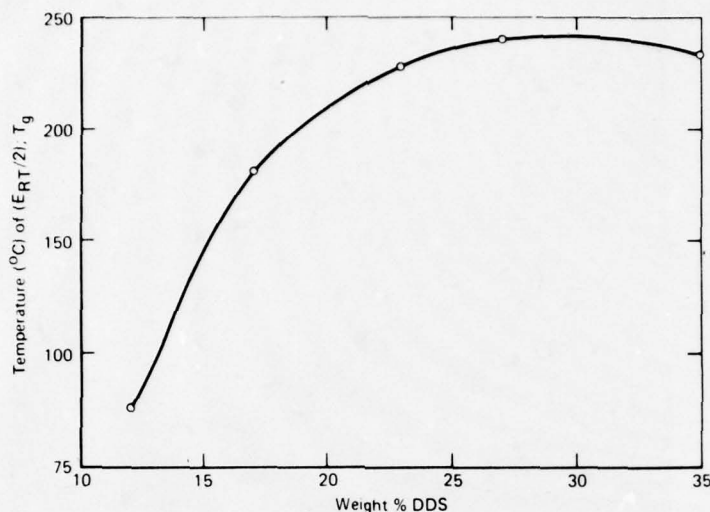


Fig. 10. A measure of the T_g ($E_{RT}/2$) versus initial wt% of DDS in TGDDM-DDS epoxies.

tained from the unreacted DDS crystals. The aggregates of unreacted DDS molecules crystallize after cooling the epoxy from its cure temperature. In addition, x-ray emission spectroscopy of fracture surfaces has detected regions of high sulfur content which are probably clusters of unreacted DDS molecules. In this technique a fracture surface is bombarded with an electron beam, and the surfaces are scanned for emitted x-rays characteristic of sulfur. Figure 11 is an x-ray map of the sulfur distribution (indicated by the white dots) superimposed on the secondary scanning electron micrograph of the fracture surface. The large concentration of sulfur in the fracture-initiation region probably results from a cluster of unreacted DDS molecules.

Bright field transmission electron microscopy studies of the network structure of strained TGDDM-DDS epoxy films have revealed microscopic heterogeneities only in the brittle, low-molecular-weight systems prepared from 10 to 15 wt% DDS. In Fig. 12(a) a strained TGDDM-DDS (10 wt% DDS) epoxy is shown to break into 2.5 to 13 nm diameter particles. At higher deformations the network breaks into ~ 2.5 nm diameter particles, as shown in Fig. 12(b). These basic 2.5 nm diameter particles are of a similar size as the TGDDM molecule.



Fig. 11. X-ray emission scanning spectroscopy map of sulfur distribution in the fracture surface of TGDDM-DDS (27 wt% DDS) epoxy which was fractured at 250°C.

Evidence that the cross-linked network topography of TGDDM-DDS epoxies can be heterogeneous is suggested from fracture topography observations. Figure 13 shows scanning electron micrographs of the fracture topography initiation region of a TGDDM-DDS (23 wt% DDS) epoxy. Undeformed particles, 1 to 5 μm in size, are embedded in the deformed, surrounding material. These undeformed particles are possible regions of high cross-linked density which are embedded in a lower cross-link density, deformable matrix.

B. Microvoid Characteristics

Little attention has been given to the microvoid characteristics in thermosets, such as epoxies, and how such microvoids can be produced during fabrication.

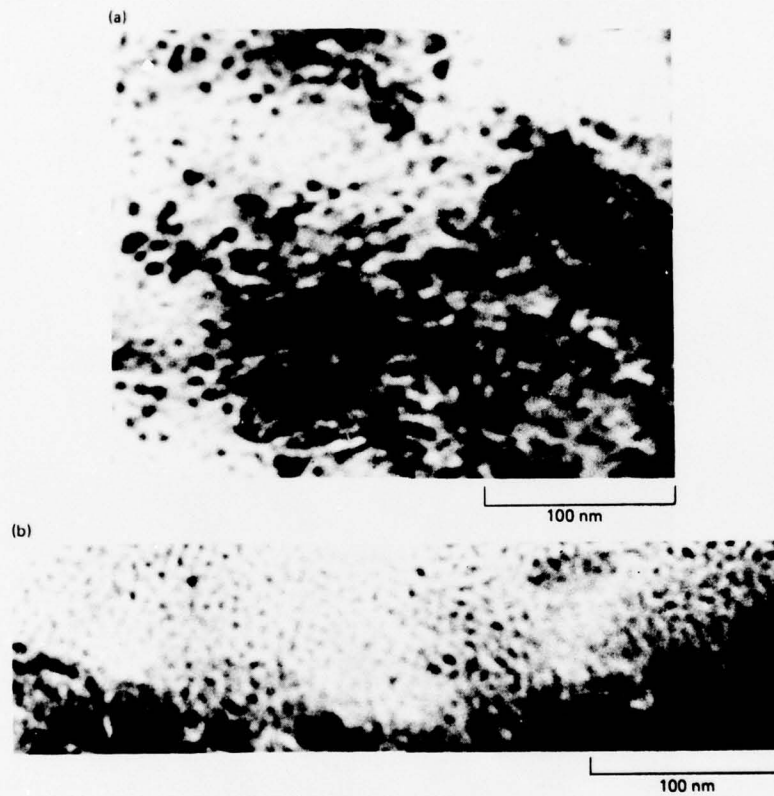


Fig. 12. Bright-field transmission electron micrographs of structure in deformed TGDDM-DDS (10 wt% DDS) epoxy.

These microvoids can have a deleterious effect on the mechanical properties by acting as stress concentrators and also on the durability by serving as a sink for the accumulation of sorbed moisture. Microvoids can result in epoxies from (1) trapped air, which can be easily avoided if the appropriate precautions are taken during fabrication; and (2) low-molecular-weight material trapped in the glass which is subsequently eliminated during postcure. This low-molecular-weight material results from either inhomogeneous mixing of epoxy monomer and curing agent and/or the inability of the constituents to react and resultant aggregation of these constituents.

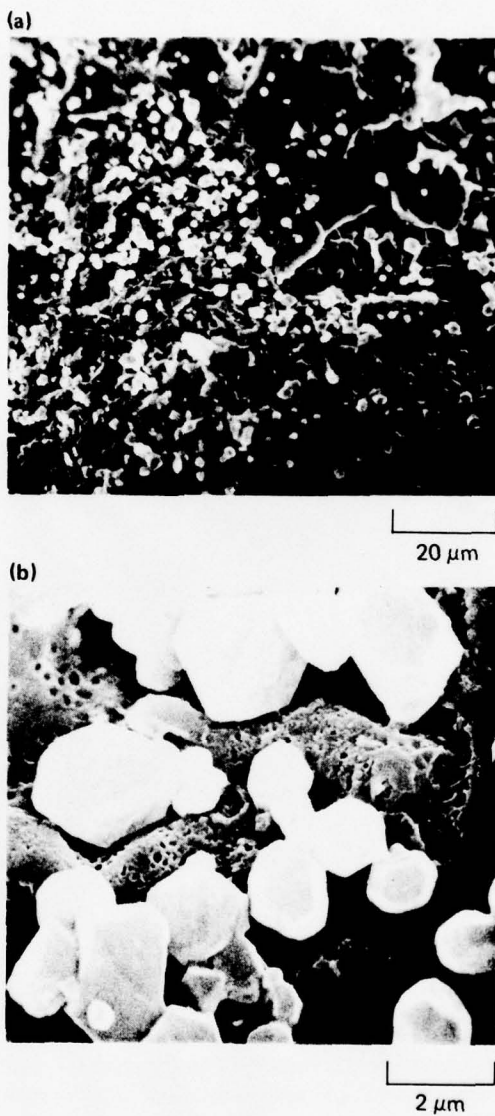


Fig. 13. Scanning electron micrographs illustrating possible undeformed regions of high cross-link density embedded in a lower cross-linked density, deformable matrix in the fracture topography initiation region of a TGDDM-DDS (23 wt% DDS) epoxy, which was fractured in tension at room temperature at a strain rate of $\sim 10^{-2}$ /min.



Fig. 14. Optical micrograph of pure DGEBA crystals suspended in an unreacted commercial epoxide.

1. The DGEBA-DETA Epoxy System

Pure DGEBA epoxy monomer crystallizes at room temperature (melting point 41.5°C), resulting in crystals that are suspended in the higher-molecular-weight liquid. In commercial DGEBA epoxides, such as Epon 828, the crystals are $\sim 15\ \mu\text{m}$ in size and predominantly in the form of square platelets, as illustrated in Fig. 14. We have demonstrated for certain cure conditions that the presence of these crystallites can result in microvoids in the postcured resin [71]. Partly curing the partially crystalline DGEBA epoxide monomer with DETA at room temperature leaves the crystals embedded in the glass. Postcuring $\geq 80^{\circ}\text{C}$ under vacuum produces $\sim 10\ \mu\text{m}$ microvoids and associated stresses in the epoxy as a result of melting the crystals and subsequent volatilization of the resultant

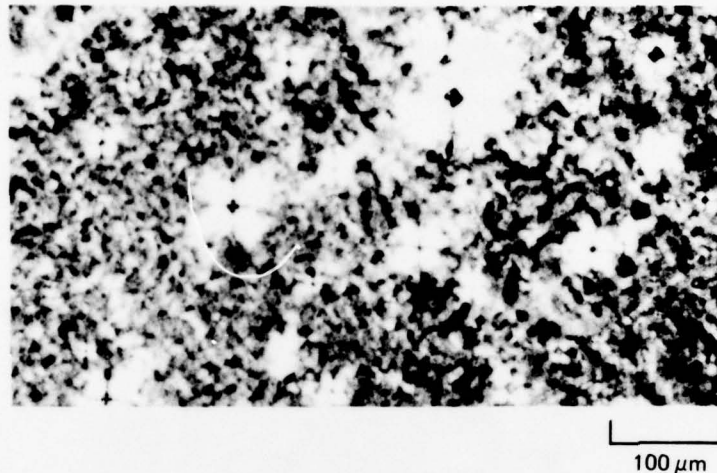


Fig. 15. Light-scattering patterns, under polarized light, produced by microvoids and surrounding stress fields in an polyamide-cured DGEBA epoxy.

liquid. Figure 15 illustrates the light-scattering patterns, under polarized light, associated with the microvoids and surrounding stress field in an amine-cured DGEBA system that was postcured at 95°C for 24 hr.

Such microvoid production can easily be avoided for DGEBA-based epoxy systems by either initially melting the crystals prior to curing or initially curing above the monomer crystalline melting point. These observations, however, do demonstrate that clusters of unreacted molecules present in an epoxy system during cure can, for certain cure conditions, result in microvoids in the finally cured glass.

2. The TGDDM-DDS Epoxy System

To obtain a TGDDM-DDS epoxy system with a high T_g , which is advantageous to limit the deleterious effects of sorbed moisture on this epoxy, requires ~30 wt% DDS in the initial TGDDM-DDS mixture (see Fig. 10). However, at these DDS concentrations, aggregates of unreacted DDS molecules can be present in the epoxy after the system forms a glass at the cure temperature. The elimination of these aggregates during subsequent cure could result in microvoids in the glass.

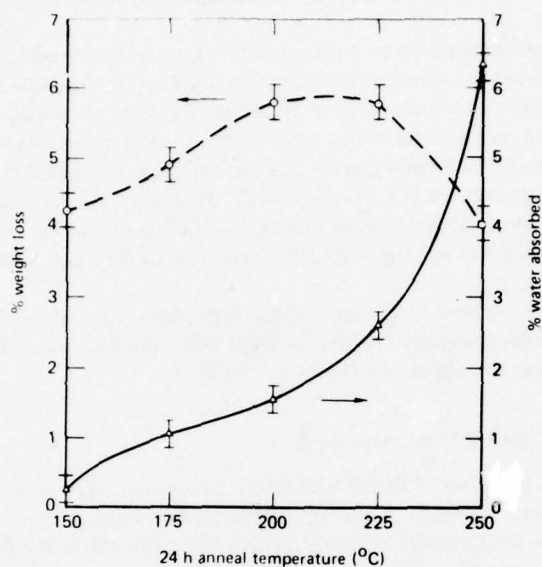


Fig. 16. Plots of weight loss and subsequent water sorption versus anneal temperature for TGDDM-DDS (27 wt% DDS) epoxy.

Microvoids are produced in the TGDDM-DDS system by elimination of unreacted, low-molecular-weight material. Figure 16 shows the progressive weight loss with increasing anneal temperatures from 150 to 250°C for a TGDDM-DDS (27 wt% DDS) epoxy originally cured at 177°C for 5 hr. In this figure the amount of water subsequently sorbed by the epoxy at 120°C in an autoclave for 3 hr is plotted versus anneal temperature. The increase in water sorption with increasing anneal temperature from 150 to 200°C is associated with microvoids produced by volatilization of unreacted low-molecular-weight material. The water sorption exhibits a maximum in the 200 to 225°C range and decreases as the anneal temperature approaches T_g at ~250°C because the microvoids partially collapse.

Hence a high T_g TGDDM-DDS epoxy system may contain microvoids which result from the elimination of aggregates of unreacted DDS molecules trapped in the glass during the early stages of cure.

III. DEFORMATION AND FAILURE MODES OF EPOXIES

The relation between the network structure, microvoid characteristics, and failure processes of epoxies has received little attention. Localized plastic flow has been reported to occur during the failure processes of epoxies [53, 55, 71, 77-84], and, in a number of cases, the fracture energies have been reported to be a factor of 2 to 3 times greater than the expected theoretical estimate for purely brittle fracture [77, 78, 82, 84-91]. However, no systematic studies have been made to elucidate the microscopic flow processes that occur during the deformation of epoxies and the relation of such flow processes to the network structure.

Recently, we have conducted studies on the failure processes of amine-cured DGEBA epoxy systems and TGDDM-DDS epoxy systems. The major findings from these studies will now be reviewed.

A. The DGEBA-DETA Epoxy System

The failure processes of DGEBA-DETA epoxies were monitored by optical and electron microscopy of thin films deformed on a metal substrate and of the fracture topographies of epoxy specimens fractured in tension as a function of temperature and strain rate. In addition, epoxy films were strained directly in the electron microscope, and the failure processes were monitored by bright-field microscopy. These studies indicate that epoxies fail by a crazing process [83, 92].

The structure of a craze is illustrated in Fig. 17. Crazes only form in tension, and craze initiation involves cavitation at a stress concentration defect or inhomogeneity in the glass. Sternstein and Ongchin [93] have suggested

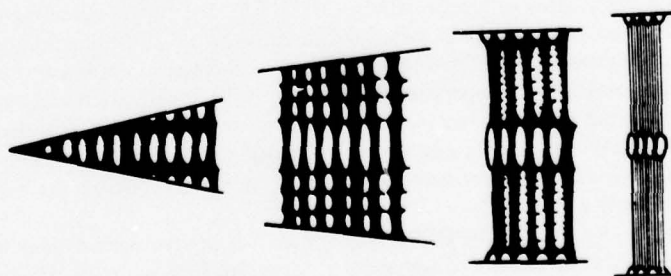


Fig. 17. The structure of a craze [99].

that cavitation results from both the tensile dilatational component of the applied stress field and a normal yielding factor. This cavitation results in a highly porous structure at the craze tip. As the craze develops, microvoids formed by the cavitation craze-initiation process coalesce and enlarge, and polymeric material flows and orients in the direction of the applied tensile stress. This flow and orientation results, as illustrated in Fig. 17, in fine, highly oriented fibrils within the well-developed craze. A crack will propagate through the craze when a cavity formed by enlargement and coalescence of microvoids attains a critical size and begins to propagate perpendicularly to the tensile stress through the craze. The amount of energy expended in the form of viscous, molecular flow during the craze process is considerable and enhances the toughness of the material. Detailed discussions of the crazing and fracture processes of polymer glasses are given by Rabinowitz and Beardmore [12] and Kambour [94].

Crazes were observed in one-stage, carbon-platinum surface replicas of DGEBA-DETA epoxy films that were adhered to a brass substrate and strained $\sim 10\%$ in tension. The replicas in Fig. 18 illustrate the craze structure. The absence of any carbon-platinum particles within regions of the craze fibrils indicates that a thin epoxy layer adhered to the replica. At the craze tip, ~ 10 nm diameter voids are produced by the tensile dilatational stress fields (Fig. 18a). These voids coalesce to form larger voids $\lesssim 100$ nm in diameter separated by 20 to 100 nm diameter fibrils. Further from the craze tip, the fibrils fracture as their length approaches ~ 100 nm. The latter phenomenon may be a consequence of the poor structural integrity of the replica.

Crazes were also found to propagate in ~ 1 μm thick DGEBA-DETA epoxy films that were strained directly in the electron microscope. An overall view of a craze consisting of coarse 100 to 1000 nm wide fibrils is shown in the bright-field transmission electron micrograph in Fig. 19(a). The region near the craze tip is shown in more detail in Fig. 19(b). The structure of the coarse ~ 1000 nm wide craze fibril shown in Fig. 19(a) is illustrated in more detail in Fig. 20. These micrographs reveal that the epoxy deforms inhomogeneously within the craze fibril (Fig. 20a) and breaks up into 6 to 9 nm diameter particles. The network structure of 6 to 9 nm diameter particles within the region of the craze fibril is illustrated in Fig. 20(b).

The fracture topographies of DGEBA-DETA epoxies fractured as a function of temperature and strain-rate were studied by optical and scanning electron microscopy. The optical micrograph shown in Fig. 21(a) illustrates the three characteristic topographic regions observed in these epoxies: (1) a coarse initiation region (dark area in the left of the micrograph); (2) a slow crack-growth, smooth, mirror-like region; and (3) a fast crack-growth, rough, parab-

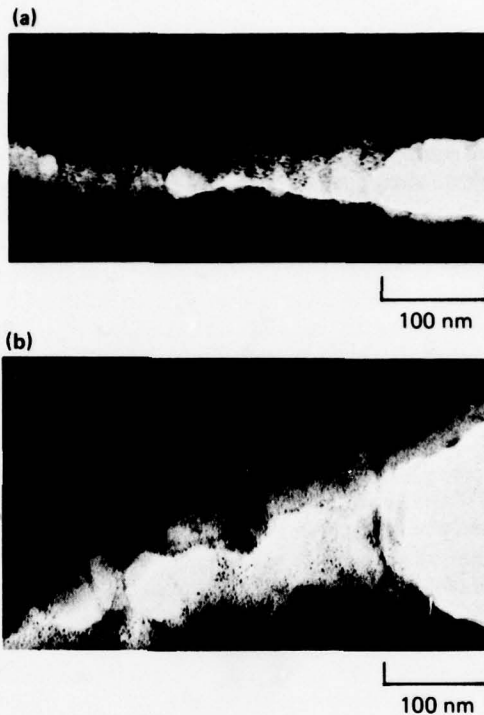


Fig. 18. Carbon-platinum surface replicas of craze structure in DGEBA-DETA (11 wt% DETA) epoxy films that were strained on a metal substrate.

ola region. The topography varies with temperature and strain rate, with the mirror-like region covering a larger portion of the fracture surface with increasing temperature and/or decreasing strain rate, as illustrated in Fig. 22.

The coarse initiation region often is found within a cavity as indicated by a cusp in the fracture topography which separates this region from the surrounding smooth, mirror-like region (Fig. 21b). The coarse structure can (1) cover a relatively small region in the center of the initiation cavity, (2) cover the entire cavity, or (3) irregularly cover parts of the cavity.

The structure of the coarse topography in the initiation region exhibited little consistency between samples or with varying temperature and strain rate. A typical range of topographies consisted of the mica-like structure illustrated

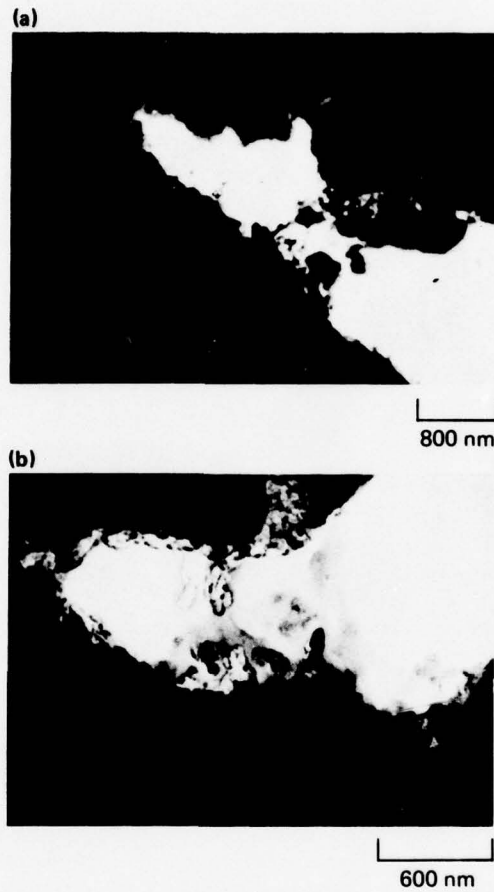


Fig. 19. Bright-field transmission electron micrographs of (a) overall craze and (b) craze tip in DGEBA-DETA (13 wt% DETA) epoxy.

in Fig. 21(c), a nodular structure, and a collapsed fibrillar topography. At temperatures nearer the T_g (i.e., at $T_g - 25^\circ\text{C}$), the fracture-initiation region in the DGEBA-DETA epoxies is either nonexistent and/or much smoother than at lower fracture temperatures.

The fracture topography initiation region characteristics can be explained

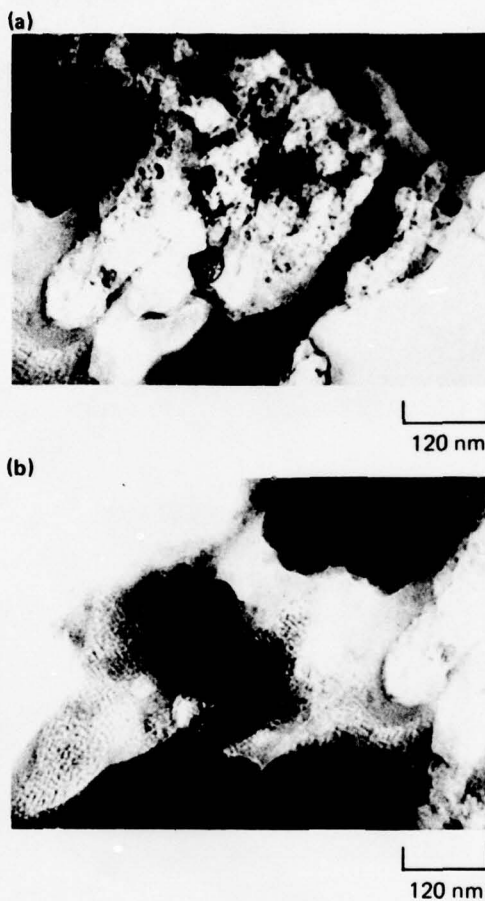


Fig. 20. Bright-field transmission electron micrographs of craze fibril structure in DGEBA-DETA (13 wt% DETA) epoxy.

in terms of a crazing failure process. Murray and Hull [95] have reported that void growth and coalescence within a craze produce a planar cavity whose thickness is that of the craze. A mica-like structure in the slow crack-growth fracture topography of polymer glasses is generally associated with crack propagation through preexisting craze material [96]. Murray and Hull [95] and



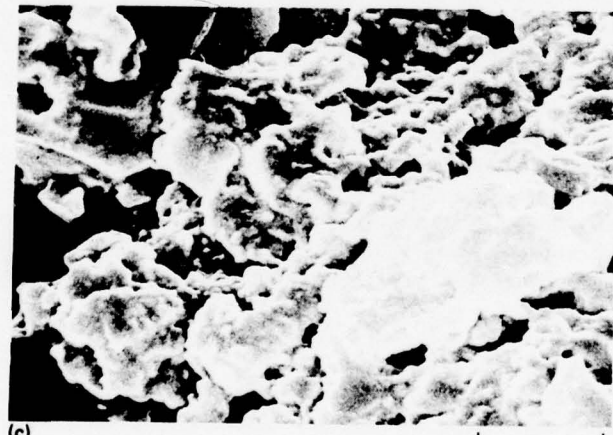
(a)

800 μm



(b)

50 μm



(c)

6.6 μm

Cornes and Haward [97] have observed irregularly furrowed or ruffled surfaces within initiation cavities in polystyrene and poly(vinyl chloride), respectively. Furthermore, there is evidence from studies on polystyrene that the initial stages of void growth and coalescence within a craze involve fracture through the center of the craze [98, 99]. In addition, the coarseness of the craze fibrils has been reported to decrease with increasing craze width and thickness [99]. These facts suggest that the coarse initiation region in epoxies results from void growth and coalescence through the center of a simultaneously growing, poorly developed craze which consists of coarse fibrils. The diameter of the broken fibrils depends on the relative rates of craze and void growth. Nodular particles and fibrillar structures that lie parallel to the fracture surface are associated with fractured craze fibrils. Doyle [100, 101] and Hoare and Hull [102] have reported broken fibrils that lie parallel to the fracture surface in polystyrene and have suggested that these fibrils are swept down onto the fracture surface as the crack passes through the craze. We cannot preclude, however, that the mica-like structure such as that observed in Fig. 21(c) results from the coalescence of a bundle of parallel microcrazes situated in slightly different planes rather than directly from the fracture of poorly formed, coarse craze fibrils. Skibo et al. [103] suggested that the mica-like structure which they observed in the noninitiation region of the fatigue-fracture topography of polystyrene is a result of the intersection of the crack plane with craze bundles. The more nodular-like topographies are similar to those observed in the fracture topographies of certain multiphase metals [104] and polyvinyl chloride [105-107]. In polyvinyl chloride, this structure has been associated with particulates in the polymer resulting from imperfect melting of resin particles [105-107]. Hence, we also cannot preclude that any heterogeneity in the epoxy structure could be partially responsible for the observed topographies.

The variation in the fracture topography initiation region which did not exhibit consistent trends with strain rate and temperature, except for the disappearance or smoothening of the coarse topographies in those specimens fractured near T_g , is a result of a number of factors: (1) the relative rates of crack and craze propagation, (2) the craze structure immediately prior to crack propagation through the craze, (3) the modification of the craze structure by crack propagation, (4) the collapsing and relaxation of the craze rem-

Fig. 21. Fracture topography of amine-cured DGEBA epoxies: (a) optical micrograph of overall topography, (b) optical micrograph of slow crack-growth region, and (c) scanning electron micrograph of initiation region.

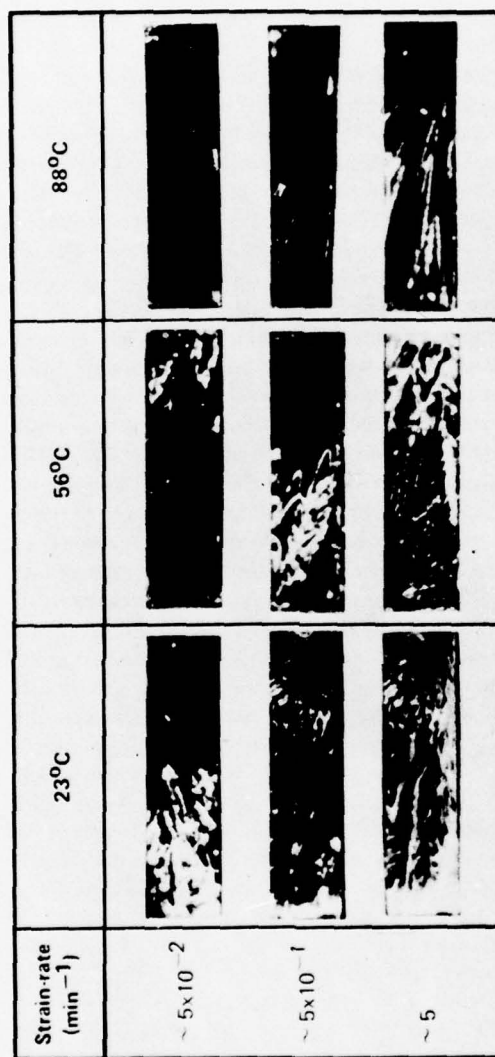


Fig. 22. Optical micrographs of overall fracture surfaces of DGEBA-DETA (9 wt% DETA) epoxies as a function of temperature and strain rate.

nants after crack propagation, and (5) the variation in the local stress fields in the vicinity of the growing craze or crack which depend on the microvoid characteristics of the epoxy.

The smooth mirror-like region of the fracture topography of DGEBA-DETA epoxies whose area increases with increasing temperature and decreasing strain rate (Fig. 22) can be attributed to a crazing process. For other polymers, this region has been associated with slow crack-growth, and its size varies with temperature, molecular weight, and strain rate [108-111]. In studies on polyester resins, Owen and Rose [112] report that the mirror-like area increases with resin flexibility. A number of workers have associated this smooth fracture topography region with slow crack-propagation through the median of the craze with subsequent relaxation of craze remnants [95, 96, 101, 102, 113, 114]. El-Hakeem et al. [114] have directly observed the masking of the microfeatures of this fracture topography region by the subsequent relaxation processes. The smoothness of the fracture topography region surrounding the coarse initiation region in DGEBA-DETA epoxies results from crack propagation either through the center or along the craze-matrix boundary interface of a thick, well-developed craze consisting of fine fibrils. The presence of fine fibrils would produce a smoother fracture topography than in the coarse initiation region, irrespective of any subsequent relaxation of craze remnants. One-stage, carbon-platinum surface replicas of the mirror-like region reveal areas consisting of 15 to 30 nm diameter particles. This granular appearance of the replica could be the result of fractured fine fibrils aligned normal to the surface. However, we cannot preclude that such structures are regions of high cross-link density. The extent of the mirror-like region is a measure of the area in which crack propagation occurs through a preformed craze [95]. For a fracture surface completely covered by the mirror-like region, crazes have grown completely across the specimen prior to any significant crack propagation [102]. Hoare and Hull [102] have suggested that this area depends on (1) the ease of cavitation and crack propagation within the craze, (2) the rate of craze nucleation and growth, and (3) the concentration of crazes. The decrease in the crazing stress with increasing temperature and/or decreasing strain rate favors craze growth which will result in a larger mirror-like region.

River markings which radiate from the fracture-initiation site are also observed in the mirror-like region, as illustrated in Fig. 21(b). These markings, which vary inconsistently between epoxy specimens, are steps formed by the subdivision of the main crack into segments running on parallel planes. This subdivision could result from the interaction of the crack front with the craze structure. Owen and Rose [112] have found that the river markings become

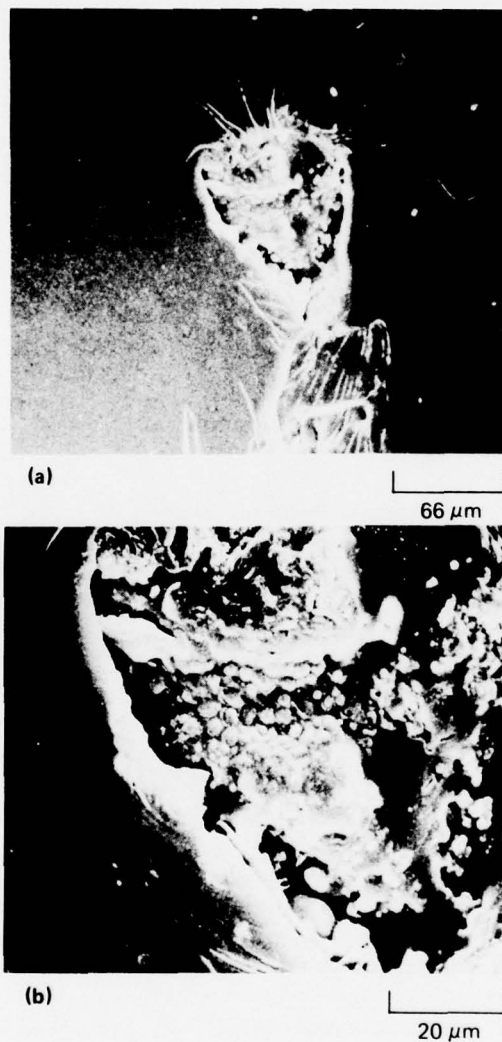


Fig. 23. Scanning electron micrographs of (a) overall fracture topography initiation cavity, (b) coarse fractured fibrils, and (c) fine fractured fibrils in TGDDM-DDS (27 wt% DDS) epoxy, fractured at room temperature at a strain rate of 10^{-2} /min.

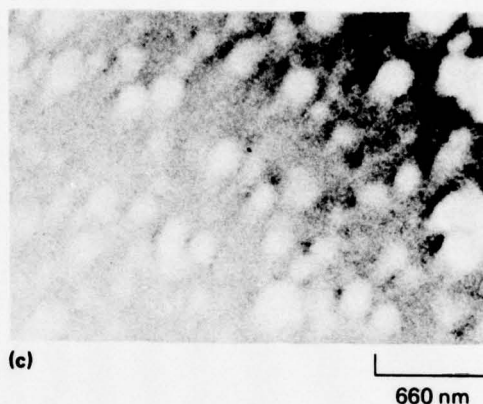


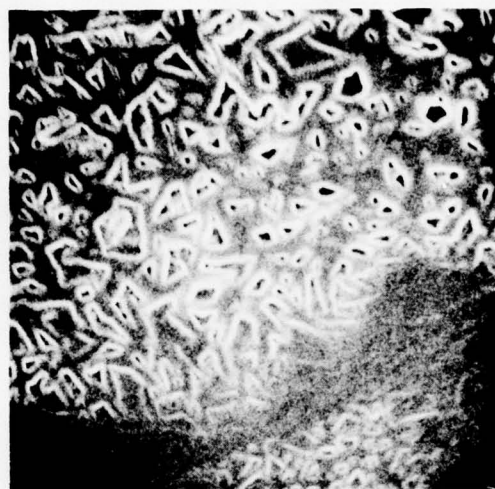
Fig. 23 (continued)

ordered and regular as the flexibility and therefore the ability to undergo crazing in polyester resins is enhanced.

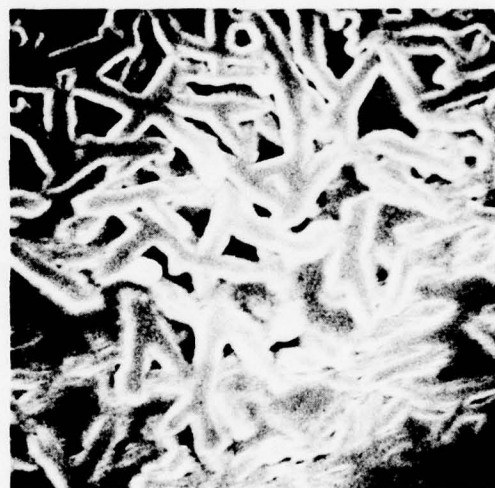
Interference colors, often observed in the mirror-like region of noncross-linked polymer glasses [6], were not evident in the fracture topography of DGEBA-DETA epoxies. Broutman and McGarry [77] also found that interference colors were absent in the fracture surfaces of cross-linked polymethyl methacrylates. They suggested that the thickness of the craze or craze remnants in the mirror-like regions of these cross-linked glasses was not large enough to cause interference with visible light. A similar explanation may apply to epoxies where the presence of cross-linking presumably inhibits the development of thick crazes.

B. The TGDDM-DDS Epoxy System

TGDDM-DDS epoxies exhibit fracture topography characteristics similar to those of the DGEBA-DETA epoxies, which indicates that they too deform and fail primarily by a crazing process. The fracture topography initiation region characteristics of a TGDDM-DDS (27 wt% DDS) epoxy are illustrated in Fig. 23. The overall fracture topography initiation cavity is illustrated in Fig. 23(a); 1 to 5 μm diameter, poorly developed, fractured fibrils are shown in Fig. 23(b); and well-developed, 100 to 200 nm diameter finer fractured fibrils are illustrated in Fig. 23(c). The size distribution of the fractured



2 μm



2 μm

Fig. 24. Scanning electron micrographs of fibrils swept onto the fracture surface in TGDDM-DDS (23 wt% DDS) epoxy, fractured at 200°C at a strain rate of 10^{-2} /min.

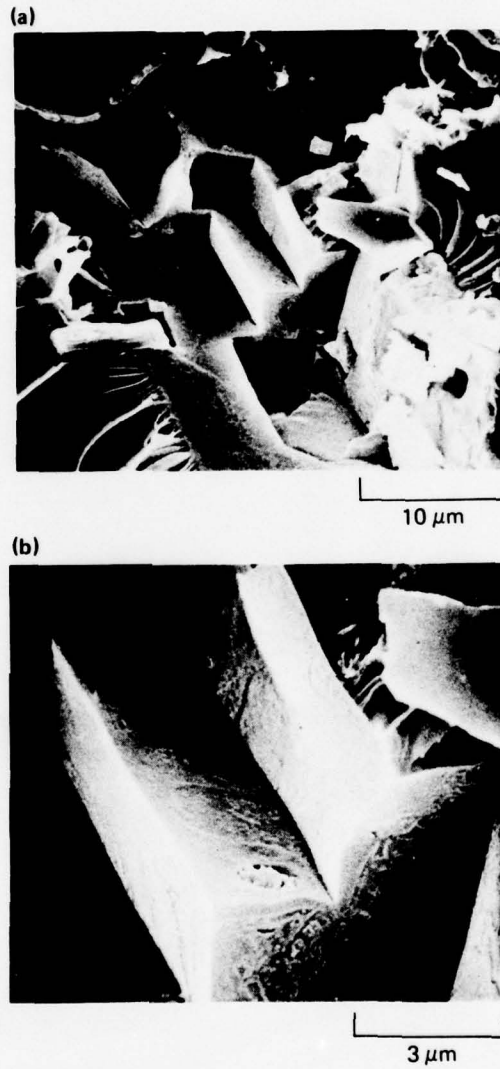


Fig. 25. Scanning electron micrographs of right-angle steps in the fracture topography initiation region of TGDDM-DDS (35 wt% DDS) epoxy fractured at 225°C at a strain rate of 10^{-2} /min.

fibrils within the initiation region depends on the relative rates of craze and crack propagation (see Section III-A). Elongated fibrils that were swept onto the fracture surface were found in the TGDDM-DDS epoxy fracture topographies as illustrated in Fig. 24.

The TGDDM-DDS epoxies also deform to a limited extent by shear banding [115]. Regular, right-angle steps were observed in the fracture topography initiation region, as illustrated in Fig. 25. A plot of the percentage of all fracture topographies that exhibited this mode of deformation as a function of test temperature is shown in Fig. 26. The regular, right-angle steps observed in $\sim 20\%$ of all room-temperature fractures (strain rate $\sim 10^{-2}$ /min) were more prevalent at higher temperatures. At and above 250°C ($T_g \approx 250^\circ\text{C}$), none of the fracture surfaces exhibited the right-angle steps because viscous flow and relaxation processes during and after crack propagation cause a smooth fracture surface and mask the fracture topography microfeatures. The increase in the percentage of fracture topographies exhibiting right-angle steps with temperature is consistent with the shear-band mode of deformation becoming more favored relative to the crazing mode with increasing temperature [21, 93, 116]. Shear-band propagation in these cross-linked glasses produces structur-

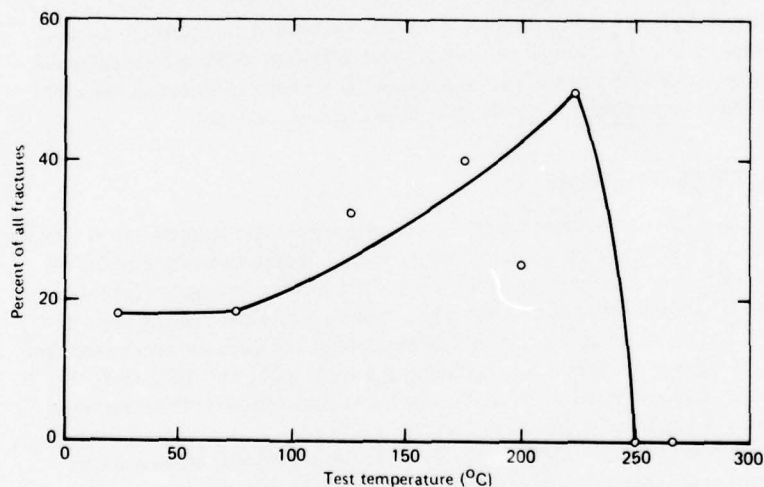


Fig. 26. Percentage of fracture topography initiation regions that exhibit right-angle steps versus temperature in TGDDM-DDS (15 to 35 wt% DDS) epoxies.

ally weak planes because of bond cleavage caused during molecular flow. Hull [117] and Mills [118] have both noted that the intersection of shear bands, which occurs at right angles, causes a stress concentration. This stress concentration is sufficient to cause a crack to propagate through the structurally weak planes caused by shear-band propagation. These phenomena produce right-angle steps in the fracture topography.

IV. EFFECTS OF SORBED MOISTURE ON DURABILITY OF EPOXIES

Epoxy composites and adhesives sorb moisture which in both laboratory and field tests deteriorates the mechanical properties, particularly at high temperatures. The effect of sorbed moisture on the physical properties and mechanical integrity of epoxies and other thermosets utilized as adhesives and composite matrices in the aerospace industry has received considerable attention [1, 2, 19, 82, 84, 86, 88, 119-179]. Despite these studies, all the basic mechanisms responsible for moisture-induced degradation of epoxies have not been identified and/or understood; hence the durability of epoxy components in the service environment is still uncertain. In this section the pertinent basic physical phenomena induced and/or modified by sorbed moisture and affecting the durability of epoxies are discussed. These phenomena include (1) lowering of T_g by sorbed moisture, (2) diffusion of sorbed moisture, (3) swelling stresses induced by sorbed moisture, (4) modification of the deformation and failure modes and the mechanical response by sorbed moisture, and (5) interaction of sorbed moisture with other environmental factors.

A. The Glass Transition

The glass transition temperature, T_g , of a polymer is that temperature at which the glass becomes a viscous liquid with a corresponding viscosity decrease of several orders of magnitude within a $\sim 10^\circ\text{K}$ temperature range. This transition is a second-order phase change and unlike a crystalline melting point occurs over a temperature range, is time dependent, and does not involve changes in extensive properties such as enthalpy and volume but only their rates of change with temperature. Near T_g , a polymer glass softens with decreases in tensile strength and increases in ductility.

Epoxies generally exhibit broad T_g 's (see Section II-A-2) because of the presence of cross-links and their heterogeneous distribution. The large-scale, cooperative segmental motions that occur at T_g require the cleavage of cross-links for certain types of morphological networks, particularly those in which regions of high cross-link density form the continuous phase.

The sorption of moisture by epoxies lowers their T_g 's and correspondingly causes them to soften at lower temperatures. The lowering of the T_g by a diluent, plasticization, is a result of a decrease in the free volume (total volume minus molar volume) of the system caused by the addition of the lower free-volume diluent. The free volume at T_g for a wide variety of glass-forming materials has been shown to be a constant and have a critical free-volume fraction of 0.025 of the total volume [180-182]. Kelley and Bueche [183] have derived an expression relating the T_g of a polymer-diluent system to that of the T_g 's of the two components. The Kelley-Bueche equation assumes that the free volume contributed by the diluent is additive to that of the polymer and that the free volumes of the mixture and components at their T_g 's are a universal constant. The Kelley-Bueche equation for the T_g of the polymer-diluent system is

$$T_g = \frac{\alpha_p V_p T_{gp} + \alpha_d (1 - V_p) T_{gd}}{\alpha_p V_p + \alpha_d (1 - V_p)} \quad (1)$$

where $T_{gp} = T_g$ of the polymer

$T_{gd} = T_g$ of the diluent

α_p = coefficient of expansion of polymer

α_d = coefficient of expansion of diluent

V_p = volume fraction of the polymer

For an epoxy-water system, the Kelley-Bueche equation must be used in a simplified form. The coefficient of expansion of amorphous water between its T_g and melting point (T_M) at 0°C is unknown. Therefore, assuming $\alpha_p \approx \alpha_d$, the Kelley-Bueche equation simplifies to

$$T_g = V_p T_{gp} + (1 - V_p) T_{gd} \quad (2)$$

Experimentally, the T_g of water has been reported in the 128 to 142°K range [184-189]. A good empirical rule [190] for most substances is

$$T_g/T_M \approx 1/2 \text{ to } 2/3 \quad (3)$$

which places the T_g of water in the 137 to 182°K range. In Fig. 27 we compare Browning's [177] experimentally determined T_g 's of a $\text{BF}_3:\text{NH}_2-\text{C}_2\text{H}_5$ catalyzed TGDDM-DDS epoxy-moisture system, which contains equilibrium

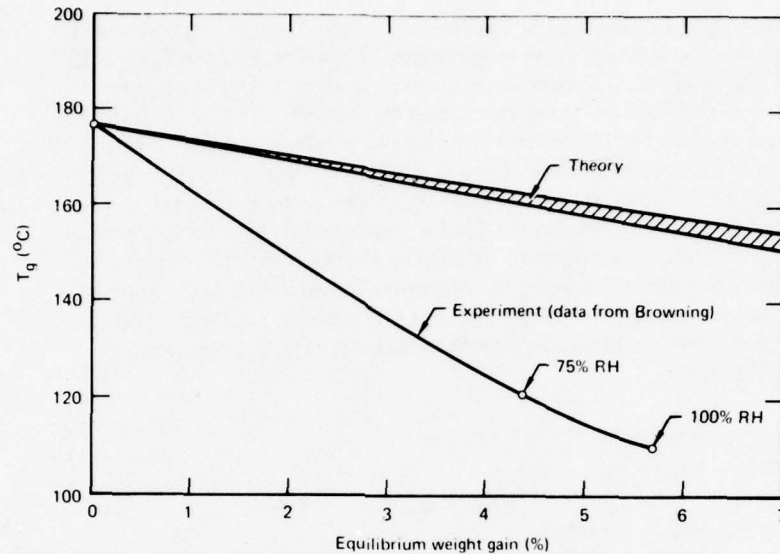


Fig. 27. Theoretical and experimental plots of T_g vs equilibrium moisture weight gain for $\text{BF}_3:\text{NH}_2-\text{C}_2\text{H}_5$ catalyzed TGDDM-DDS (24 wt% DDS) epoxy-moisture system.

amounts of sorbed moisture, with the theoretically calculated values of T_g determined from Eq. (2). The upper limits of the theoretical plot are calculated assuming a T_g of water of 182°K , whereas the lower limits are determined utilizing a T_g of 135°K . The experimental data points are well below the theoretical predictions. This discrepancy could be caused by the following phenomena: (1) the strong hydrogen-bonding capability of water could produce anomalous effects, or (2) if the epoxy has a heterogeneous-cross-link density distribution, moisture will preferentially sorb in the regions of low cross-link density. The regions of low cross-link density control the flow processes that occur at T_g . Equilibrium moisture gains are determined by assuming a uniform moisture distribution. However, a nonuniform distribution could lead to local moisture concentrations in low cross-link density regions that are considerably greater than those implied for a uniform moisture distribution. Hence the depression of T_g may be greater than that expected for a homogeneous distribution of sorbed water. Therefore, the depression of

T_g of TGDDM-DDS epoxies by sorbed moisture is considerably greater than that predicted theoretically.

The plasticization of epoxies by sorbed moisture has generally been reported to be reversible since desorption of moisture from the polymer regenerates the original physical and mechanical properties [1, 2, 19, 82, 84, 86, 88, 119-179]. However, in many environments, irreversible, permanent-damage regions can easily be produced in epoxies during the moisture sorption and desorption processes. These phenomena will be discussed in later sections.

B. Diffusion

The durability of epoxies in many aerospace service environments depends on the degree of deterioration of the high-temperature mechanical properties caused by the plasticizing effect of sorbed moisture and whether this phenomenon is adequately considered during the design stage. The previous relative-humidity-time-temperature exposure of the epoxy component and the diffusion characteristics of moisture in this component determine the moisture profile and the resultant mechanical response of the material. Hence the diffusion characteristics of moisture in an epoxy component are critical factors for predicting mechanical response and durability in a given service environment.

Many diffusion processes can be adequately described by Fick's laws of diffusion [191]. A number of workers have successfully applied Fick's second law of diffusion to the sorption and desorption of moisture in epoxies and epoxy composites and have predicted the moisture profiles as a function of time for specific environmental conditions [1, 2, 156, 158, 165, 166, 167, 169, 175, 177, 178]. Fick's second law for one-dimensional diffusion is given by

$$\frac{dc}{dt} = D \frac{d^2 c}{dx^2} \quad (4)$$

where c is concentration, D is the diffusion coefficient, and x is the distance the moisture has advanced from a given boundary. Equation (4) has been solved for the case of a flat sheet sorbing vapor at both faces under constant environmental conditions. The solution for the fraction of the equilibrium amount of moisture sorbed in time t [$M(t)$] is given by

$$M(t) = \frac{4}{\pi} \left(\frac{Dt}{\pi} \right)^{1/2} \quad (5)$$

where ℓ is the plate thickness [192]. From linear plots of $M(t)$ vs $(t)^{1/2}$, the Fickian behavior in composites, corrected for volume effects, was identical with that of the neat resins [156, 158]. The rates of moisture sorption increased with temperature, and the equilibrium amount of moisture was directly proportional to the relative humidity.

At high moisture contents ($M(t) \geq 0.6$), Eq. (5) does not hold, and a number of methods have been used to determine the moisture profiles in epoxies and epoxy composites. Estimates within 15% of the moisture content and its distribution have been obtained from a series solution of Eq. (4) by Shen and Springer [169] and from a hyperbolic tangent method developed by McKague [168]. Bohlmann and Derby [178] have noted that a numerical-methods technique utilizing a computer program [193] must be used to account for the moisture profile for transient conditions with different relative humidities at each surface.

The utilization of Fickian diffusion as the controlling mechanism to predict the concentration and distribution of sorbed moisture and corresponding deterioration in the high-temperature mechanical properties can lead to serious errors in the durability predictions of epoxies in many environments. Any damage induced in the epoxy or epoxy composite by fabrication and/or environmental conditions can cause deviations from Fickian diffusion and accelerate moisture sorption.

Non-Fickian diffusion has been observed in polymers [194] in which the diffusion coefficient also becomes time and concentration dependent. This type of diffusion has generally been attributed to interaction between the polymer and penetrant [195-202], voids in the polymer [203-207], and clustering of the penetrant in the polymer [194, 208-212].

Non-Fickian diffusion of moisture in epoxies and epoxy composites generally results from the perturbation of the diffusion processes by microvoids and/or cracks. These voids or cracks can be caused by many factors such as one or a combination of the following phenomena: (1) swelling stresses induced by the sorbed moisture (see Section IV-C), (2) craze cavitation (see Section IV-D), (3) formation of water clusters and their subsequent elimination from the glass (see Section V), and (4) high surface tensile stresses resulting from temperature and moisture gradients (see Section V).

Sorbed moisture can modify the epoxy network and therefore the moisture diffusion characteristics in that network. These network modifications can be (1) bond cleavage as a result of swelling stresses [179] and/or relaxation of fabrication stresses, (2) formation of additional cross-links by moisture-enhanced mobility of unreacted groups, and (3) modification of the free volume and/or microvoid characteristics.

In epoxy composites, anomalous diffusion can also occur as a result of (1) accelerated diffusion along the fiber-matrix boundary interface because the presence of voids at the interface creates a preferential diffusion path [175], and (2) stress-biased diffusion caused by anisotropic swelling stresses in the composite [213].

Hence a number of phenomena, some of which have been alluded to in this section and will be discussed in greater depth in subsequent sections, can cause non-Fickian diffusion of moisture in epoxies and epoxy composites. This non-Fickian diffusion, if not considered during the design stage of an epoxy component, can seriously modify the durability in many long-term applications.

C. Swelling

Sorbed moisture causes epoxies to swell [1, 175, 177]. The swelling stresses generated by the sorbed moisture can significantly affect the durability of epoxies in many environments. Swelling stresses caused by moisture gradients, together with other stresses inherent in the material, such as fabrication stresses, can be sufficiently large to cause localized fracture of the polymer [177] (see Section IV-D). For example, the crazing of polystyrene on sorption of normal hydrocarbons has been shown to result from a coupling of the relaxation of orientation stresses frozen into the glass and the swelling stresses which are produced at the boundary between the swollen, outer regions of the glass and the unswollen core [214-218]. Furthermore, Fourier-transform IR spectroscopy suggests that the swelling stresses are sufficient to cleave bonds in the cross-linked, TGDDM-DDS epoxy system [179]. Although the moisture-induced swelling of epoxies generally results in only a 1 to 2% thickness increase, these dimensional changes can result in high stresses in a composite where the fibers constrain the swelling.

For durability predictions of epoxies, the local magnitude of the swelling stresses and strains and at what stress or strain they produce permanent damage in the epoxy glass must be known. Halpin [175] has calculated the dilatational strains in epoxies assuming volume additivity and a homogeneous water distribution. However, the experimentally observed swelling strains were greater than predicted by theory by a factor of three at moisture contents $\leq 2\%$. The swelling of elastomers by diluents can be adequately treated by the kinetic theory of rubber elasticity utilizing Gaussian statistics [67, 219, 220]. However, the swelling of a nonuniform, high cross-link density epoxy glass is considerably more difficult to treat on a fundamental level. Gaussian statistics cannot be utilized at high cross-link densities. Also, a heterogeneous cross-link density distribution could produce nonuniform diffusion at low concentrations

as has been suggested for other heterogeneous systems [221-225]. In these systems, some of the penetrant molecules are envisaged to diffuse faster along certain unspecified paths.

To compute the moisture sorption levels for specific environmental conditions that cause network modification and subsequent growth of permanent damage regions in epoxies requires (1) further experimental and theoretical studies on moisture-induced swelling stresses and strains, and (2) a detailed knowledge of the network structure and the stress levels in the presence of moisture at which damage occurs in the network.

D. Modes of Deformation and Failure and Mechanical Response

In Section III, evidence is presented to show that crazing is the predominant mode of deformation and failure in the TGDDM-DDS and DGEBA-DETA epoxy systems. In any durability prediction, it is vital to understand how sorbed moisture modifies the crazing process and mechanical response. Sorbed low-molecular-weight liquids generally cause failure in polymers by inducing crazing or cracking at stresses much lower than those observed in their absence. Numerous studies [22, 82, 84, 86, 88, 94, 170-172, 211, 214-218, 225-269] on the interaction of low-molecular-weight diluent molecules on the crazing process have illustrated that this phenomenon is complex and not completely understood on a molecular level. This section reviews the basic physical phenomena responsible for modification of the crazing process in the presence of low-molecular-weight diluent molecules, presents evidence that sorbed moisture modifies the crazing process and mechanical response of TGDDM-DDS epoxies, and discusses the implications of these findings in relation to the durability of TGDDM-DDS epoxies.

The modification of craze initiation and propagation by the presence of diluents can occur as a result of plasticization [227] and/or surface energy reduction [234]. The presence of the diluent at the craze tip can reduce the surface energy of the polymer, facilitating the creation of a new surface [263]. For an sorbed diluent layer at least a few molecules thick, the interfacial surface energy participating in craze cavitation can be reduced from the higher polymer-air surface energy value. The plasticization of the polymer at the craze tip by the diluent lowers the shear yield stress which is also active in the craze cavitation process. The stress concentration at the craze tip increases the fractional free volume of the polymer which both enhances sorption of the diluent and lowers the T_g of the polymer [22, 263].

Andrews and co-workers [231, 244, 249] have shown that solvent craze formation (W) is governed by the cavitation properties of a solvated zone of polymer at the craze tip:

$$W = 4.84(h\gamma/p)^{2/3} + 0.66Y\psi hf \quad (6)$$

where h is the craze thickness, γ the interfacial energy of the voids, p the mean distance between the void centers, f the void fraction, Y the shear yield stress, and ψ a constant with a value of 4.4. These threshold conditions for craze cavitation depend on the work necessary to produce plastic yielding and the work necessary to create void interfaces. The yield stress is strongly temperature dependent relative to the surface energy term. Andrews and co-workers showed that W decreases with temperature and that, above a critical temperature T_c , W assumes a minimum constant value W_0 . The temperature T_c has been associated with the T_g of the plasticized swollen polymer at the craze tip. The yield stress term in Eq. (1) reduces to near zero at T_g because $Y \approx 0$ at or above T_g . When $Y \approx 0$, W is dependent only on the temperature-independent surface energy term.

More recently, Kambour and co-workers [250] have suggested that the plasticization effect is the more important factor in solvent crazing. They reported that the solvent-crazing resistance of undiluted polystyrene is the same as that of the preplasticized polystyrene in air. This finding implies that the presence of a liquid/polymer interface is not critical to crazing effectiveness of a given diluent. These workers, therefore, concluded that liquids do not appear to reduce crazing resistance by flowing into and wetting the surface of holes as they form.

There have been a number of efforts to correlate the modification of the craze-crack behavior of the polymer in the presence of a diluent with the solubility parameters of the polymer and diluent. Bernier and Kambour [233] studied the effect of a variety of liquids on the failure of poly(2,6-dimethyl-1,4-phenylene oxide). They concluded that a liquid acts as a solvent when its solubility parameter is close to that of the polymer. When the difference between the solubility parameters of the liquid and polymer is small, the liquid promotes cracking; when this difference is large, crazing is enhanced. Vincent and Raha [240], however, found that a more effective representation of the solvent-cracking versus crazing behavior is obtained by considering the capacity of each liquid-to-hydrogen bond in addition to its solubility parameter.

Kambour and co-workers [233, 239] have also shown a close correlation between the critical strain for craze or crack formation (ϵ_c) and the solubility parameter of the diluent. Subsequently, Andrews and Bevan [244] found that the work of solvent craze formation (W) above the T_g of the plasticized polymer at the craze tip is a smooth function of the difference in the solubility parameters of the polymer (δ_p) and the diluent (δ_d), ($\delta_p - \delta_d$). These workers also found that W exhibits a minimum at $\delta_p \approx \delta_d$. More recently, Mai

[269] has reported that $W\text{-}\delta_d$ relations are not affected by hydrogen bonding. Despite these reported correlations between the solubility parameters of polymer and diluent and the work of craze cavitation formation, the modification of craze initiation and propagation in a specific polymer by a given diluent cannot be predicted a priori. The polymer-diluent interactions on a molecular level and the effect of these interactions on plasticization and swelling behavior at the craze tip are not understood. For example, the role of factors, such as the size and shape of the diluent molecule [270, 271], the rotational isomeric configurations of the polymer, and the flexibility of the polymer chains in polymer-diluent interactions, are not fully understood.

There are a number of additional phenomena that play a significant role in solvent crazing. For an initially undiluted polymer that is stressed in a diluent environment, Williams and co-workers [236, 245, 253, 260, 267] have determined that the craze growth rate is controlled by the slower of either the relaxation processes of the polymer or the rate of flow of the diluent through the porous craze structure. Mai and co-workers [265, 269] have investigated the effects of diluents on polymer fracture toughness as a function of crack velocity. Hopfenberg and co-workers [214-218] have shown that solvent crazing can be significantly enhanced by any orientation present in the polymer. Crazing has been shown to occur at the boundary between the outer swollen gel and the unpenetrated glassy core of the polymer when the combined orientation and swelling stresses are sufficiently large to cause craze cavitation and propagation. Subtle differences in polymer orientation can result in significant changes in the rate of solvent crazing. These workers also found that crazing can occur upon either sorption or desorption of the diluent from the glassy polymer which depend on variations in the thermal and mechanical histories of the glass.

Distribution of the diluent within the polymer is another significant factor affecting craze initiation and growth characteristics. Andrews and co-workers [231, 244, 249] assume an initial homogeneous distribution of diluent within the polymer, but in many service environments clustering of the diluent in the polymer may occur. For example, sorption of the diluent into the polymer at elevated temperatures could cause the polymer to be saturated with the diluent. When the polymer is subsequently cooled, the solubility of the diluent in the polymer is lowered, and regions of high diluent concentration or even diluent clusters can form in the polymer [212, 270, 271]. Dynamic mechanical studies of such polymer-diluent systems suggest that the regions of high diluent concentration are small, ~ 10 nm [270, 271]. These regions would preferentially be highly plasticized which would lower the local shear yield stress and favor cavitation. Within these regions of high diluent concen-

tration the surface energy associated with void formation would also be lowered if the surface tension of the diluent were lower than that of the polymer [272, 273]. It is possible that the regions of high diluent concentration, because of their small size, would favor craze cavitation but not significantly plasticize the craze fibrils. For these conditions, crazes would form more easily, but the fibrils would possess good load-bearing capability. This hypothesis may explain why poor solvents act as good crazing agents because of their tendency to cluster, whereas good solvents act as cracking agents because they are homogeneously distributed throughout the glass, thereby plasticizing and softening the craze fibrils.

There have been few studies on the modification of the modes of deformation and failure of thermosets by water [84, 86, 88, 170, 172]. Generally, such studies reported changes in fracture toughness induced by water with no attempt to explain such changes in terms of modification of the microscopic modes of deformation and failure.

We have recently studied the effect of sorbed moisture on the tensile mechanical properties and fracture topographies of TGDDM-DDS (27 wt% DDS) epoxy as a function of test temperature. In Fig. 28 the tensile strength, ultimate elongation, and Young's modulus of both initially wet and dry epoxies are shown as a function of test temperature. The wet epoxies exhibit lower tensile strengths, ultimate elongations, and moduli than the dry epoxies from room temperature to 150°C. Plasticization of the epoxy, including a softening of the craze fibrils by the sorbed moisture, could cause such a deterioration in the mechanical properties. Above 150°C, the mechanical properties of both the initially wet and dry epoxies start to merge because significant amounts of moisture are eliminated from the wet glasses during the time of the test.

The microscopic yield stress (that stress at the onset of nonlinear behavior in the tensile stress-strain curve) is shown in Fig. 29 as a function of test temperature for both initially wet and dry TGDDM-DDS (27 wt% DDS) epoxies. (This yield stress is closely associated with the onset of localized flow and cavitation.) The microscopic yield stress of the wet epoxies is lower than that of the dry glasses from room temperature to 150°C, as shown in Fig. 29. Above 150°C, the yield stresses of the wet and dry epoxies merge because water is eliminated from the wet specimens during the test.

From room temperature to 150°C, the lower yield stresses of the epoxies containing 4 wt% sorbed moisture, relative to those of the dry epoxies, are equivalent to lowering the dry yield stresses 100 to 125°C on the temperature scale. However, the T_g of this epoxy is lowered only ~60°C by ~4 wt% sorbed moisture (see Fig. 27). These observations imply that the craze cavitation stress is more susceptible to sorbed moisture than the main T_g . Hence the

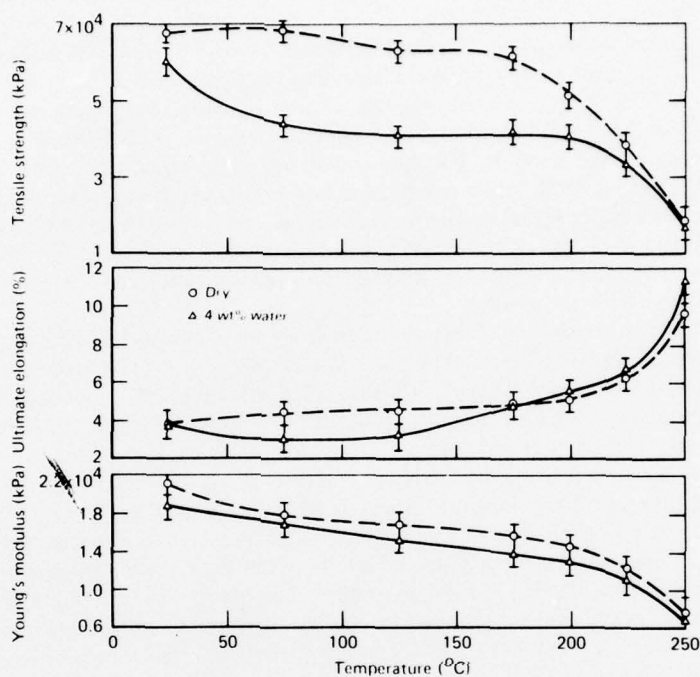


Fig. 28. Tensile strength, ultimate elongation, and Young's modulus of initially wet (~ 4 wt% sorbed moisture) and dry TGDDM-DDS (27 wt% DDS) epoxies as a function of test temperature (strain rate $\sim 10^{-2}$ /min).

magnitude the T_g is lowered on the temperature scale by sorbed moisture cannot be utilized to predict any modification of the formation of permanent damage regions in these epoxies. The craze cavitation stress is more sensitive to sorbed moisture than the T_g for a heterogeneous distribution of moisture in the epoxy. High moisture concentrations in localized regions enhance cavitation by plasticization which results in a lower local shear yield stress. The overall T_g of the epoxy, however, is generally measured on a macroscopic level and is not sensitive to high local moisture concentrations. The surface energy for formation of a fresh surface when cavitation occurs is not enhanced by the presence of local concentrations of moisture because the surface tension of water (7.2 Pa) is greater than that of the epoxy (~ 4 to 5 Pa) [274].

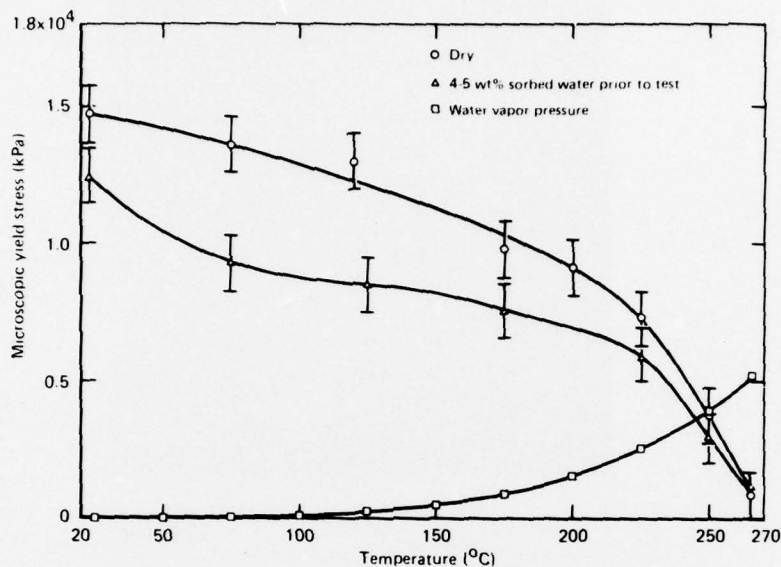


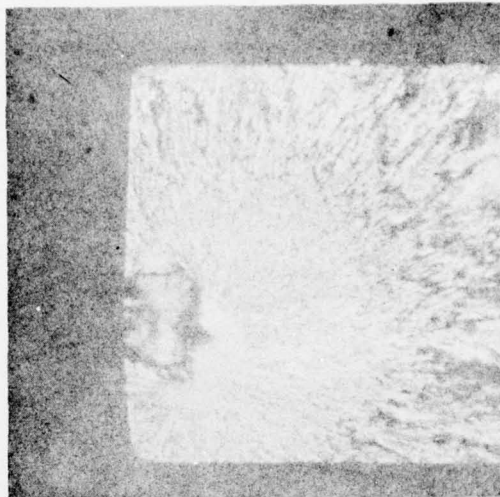
Fig. 29. Microscopic yield stress (strain rate $\sim 10^{-2}$ /min) of initially wet (~ 4 wt% sorbed moisture) and dry TGDDM-DDS (27 wt% DDS) epoxies and water vapor pressure as a function of temperature.

(Moisture was introduced into the TGDDM-DDS epoxies at 135°C in an autoclave, and the samples were then cooled to room temperature. The decrease in solubility of moisture in epoxies on lowering the temperature results in local regions of high moisture concentrations [212, 270, 271].)

Fracture topography studies also indicate that craze deformation and failure modes in epoxies are modified by sorbed moisture. The optical micrographs in Fig. 30 compare the room-temperature fracture topography of a dry TGDDM-DDS (27 wt% DDS) epoxy with one containing ~ 4 wt% sorbed water. The smooth, mirror-like region in the wet sample is considerably larger than in the dry sample. The extent of the mirror-like region is a measure of

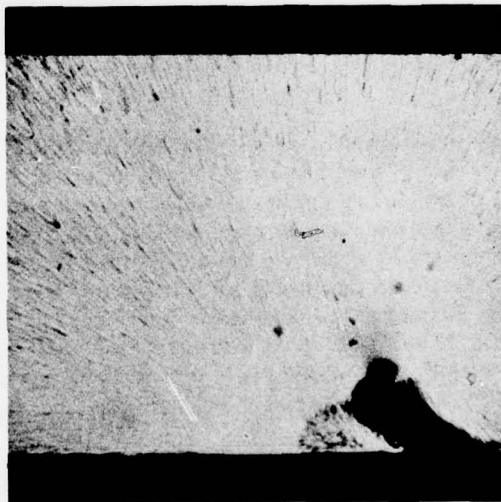
Fig. 30. Optical micrographs of room-temperature fracture surfaces of (a) dry and (b) wet (4 wt% sorbed moisture) TGDDM-DDS (27 wt% DDS) epoxy.

(a) Dry



1.25 mm

(b) 4% Water



1.25 mm

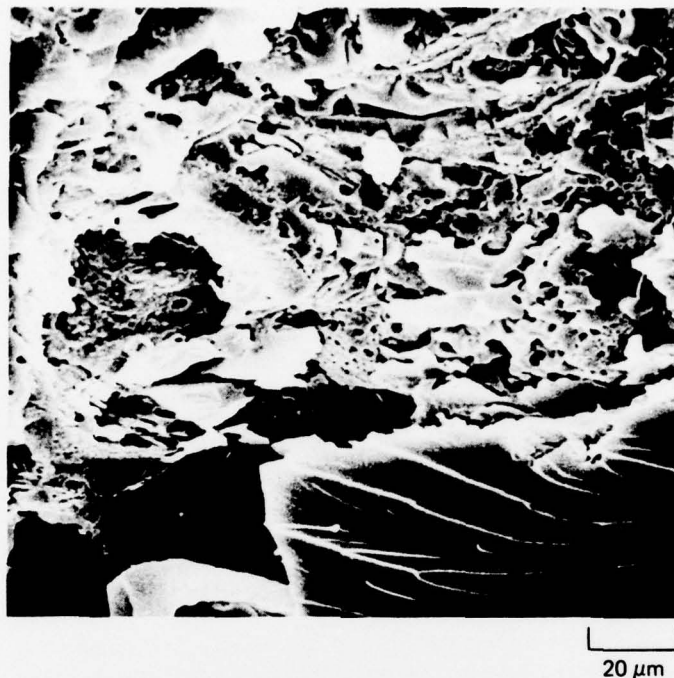


Fig. 31. Scanning electron micrograph of cavities in the fracture topography initiation region of wet TGDDM-DDS (27 wt% DDS) epoxy (4 wt% sorbed moisture) which was fractured at room temperature at a strain rate of $\sim 10^{-2}$ /min.

the area in which crack propagation occurs through a preformed craze. Hoare and Hull [102] suggested that this area depends on the ease of craze growth, crack nucleation, and crack growth within the craze. The area of the mirror-like region increases with test temperatures as illustrated in Fig. 22. The extent of this region in the wet specimen that fractured at room temperature is equivalent to that in a dry specimen fractured at 125°C.

Scanning electron micrographs of the fracture topography initiation regions in the wet TGDDM-DDS epoxies reveal numerous cavities, as illustrated in Fig. 31. The cavities are more numerous than those observed in dry epoxy glasses fractured under similar conditions. This observation suggests that sorbed moisture in these epoxies enhances cavitation.

Hence the data illustrated in Figs. 28-31 suggest that sorbed moisture lowers the craze initiation and propagation stresses in TGDDM-DDS epoxies. The sorbed moisture has a more severe effect on the crazing process than the T_g , probably as a result of the presence of islands of high moisture concentration.

The enhancement of craze cavitation and propagation in TGDDM-DDS epoxies by sorbed moisture directly affects the durability of these glasses in humid environments. The plasticizing effect of sorbed moisture on TGDDM-DDS epoxies is already abnormally large (see Section IV-A). However, local concentrations of sorbed moisture lower the local shear yield stress to an even greater extent than that expected from the observed, macroscopic lowering of the T_g . Such high, local moisture concentrations can form in microvoids, in the porous structure of a preformed craze, or from moisture sorption at elevated temperature followed by exposure of the epoxy to lower temperature. The ease of diffusion of moisture through a porous craze structure and its accumulation near the craze tip where it enhances cavitation must be considered a significant mechanism for the growth of permanent damage regions in these glasses in humid environments, particularly in view of the low stress levels at which cavitation generally occurs in polymer glasses (Fig. 29).

V. FACTORS THAT CONTROL THE DURABILITY OF EPOXIES

In service environment, the durability of epoxies depends on a complex number of interacting phenomena. The factors that control the critical path to ultimate failure or unacceptable damage depend specifically on the particular environmental conditions. In this section, all possible factors that generally affect the durability of epoxies in service environments are reviewed, and some of the critical environments that affect the durability of epoxies and the difficulties in predicting their long-term durability are discussed.

The durability of an epoxy component depends on the structure and physical state of the epoxy after cure and fabrication. Figure 32 illustrates the primary phenomena that are dependent on cure and fabrication conditions and that also affect the durability of epoxies. These phenomena include the network structure, microvoid characteristics (considered in Section II), and fabrication stresses. Stresses can arise in the epoxy during fabrication from (1) shrinkage of the epoxy during cure, (2) temperature gradients within the sample during cure, and (3) the mismatch in the coefficients of expansion of the epoxy matrix and fiber in an epoxy composite [275, 276]. Temperature gradients, which are worse in thick specimens, can cause one region of the epoxy to form a glass prior to other regions during cure. Once the epoxy has formed a glass at the cure temperature, stresses develop in a composite on

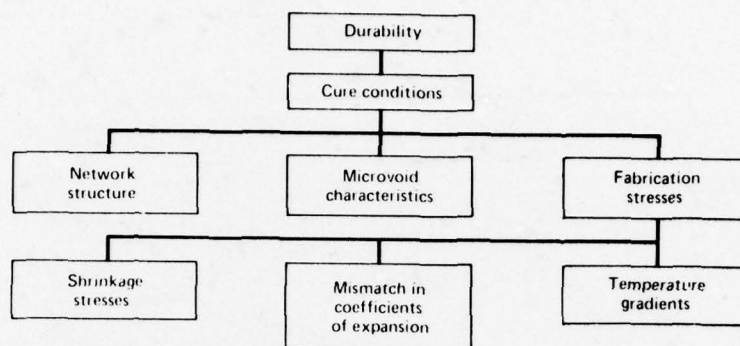


Fig. 32. Schematic of cure and fabrication factors that affect the durability of epoxies.

cooling to room temperature because of the difference in the coefficients of expansion of matrix and filler. Such stresses are complex and intimately depend on the distribution of the fibers in the epoxy matrix. The theoretical treatment of the stresses and strains that arise from thermal expansion and shrinkage differences in composites has recently been reviewed by Hale [277].

Several environmental factors can cause growth of the flaws produced during cure and fabrication and/or formation of new permanent damage regions. Figure 33 illustrates the environmental factors that contribute to the formation of permanent damage regions and, hence, directly limit the durability of epoxies. The primary environmental factors are service stresses, humidity, temperature, and solar radiation.

Normal service stresses, particularly in combination with environmental and fabrication stresses, can cause formation of permanent damage regions in epoxies. Solar radiation can induce surface cross-linking and/or a lowering of molecular weight which will cause surface stresses and possible microcracking [278]. (There is no evidence, at present, to suggest that TGDDM-DDS epoxies are particularly susceptible to radiation-induced chemical changes.)

Temperature effects can also contribute to the formation of permanent damage regions. High temperatures can cause trapped, unreacted, low-molecular-weight material to be evolved from the epoxy, resulting in microvoids (see Section II-B). Thermal gradients can cause stresses in epoxy components. Such gradients can be caused by sunlight heating only one surface or from a thermal spike caused by aerodynamic heating during high-speed dashes by an aircraft followed by rapid cooling when speed is reduced.

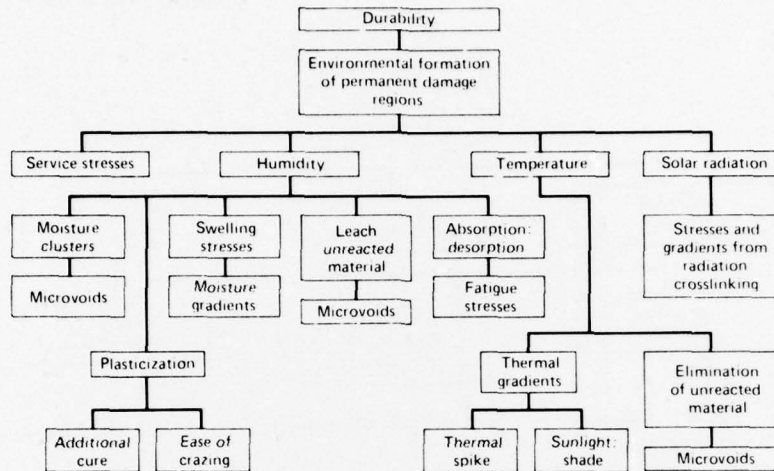


Fig. 33. Schematic of environmental factors that affect the durability of epoxies.

The sorption of moisture by epoxies can cause a number of phenomena which may contribute to the formation of permanent damage regions. Moisture-induced plasticization, in addition to enhancing crazing, increases the mobility within the epoxy which may lead to additional cure. Sorbed moisture causes swelling stresses which are particularly serious at the boundary between the outer swollen region and the inner unswollen core. The sorption and desorption of moisture causes oscillatory swelling stresses which are equivalent to subjecting the epoxy to fatigue. The sorption and desorption of moisture could result in leaching from the epoxy any unreacted, low-molecular-weight material, resulting in microvoids. The formation of water clusters (see Section IV-D) and their subsequent elimination can also result in the formation of microvoids in epoxies. Bair and Johnson [212] have directly shown that cavities are produced in a polyethylene-water system by such a mechanism.

There are many possible critical paths involving the effects of the original network structure, microvoid characteristics, and fabrication stresses together with service stresses, moisture, temperature, and solar radiation exposure of epoxies that will lead to formation and/or growth of permanent damage regions. The critical path that causes damage and that predominates in a given

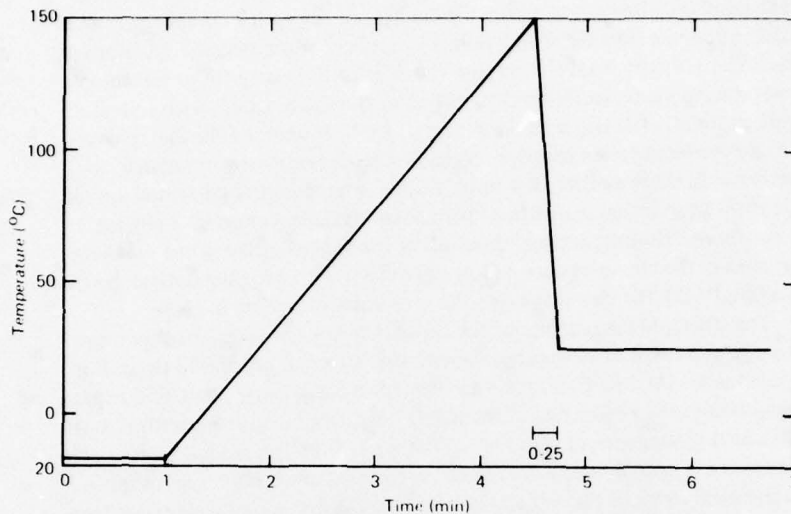


Fig. 34. Thermal spike experienced by outer surface of epoxy component as a result of a supersonic maneuver.

service environment often depends on a complex series of interacting phenomena which were illustrated as separate entities in Figs. 32 and 33.

The most extreme environmental conditions experienced by components on a fighter aircraft occur during a supersonic dash. The aircraft dives from high altitudes (outer surface temperature -20 to -55°C) into a supersonic, low-altitude run during which the surface temperature rises in minutes to 100 to 150°C as a result of aerodynamic heating. On reduction of speed, the outer surface temperature drops extremely rapidly. In Fig. 34 a temperature profile of the outer surface of the aircraft component as a function of time illustrates the thermal spike that the outer surface receives during the supersonic maneuver. This particular thermal spike has been utilized by McKague [168] and Browning [177] in their studies of the simulation of real-life environmental conditions on the durability of epoxies and epoxy composites. McKague [168] found that epoxy laminates are damaged after thermal-spike exposures as indicated by abnormal increases in moisture sorption. Browning [177] found similar evidence of thermal-spike-induced damage in unfilled TGDDM-DDS epoxies. After exposure to thermal spikes, this epoxy exhibited numerous surface microcracks. Browning [177] suggests that damage occurs during

the rapid cool-down portion of the spike at which the rate is $\sim 500^\circ\text{C}/\text{min}$. The rapid cool-down rate causes the exterior of the epoxy component to be cooler than the interior, which results in surface tensile stresses. In addition, moisture is driven from the exterior but not from the interior of the component during the temperature-rise portion of the spike, which leads to a moisture gradient. The larger swelling stresses in the interior of the material relative to the less swollen exterior results in surface tensile stresses which, together with those stresses that result from the temperature gradients, are sufficiently large to cause growth of permanent damage regions by a crazing mechanism. During the short duration of the thermal spike, some moisture remains in the epoxy surface region and lowers the craze cavitation stress (see Section IV-D), thereby enhancing the possibility of surface damage.

The less rapid heating rate of the thermal spike could also possibly cause damage as a result of expanding, superheated steam momentarily trapped in a microvoid. At 150°C , a small vapor pressure could cause microvoid expansion because the yield stress of the highly plasticized microvoid walls is negligible at this temperature. (In Fig. 29 the water vapor pressure is plotted as a function of temperature; at 150°C the vapor pressure is similar in magnitude to the yield stress of the wet epoxy assuming the dry epoxy yield stress-temperature plot is shifted 100 to 125°C on the temperature scale by sorbed moisture.) At MDRL, moisture-saturated epoxies have been rapidly heated by introduction into a preheated oven in the 50 to 150°C range. Mechanical property and fracture topography observations do not indicate any significant evidence of microvoid growth as a result of water vapor pressure. Therefore, at present, the primary mode of damage during a thermal spike occurs during the rapid cool-down period.

The thermal spike utilized by McKague [168] and Browning [177] is one of the more severe spikes in terms of maximum temperature and rate of cool-down. Recently, Bohlmann and Derby [178] found no evidence of damage in graphite-epoxy laminates for the less-severe thermal spike condition which the Space Shuttle Orbiter will experience (assuming a cool-down rate of only $4^\circ\text{C}/\text{min}$).

For less-severe environmental conditions than those that involve supersonic maneuvers, it is, at present, difficult to predict the long-term effects of fabrication and environmental factors on the durability of epoxies in specific environments. Such a priori predictions require knowledge of the structure-property relations of epoxies, the magnitude and/or duration of fabrication, environmental and service stresses placed on the material, and a detailed understanding of other fabrication and environmental factors alluded to in Figs. 32 and 33. However, the present state of knowledge of epoxies and composite materials does not yield all such required information.

Furthermore, an understanding of the interactions of the various fabrication and environmental factors that affect the durability of thermosets or their composites has received little attention. Blaga and Yamasaki [159] have studied and suggested the critical phenomena affecting the weathering of glass-reinforced polyesters. In their studies they propose that damage occurs in surface regions under the combined action of radiation-induced tensile stresses in the surface region together with physically induced stress fatigue. Tensile stresses in the surface region are caused by shrinkage of the matrix that results from cross-linking induced by the UV radiation. Stress fatigue is imposed on the composite system by physically induced alternating stresses produced by cyclic variation of temperature and probably moisture resulting from thermal and moisture gradients and inhomogeneities. The resin in the interface region is damaged by stress fatigue resulting from the differential dimensional changes between glass and matrix, induced by moisture and/or temperature cyclic variations. Under the influence of alternating cyclic stresses and in conjunction with chemical degradation of the matrix, the interface region undergoes cracking, fracture, and fiber delamination. These workers note that the stresses at the interface are complex.

VI. CONCLUSIONS

The structure-property relations of TGDDM-DDS and DGEBA-DETA epoxies, the effects of sorbed moisture, and the fabrication and environmental factors that control the durability of epoxies have been reviewed. The primary conclusions are summarized as follows.

A. Structure-Property Relations

The modes of deformation and failure and mechanical response of epoxies are controlled by the epoxy network structure and microvoid characteristics.

The cross-link-density distribution in epoxy networks can be heterogeneous with regions of low cross-link density controlling the flow processes. Steric and diffusional restrictions inhibit cross-link reactions during the latter stages of cure and limit the overall achievable cross-link density.

Microvoids, which act as stress concentrations and sinks for sorbed moisture, can be formed in epoxies as a result of clusters of unreacted, low-molecular-weight material ejected from the epoxies during cure.

The epoxies deform and fail predominantly by a crazing process. The TGDDM-DDS epoxies also deform to a limited extent by shear banding.

B. Sorbed Moisture

Epoxyes are plasticized by sorbed moisture, and their T_g 's are lowered to a greater extent than predicted from free-volume considerations. Strong hydrogen bonding or the preferential accumulation of moisture in regions of low cross-link density could explain the anomalous plasticization.

Moisture diffusion in epoxyes can be adequately described by Fick's laws of diffusion. Non-Fickian diffusion with accelerated moisture sorption will occur, however, in environments that cause microvoid or crack formation in the epoxyes.

Local swelling stresses generated by the sorption of moisture in epoxyes cannot be predicted accurately without a detailed knowledge of the epoxy network structure and the moisture distribution within the network.

Sorbed moisture enhances the craze cavitation and propagation processes in the epoxyes by plasticization. The craze cavitation stress is more susceptible to sorbed moisture than T_g , particularly when microscopic regions of high-moisture concentration are present in the epoxy. Therefore, modification of T_g by sorbed moisture cannot alone be utilized as a sensitive guide to predict deterioration in the mechanical response and durability of epoxyes.

C. Durability

Permanent damage regions can form on the surface of epoxy components when aircraft perform supersonic maneuvers. Such maneuvers can impose surface tensile stresses greater than the epoxy craze cavitation stress as a result of severe temperature and moisture gradients.

To predict the durability of epoxyes with confidence in less extreme environmental conditions requires a detailed knowledge of the service environment, the structure-property relations of epoxyes, the effect of fabrication and environmental factors, and their complex interactions on the formation of permanent damage regions. The present knowledge of epoxyes and composite materials is not sufficiently advanced to achieve accurate predictions.

Acknowledgments

We wish to acknowledge Dr. D. R. Ulrich of the Air Force Office of Scientific Research and Drs. D. P. Ames and C. J. Wolf of McDonnell Douglas Research Laboratories for their support and encouragement of this work.

Research sponsored in part by the McDonnell Douglas Independent Re-

search and Development Program and in part by the Air Force Office of Scientific Research/AFSC, United States Air Force, under Contract No. F44620-76-C-0075. The United States Government is authorized to reproduce and distribute reprints for governmental purposes notwithstanding any copyright notation hereon.

REFERENCES

- [1] Air Force Durability Workshop, Battelle Columbus Laboratories, September 1975.
- [2] Air Force Conference on The Effects of Relative Humidity and Temperature on Composite Structures, University of Delaware, March, 1976, AFOSR-TR-77-0030 (1977).
- [3] J. P. Berry, *J. Polym. Sci.*, **50**, 107 (1961).
- [4] J. P. Berry, *Ibid.*, **50**, 313 (1961).
- [5] R. F. Boyer, *Rubber Chem. Technol.*, **36**, 1301 (1963).
- [6] R. P. Kambour, *J. Polym. Sci.*, **A3**, 1713 (1965).
- [7] R. P. Kambour, *Polym. Eng. Sci.*, **8**, 281 (1968).
- [8] R. P. Kambour, *Appl. Polym. Symp.*, **7**, 215 (1968).
- [9] J. Heijboer, in *Macromolecular Chemistry* (O. Wichterle and B. Sedlacek, eds.), Wiley-Interscience, New York, 1968, p. 3755.
- [10] E. H. Andrews, *Fracture in Polymers*, Elsevier, New York, 1968.
- [11] S. M. Aharoni, *J. Appl. Polym. Sci.*, **16**, 3275 (1972).
- [12] S. Rabinowitz and P. Beardmore, *Crit. Rev. Macromol. Sci.*, **1**, 1 (1972).
- [13] R. J. Morgan, *J. Polym. Sci., Polym. Phys. Ed.*, **11**, 1271 (1973).
- [14] J. R. Kastelic and E. Baer, *J. Macromol. Sci.-Phys.* **B7**(4), 679 (1973).
- [15] R. J. Morgan and L. E. Nielsen, *Ibid.*, **B9**(2), 239 (1974).
- [16] A. J. Kovacs, *Adv. Polym. Sci.*, **3**, 394 (1964).
- [17] M. H. Litt and A. V. Tobolsky, *J. Macromol. Sci.-Phys.*, **B1**(3), 433 (1967).
- [18] R. F. Boyer, *Polym. Eng. Sci.*, **8**, 161 (1968).
- [19] R. J. Morgan and J. E. O'Neal, *Polym. Plast. Technol. Eng.*, **5**(2), 173 (1975).
- [20] S. E. B. Petrie, in *Polymeric Materials: Relationships between Structure and Mechanical Behavior* (E. Baer and S. V. Radcliffe, eds.), American Society for Metals, 1975, p. 55.
- [21] R. J. Morgan and J. E. O'Neal, *J. Polym. Sci., Polym. Phys. Ed.*, **14**, 1053 (1976).
- [22] A. N. Gent, *J. Mater. Sci.*, **5**, 925 (1970).
- [23] E. H. Andrews, in *The Physics of Glassy Polymers* (R. N. Haward, ed.), Applied Science Publishers, 1973, Chap. 7.

D-A073 930

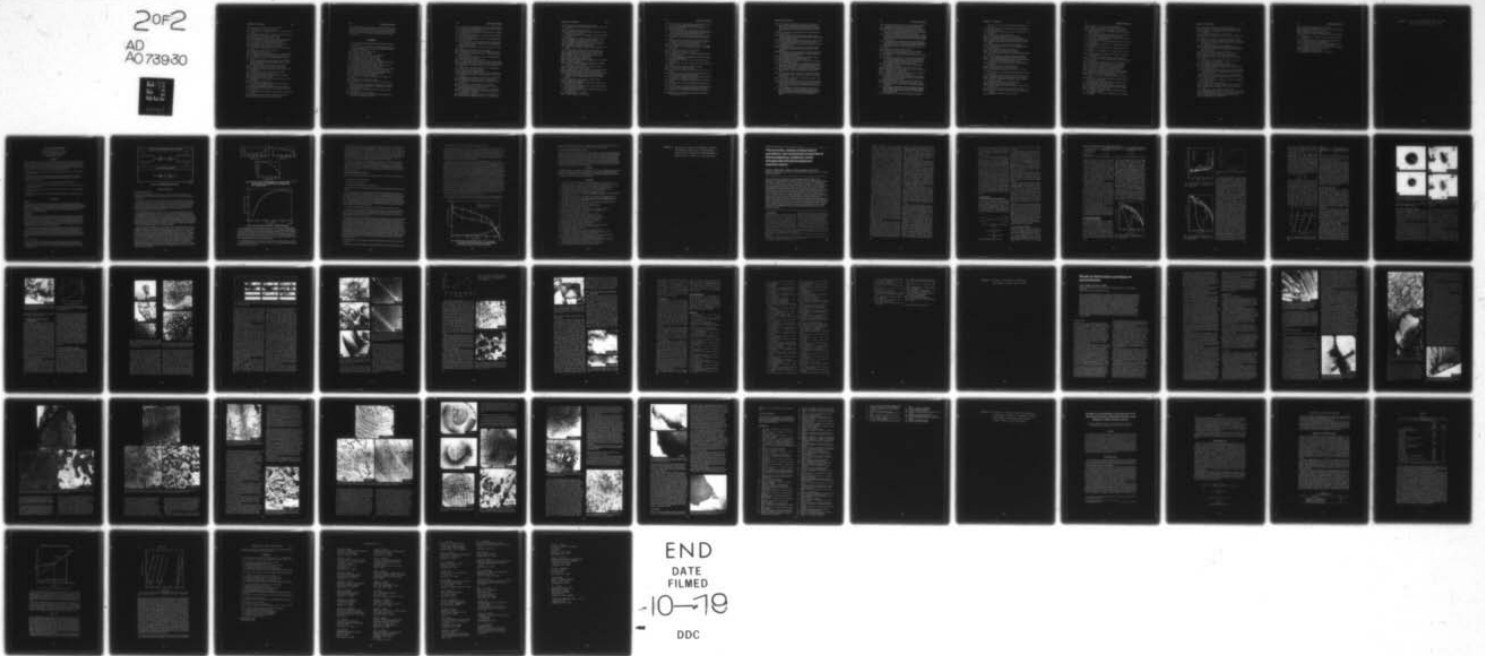
MCDONNELL DOUGLAS RESEARCH LABS ST LOUIS MO
THE RELATION BETWEEN THE CHEMICAL AND PHYSICAL STRUCTURE AND TH--ETC(U)
JUN 79 R J MORGAN, J E O'NEAL F44620-76-C-0075
MDC-Q0653 NL

F/G 11/9

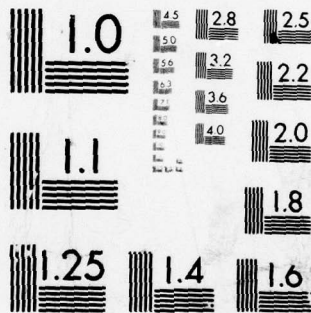
UNCLASSIFIED

2 of 2

AD
AO 739-30



END
DATE
FILMED
10-19
DDC



MICROCOPY RESOLUTION TEST CHART
NATIONAL BUREAU OF STANDARDS-1963-A

- [24] D. Katz and A. V. Tobolsky, *Polymer*, **4**, 417 (1963).
- [25] T. K. Kwei, *J. Polym. Sci.*, **A1**, 2977 (1963).
- [26] A. S. Kenyon and L. E. Nielsen, *J. Macromol. Sci.-Chem.*, **A3**(2), 275 (1969).
- [27] R. P. Krehling and D. E. Kline, *J. Appl. Polym. Sci.*, **13**, 2411 (1969).
- [28] J. P. Bell, *J. Polym. Sci., Part A-2*, **8**, 417 (1970).
- [29] T. Murayama and J. P. Bell, *Ibid.*, **8**, 437 (1970).
- [30] M. A. Acitelli, R. B. Prime, and E. Sacher, *Polymer*, **12**, 335 (1970).
- [31] R. G. C. Arridge and J. H. Speake, *Ibid.*, **12**, 443, 450 (1972).
- [32] P. V. Sidiyakin, *Vysokomol. Soedin.*, **A14**, 979 (1972).
- [33] T. Hirai and D. E. Kline, *J. Appl. Polym. Sci.*, **16**, 3145 (1972).
- [34] R. B. Prime and E. Sacher, *Polymer*, **13**, 455 (1972).
- [35] P. G. Babayevsky and J. K. Gillham, *J. Appl. Polym. Sci.*, **17**, 2067 (1973).
- [36] T. Hirai and D. E. Kline, *Ibid.*, **17**, 31 (1973).
- [37] E. Sacher, *Polymer*, **14**, 91 (1973).
- [38] D. A. Whiting and D. E. Kline, *J. Appl. Polym. Sci.*, **18**, 1043 (1974).
- [39] J. K. Gillham, J. A. Benci, and A. Noshay, *Ibid.*, **18**, 951 (1974).
- [40] L. E. Nielsen, *J. Macromol. Sci.-Rev. Macromol. Chem.*, **C3**(1), 69 (1969).
- [41] L. E. Nielsen, *Crosslinking-Effect on Physical Properties of Polymers*, Monsanto/Washington University/ONR/ARPA Association, Report HPC-68-57, May 1968.
- [42] T. S. Carswell, *Phenoplasts*, Interscience, New York, 1947.
- [43] T. G. Rochow and F. G. Rowe, *Anal. Chem.*, **21**, 261 (1949).
- [44] R. A. Spurr, E. H. Erath, H. Myers, and D. C. Pease, *Ind. Eng. Chem.*, **49**, 1839 (1957).
- [45] E. H. Erath and R. A. Spurr, *J. Polym. Sci.*, **35**, 391 (1959).
- [46] T. G. Rochow, *Anal. Chem.*, **33**, 1810 (1961).
- [47] E. H. Erath and M. Robinson, *J. Polym. Sci., Part C*, **3**, 65 (1963).
- [48] H. P. Wohnsiedler, *Ibid.*, **3**, 77 (1963).
- [49] D. H. Solomon, B. C. Loft, and J. D. Swift, *J. Appl. Polym. Sci.*, **11**, 1593 (1967).
- [50] R. E. Cuthrell, *Ibid.*, **11**, 949 (1967).
- [51] A. N. Neverov, N. A. Birkina, Yu. V. Zherdev, and V. A. Kozlov, *Vysokomol. Soedin.*, **A10**, 463 (1968).
- [52] G. Nenkov and M. Mikhailov, *Makromol. Chem.*, **129**, 137 (1969).
- [53] B. E. Nelson and D. T. Turner, *J. Polym. Sci., Polym. Phys. Ed.*, **10**, 2461 (1972).
- [54] L. G. Bozveliev and M. G. Mihajlov, *J. Appl. Polym. Sci.*, **17**, 1963, 1973 (1973).
- [55] R. J. Morgan and J. E. O'Neal, *Polym. Prepr.*, **16**(2), 610 (1975).
- [56] K. Selby and L. E. Miller, *J. Mater. Sci.*, **10**, 12 (1975).

search and Development Program and in part by the Air Force Office of Scientific Research/AFSC, United States Air Force, under Contract No. F44620-76-C-0075. The United States Government is authorized to reproduce and distribute reprints for governmental purposes notwithstanding any copyright notation hereon.

REFERENCES

- [1] Air Force Durability Workshop, Battelle Columbus Laboratories, September 1975.
- [2] Air Force Conference on The Effects of Relative Humidity and Temperature on Composite Structures, University of Delaware, March, 1976, AFOSR-TR-77-0030 (1977).
- [3] J. P. Berry, *J. Polym. Sci.*, **50**, 107 (1961).
- [4] J. P. Berry, *Ibid.*, **50**, 313 (1961).
- [5] R. F. Boyer, *Rubber Chem. Technol.*, **36**, 1301 (1963).
- [6] R. P. Kambour, *J. Polym. Sci.*, **A3**, 1713 (1965).
- [7] R. P. Kambour, *Polym. Eng. Sci.*, **8**, 281 (1968).
- [8] R. P. Kambour, *Appl. Polym. Symp.*, **7**, 215 (1968).
- [9] J. Heijboer, in *Macromolecular Chemistry* (O. Wichterle and B. Sedlacek, eds.), Wiley-Interscience, New York, 1968, p. 3755.
- [10] E. H. Andrews, *Fracture in Polymers*, Elsevier, New York, 1968.
- [11] S. M. Aharoni, *J. Appl. Polym. Sci.*, **16**, 3275 (1972).
- [12] S. Rabinowitz and P. Beardmore, *Crit. Rev. Macromol. Sci.*, **1**, 1 (1972).
- [13] R. J. Morgan, *J. Polym. Sci., Polym. Phys. Ed.*, **11**, 1271 (1973).
- [14] J. R. Kastelic and E. Baer, *J. Macromol. Sci.-Phys.* **B7**(4), 679 (1973).
- [15] R. J. Morgan and L. E. Nielsen, *Ibid.*, **B9**(2), 239 (1974).
- [16] A. J. Kovacs, *Adv. Polym. Sci.*, **3**, 394 (1964).
- [17] M. H. Litt and A. V. Tobolsky, *J. Macromol. Sci.-Phys.*, **B1**(3), 433 (1967).
- [18] R. F. Boyer, *Polym. Eng. Sci.*, **8**, 161 (1968).
- [19] R. J. Morgan and J. E. O'Neal, *Polym. Plast. Technol. Eng.*, **5**(2), 173 (1975).
- [20] S. E. B. Petrie, in *Polymeric Materials: Relationships between Structure and Mechanical Behavior* (E. Baer and S. V. Radcliffe, eds.), American Society for Metals, 1975, p. 55.
- [21] R. J. Morgan and J. E. O'Neal, *J. Polym. Sci., Polym. Phys. Ed.*, **14**, 1053 (1976).
- [22] A. N. Gent, *J. Mater. Sci.*, **5**, 925 (1970).
- [23] E. H. Andrews, in *The Physics of Glassy Polymers* (R. N. Haward, ed.), Applied Science Publishers, 1973, Chap. 7.

- [57] J. L. Racich and J. A. Koutsky, *Bull. Am. Phys. Soc.*, **20**, 456 (1975).
- [58] M. I. Karyakina, M. M. Mogilevich, N. V. Maiorova, and A. V. Udalova, *Vysokomol. Soedin.*, **A17**, 466 (1975).
- [59] M. V. Maiorova, M. M. Mogilevich, M. I. Karyakina, and A. V. Udalova, *Ibid.*, **A17**, 471 (1975).
- [60] V. M. Smartsev, A. Ye. Chalykh, S. A. Nenakhov, and A. T. Sanzharovskii, *Ibid.*, **A17**, 836 (1975).
- [61] H. Lee and K. Neville, *Handbook of Epoxy Resins*, McGraw-Hill, New York, 1967, Chap. 5.
- [62] J. A. Manson, S. L. Kim, and L. H. Sperling, *Influence of Crosslinking on the Mechanical Properties of High T_g Polymers*, Technical Report AFML-TR-76-124 (1976).
- [63] B. Wunderlich and A. Mehta, *J. Polym. Sci., Polym. Phys. Ed.*, **12**, 255 (1974).
- [64] S. M. Aharoni, *J. Appl. Polym. Sci.*, **19**, 1103 (1975).
- [65] K. Neki and P. H. Geil, *J. Macromol. Sci.-Phys.*, **B8**(1-2), 295 (1973).
- [66] A. J. Chompff, *Am. Chem. Soc., Div. Org. Coat. Plast. Chem., Prepr.*, **36**(2), 529 (1976).
- [67] P. J. Flory, *Principles of Polymer Chemistry*, Cornell University Press, Ithaca, New York, 1953, Chap. 9.
- [68] E. G. K. Pritchett, *Chem. Ind.*, **2**, 95 (1949).
- [69] N. J. L. Megson, *Phenolic Resin Chemistry*, Academic, New York, 1958.
- [70] D. H. Solomon, *J. Macromol. Sci.-Rev. Macromol. Chem.*, **C1**, 179 (1967).
- [71] R. J. Morgan and J. E. O'Neal, *J. Macromol. Sci.-Phys.*, **B15**(1), 139 (1978).
- [72] J. P. Bell and W. T. McCarvill, *J. Appl. Polym. Sci.*, **18**, 2243 (1974).
- [73] P. L. Jain, *J. Polym. Sci.*, **31**, 210 (1958).
- [74] D. W. Ovenall, *J. Polym. Sci.*, **B1**, 37 (1963).
- [75] M. A. Kennan and D. A. Smith, *J. Appl. Polym. Sci.*, **11**, 1009 (1967).
- [76] D. A. Smith, *Am. Chem. Soc., Div. Org. Coat. Plast. Chem., Prepr.*, **27**, 321 (1967).
- [77] L. J. Broutman and F. J. McGarry, *J. Appl. Polym. Sci.*, **9**, 609 (1965).
- [78] R. Griffiths and D. G. Holloway, *J. Mater. Sci.*, **5**, 302 (1970).
- [79] R. L. Patrick, W. G. Gehman, L. Dunbar, and J. A. Brown, *J. Adhes.*, **3**, 165 (1971).
- [80] P. B. Bowden and J. A. Dukes, *J. Mater. Sci.*, **7**, 52 (1972).
- [81] R. L. Patrick, in *Treatise on Adhesion and Adhesives*, Vol. 3 (R. L. Patrick, ed.), Dekker, New York, 1973, p. 163.
- [82] R. J. Young and P. W. R. Beaumont, *J. Mater. Sci.*, **10**, 1343 (1975).
- [83] R. J. Morgan and J. E. O'Neal, *Am. Chem. Soc., Div. Org. Coat. Plast. Chem., Prepr.*, **36**(2), 689 (1976).
- [84] A. Christiansen and J. B. Shortall, *J. Mater. Sci.*, **11**, 1113 (1976).
- [85] S. Mostovoy and E. J. Ripling, *J. Appl. Polym. Sci.*, **10**, 1351 (1966).

- [86] S. Mostovoy and E. J. Ripling, *Ibid.*, **15**, 641 (1971).
- [87] A. T. DiBenedetto and A. D. Wambach, *Int. J. Polym. Mater.*, **1**, 159 (1972).
- [88] A. D. S. Diggwa, *Polymer*, **15**, 101 (1974).
- [89] W. D. Bascom, R. L. Cottingham, R. L. Jones, and P. Peyser, *J. Appl. Polym. Sci.*, **19**, 2545 (1975).
- [90] P. G. Babayevskii and Ye. B. Trostyanskaya, *Vysokomol. Soedin.*, **A17**, 906 (1975).
- [91] R. A. Gledhill and A. J. Kinloch, *J. Mater. Sci.*, **10**, 1263 (1975).
- [92] R. J. Morgan and J. E. O'Neal, *Ibid.*, **12**, 1966 (1977).
- [93] S. S. Sternstein and L. Ongchin, *Polym. Prepr.*, **10**, 1117 (1969).
- [94] R. P. Kambour, *J. Polym. Sci., Macromol. Rev.*, **7**, 1 (1973).
- [95] J. Murray and D. Hull, *Polymer*, **10**, 451 (1969).
- [96] S. Rabinowitz, A. R. Krause, and P. Beadmore, *J. Mater. Sci.*, **8**, 11 (1973).
- [97] P. L. Cornes and R. N. Haward, *Polymer*, **15**, 149 (1974).
- [98] J. Murray and D. Hull, *J. Polym. Sci., Part A-2*, **8**, 1521 (1970).
- [99] P. Beahan, M. Bevis, and D. Hull, *J. Mater. Sci.*, **8**, 162 (1972).
- [100] M. J. Doyle, *J. Polym. Sci., Polym. Phys. Ed.*, **13**, 127 (1975).
- [101] M. J. Doyle, *J. Mater. Sci.*, **10**, 300 (1975).
- [102] J. Hoare and D. Hull, *Ibid.*, **10**, 1861 (1975).
- [103] M. D. Skibo, R. W. Hertzberg, and J. A. Manson, *Ibid.*, **11**, 479 (1976).
- [104] J. E. O'Neal, Unpublished.
- [105] G. Pezzin, G. Ajroldi, T. Casiraghi, C. Garbuglio, and G. Vittadini, *J. Appl. Polym. Sci.*, **16**, 1839 (1972).
- [106] R. G. Faulkner, *J. Macromol. Sci.-Phys.*, **B11**(2), 251 (1975).
- [107] R. P. Chartoff, *Polymer*, **16**, 470 (1975).
- [108] F. Zandeman, *Publ. Sci. Tech. Minist. Air (Fr.)*, **291**, Chap. 4 (1954).
- [109] S. B. Newman and I. Wolock, *J. Appl. Phys.*, **29**, 49 (1958).
- [110] I. Wolock and S. B. Newman, in *Fracture Processes in Polymeric Solids* (B. Rosen, ed.), Wiley-Interscience, New York, 1964, Chap. IIc.
- [111] R. J. Bird, J. Mann, G. Pogany, and G. Rooney, *Polymer*, **7**, 307 (1966).
- [112] M. J. Owen and R. G. Rose, *J. Mater. Sci.*, **10**, 1711 (1975).
- [113] M. J. Doyle, *Ibid.*, **10**, 159 (1975).
- [114] H. El-Hakeem, G. P. Marshall, E. I. Zichy, and L. E. Culver, *J. Appl. Polym. Sci.*, **19**, 3093 (1975).
- [115] R. J. Morgan and J. E. O'Neal, *Am. Chem. Soc., Div. Org. Coat. Plast. Chem., Prepr.*, **37**(2), 480 (1977).
- [116] R. N. Haward, B. M. Murphy, and E. F. T. White, *J. Polym. Sci., Part A-2*, **9**, 801 (1971).
- [117] D. Hull, *Acta Metall.*, **8**, 11 (1960).
- [118] N. J. Mills, *J. Mater. Sci.*, **11**, 363 (1976).

- [119] H. W. Eickner, *Environmental Exposure of Adhesive-Bonded Metal Lap Joints*, Technical Report WADC-TR-59-564, 1960.
- [120] K. E. Kimball, Forest Products Laboratory, Technical Report No. WADC-TR-55-319 (1962).
- [121] G. Epstein and Banderuk, *The Craze Phenomena and Its Effects in Filament-Wound Vessels*, 19th Annual Technical Conference, Society of Plastics Industries, Reinforced Plastics Division, 1964.
- [122] J. A. Kies, *The Strength of Glass Fibers and the Failure of Filament Wound Pressure Vessels*, Naval Research Laboratory Report 6034, 1964.
- [123] G. R. Irwin, *Moisture Assisted Slow Crack Extension in Glass Plates*, Naval Research Laboratory Memorandum Report 1678, 1966.
- [124] L. H. Sharpe, *Appl. Polym. Symp.*, **3**, 353 (1966).
- [125] I. G. Romanenkov and Z. P. Machavariari, *Sov. Plast.*, **5**, 49 (1966).
- [126] K. H. G. Ashbee, F. C. Frank, and R. C. Wyatt, *Proc. R. Soc.*, **A300**, 415 (1967).
- [127] D. J. Steel, *Trans. Plast. Inst.*, **35**, 116, 429 (1967).
- [128] I. G. Romanenkov, *Sov. Plast.*, **6**, 74 (1967).
- [129] J. L. Parham and E. A. Verchot, U.S. Army Missile Command Report No. RS-TR-67-6 (1967).
- [130] N. C. W. Judd, Royal Aircraft Establishment, Farnborough, Final Report RAE-TR-67042 (1967).
- [131] I. Wolcock and H. P. Ewing, *Proceedings of 12th National SAMPE Meeting*, 1967.
- [132] R. Slysh, *Am. Chem. Soc., Org. Coat. Plast. Chem., Prepr.*, **28**(1), 456 (1968).
- [133] J. R. Griffith and J. E. Quick, *Ibid.*, **28**(1), 476 (1968).
- [134] L. A. Liebowitz, *Ibid.*, **28**(1), 479 (1968).
- [135] D. I. James, R. H. Norman, and M. H. Stone, *Plast. Polym.*, **36**, 21, 121 (1968).
- [136] V. R. Dietz, *Interaction of Water Vapor with Pristine E-Glass Fiber*, Naval Research Laboratory Report 6812 (1968).
- [137] J. C. Halpin and N. J. Pagano, *Proceedings 6th Annual Meeting Society Engineering Science*, Springer, New York, 1969.
- [138] J. L. Parham, U.S. Army Missile Command Report No. RS-TR-70-8, (1970).
- [139] T. R. Walton and J. E. Cowling, Naval Research Laboratory Report 7077, 1970.
- [140] N. Fried, in *Mechanics of Composite Materials* (F. W. Wendt, H. Liebowitz, and N. Perrone, eds.), Pergamon, New York, 1970, p. 813.
- [141] J. L. Parham, U.S. Army Missile Command Report No. RL-TR-71-S, 1971.
- [142] R. B. Bonk and D. A. Teetsel, Picatinny Arsenal Technical Report 2102 (Addendum No. 9), 1971.

- [143] P. W. R. Beaumont and B. Harris, *The Effects of Environment or Fatigue and Crack Propagation in Carbon-Fibre-Reinforced Epoxy Resin*, Plastics Institute, International Conference on Carbon Fibres, Their Composites and Applications, London, Paper 49, A71-20892, 1971.
- [144] M. L. Sartelli and R. A. Simon, *Proceedings of the 26th SPI Annual Conference*, 1971.
- [145] Convair Aerospace Final Report, *Development of Design Data for Graphite Reinforced Epoxy and Polyimide Composites*, Contract NASA-26198, NASA-MSFC, 1970-71.
- [146] Convair Aerospace Final Report, *Advanced Composite Applications for Spacecraft and Missiles*, Contract F33615-70-C-1442, 1970-71.
- [147] J. C. Leslie, *Hercules Analysis of the Composite Aging Problem*, Report No. H400-12-1-6, 1971.
- [148] C. E. Browning, *The Effects of Moisture on the Properties of High Performance Structural Resins and Composites*, Project No. 7340 AFML, 1971.
- [149] A. P. Penton and J. L. Perry, *Investigation on Graphite Filament Reinforced Plastic Composites*, Philco-Ford, Aero. Div. Final Report, Contract No. N00019-70-C-0439, 1971.
- [150] R. D. Edzell, *The Effects of Moisture Sorption on Epoxies*, Naval Ordnance Laboratory Report NOLTR72-108, 1972.
- [151] H. L. Young and W. L. Greever, *6th St. Louis Symposium, Composite Materials in Engineering*, 1972.
- [152] W. L. Greever, *High-Temperature Strength Degradation of Composites during Ambient Aging, Hercules, Inc.*, Final Report, Contract No. 70-000-22 to General Dynamics, Convair Contract NAS 8-27435, 1972.
- [153] L. M. Lackman, D. O. Losee, J. A. Rohlen, and T. T. Matoi, *Advanced Composites Data for Aircraft Structural Design*, AFML-TR-70-58, 1972.
- [154] C. E. Browning, *The Effects of Moisture on the Properties of High Performance Epoxy Resins and Composites*, Technical Report AFML-TR-72-94, 1972.
- [155] J. R. Romans, A. G. Sands, and J. E. Cowling, *Ind. Eng. Chem., Prod. Res. Dev.*, **11**(3), 261 (1972).
- [156] J. Hertz, *Investigation into the High-Temperature Strength Degradation of Fiber-Reinforced Resin Composites during Ambient Aging, General Dynamics, Convair*, Final Report GDCA-DBG73-005, Contract NAS 8-27435, 1973.
- [157] C. E. Browning and J. M. Whitney, *The Effects of Moisture on the Properties of High Performance Structural Resins and Composites*, Society of the Plastics Industry, Reinforced Plastics Division, Proceedings of the 28th Annual Technical Conference, Washington, D.C., 1973.

- [158] J. F. Carpenter, *Moisture Sensitivity of Epoxy Composites and Structural Adhesives*, McDonnell Aircraft Report MDC A2640, 1973.
- [159] A. Blaga and R. S. Yamasaki, *J. Mater. Sci.*, **8**, 654, 1331 (1973).
- [160] K. E. Hofer, Jr., N. Rao, and D. Larsen, *Development of Engineering Data on the Mechanical and Physical Properties of Advanced Composite Materials*, Technical Report AFML-TR-72-205, 1974.
- [161] J. L. Kardos, M. J. Michno, Jr., and T. A. Duffy, *Investigation of High Performance Short Fiber Reinforced Plastics*, Washington Univ., Naval Air Systems Command Final Technical Report, Contract No. N00019-73-0358, 1974.
- [162] C. E. Browning, *Effects of Moisture on the Properties of High Performance Structural Resins and Composites*, Composite Materials-Testing and Design, 3rd Conference, ASTM, ASTM STP546, 1974, p. 284.
- [163] D. H. Kaeble, P. J. Dynes, L. W. Crane, and L. Maus, *J. Adhes.*, **7**, 25 (1975).
- [164] O. Ishai, *Polym. Eng. Sci.*, **15**, 486, 491 (1975).
- [165] R. M. Verette, *Temperature/Humidity Effects on the Strength of Graphite/Epoxy Laminates*, AIAA Paper No. 75-1011, 1975.
- [166] E. L. McKague, Jr., J. E. Halkias, and J. D. Reynolds, *J. Compos. Mater.*, **9**, 2 (1975).
- [167] D. A. Scola, *A Study to Determine the Mechanisms of S-Glass/Epoxy Resin Composite Degradation Due to Moisture and Solvent Environments*, The Society of Plastics Industry, 30th Annual Technical Conference, Reinforced Plastics/Composites Institute, 1975.
- [168] E. L. McKague, *Life Assurance of Composite Structures*, Technical Report AFML-TR-75-51, 1975.
- [169] C. H. Shen and G. S. Springer, *J. Compos. Mater.*, **10**, 2 (1976).
- [170] G. Pritchard, R. G. Rose, and N. Taneja, *J. Mater. Sci.*, **11**, 718 (1976).
- [171] G. A. Pogany, *Polymer*, **17**, 690 (1976).
- [172] R. J. Young and P. W. R. Beaumont, *J. Mater. Sci.*, **11**, 776 (1976).
- [173] Y. Weitsman, *J. Compos. Mater.*, **10**, 193 (1976).
- [174] C. E. Browning, G. E. Husman, and J. M. Whitney, *Moisture Effect in Epoxy Matrix Composites*, *Composite Materials-Testing and Design*, 4th Conference, ASTM, STP, 1976.
- [175] AFML/AFOSR, *Mechanics of Composites Review*, Dayton, 1976.
- [176] R. L. Levy, *Mechanism by which Moisture Influences the Elevated Temperature Properties of Epoxy Resins*, Technical Report AFML-TR-76-190, 1976.
- [177] C. E. Browning, "The Mechanism of Elevated Temperature Property Losses in High Performance Structural Epoxy Resin Matrix Materials after Exposures to High Humidity Environments," Ph.D. Thesis, University of Dayton, 1976.
- [178] R. E. Bohlmann and E. A. Derby, *Moisture Diffusion in Graphite/*

- Epoxy Laminates: Experimental and Predicted*, AIAA Paper No. 77-399, 1977.
- [179] R. L. Levy, *Mechanism of Epoxy Moisture Effects*, Technical Report AFML-TR-77-41, 1977.
- [180] M. L. Williams, R. F. Landel, and J. D. Ferry, *J. Am. Chem. Soc.*, **77**, 3701 (1955).
- [181] F. Bueche, *J. Chem. Phys.*, **24**, 418 (1956).
- [182] M. H. Cohen and D. Turnbull, *Ibid.*, **31**, 1164 (1959).
- [183] F. N. Kelley and F. Bueche, *J. Polym. Sci.*, **50**, 549 (1961).
- [184] L. G. Dowell and A. P. Rinfret, *Nature (London)*, **188**, 1144 (1960).
- [185] M. Sugisaki, H. Suga, and S. Seki, *Bull. Chem. Soc. Jpn.*, **41**, 2591 (1968).
- [186] A. Korosi and B. M. Fabus, *Anal. Chem.*, **40**, 157 (1968).
- [187] N. H. Fletcher, *The Chemical Physics of Ice*, Cambridge University Press, 1970, Chap. 3.
- [188] R. Frank, *Water*, Vol. 1, Plenum, New York, 1972.
- [189] Y. Y. Tan and G. Challa, *Polymer*, **17**, 739 (1976).
- [190] L. E. Nielsen, *Mechanical Properties of Polymers*, Reinhold, New York, 1962, p. 27.
- [191] J. Crank, *The Mathematics of Diffusion*, Clarendon, Oxford, 1957.
- [192] C. J. Van Amerongen, *Rubber Chem. Technol.*, **37**, 871 (1964).
- [193] A. J. King, "Multicomponent Diffusion (1-D)," in *Computer Program User's Manual No. 61014*, Hercules Corporation, 1976.
- [194] J. Crank and G. S. Park, *Diffusion in Polymers*, Academic, London, 1958, Chap. 5.
- [195] E. W. Russel, *Nature (London)*, **165**, 91 (1950).
- [196] I. Narisawa, *J. Polymer. Sci., A-2*, **10**, 1789 (1972).
- [197] D. A. Blackadder and J. S. Keniry, *J. Appl. Polym. Sci.*, **17**, 351 (1973).
- [198] C. H. M. Jacques, H. B. Hopfenberg, and V. Stannett, *Polym. Eng. Sci.*, **13**, 81 (1973).
- [199] C. Clark-Monks and B. Ellis, *J. Colloid Interface Sci.*, **44**, 37 (1973).
- [200] H. Yasuda and A. Peterlin, *J. Appl. Polym. Sci.*, **17**, 433 (1973).
- [201] Y. J. Chang, C. T. Chen, and A. V. Tobolsky, *J. Polym. Sci., Polym. Phys. Ed.*, **12**, 1 (1974).
- [202] G. Skirrow and K. R. Young, *Polymer*, **15**, 771 (1974).
- [203] D. R. Paul, *J. Polym. Sci., A-2*, **7**, 1811 (1969).
- [204] E. Drioli, L. Nicolais, and A. Ciferri, *J. Polym. Sci., Polym. Chem. Ed.*, **11**, 3327 (1973).
- [205] H. Hoso and W. N. Findley, *Polym. Eng. Sci.*, **13**, 225 (1973).
- [206] S. A. Steen, S. K. Sen, and A. K. Rao, *J. Macromol. Sci.-Phys.*, **B-10**, 507 (1974).
- [207] Z. Miyagi and H. Tanaka, *Polymer*, **16**, 441 (1975).

- [208] P. E. Rouse, Jr., *J. Am. Chem. Soc.*, **69**, 1068 (1947).
- [209] R. M. Barrer and J. A. Barrie, *J. Polym. Sci.*, **28**, 377 (1958).
- [210] J. A. Barrie and D. Machin, *Trans. Faraday Soc.*, **67**, 244 (1971).
- [211] K. Matsushige, E. Baer, and S. V. Radcliffe, *J. Macromol. Sci. - Phys.*, **B11**(4), 565 (1975).
- [212] H. E. Bair and G. E. Johnson, *Analytical Calorimetry*, Vol. 4 (R. S. Porter and J. F. Johnson, eds.), Plenum, New York, 1976.
- [213] D. C. Ruhmann and E. M. Wu, *Am. Chem. Soc., Div. Org. Coat. Plast. Chem., Prepr.*, **31**(1), 501 (1971).
- [214] A. S. Michaels, H. J. Bixler, and H. B. Hopfenberg, *J. Appl. Polym. Sci.*, **12**, 991 (1968).
- [215] H. B. Hopfenberg, R. H. Holley, and V. T. Stannett, *Polym. Eng. Sci.*, **9**, 242 (1969).
- [216] R. H. Holley, H. B. Hopfenberg, and V. T. Stannett, *Ibid.*, **10**, 376 (1970).
- [217] B. R. Baird, H. B. Hopfenberg, and V. T. Stannett, *Ibid.*, **11**, 4, 274 (1971).
- [218] C. H. M. Jacques, H. B. Hopfenberg, and V. Stannett, *J. Appl. Polym. Sci.*, **18**, 223 (1974).
- [219] R. S. Stein and A. V. Tobolsky, *Text. Res. J.*, **18**, 302 (1948).
- [220] L. R. G. Treloar, *The Physics of Rubber Elasticity*, 2nd ed., Clarendon, Oxford, 1958.
- [221] B. H. Zimm and J. L. Lundberg, *J. Phys. Chem.*, **13**, 276 (1956).
- [222] A. H. Gent and T. H. Kuon, *Macromolecules*, **2**, 262 (1969).
- [223] A. H. Gent and T. H. Kuon, *J. Polym. Sci., A-2*, **9**, 927 (1971).
- [224] S. S. Sternstein, *J. Macromol. Sci. - Phys.*, **B6**(1), 243 (1972).
- [225] D. G. LeGrand, *J. Appl. Polym. Sci.*, **20**, 1573 (1976).
- [226] C. Gurney and Z. Borysowsky, *Proc. Phys. Soc.*, **A61**, 446 (1948).
- [227] B. Maxwell and L. F. Rahm, *Ind. Eng. Chem.*, **41**, 1988 (1949).
- [228] J. J. Benbow, *Proc. Phys. Soc.*, **B78**, 970 (1961).
- [229] H. A. Stuart, G. Markowski, and D. Jeschke, *Kunststoffe*, **54**, 618 (1964).
- [230] J. B. Howard, in *Engineering Design for Plastics* (E. Baer, ed.), Reinhold, New York, 1964, p. 742.
- [231] E. H. Andrews and L. Bevan, *Physical Basis of Yield and Fracture*, Institute of Physics, London, 1966, p. 209.
- [232] C. Gurney and J. Hunt, *Proc. R. Soc. London*, **A299**, 509 (1967).
- [233] G. A. Bernier and R. P. Kambour, *Macromolecules*, **1**, 393 (1968).
- [234] R. J. Bergen, Jr., *SPE J.*, **24**, 77 (1968).
- [235] I. S. Lyakhovich, I. N. Musayelyan, and N. M. Chirkov, *Vysokomol. Soedin.*, **A10**, 715 (1968).
- [236] G. P. Marshall, L. E. Culver, and J. G. Williams, *Proc. R. Soc.*, **A319**, 165 (1970).

- [237] G. Menges and H. Schmidt, *Plast. Polym.*, **38**, 13 (1970).
- [238] G. P. Marshall, L. E. Culver, and J. G. Williams, *Ibid.*, **38**, 95 (1970).
- [239] R. P. Kambour, E. E. Romagosa, and C. L. Gruner, *Macromolecules*, **5**, 335 (1972).
- [240] P. I. Vincent and S. Raha, *Polymer*, **13**, 283 (1972).
- [241] M. F. Parrish and N. Brown, *Nature (London), Phys. Sci.*, **237**(77), 122 (1972).
- [242] N. Brown and M. F. Parrish, *J. Polym. Sci., Part B*, **10**, 777 (1972).
- [243] A. Hiltner, J. A. Kastelic, and E. Baer, in *Advances in Polymer Science and Engineering* (K. D. Pae, D. R. Morrow, and Yu Chen, eds.), Plenum, New York, 1972, p. 335.
- [244] E. H. Andrews and L. Bevan, *Polymer*, **13**, 337 (1972).
- [245] I. D. Graham, G. P. Marshall, and J. G. Williams, *Proceedings of the International Conference on Dynamic Crack Propagation*, Noordhoff, Leyden, 1972, p. 261.
- [246] H. G. Olf and A. Peterlin, *Polymer*, **14**, 78 (1973).
- [247] N. Brown, *J. Polym. Sci., (Polym. Phys. Ed.)*, **11**, 2099 (1973).
- [248] S. Fischer and N. Brown, *J. Appl. Phys.*, **44**, 4322 (1973).
- [249] E. H. Andrews, G. M. Levey, and J. Willis, *J. Mater. Sci.*, **8**, 1000 (1973).
- [250] R. P. Kambour, C. L. Gruner, and E. E. Romagosa, *J. Polym. Sci., Polym. Phys. Ed.*, **11**, 1879 (1973).
- [251] H. G. Olf and A. Peterlin, *Ibid.*, **12**, 2209 (1974).
- [252] E. H. Andrews and G. M. Levy, *Polymer*, **15**, 599 (1974).
- [253] J. G. Williams, G. P. Marshall, I. Graham, and E. L. Zichy, *Pure Appl. Chem.*, **39**, 275 (1974).
- [254] G. P. Marshall and J. G. Williams, in *Deformation and Fracture of High Polymers* (H. H. Kausch, J. A. Hassell, and R. I. Jaffee, eds.), Plenum, New York, 1974, p. 557.
- [255] D. McCammond and C. A. Ward, *Polym. Eng. Sci.*, **14**, 831 (1974).
- [256] B. L. Earl, R. J. Loneragan, J. Markham, and M. Crook, *J. Appl. Polym. Sci.*, **18**, 245 (1974).
- [257] B. L. Earl, M. Crook, R. J. Loneragan, J. H. T. Johns, and J. Markham, *Ibid.*, **18**, 857 (1974).
- [258] Y. W. Mai, *J. Mater. Sci.*, **9**, 1896 (1974).
- [259] J. R. Martin and J. F. Johnson, *J. Appl. Polym. Sci.*, **18**, 3227 (1974).
- [260] J. G. Williams and G. P. Marshall, *Proc. R. Soc. London*, **A342**, 55 (1975).
- [261] N. Brown and Y. Imai, *J. Appl. Phys.*, **46**, 4130 (1975).
- [262] N. Brown and Y. Imai, *J. Polym. Sci., Polym. Lett. Ed.*, **13**, 511 (1975).
- [263] A. Peterlin and H. G. Olf, *J. Polym. Sci., Polym. Symp.*, **50**, 243 (1975).
- [264] G. W. Weidmann and J. G. Williams, *Polymer*, **16**, 921 (1975).
- [265] Y. W. Mai, *J. Mater. Sci.*, **10**, 943 (1975).

- [266] Y. Imai and N. Brown, *Ibid.*, **11**, 417, 425 (1976).
- [267] I. D. Graham, J. G. Williams, and E. L. Zichy, *Polymer*, **17**, 439 (1976).
- [268] Y. W. Mai, *J. Mater. Sci.*, **11**, 303 (1976).
- [269] Y. W. Mai and A. G. Atkins, *Ibid.*, **11**, 677 (1976).
- [270] R. J. Morgan, L. E. Nielsen, and R. Buchdahl, *Polym. Prepr.*, **12**, 687 (1971).
- [271] R. J. Morgan and L. E. Nielsen, *J. Polym. Sci., Polym. Phys. Ed.*, **10**, 1575 (1972).
- [272] G. R. Irwin, *Handbuch der Physik*, Springer, Berlin, 1958, p. 551.
- [273] J. C. Fisher, *J. Appl. Phys.*, **19**, 1062 (1948).
- [274] E. G. Shafrin, in *Polymer Handbook*, 2nd ed. (J. Brandrup and E. H. Immergut, eds.), Wiley, New York, 1975, Chap. III-221.
- [275] L. E. Nielsen and T. B. Lewis, *J. Polym. Sci., Part A-2*, **7**, 1705 (1969).
- [276] R. J. Morgan, *J. Mater. Sci.*, **9**, 1219 (1974).
- [277] D. K. Hale, *Ibid.*, **11**, 2105 (1976).
- [278] A. Blaga and R. S. Yamasaki, *Ibid.*, **11**, 1513 (1976).

APPENDIX D: Epoxies as Composite Matrices, Org. Plast.
Coat. Preprints (ACS) 38, 485 (1978)

Epoxies as Composite Matrices*

Roger J. Morgan and James E. O'Neal
McDonnell Douglas Research Laboratories
McDonnell Douglas Corporation
St. Louis, Missouri 63166

Introduction

High-performance epoxy-graphite or epoxy-boron fiber composites are often utilized in extreme service environments, particularly in the aerospace industry. A number of laboratory and field studies have indicated that the combined effects of sorbed moisture and thermal environment can cause significant changes in the mechanical response of these materials [1,2]. The long-term, in-service durability of epoxy composites is unknown primarily because:

- (1) long-term, in-service aging characteristics are difficult to simulate by short-term laboratory and/or field tests, and
- (2) the basic phenomena responsible for the changes in the epoxy matrix, the epoxy-fiber interfacial region, and the overall mechanical response of the composite have not all been identified and/or understood.

There are three basic areas necessary for meaningful epoxy durability predictions:

- (1) the structure of epoxies, their modes of deformation and failure, and the structural parameters controlling these modes;
- (2) the effects of sorbed moisture on the epoxy structure, properties, and modes of deformation and failure; and
- (3) the complex fabrication and environmental phenomena affecting the durability in service environments.

Experimental

Material

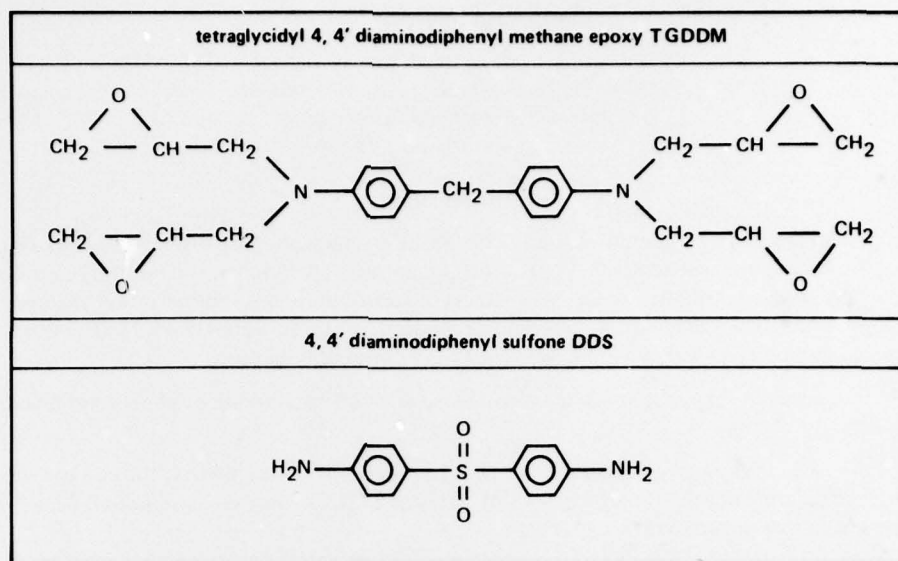
The primary epoxy system considered in this paper is diaminodiphenyl sulfone (Ciba-Geigy, Eporal)-cured tetraglycidyl 4,4' diaminodiphenyl methane (Ciba Geigy, MY720) epoxy (TGDDM-DDS). The structures of the unreacted TGDDM epoxide and DDS amine monomers are illustrated in Fig. 1. This TGDDM-DDS epoxy system is the primary matrix utilized in aerospace high-performance epoxy-fiber composites.

Experiments

TGDDM-DDS epoxy specimens suitably shaped for tensile mechanical property, fracture topography, x-ray emission spectroscopy, and density measurements were prepared in silicone rubber molds and cured for 1 h at 150°C and 5 h at 177°C. Thinner epoxy films for physical structure studies by bright-field transmission electron microscopy and electron diffraction studies were prepared between salt crystals. TGDDM-DDS epoxies of various initial compositions (10-35 wt% DDS) exposed to various environments were investigated.

A table-model tensile tester (Instron TM-S-1130) was used to determine the mechanical properties. An electron microscope (JEOL model JEM 100B) was used in the scanning mode for fracture topography and x-ray emission spectroscopy studies and in the transmission mode for the diffraction and bright-field studies. An optical microscope (Zeiss Ultraphot II) was also used for fracture topography studies. Density measurements were performed on a Mettler M-5 microbalance.

*Research sponsored by the Air Force Office of Scientific Research/AFSC, United States Air Force, under Contract No. F44620-76-C-0075. The United States Government is authorized to reproduce and distribute reprints for governmental purposes notwithstanding any copyright notation hereon.



GP77-0731-4

Figure 1 The TGDDM-DDS epoxy system.

Results and Discussion

Structure-Property Studies

The major structural parameters controlling the modes of deformation and failure and the mechanical response of epoxies are the crosslinked network structure and the microvoid characteristics [3-11].

Generally, the cure process and final network structure of epoxies have been estimated from the chemistry of the system, if the curing reactions are known and assumed to go to completion, and experimental techniques such as infrared spectra, swelling, dynamic mechanical, thermal conductivity, and differential scanning calorimetry measurements [12-26]. However, in many epoxy systems, the chemical reactions are diffusion controlled and incomplete and there is a heterogeneous distribution in the crosslink density.

The TGDDM-DDS epoxy system, cured at 177°C, is not highly crosslinked despite the tetra-functionality of the TGDDM epoxide. We have monitored the tensile mechanical properties of the TGDDM-DDS epoxy system as a function of composition (10-35 wt% DDS) and test temperature (23°-250°C). Figure 2 is a plot of tensile strength, ultimate elongation, and Young's modulus from 23°-250°C for a TGDDM-DDS (35 wt% DDS) epoxy. The gradual decrease in tensile strength and modulus and the increase in ultimate elongation from 200°-250°C suggests that a broad glass transition exists in this temperature range. Ultimate extensions of $\geq 15\%$ near T_g for epoxies with 15-35 wt% DDS suggests these glasses are not highly crosslinked.

A plot of T_g versus initial DDS concentration, shown in Fig. 3, confirms that these epoxies are not highly crosslinked. [The temperatures representative of these broad T_g 's were taken as those temperatures at which the room-temperature modulus (E_{RT}) decreased by half (i.e., $E_{RT}/2$)]. From 10-25 wt% DDS, the T_g rises with increasing DDS concentration because of corresponding increases in molecular weight and/or crosslink density. The T_g exhibits a maximum of $\sim 250^\circ\text{C}$ at ~ 30 wt% DDS and subsequently decreases for higher DDS concentrations. For epoxies prepared from > 25 wt% DDS, steric and diffusional restrictions evidently inhibit additional epoxy-amine reactions. Above ~ 30 wt% DDS concentrations, unreacted DDS molecules plasticize the epoxy system and decrease the T_g . However, 37 wt% DDS is required to consume half the TGDDM epoxide groups when only epoxide/primary-amine reactions occur. Hence, the maximum in T_g at 30 wt% DDS suggests that less than half the TGDDM epoxide groups have reacted when 100% of the DDS is consumed.

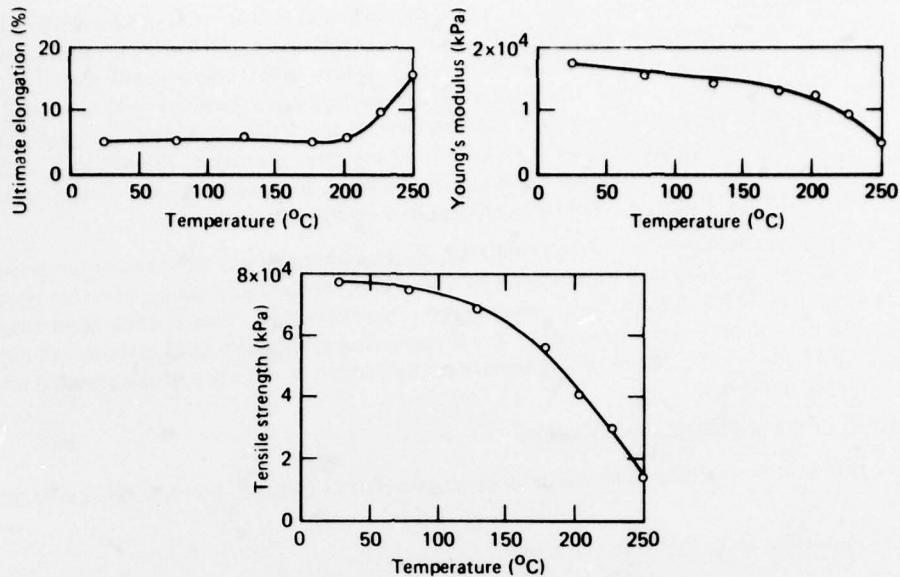
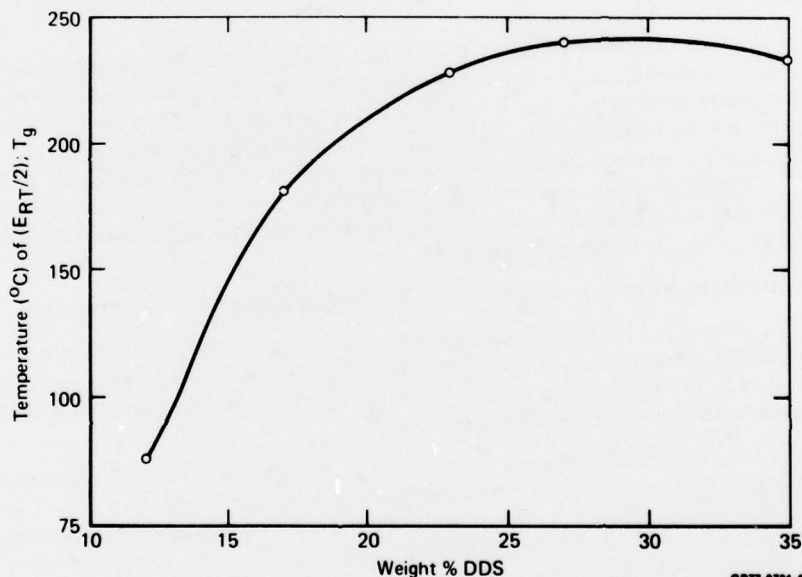


Figure 2 Tensile strength, ultimate elongation, and Young's modulus versus temperature for TGDDM-DDS (35 wt% DDS) epoxy (10^{-2} /min strain rate).

QP77-0731-8



QP77-0731-10

Figure 3 T_g versus initial wt% of DDS in TGDDM-DDS epoxies.

After cure, aggregates of unreacted DDS molecules have been detected in TGDDM-DDS (>25 wt% DDS) epoxies by both electron diffraction and x-ray emission spectroscopy studies. Electron diffraction patterns were obtained from thin films prepared from >25 wt% DDS that were similar to those obtained from the unreacted DDS crystals. The aggregates of unreacted DDS molecules crystallize after cooling the epoxy from its cure temperature. In addition, x-ray emission spectroscopy studies of fracture surfaces have detected regions of high sulfur content which are probably clusters of unreacted DDS molecules.

The TGDDM-DDS epoxy networks consist of regions of high-crosslink density as indicated by bright-field transmission electron microscopy in the 2-15 nm range and by scanning electron microscopy in the 1-5 μ m range.

Microvoids can have a deleterious effect on the mechanical properties of epoxies by acting as stress concentrators and also on the durability by serving as a sink for the accumulation of sorbed moisture. To obtain a TGDDM-DDS epoxy system with a high T_g , which is advantageous to limit the deleterious effects of sorbed moisture on this epoxy, requires ~ 30 wt% DDS in the initial TGDDM-DDS mixture (see Fig. 3). However, at these DDS concentrations, aggregates of unreacted DDS molecules can be trapped in the epoxy after the system forms a glass at the cure temperature. Thermal-anneal/moisture-sorption/mechanical-property studies indicate that elimination of these aggregates during cure results a microvoids in the glass.

The fracture topographies of TGDDM-DDS epoxies fractured as a function of temperature and strain-rate indicate that these glasses predominantly deform and fail by a crazing process. These epoxies also deform to a limited extent by shear banding as indicated by regular right-angle steps in the fracture topography. The deformation of TGDDM-DDS epoxies will depend on the size and concentration of any regions of high-crosslink density and the material interconnecting such regions.

Effects of Sorbed Moisture on Epoxies

The pertinent basic physical phenomena in epoxies induced and/or modified by sorbed moisture are

- (1) lowering of T_g by sorbed moisture,
- (2) diffusion of sorbed moisture,
- (3) swelling stresses induced by sorbed moisture, and
- (4) modification of the deformation and failure modes and the mechanical response by sorbed moisture.

The sorption of moisture by epoxies lowers their T_g 's and correspondingly causes them to soften at lower temperatures. Kelley and Bueche [27] have derived an expression relating the T_g of a polymer-diluent system to that of the T_g 's of the two components. This expression assumes that the free volume contributed by the diluent is additive to that of the polymer and that the free volumes of the mixture and components at their T_g 's are a universal constant. However, the T_g 's of TGDDM-DDS epoxy-moisture systems, containing equilibrium amounts of sorbed moisture, are considerably lower than those predicted by the Kelley-Bueche expression. This discrepancy could be caused by the following phenomena:

- (1) the strong hydrogen-bonding capability of water could produce anomalous effects or
- (2) if the epoxy has a heterogeneous-crosslink density distribution, moisture will preferentially sorb in regions of low-crosslink density. The regions of low-crosslink density control the flow processes that occur at T_g . Hence, the depression of T_g may be greater than that expected for a homogeneous distribution of sorbed water.

The durability of epoxies and epoxy-composites in many aerospace service environments depends on the degree of deterioration of the high-temperature mechanical properties caused by the plasticizing effect of sorbed moisture. The previous relative-humidity/time/temperature exposure of the epoxy component and the diffusion characteristics of moisture in this component determine the moisture profile and the resultant mechanical response of the material. Hence, the diffusion characteristics of moisture in an epoxy component are critical factors for predicting mechanical response and durability in a given service environment. Fickian diffusion has been utilized successfully as the controlling mechanism to predict the concentration and distribution of sorbed moisture [28-30] and corresponding deterioration of high-temperature mechanical properties. Moisture sorption can, however, cause formation of permanent damage regions or modification of the epoxy network which will result in deviations from Fickian diffusion and accelerate moisture sorption. These structural modifications can be

- (1) bond cleavage or crack formation as a result of swelling stresses and/or relaxation of fabrication stresses,
- (2) formation of additional crosslinks by moisture-enhanced mobility of unreacted groups, and

(3) modification of the free volume and/or microvoid characteristics.

Sorbed moisture causes epoxies to swell [1, 31, 32]. The swelling stresses caused by moisture gradients, together with other stresses inherent in the material, such as fabrication stresses, can be sufficiently large to cause localized fracture of the polymer [32]. However, to compute the moisture sorption levels for specific environmental conditions that cause network modification and subsequent growth of permanent damage regions in epoxies requires a detailed knowledge of the network structure and the stress levels in the presence of moisture where damage occurs in the network. This type of information is not yet available.

Sorbed moisture acts as a solvent crazing agent in TGDDM-DDS epoxies. The microscopic yield stress (that stress at the onset of non-linear behavior in the tensile stress-strain curve) is shown in Fig. 4 as a function of test temperature for both initially wet and dry TGDDM-DDS (27 wt% DDS) epoxies. The microscopic yield stress of the wet epoxies is lower than that of the dry glasses from room temperature to 150°C. Above 150°C, the yield stresses of the wet and dry epoxies merge because water is eliminated from the wet specimens during the test. From room temperature to 150°C, the lower yield stresses of the epoxies containing 4 wt% sorbed moisture, relative to those of the dry epoxies, are equivalent to lowering the dry yield stresses 100°-125°C on the temperature scale. However, the T_g of this epoxy is lowered only ~60°C by ~4 wt% sorbed moisture. These observations imply that the craze cavitation stress is more susceptible to sorbed moisture than the main T_g . Hence, the magnitude T_g is lowered on the temperature scale by sorbed moisture cannot be utilized to predict any modification of the formation of permanent damage regions in these epoxies. The craze cavitation stress is more sensitive to sorbed moisture than the T_g for a heterogeneous distribution of moisture in the epoxy. High moisture concentrations in localized regions enhance cavitation by plasticization which results in a lower local shear yield stress. The overall T_g of the epoxy, however, is generally measured on a macroscopic level and is not sensitive to high local moisture concentrations. The large mirror-like region and the numerous cavities observed in the fracture topography initiation region of wet epoxies also indicate that the craze initiation and growth processes are enhanced by sorbed moisture.

The ease of diffusion of moisture through a porous craze structure and its accumulation near the craze tip where it enhances cavitation must be considered a significant mechanism for the

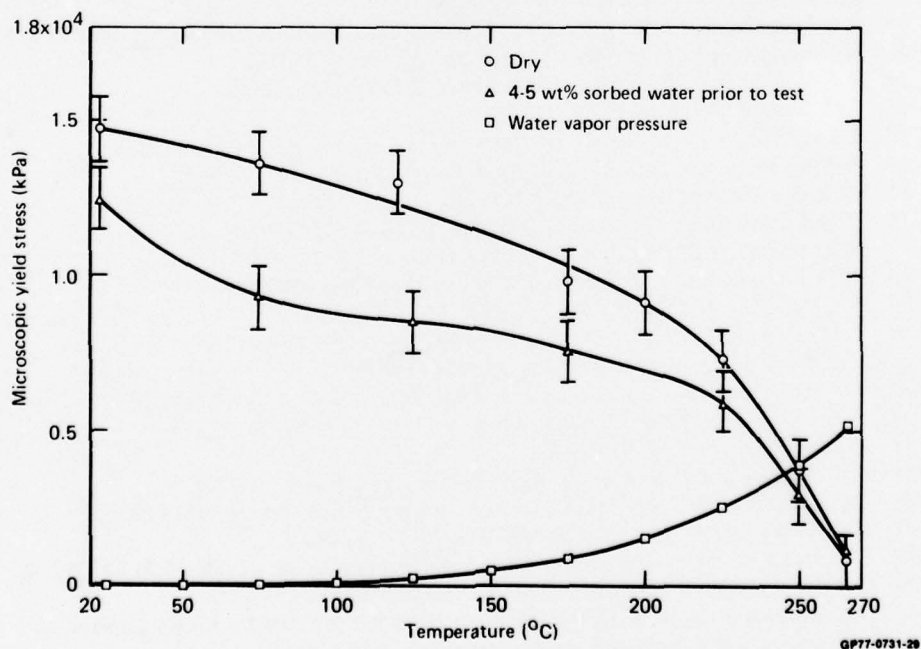


Figure 4 Microscopic yield stress (strain-rate $\sim 10^{-2}$ /min) of both initially wet (~4 wt% sorbed moisture) and dry TGDDM-DDS (27 wt% DDS) epoxies as a function of temperature.

growth of permanent damage regions in these glasses in humid environments, particularly in view of the low stress levels at which cavitation generally occurs in polymer glasses.

Factors that Control the Durability of Epoxies

In the service environment, the durability of epoxies depends on a complex number of interacting phenomena. The factors that control the critical path to ultimate failure or unacceptable damage depend specifically on the particular environmental conditions. In the presentation, all possible factors that generally effect the durability of epoxies in service environments are reviewed, and some of the critical environments that affect the durability of epoxies and the difficulties in predicting the long-term durability of epoxies are discussed. These factors include the network structure, microvoid characteristics and fabrication stresses, and environmental factors such as service stresses, humidity, temperature, and solar radiation.

Conclusion

TGDDM-DDS epoxies are not highly crosslinked because of steric and diffusional restrictions; they deform and fail predominantly by a crazing process. The durability of TGDDM-DDS epoxies depends on a complex number of interacting phenomena, including sorbed moisture which acts as a plasticizer and a swelling and solvent crazing agent.

References

1. *Air Force Durability Workshop, Battelle Columbus Laboratories, September (1975).*
2. *Air Force Conference on the Effects of Relative Humidity and Temperature on Composite Structures, University of Delaware, March, 1976. AFOSR-TR-77-0030 (1977).*
3. R.J. Morgan and J.E. O'Neal, *Org. Plast. Coat. Preprints (ACS)* **34(2)**, 195 (1974).
4. R.J. Morgan and J.E. O'Neal, *Polym. Plast. Tech. and Eng.* **5(2)**, 173 (1975).
5. R.J. Morgan and J.E. O'Neal, *Polymer Preprints* **16(2)**, 610 (1975).
6. R.J. Morgan and J.E. O'Neal, in *Toughness and Brittleness of Plastics, Advances in Chemistry Series 154, Ch. 2 (1976).*
7. R.J. Morgan and J.E. O'Neal, *Org. and Plast. Coat. Preprints (ACS)* **36(2)**, 689 (1976).
8. R.J. Morgan and J.E. O'Neal, in *Chemistry and Properties of Crosslinked Polymers, Ed. S.S. Labana, Academic Press, 1977, p. 289.*
9. R.J. Morgan and J.E. O'Neal, *Org. and Plast. Coat. Preprints (ACS)* **37(2)**, 480 (1977).
10. R.J. Morgan and J.E. O'Neal, *J. Mater. Sci.* **12**, 1966 (1977).
11. R.J. Morgan and J.E. O'Neal, *J. Macromol. Sci-Phys. (in press).*
12. T.K. Kwei, *J. Polym. Sci.* **A1**, 2977 (1963).
13. A.S. Kenyon and L.E. Nielsen, *J. Macromol. Sci.-Chem.* **A3(2)**, 275 (1969).
14. R.P. Krehling and D.E. Kline, *J. Appl. Polym. Sci.* **13**, 2411 (1969).
15. J.P. Bell, *J. Polym. Sci.* **A-2**, **8**, 417 (1970).
16. T. Murayama and J.P. Bell, *J. Polym. Sci.* **A-2**, **8**, 437 (1970).
17. M.A. Acitelli, R.B. Prime and E. Sacher, *Polymer* **12**, 335 (1971).
18. R.G.C. Arridge and J.H. Speake, *Polymer* **12**, 443 and 450 (1972).
19. P.V. Sidiyakin, *Vysokomol. soyed.*, **A14**, No. 5, 979 (1972).
20. T. Hirai and D.E. Kline, *J. Appl. Polym. Sci.* **16**, 3145 (1972).
21. R.B. Prime and E. Sacher, *Polymer* **13**, 455 (1972).
22. P.G. Babayevsky and J.K. Gillham, *J. Appl. Polym. Sci.* **17**, 2067 (1973).
23. T. Hirai and D.E. Kline, *J. Appl. Polym. Sci.* **17**, 31 (1973).
24. E. Sacher, *Polymer* **14**, 91 (1973).
25. D.A. Whiting and D.E. Kline, *J. Appl. Polym. Sci.* **18**, 1043 (1974).
26. J.K. Gillham, J.A. Benci and A. Noshay, *J. Appl. Polym. Sci.* **18**, 951 (1974).
27. F.N. Kelley and F. Bueche, *J. Polym. Sci.* **50**, 549 (1961).
28. E.L. McKague, *Life Assurance of Composite Structures, AFML-TR-75-51 (1975).*
29. C.H. Shen and G.S. Springer, *J. Composite Materials* **10**, 2 (1976).
30. R.E. Bohlmann and E.A. Derby, *Moisture Diffusion in Graphite/Epoxy Laminates: Experimental and Predicted, AIAA Paper No. 77-399 (1977).*
31. *AFML/AFOSR, Mechanics of Composites Review, Dayton (1976).*
32. C.E. Browning, *Ph. D. Thesis, University of Dayton (1976).*

APPENDIX E: The Structure, Modes of Deformation and Failure
and Mechanical Properties of Diaminodiphenyl
Sulfone Cured Tetraglycidyl 4,4'Diaminodiphenyl
Methane Epoxy, J. Mater. Sci. 14, 109 (1979)

The structure, modes of deformation and failure, and mechanical properties of diaminodiphenyl sulphone-cured tetraglycidyl 4,4' diaminodiphenyl methane epoxy*

ROGER J. MORGAN[†], JAMES E. O'NEAL, DANIEL B. MILLER[‡]
McDonnell Douglas Research Laboratories, McDonnell Douglas Corporation, St. Louise, Missouri 63166, USA

The tensile mechanical properties of diaminodiphenyl sulphone (DDS) - cured tetraglycidyl 4,4' diaminodiphenyl methane (TGDDM) epoxies [TGDDM-DDS (12 to 35 wt % DDS)] are reported as a function of temperature and strain rate. TGDDM-DDS (20 to 35 wt % DDS) epoxies, which exhibit broad T_g s near 250° C, are not highly cross-linked glasses because diffusional and steric restrictions limit their cross-link density. TGDDM-DDS (10 to 20 wt % DDS) epoxies are more brittle with lower T_g s as a result of lower molecular weights and/or lower cross-link densities. Electron diffraction and X-ray emission spectroscopy studies indicate that TGDDM-DDS (>25 wt % DDS) epoxies contain crystalline regions of unreacted DDS which can be eliminated from these epoxies during cure resulting in microvoids. TGDDM-DDS (12 to 35 wt % DDS) epoxies predominantly deform and fail in tension by crazing, as indicated by fracture topography studies. These glasses also deform by shear banding as indicated by right-angle steps in the fracture topography initiation region and mixed modes of deformation that involve both crazing and shear banding. No evidence was found for heterogeneous cross-link density distributions in TGDDM-DDS (15 to 35 wt % DDS) epoxies on straining films in the electron microscope.

1. Introduction

Epoxies, when utilized as composite matrices and adhesives in aerospace structural components, are often exposed to extreme environments. The durability of epoxies in such environments is difficult to predict without a knowledge of the structure, modes of deformation and failure, and mechanical response relations of these materials and how such relations are modified by fabrication

procedures and the service environment. The structure-property relationships of epoxy glasses, however, have received little attention compared with other commonly utilized polymer glasses.

The network structure and microvoid characteristics of epoxies are the primary structural components that control the modes of deformation and failure and mechanical response [1-4].

The network structure of epoxies varies with

*Research sponsored by the Air Force Office of Scientific Research/AFSC, United States Air Force, under Contract No. F44620-76-0075. The United States Government is authorized to reproduce and distribute preprints for governmental purposes notwithstanding any copyright notation hereon.

[†]Present address: Lawrence Livermore Laboratory, L-338, University of California, P.O. Box 808, Livermore, Ca 94550, USA.

[‡]National Science Foundation Faculty Research Participant: NSF Grant No. SER 76-04721. Present address: Physical Science Division, Forest Park Community College, St. Louis, Missouri, USA.

© 1979 Chapman and Hall Ltd. Printed in Great Britain.

chemical composition and cure conditions. Generally, the cure reactions and final network structure of epoxies have been estimated from (a) the chemistry of the system, if the cure reactions were known and assumed to go to completion, and (b) experimental techniques such as infra-red spectroscopy, swelling, dynamic mechanical, thermal conductivity, differential scanning calorimetry, viscosity, and dielectrometry measurements [5-22]. However, in certain epoxy systems, the chemical reactions may be diffusion-controlled and never go to completion, and a heterogeneous distribution in the cross-link density may also occur. For certain cure conditions, high cross-link density regions from 6 to 10^4 nm in diameter have been observed in cross-linked resins [1-4, 7, 23-44]. The conditions for formation of a heterogeneous rather than a homogeneous system depend on polymerization conditions (i.e., temperature, solvent and/or chemical composition). The ordered regions have been described as agglomerates of colloidal particles [28, 29] or floccules [31] in a lower molecular weight interstitial fluid. Solomon *et al.* [30] suggested that a two-phase system is produced by microgelation prior to the formation of a macrogel. These microgel regions may originate in the initial stages of polymerization from the formation of micro-regions of aggregates of primary polymer chains [40, 45]. Kenyon and Nielsen [7] suggested that the highly cross-linked microgel regions are loosely connected during the latter stages of the cure process. Heterogeneities also can result from either configurational restrictions leading to excessive intramolecular cross-linking [46] or from the chemical composition of the epoxy network formed at a given time being different from that of the chemical composition of the monomer mixture [47]. The high cross-link density regions have been reported to be only weakly attached to the surrounding matrix [28, 29, 31], and their size varies with cure conditions [28], proximity of surfaces [31, 41], and the presence of solvents [7, 30].

Recently, we have studied the network structure of diethylene triamine (DETA)-cured bisphenol-A-diglycidyl ether (DGEBA) epoxies by straining films directly in the electron microscope [3]. These epoxies were found to consist of 6 to 9 nm diameter particles which remain intact when flow occurs. We suggest that these particles are intramolecularly cross-linked, molecular domains. The 6 to 9 nm diameter particles interconnect to form

larger 20 to 35 nm diameter aggregates which are observed in patches on surfaces and in thin films of DGEBA-DETA epoxies. Two types of network structures were observed in these studies: (a) regions of high cross-link density embedded in a low- or non-cross-linked matrix and (b) low- or non-cross-linked density regions embedded in a high cross-link density matrix.

Microvoids in epoxies act as stress concentrators and sinks for sorbed moisture and will, therefore, deteriorate the mechanical response. These microvoids can be formed during cure as a result of evolution of trapped, low molecular weight material. The low molecular weight material may be air, moisture, or clusters of unreacted epoxy constituents. The latter may result from inhomogeneous mixing and/or microscopic phase separation of the constituents prior to or during cure. For example, the ability of DGEBA epoxide monomer to crystallize as a separate phase in polyamide-cured DGEBA epoxies has been shown to subsequently cause microvoids in these epoxies for certain cure conditions [1, 2, 4].

The relation between the network structure, microvoid characteristics and failure processes of epoxies has received little attention. Localized plastic flow has been reported to occur during the deformation and failure of epoxies [1-4, 34, 36, 48-54], and in a number of cases, the fracture energies have been reported to be a factor of two to three times greater than the expected theoretical estimate for purely brittle fracture [36, 48, 49, 53-64].

Recent studies revealed that the mode of deformation and failure in DGEBA-DETA epoxy films either strained directly in the electron microscope or strained on a metal substrate is a crazing process [3]. The fracture topographies of bulk DGEBA-DETA epoxy glasses fractured as a function of temperature and strain rate were also interpreted in terms of a crazing process. The flow processes that occurred within craze fibrils during deformation of DGEBA-DETA epoxy films strained in the electron microscope depended on the network structure. Deformation of the network consisting of high cross-link density particles embedded in a deformable, low cross-link density matrix occurred by preferential deformation of the low cross-link density regions without causing cleavage of the high cross-link density regions. However, deformation of the network consisting of low cross-link density regions embedded in a

high cross-link density matrix involved network cleavage and flow in the high cross-link density regions simultaneously as flow with little network cleavage occurred in the neighbouring low cross-link density regions.

In this study, our objective was to characterize further the structure/deformation/mechanical property relations of epoxies. The amine-cured tetrafunctional epoxide studied was tetraglycidyl 4,4'-diaminodiphenyl methane epoxide (TGDDM) cured with diaminodiphenyl sulphone (DDS). This epoxy system is currently one of the most commonly utilized in the aerospace industry. A series of epoxies was cured from different TGDDM-DDS compositions, and the tensile mechanical properties were monitored as a function of test temperature and strain rate. The structure and microvoid characteristics were monitored by (a) X-ray emission spectroscopy measurements, (b) electron diffraction measurements, and (c) weight-loss/moisture-sorption studies as a function of anneal temperature. Fracture topography studies were utilized to monitor the modes of deformation and failure of these glasses. In addition, epoxy films were strained directly in the electron microscope to further elucidate the structure of these epoxies.

2. Experimental

2.1. Materials and sample preparation

The epoxy system studied was a diaminodiphenyl sulphone (Ciba Geigy, Eporal)-cured tetraglycidyl 4,4'-diaminodiphenyl methane (Ciba Geigy, MY720) epoxy (TGDDM-DDS). The structure of the unreacted TGDDM epoxide and DDS monomers are illustrated in Fig. 1. The TGDDM epoxide monomer is a liquid at room temperature, whereas

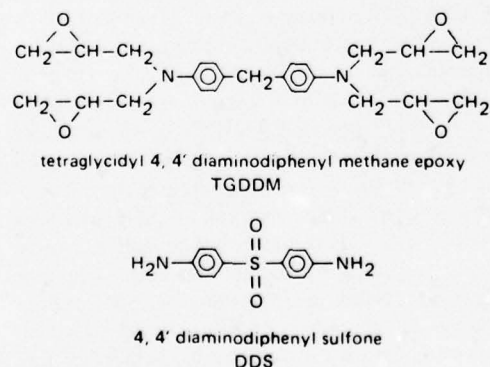


Figure 1 The TGDDM-DDS epoxy system.

the DDS is a crystalline powder with a melting point of 162°C.

For sample preparation, the fabrication techniques developed by Fanter [65] were utilized. A master batch of TGDDM was heated to 75°C, and the DDS was added slowly while the mixture was stirred. This mixture was then held at 75°C for 3 h, periodically stirred, and poured into vials and stored at -20°C. TGDDM-DDS mixtures were prepared in the 10 to 35 wt% DDS range. (For TGDDM-DDS mixtures containing ≥ 30 wt% DDS, the solid DDS did not all dissolve using this procedure; it did dissolve at the higher temperatures utilized during cure.)

Table I illustrates the percentage by weight of DDS required for (1) all primary and secondary amines in the DDS to react and (2) only primary amines in the DDS to react with 50 or 100% of the epoxide groups in the tetrafunctional TGDDM molecules.

In order to prepare dumb-bell-shaped specimens suitable for tensile mechanical property studies, the TGDDM-DDS mixture was heated to 165°C. After 20 min at 165°C, the mixture was degassed in a vacuum chamber, reheated to 165°C, and then poured into dumb-bell-shaped silicone rubber moulds. The specimens were cured at 150°C for 1 h, followed by 5 h at 177°C, cooled to room temperature, and removed from the moulds. The specimens had a gauge length of 3.0 cm, a width of 0.4 cm within the gauge length, and a thickness of 0.6 mm.

Epoxy films, $\sim 1 \mu\text{m}$ thick, suitable for straining directly in the electron microscope, were prepared between salt crystals. The cure conditions were similar to those utilized in preparing the dumb-bell-shaped specimens. After cure, the crystals were dissolved in water, and the film was washed with distilled water. Specimens, 2 mm square, were cut from the epoxy film. Thinner, 100 nm thick films were prepared by a similar procedure for electron diffraction and bright-field transmission studies.

Dumb-bell-shaped specimens were also used for weight loss/moisture sorption studies.

2.2. Experimental procedure

A table model tensile tester (Instron TM-S-1130) was used to determine the tensile mechanical properties of the TGDDM-DDS epoxies in the 10^{-2} to 10^1 min^{-1} strain rate region from 23 to 265°C.

A scanning reflection electron microscope (JEOL model JEM-100B) and optical microscope (Zeiss Ultraphot II) were used for fracture topo-

TABLE I Theoretical reaction mixtures for TGDDM-DDS epoxy system

	100% TGDDM epoxide groups react	50% TGDDM epoxide groups react
100% DDS primary and secondary amines react	37 wt % DDS	23 wt % DDS
100% DDS primary amines react	54 wt % DDS	37 wt % DDS

graphy studies. For the electron microscope studies, the fracture surfaces were coated with gold while the sample was rotated in vacuum.

For the X-ray emission spectroscopy (XES) studies, uncoated fracture surfaces were exposed to the electron beam, and the surface was scanned for X-rays characteristic of sulphur. The sulphur distribution (as indicated by the relative concentration of white dots) is superimposed on a secondary electron micrograph of the fractured surface. A lithium-drifted silicon X-ray detector (Kevex) was utilized in conjunction with a data analysis system (Tracor Northern).

Bright-field transmission electron microscopy (TEM) was used to monitor the morphology of $\sim 1 \mu\text{m}$ thick films that were strained directly in the electron microscope. The 2 mm square, epoxy specimens were fastened to standard cartridge specimen holders with cement (Duclo, E. I. DuPont). The specimen holder was attached to an EM-SEH specimen elongation holder which was introduced into the microscope via the side-entry goniometer. The specimens were deformed in the microscope at a strain rate of $\sim 10^{-2} \text{ min}^{-1}$. Selected area electron diffraction studies were also performed on thinner, $\sim 100 \text{ nm}$ thick films using the microscope in the electron diffraction mode.

Weight loss/moisture sorption measurements were performed by annealing specimens in a tube furnace in a He atmosphere for 24 h. The specimens were weighed before and after annealing and again after a 3 h exposure to steam in a 120°C autoclave.

3. Results and discussion

3.1. Mechanical properties

The tensile mechanical properties of the TGDDM-DDS epoxies were determined as a function of composition (12 to 35 wt % DDS) and temperature (23 to 265°C) at a strain rate of $\sim 10^{-2} \text{ min}^{-1}$. In Figs. 2, 3, and 4 the tensile strengths, ultimate elongations, and Young's moduli are plotted as a function of temperature for TGDDM-DDS (12 to 35 wt % DDS) epoxies. The decreases in tensile strengths and moduli and increase in ultimate elongations with increasing temperature from 200

to 250°C for TGDDM-DDS (23 to 35 wt % DDS) epoxies indicate that these glasses exhibit broad glass transitions near 250°C . The 10 to 17% ultimate elongations exhibited by the TGDDM-DDS (23 to 35 wt % DDS) epoxies from 200 to 250°C suggests that these glasses are not highly cross-linked despite the tetrafunctionality of the TGDDM epoxide. TGDDM-DDS (10 to 20 wt % DDS) epoxies exhibit lower T_g s and corresponding softer mechanical properties at lower temperatures than those epoxies prepared from higher DDS concentrations. The TGDDM-DDS (12 wt % DDS) epoxy exhibits $< 10\%$ ultimate elongation near its T_g , thus indicating that a more brittle, lower molecular weight epoxy is formed with $\sim 10 \text{ wt } \%$ DDS than is formed at higher DDS concentrations.

A plot of T_g as a function of initial DDS concentration, shown in Fig. 5, confirms that TGDDM-DDS epoxies are not highly cross-linked. [The temperatures representative of the broad T_g s were taken as those temperatures at which the room temperature modulus (E_{RT}) decreased by half (i.e., $E_{RT}/2$).] From 10 to 25 wt % DDS, the

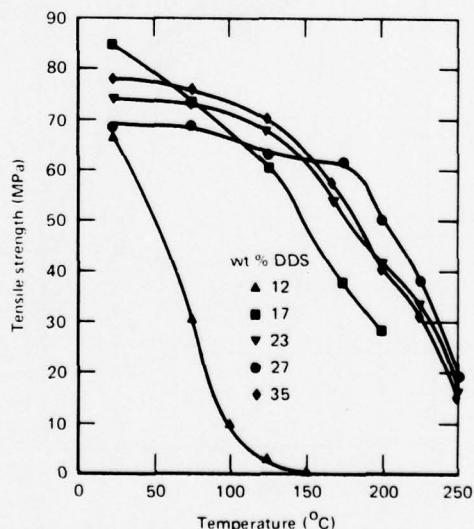


Figure 2 Tensile strength ($\pm 2 \text{ MPa}$) (strain rate $\sim 10^{-2} \text{ min}^{-1}$) versus temperature for TGDDM-DDS (12 to 35 wt % DDS) epoxies.

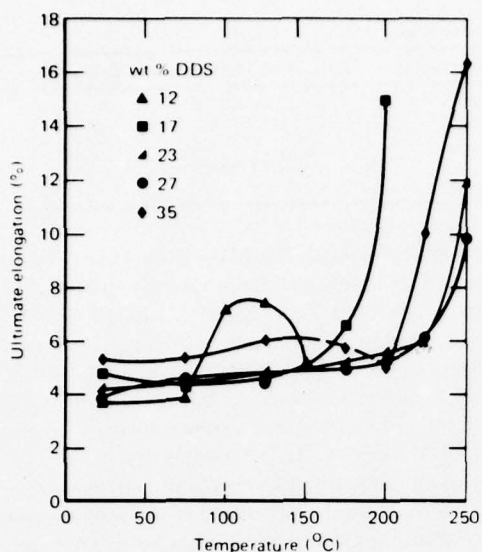


Figure 3 Ultimate elongation ($\pm 0.2\%$) (strain rate $\sim 10^{-2}$ min^{-1}) versus temperature for TGDDM-DDS (12 to 35 wt% DDS) epoxies.

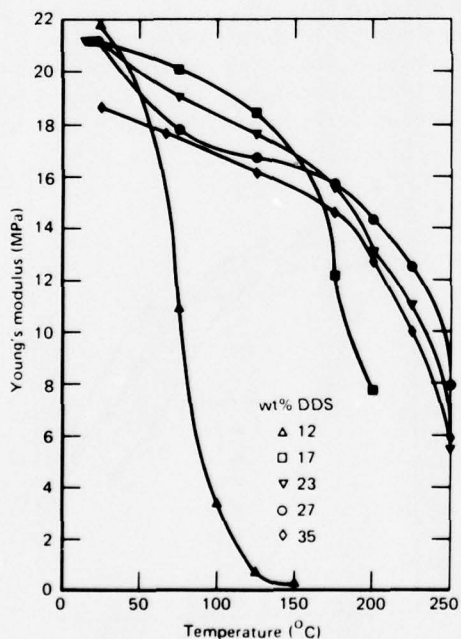


Figure 4 Young's modulus (± 1 MPa) (strain rate $\sim 10^{-2}$ min^{-1}) versus temperature for TGDDM-DDS (12 to 35 wt% DDS) epoxies.

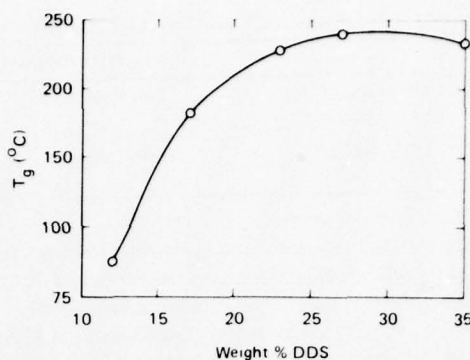


Figure 5 T_g versus initial wt% of DDS in TGDDM-DDS epoxies.

T_g rises with increasing DDS concentration because of corresponding increases in molecular weight and/or cross-link density. The T_g exhibits a maximum of $\sim 250^\circ\text{C}$ at ~ 30 wt% DDS and subsequently decreases for higher DDS concentrations. For epoxies prepared from $\lesssim 25$ wt% DDS, steric and diffusional restrictions evidently inhibit additional epoxy-amine reactions. Examinations of molecular models of the tetrafunctional TGDDM molecule indicate that the epoxide groups are sterically restricted which inhibits their ability to react with the primary amine hydrogens of the DDS. In addition, after gelation at the cure temperature, unreacted groups have difficulty approaching one another spatially because of mobility restrictions produced by the glassy state and the network cross-links. Above ~ 30 wt% DDS concentrations, unreacted DDS molecules plasticize the epoxy system and decrease the T_g (evidence for the presence of unreacted DDS molecules in these epoxies is presented in Sections 3.2 and 3.3). However, 37 wt% DDS is required to consume half the TGDDM epoxide groups when only epoxide-primary amine reactions occur (Table I). Hence, the maximum in T_g at ~ 30 wt% DDS suggests that less than half the TGDDM epoxide groups have reacted when only epoxide-primary amine reactions occur and steric and diffusional restrictions inhibit further reactions. It seems doubtful that networks in which only half of the epoxide groups have reacted would exhibit the respectable mechanical properties shown by the TGDDM-DDS (20 to 35 wt% DDS) epoxies. Evidently, other cure reactions, in addition to the epoxide-primary amine reactions, are occurring and possibly involve (1) epoxide homopolymerization, (2) epoxide-

secondary amine reactions and (3) internal cyclization within the TGDDM epoxide as a result of hydroxyl and/or secondary amines reacting with adjacent unreacted epoxides.

In the $(T_g - 50)$ to T_g temperature range, TGDDM-DDS (17 to 35 wt% DDS) epoxies exhibit definite yield stresses where the stress remains constant with increasing strain. The strain rate dependence of the yield stress in this temperature range was investigated for TGDDM-DDS (27 wt% DDS) epoxy to determine if the data for this cross-linked glass fit Eyring's theory of stress-activated viscous flow for polymers [66]. This theory predicts [67] that the yield stress (σ_y) is a linear function of the logarithm of the strain rate ($\dot{\epsilon}$) at constant temperature T , i.e.,

$$\frac{d\sigma_y}{d \ln \dot{\epsilon}} = \frac{2kT}{v} \quad (1)$$

where k is Boltzmann's constant and v is the activation volume which is associated with that volume displaced when a chain segment jumps when acted upon by an applied stress. The data for TGDDM-DDS (27 wt% DDS) epoxy fit the Eyring model as illustrated by the linear plots of σ_y versus $\log \dot{\epsilon}$ at 225, 250 and 265°C in Fig. 6. The values of the activation volume at each temperature are shown in Table II and are within the range of values (i.e., $v = 3$ to 15 nm^3) reported for non-cross-linked polymers [68-74] and one cross-linked epoxy resin system [75]. These observations suggest that either regions of low cross-link density control the flow processes of this epoxy near T_g and/or the rupturing of cross-

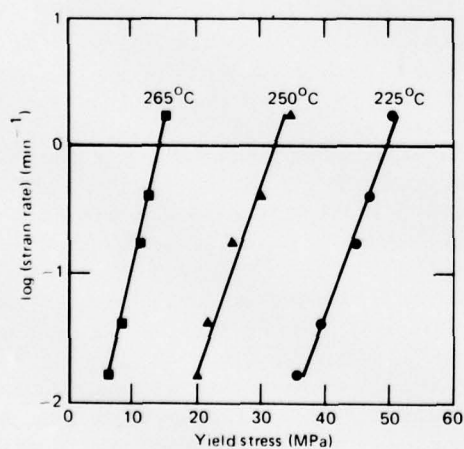


Figure 6 Log (strain rate) versus yield stress for TGDDM-DDS (27 wt% DDS) epoxy as a function of temperature.

TABLE II

Temperature ($^{\circ}\text{C}$)	Activation volume, $v(\text{nm}^3)$
225	8.0
250	7.9
265	11.7

links does not significantly affect the activation volume in this temperature range.

The larger value of the activation volume at 265°C compared with values at the lower temperatures may be a result of additional cross-links which form during testing. At 265°C, the epoxy rapidly discolours because of the formation of free radicals [4] associated with complex oxidative cross-linking reactions. (The enhanced mobility of the epoxy at 265°C allows such reactions to occur rapidly.) Hence, this larger value of the activation volume suggests that an increase in cross-link density will significantly increase the activation volume. However, such an interpretation must be treated with caution because the physical meaning of v on a molecular level is still unclear [67].

3.2. Electron diffraction

The data presented in Section 3.1 suggest that unreacted DDS molecules may be present in TGDDM-DDS (≈ 25 wt% DDS) epoxies. Previous studies on polyamide-cured bisphenol-A-diglycidyl ether epoxies have shown that unreacted epoxide monomer can recrystallize in the partially cured resin [4]. Hence, electron diffraction studies were performed on TGDDM-DDS (≈ 25 wt% DDS) epoxy films to determine if any liquid clusters of unreacted DDS molecules recrystallized within these glasses.

Several electron diffraction patterns of DDS powder on a carbon film were produced. A typical selected area diffraction (SAD) pattern illustrating a polycrystalline pattern of DDS is shown in Fig. 7a. For a hexagonal form, the unit cell dimensions of DDS were determined to be $a = 0.526 \text{ nm}$ and $c = 1.236 \text{ nm}$. From these unit cell dimensions, a complete list of interplanar spacings was calculated to obtain a standard pattern for DDS.

TGDDM-DDS (≈ 25 wt% DDS) epoxy films exhibited electron diffraction patterns from isolated regions. Such regions, which were $\approx 1 \mu\text{m}$ in size, appeared as dark but indistinct regions in bright field transmission electron micrographs. The SAD pattern originating from such a region is illustrated in Fig. 7b. The interplanar spacing determined from this pattern agreed with those of the calculated standard DDS pattern, indicating that

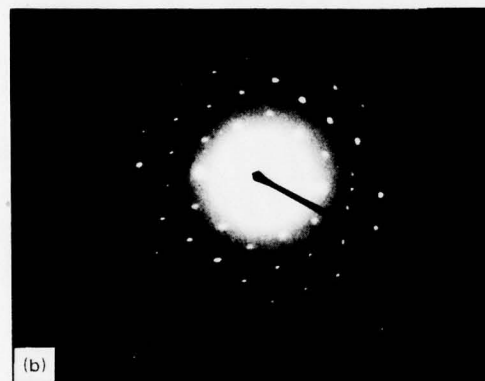


Figure 7 Selected area electron diffraction pattern of (a) DDS powder (polycrystalline) and (b) unreacted DDS crystalline region in TGDDM-DDS (35 wt% DDS) epoxy.

DDS crystalline regions are present in the TGDDM-DDS (≥ 25 wt% DDS) epoxy films.

3.3. X-ray emission spectroscopy

X-ray emission spectroscopy (XES) studies were conducted on TGDDM-DDS (≥ 25 wt% DDS) epoxies to detect regions of high sulphur content. The detection of such regions would imply the presence of unreacted DDS clusters because sulphur atoms are present only in the DDS molecule (see Fig. 1).

In this technique a fracture surface is bombarded with an electron beam, and the surface is scanned for X-rays characteristic of sulphur. The validity of XES to detect concentrations of DDS was established by monitoring DDS crystalline powder which was sprinkled onto a carbon background. A scanning electron micrograph of such DDS particles is shown in Fig. 8a. The sulphur distribution (as indicated by the relative concentration of white dots) is superimposed on this micrograph in Fig. 8b,

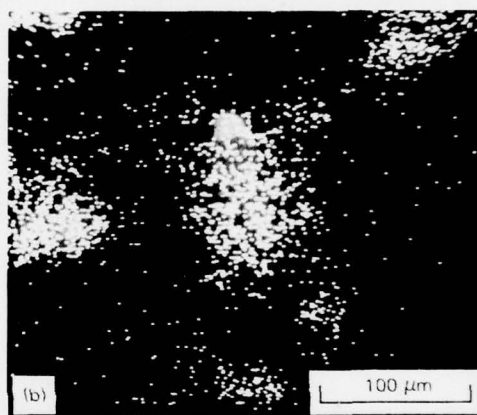
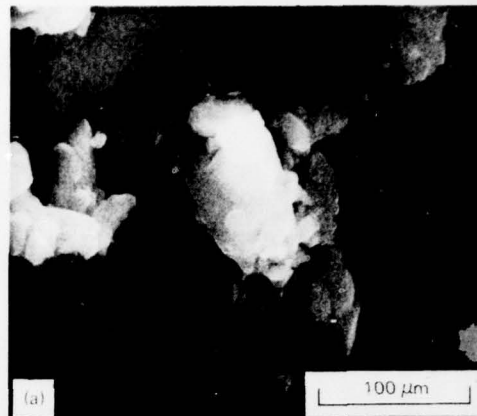


Figure 8 (a) Scanning electron micrograph of DDS crystalline powder and (b) X-ray emission scanning spectroscopy map of sulphur distribution in the same micrograph.

thus illustrating that particles of DDS $\geq 10 \mu\text{m}$ in size can be detected by this technique. Similar regions were observed in isolated areas of the fracture surfaces of TGDDM-DDS (≥ 25 wt% DDS) epoxies. In Fig. 9 an XES map of the sulphur distribution in the fracture surface of TGDDM-DDS (27 wt% DDS) epoxy is illustrated. The large concentration of sulphur in the fracture-initiation region probably results from a cluster of unreacted DDS molecules which acted as a site for craze/crack initiation. Regions $\geq 10 \mu\text{m}$ in size were not detected by this technique.

XES was also evaluated as a technique to monitor chemically different regions of polymers, such as cross-link density distribution, in the 10 nm size range. From extensive studies on TGDDM-DDS epoxies and polycarbonate-siloxane block copolymers, we have concluded that this technique

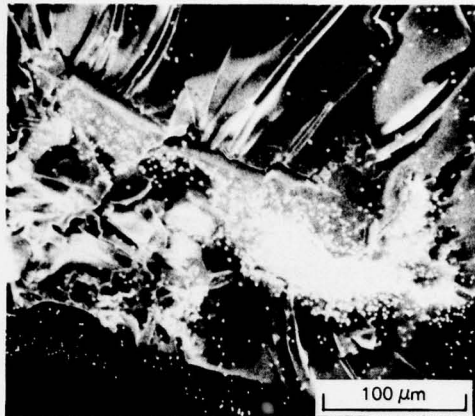


Figure 9 X-ray emission scanning spectroscopy map of sulphur distribution in the fracture surface of TGDDM-DDS (27 wt % DDS) epoxy.

is sensitive only to distinct, $\geq 10 \mu\text{m}$ sized, chemically different regions in polymers.

3.4. Weight loss/moisture sorption measurements

We have shown by optical microscopy that unreacted islands of epoxide monomer present in amide-cured bisphenol-A-diglycidyl ether epoxies can produce microvoids by diffusing out of these epoxies when they are annealed below T_g [4]. Microvoids are undesirable in epoxies because they act as stress concentrators, and also serve as a sink for sorbed moisture which deteriorates the mechanical integrity [76]. The weight lost and the subsequent moisture sorbed by TGDDM-DDS (27 wt % DDS) epoxy, as a function of a 24 h anneal from 150 to 250°C, were measured to determine if any clusters of unreacted DDS were eliminated from this epoxy, thus producing microvoids. The production of microvoids is expected to cause an increase in the amount of moisture sorbed by the epoxy. (Optical microscopy was not used in these studies because the size of the DDS clusters was generally $< 1 \mu\text{m}$ and, hence, any microvoids formed from such clusters would be too small to be detected by this technique.)

Fig. 10 shows the progressive weight loss with increasing anneal temperatures from 150 to 250°C for the TGDDM-DDS (27 wt % DDS) epoxy which was originally cured at 177°C for 5 h. The amount of moisture subsequently sorbed by the epoxy at 120°C in an autoclave for 3 h after annealing at 150 to 250°C is plotted versus anneal temperature.

116

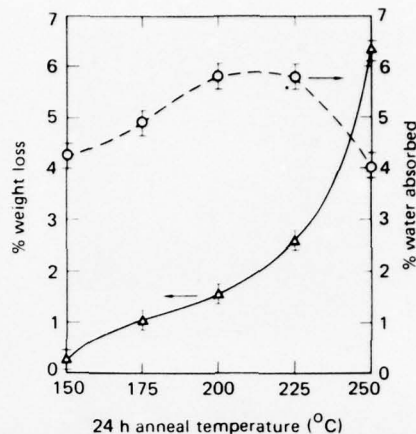


Figure 10 Plots of weight loss and subsequent moisture sorption versus anneal temperature for TGDDM-DDS (27 wt % DDS) epoxy.

The increase in sorbed moisture with increasing anneal temperature from 150 to 200°C is associated with microvoids produced by the elimination of unreacted DDS clusters. The sorbed moisture exhibits a maximum at 200 to 225°C and decreases as the anneal temperature approaches T_g at $\sim 245^\circ\text{C}$. We associate this maximum and the subsequent decrease in moisture sorption with the enhanced mobility of the epoxy at these higher temperatures, causing a partial collapsing of the microvoids and a possible increase in the cross-link density. Both of these phenomena will decrease the moisture sorption capabilities of the epoxy.

Hence, it is possible that once TGDDM-DDS ($\geq 25 \text{ wt } \% \text{ DDS}$) epoxies form glasses at their cure temperatures, subsequent curing can cause elimination of unreacted clusters of DDS resulting in microvoids.

3.5. Fracture topography studies

The fracture topographies of TGDDM-DDS (12 to 35 wt % DDS) epoxies were studied by optical and scanning electron microscopy as a function of temperature and strain rate. Three characteristic topographic regions were observed in these epoxies: (1) a coarse initiation cavity, (2) a slow crack growth, smooth, mirror-like region, and (3) a fast crack growth, rough region. The fracture topography features were generally similar to those observed in our studies of amine- and amide-cured disphenol-A-diglycidyl ether epoxies [3, 4] and can be interpreted in terms of a crazing deformation and failure process. However, the TGDDM-DDS

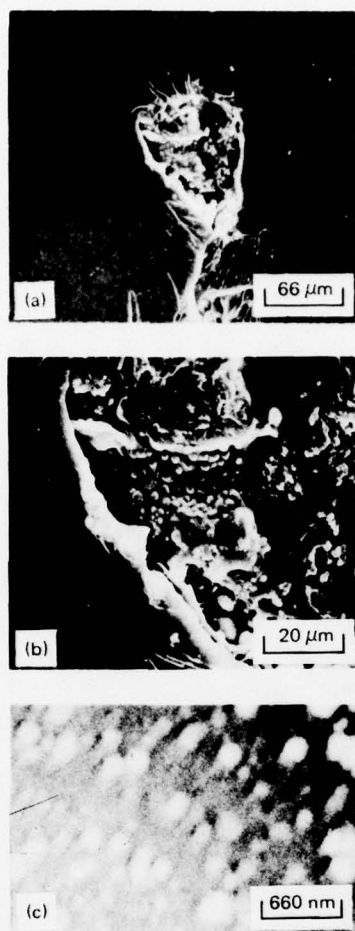


Figure 11 Scanning electron micrographs of (a) overall fracture topography initiation cavity, (b) coarse fractured fibrils and (c) fine fractured fibrils in TGDDM-DDS (27 wt% DDS) epoxy, fractured at room temperature at a strain rate of 10^{-2} min^{-1} .

fracture topography initiation regions also exhibit unique features as a result of shear-band deformation which occurs in $\sim 20\%$ of room temperature fractured specimens. These unique topographical features will be considered later in this section.

A typical fracture topography initiation region characteristic of a TGDDM-DDS epoxy that deformed and failed by a crazing process is illustrated in Fig. 11. The overall fracture topography initiation cavity is illustrated in Fig. 11a; 1 to 5 μm diameter, poorly developed, fractured fibrils are shown in Fig. 11b, and well-developed, 100 to 200 nm diameter, finer fractured fibrils are illustrated in Fig. 11c. This coarse initiation region

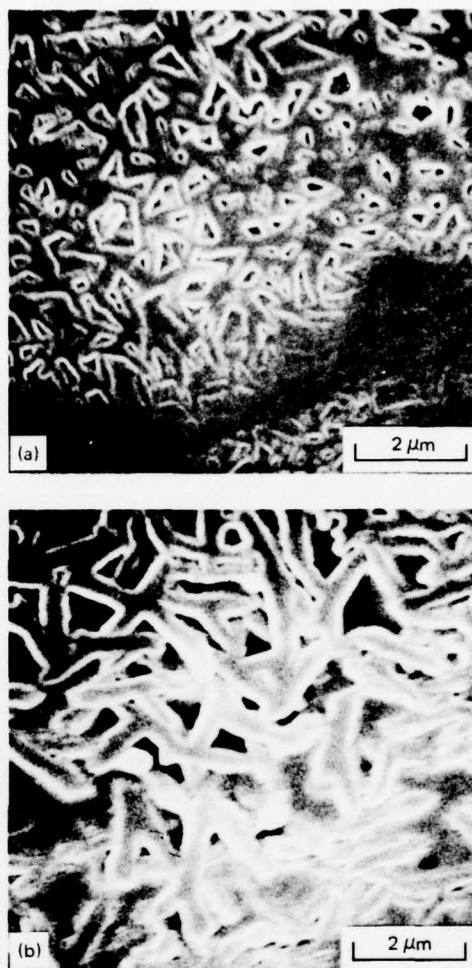


Figure 12 Scanning electron micrographs of fibrils swept onto the fracture surface in TGDDM-DDS (23 wt% DDS) epoxy, fractured at 200°C at a strain rate of 10^{-2} min^{-1} .

results from void growth and coalescence through the centre of a simultaneously growing, poorly developed craze, which generally consists of coarse fibrils [3, 4, 77-81]. The diameters of the fractured fibrils depend on the relative rates of craze and void growth. These relative rates vary for different stages of craze-crack growth and depend on complex local stress fields which change from specimen to specimen because of different flaw characteristics. Above 100°C, the fracture topography initiation regions are smoother than at lower temperatures because the enhanced mobility of the glass allows relaxation of the topographical features. Elongated fibrils that have been swept

Temperature (°C)	Strain rate (min ⁻¹)		
	$\sim 2 \times 10^{-2}$	$\sim 2 \times 10^{-1}$	~ 2
200			
225			
250			
265			

Figure 13 Optical micrographs of overall fracture topographies of TGDDM- DDS (27 wt% DDS) epoxies as a function of temperature and strain rate.

onto the fracture surface as the crack passes through the craze were also observed in the fracture topography initiation region and immediate surroundings for specimens fractured at $\geq 100^\circ\text{C}$, as illustrated in Fig. 12. Similar topographies of fractured fibrils that lie parallel to the surface have been reported by Doyle [82, 83] and Hoare and Hull [84] for polystyrene and by the authors for DGEBA-DETA epoxies [3].

The smooth mirror-like region of the fracture topography of TGDDM-DDS epoxies whose area increases with increasing temperature and decreasing strain rate (Fig. 13) can be attributed to a crazing process. Similar observations have been reported for DGEBA-DETA epoxies [3]. For other polymers, this region has been associated with slow crack growth, and its size varies with temperature, molecular weight and strain rate [85-89]. For polyester resins, Owen and Rose [90] report that the mirror-like area increases with resin flexibility. This smooth topography is associated with slow crack propagation through the median or along the craze-matrix boundary interface of a thick, well-developed craze consisting of fine fibrils [77, 78, 83, 84, 91-95]. Furthermore the increased mobility of the glass near T_g enhances relaxation of the topographical features, thus also favouring a smooth surface.

Interference colours, often observed in the mirror-like region of non-cross-linked polymer glasses [96], were not evident in the fracture topography of TGDDM-DDS epoxies. The absence of such colours in other cross-linked polymers [3, 4, 48] suggests that the thickness of the craze or craze remnants in the mirror-like

regions of these cross-linked glasses was not large enough to cause interference with visible light.

The TGDDM-DDS epoxies also deform to a limited extent by shear banding. Regular, right-angle steps were observed in the fracture topography initiation region, all illustrated in Fig. 14. The topography of the right-angle steps exhibits a finer structure at higher magnifications as shown in Fig. 15 where both faces of a right-angle step and their line of intersection are illustrated. Attached to each face is a thin, deformed layer ($\sim 100\text{ nm}$ thick) of material that consists of rectangular or square-shaped voids and protrusions with dimensions of 100 to 500 nm. These structures are aligned parallel to the line at which the larger perpendicular planes intersect. This topography suggests that the larger shear bands consist of packets of micro-shear bands whose thickness of $\sim 100\text{ nm}$ is that of the larger bands. Wu and Li [97] have characterized two shear band deformation processes in polystyrene; one appears as fine shear bands and the other as diffuse shear zones. Also, for shear bands that propagate in epoxies under compression, Bowden and Jukes [98] report that the matrix material outside the bands does not undergo any permanent plastic deformation. Certainly, a sharp boundary between the deformed material in a shear band and the undeformed immediate surroundings is consistent with the thin layer of deformed material observed in the shear planes in Fig. 15.

The percentage of all fractures in which regular right-angle steps were prevalent in the initiation region is plotted as a function of test temperature in Fig. 16. At and above 250°C ($T_g \approx 250^\circ\text{C}$), none

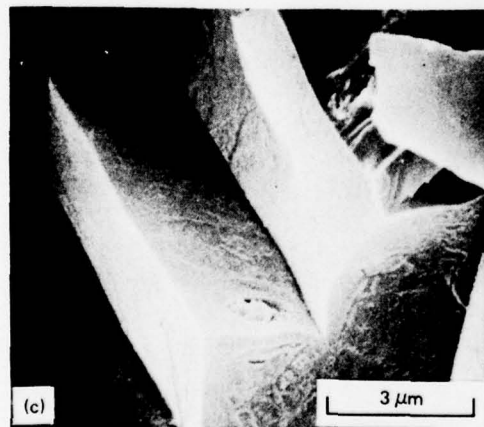
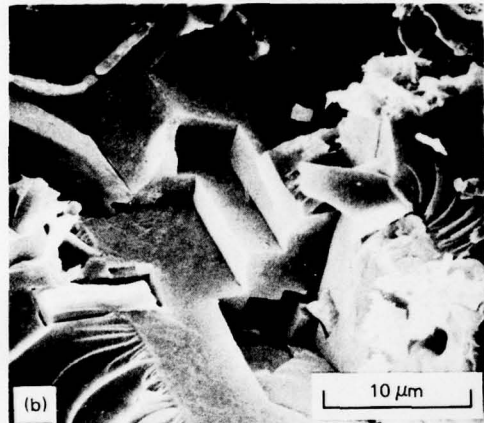
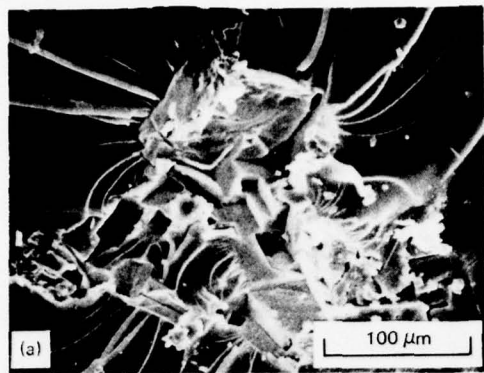


Figure 14 Scanning electron micrographs of right-angle steps in the fracture topography initiation region of TGDDM-DDS (35 wt% DDS) epoxy fractured at 225°C at a strain rate of 10^{-2} min^{-1} .

of the fracture surfaces exhibited the right-angle steps because viscous flow and relaxation processes during and after crack propagation cause a smooth fracture surface and mask the fracture topography

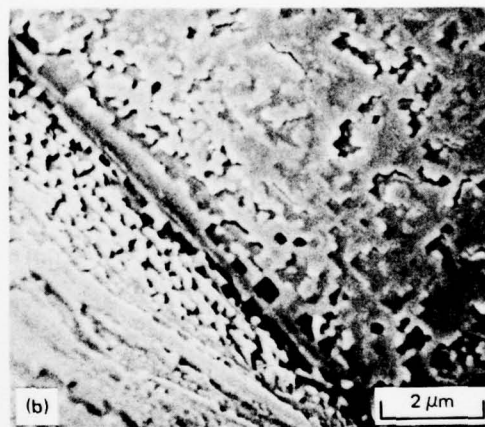
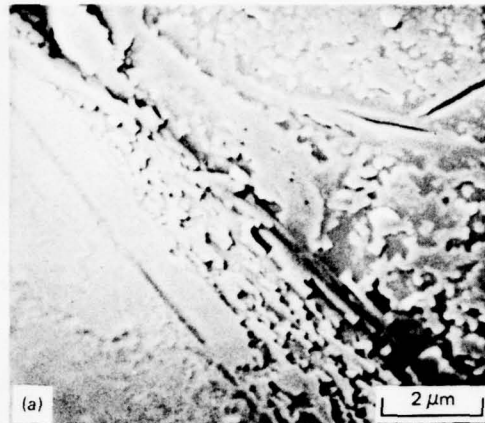


Figure 15 Scanning electron micrographs of the fine structure exhibited at the intersection of both faces of a right-angle step in the fracture topography initiation region of TGDDM-DDS (27 wt% DDS) epoxy fractured at 225°C at a strain rate of 1 min^{-1} .

microfeatures. The increase in the percentage of fracture topographies exhibiting right-angle steps with temperature is consistent with the shear band mode of deformation becoming more favoured relative to the crazing mode with increasing temperature [99-101]. Also, Bowden [67] has noted that the rate at which shear bands develop is controlled by the rate of strain softening and the strain rate sensitivity of the flow stress. The relatively low magnitudes of $d\sigma_y/d\ln\dot{\epsilon}$ of 2.5 to 3.5 MN m^{-2} for TGDDM-DDS epoxies above 200°C (ascertained from Fig. 6) compared with values quoted for poly(methyl methacrylate) of 5 to 9 MN m^{-2} [67] suggest that shear band deformation is favourable for TGDDM-DDS epoxies above 200°C.

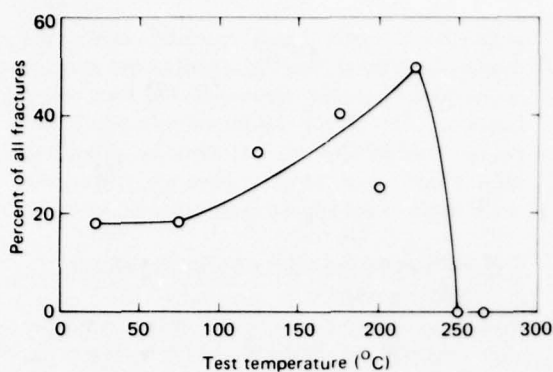


Figure 16 Percentage of fracture topography initiation regions that exhibit right-angle steps versus temperature in TGDDM-DDS (15 to 35 wt % DDS) epoxies.

Shear bands, which propagate at 45° to the applied tensile load direction and therefore intersect at right-angles, produce structurally weak planes in cross-linked glasses because of bond cleavage that is caused during molecular flow. Hull [102] and Mills [103] have both noted that the intersection of shear bands causes a stress concentration that is sufficient to cause a crack to propagate through the thin, structurally weak planes caused by shear band propagation. These phenomena produce the unique right-angle steps in the fracture topography of TGDDM-DDS epoxies that have not yet been observed in any other polymeric materials. Generally, the planes of the shear bands were $\sim 45^\circ$ to the applied tensile load direction. However, in some cases, significant deviations from the 45° angle were observed because of complex, local stress fields in the fracture initiation region.

The fracture topography initiation regions that exhibited right-angle steps were surrounded by a smooth, mirror-like topography region. At lower temperatures this region is associated with craze propagation [77, 78, 83, 84, 91-95]. Hence, at faster crack velocities, the initial mode of deformation that was predominantly a shear band mode changes to a crazing mode.

The ability of TGDDM-DDS epoxies to deform by shear banding, particularly near T_g , allows these glasses to exhibit the high-temperature ultimate elongations illustrated in Fig. 3. In comparison, for certain polyimides that deform only by crazing [104], the ultimate elongation decreases with increasing temperature because the softening of the craze fibrils limits their load-bearing capability, enhances crack propagation, and thus limits the ultimate elongation. The shear-band deformation in TGDDM-DDS epoxies, however, enhances the

120

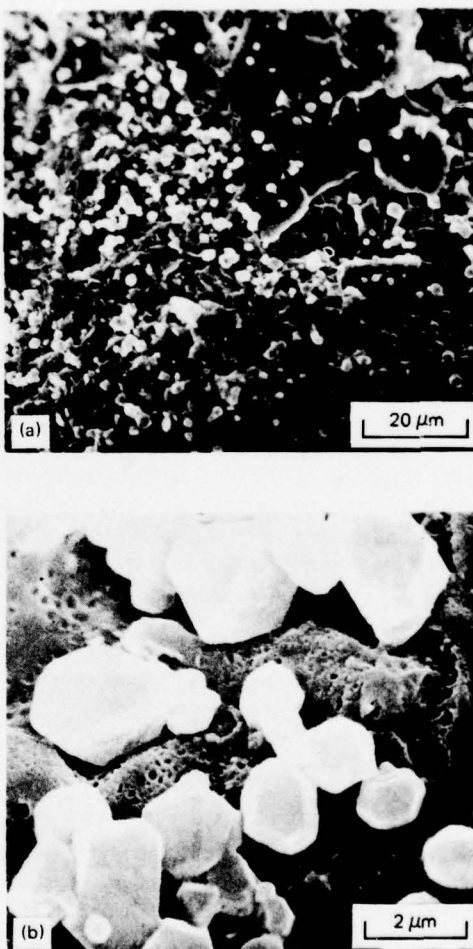


Figure 17 Scanning electron micrographs of regularly-shaped structures embedded in the porous craze fracture topography initiation region of a TGDDM-DDS (23 wt % DDS) epoxy, which was fractured at room temperature at a strain rate of $\sim 10^{-2} \text{ min}^{-1}$.

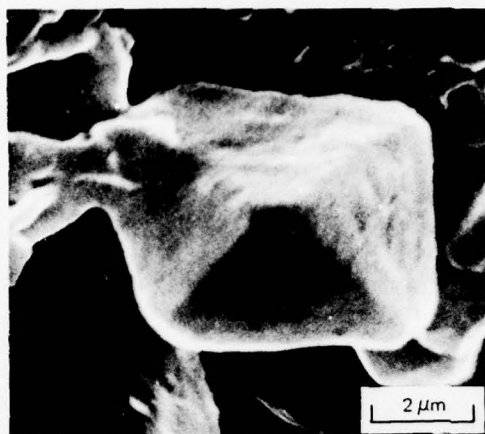


Figure 18 Scanning electron micrograph of regularly shaped structure embedded in the porous craze fracture topography initiation region of a TGDDM–DDS (12 wt % DDS) epoxy, which was fractured at 75°C at a strain rate of $\sim 10^{-2} \text{ min}^{-1}$.

high-temperature ductility without leading to premature failure.

In the fracture topography initiation region, regularly-shaped structures occasionally were found embedded in the porous craze structure as illustrated in Figs. 17 and 18. Such structures are not crystallites of unreacted DDS, for the following reasons: (1) such regular shapes were not observed in the micrographs of unreacted DDS powder (Fig. 8a); (2) clusters of these structures $\lesssim 10 \mu\text{m}$ in size did not exhibit higher sulphur contents than their surroundings as determined by XES; and (3) these regular structures were observed in TGDDM–DDS (12 wt % DDS) epoxies, whereas regions of unreacted DDS were found only in TGDDM–DDS ($\lesssim 25 \text{ wt } \% \text{ DDS}$) epoxies (Sections 3.2 and 3.3). In addition, it is difficult to envisage such regularly-shaped regions of high cross-link density, which would be less susceptible to deformation than their surroundings, being present in these TGDDM–DDS epoxies. The most plausible explanation of these regularly-shaped structures is a result of a mixed mode of deformation in which numerous shear bands develop in a region where craze growth also occurs. Perpendicular cracks develop where shear bands intersect at right-angles, and these cracks interconnect with neighbouring perpendicular cracks to produce the assortment of regular structures illustrated in Figs. 17 and 18. The variety of regular structures, most of which contain some perpendicular planes, results from the numerous three-dimensional positions that

perpendicular shear bands can have relative to neighbouring shear bands which also meet at right-angles. The complex nature of the local stress fields in this mixed deformation mode could further complicate the situation by producing local deviations of the shear band planes from the $\sim 45^\circ$ angle to the applied tensile load direction.

3.6. Films strained directly in the electron microscope

Significant information on the failure processes and structure of DGEBA–DETA epoxies was found from bright-field transmission electron micrographs of $\sim 1 \mu\text{m}$ thick epoxy films strained directly in the microscope [4]. Similar studies were conducted on TGDDM–DDS (10 to 35 wt % DDS) epoxies. On straining TGDDM–DDS epoxies in the electron microscope, cracks propagated rapidly without detection of crazing or shear band modes of deformation. However, prior to crack propagation, microscopic heterogeneities were observed in the more brittle epoxies prepared from 10 to 15 wt % DDS which possess poorer network structures than epoxies prepared from higher DDS concentrations. In Fig. 19a, a strained TGDDM–DDS (10 wt % DDS) epoxy is shown to break into 2.5 to 13 nm diameter particles. At higher deformation, the network breaks into $\sim 2.5 \text{ nm}$ dia-

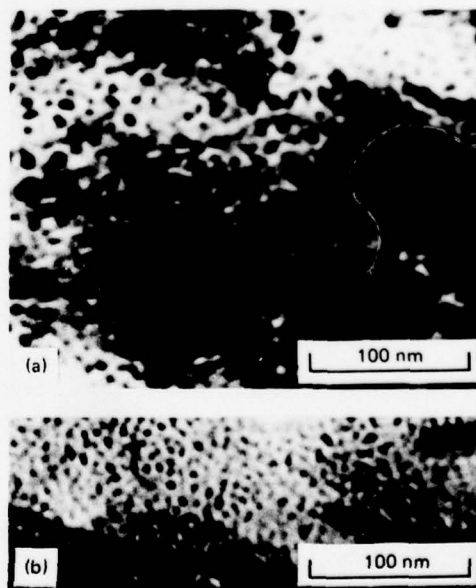


Figure 19 Bright-field transmission electron micrographs of structure in deformed TGDDM–DDS (10 wt % DDS) epoxy.

meter particles, as shown in Fig. 19b. These basic 2.5 nm diameter particles are of a similar size as the TGDDM epoxide molecule. The lack of any heterogeneities in the TGDDM-DDS (15 to 35 wt% DDS) epoxies suggests that these epoxies possess a uniform cross-link density distribution. The symmetry of the tetrafunctional TGDDM epoxide molecule would favour such a uniform distribution for a network formed as a result of primary amine/epoxide reactions.

4. Conclusions

(1) TGDDM-DDS (20 to 35 wt% DDS) epoxies, which exhibit broad T_g s near 250°C, are not highly cross-linked glasses as indicated by (a) their glassy state, high-temperature ductility and (b) the values of their activation volumes associated with the flow processes which are similar to non-cross-linked polymer glasses. Diffusional and steric restrictions inhibit the formation of high cross-link density TGDDM-DDS epoxies despite the tetrafunctionality of the TGDDM epoxide. TGDDM-DDS (10 to 20 wt% DDS) epoxies exhibit progressively lower T_g s and more brittle mechanical responses with decreasing DDS concentrations as a result of low molecular weight and/or low cross-link densities.

(2) Electron diffraction and X-ray emission spectroscopy studies indicate that TGDDM-DDS (≥ 25 wt% DDS) epoxies contain crystalline regions of unreacted DDS as a result of steric and diffusional restrictions limiting the cure reactions. Such DDS clusters can be eliminated from these epoxies during the cure process resulting in microvoids in the glasses.

(3) TGDDM-DDS (12 to 35 wt% DDS) epoxies predominantly deform and fail in tension by a crazing process as indicated by fracture topography studies. These glasses also deform to a limited extent by shear banding as indicated by unique, regular right-angle steps in the fracture topography initiation region. The shear band mode of deformation becomes more predominant with increasing temperature and is the primary mode of deformation during the initial stages of fracture just below T_g . Fracture topographical features also indicate that mixed modes of deformation that involve both shear banding and crazing can occur in these epoxies. The shear-band mode of deformation enhances the high-temperature ductility of these TGDDM-DDS epoxies.

(4) The lack of any heterogeneities on straining films of TGDDM-DDS (15 to 35 wt% DDS)

epoxies in the electron microscope suggests that these glasses possess a uniform cross-link density distribution. However, TGDDM-DDS (10 to 15 wt% DDS) epoxies, which possess poorer network structures, break into ~ 2.5 nm diameter particles which are similar in size to the TGDDM epoxide molecule.

Acknowledgements

We wish to acknowledge Mr R. Helling (summer student, MDRL) for assistance in sample preparation and mechanical property measurements, Mr D. L. Fanter (MDRL) for assistance in sample preparation, and Dr D. R. Ulrich (AFOSR), Lt Col R. W. Haffner (AFOSR), Dr D. P. Ames (MDRL) and Dr C. J. Wolf (MDRL) for their support and encouragement of this work.

References

1. R. J. MORGAN and J. E. O'NEAL, *Polymer Preprints* **16** (1975) 610.
2. *Idem*, "Chemistry and Properties of Cross-linked Polymers," edited by S. S. Labana (Academic Press, New York, 1977) p. 289.
3. *Idem*, *J. Mater. Sci.* **12** (1977) 1966.
4. *Idem*, *J. Macromol. Sci. Phys.* **B15** (1978) 139.
5. D. KATZ and A. V. TOBOLSKY, *Polymer* **4** (1963) 417.
6. T. K. KWEL, *J. Polymer. Sci.* **A1** (1963) 2977.
7. A. S. KENYON and L. E. NIELSEN, *J. Macromol. Sci. -Chem.* **A3** (1969) 275.
8. R. P. KREHLING and D. E. KLINE, *J. Appl. Polymer Sci.* **13** (1969) 2411.
9. J. P. BELL, *J. Polymer Sci. A-2* **8** (1970) 417.
10. T. MURAYAMA and J. P. BELL, *ibid.* **8** (1970) 437.
11. M. A. ACITELLI, R. B. PRIME and E. SACHER, *Polymer* **12** (1971) 335.
12. R. G. C. ARRIDGE and J. H. SPEAKE, *ibid.* **12** (1972) 443, 450.
13. P. V. SIDYAKIN, *Vysokomol. soyed.* **A14** (1972) 979.
14. T. HIRAI and D. E. KLINE, *J. Appl. Polymer. Sci.* **16** (1972) 3145.
15. R. B. PRIME and E. SACHER, *Polymer* **13** (1972) 455.
16. P. G. BABAYEVSKY and J. K. GILLHAM, *J. Appl. Polymer Sci.* **17** (1973) 2067.
17. T. HIRAI and D. E. KLINE, *J. Appl. Polymer Sci.* **17** (1973) 31.
18. E. SACHER, *Polymer* **14** (1973) 91.
19. D. A. WHITING and D. E. KLINE, *J. Appl. Polymer Sci.* **18** (1974) 1043.
20. J. K. GILLHAM, J. A. BENCI and A. NOSHAY, *ibid.* **18** (1974) 951.
21. J. F. CARPENTER, 21st National SAMPE Symposium, Los Angeles, April (1976).
22. L. T. PAPPALARDO, *J. Appl. Polymer Sci.* **21** (1977) 809.

23. T. S. CARSWELL, "Phenoplasts" (Interscience, New York, 1947).
24. T. G. ROCHOW and F. G. ROWE, *Anal. Chem.* **21** (1949) 261.
25. R. A. SPURR, E. H. ERATH, H. MYERS and D. C. PEASE, *Ind. Eng. Chem.* **49** (1957) 1839.
26. E. H. ERATH and R. A. SPURR, *J. Polymer Sci.* **35** (1959) 391.
27. T. G. ROCHOW, *Anal. Chem.* **33** (1961) 1810.
28. E. H. ERATH and M. ROBINSON, *J. Polymer Sci. C 3* (1963) 65.
29. H. P. WOHNSIEDLER, *ibid.* (1963) 77.
30. D. H. SOLOMON, B. C. LOFT and J. D. SWIFT, *J. Appl. Polymer Sci.* **11** (1967) 1593.
31. R. E. CUTHRELL, *ibid.* **11** (1967) 949.
32. A. N. NEVEROV, N. A. BIRKINA, Yu. V. ZHERDEV and V. A. KOZLOV, *Vysokomol. soyed.* **A10** (1968) 463.
33. G. NENKOV and M. MIKHAILOV, *Makromol. Chem.* **129** (1969) 137.
34. B. E. NELSON and D. T. TURNER, *J. Polymer Sci. (Phys. Ed.)* **10** (1972) 2461.
35. L. G. BOZVELIEV and M. G. MIHAJLOV, *J. Appl. Polymer Sci.* **17** (1973) 1963, 1973.
36. K. SELBY and L. E. MILLER, *J. Mater. Sci.* **10** (1975) 12.
37. R. J. MORGAN and J. E. O'NEAL, *Polymer Plast. Tech. Eng.* **5** (1975) 173.
38. M. V. MAIOROVA, M. M. MOGILEVICH, M. I. KARYAKINA and A. V. UDALOVA, *Vysokomol. soyed.* **A17** (1975) 471.
39. V. M. SMARTSEV, A. Ye. CHALYKH, S. A. NENAKHOV and A. T. SANZHAROVSKII, *ibid.* **A17** (1975) 836.
40. M. I. KARYAKINA, M. M. MOGILEVICH, N. V. MAIOROVA and A. V. UDALOVA, *ibid.* **A17** (1975) 466.
41. J. L. RACICH and J. A. KOUTSKY, *J. Appl. Polymer Sci.* **20** (1976) 2111.
42. K. SELBY and M. O. W. RICHARDSON, *J. Mater. Sci.* **11** (1976) 786.
43. J. A. MANSON, S. L. KIM, and L. H. SPERLING, "Influence of Crosslinking on the Mechanical Properties of High T_g Polymers," Technical Report AFML-TR-76-124 (1976).
44. S. L. KIM, M. D. SKIBO, J. A. MANSON, R. W. HERTZBERG and J. JANISZEWSKI, *Polymer Eng. Sci.* (in press).
45. G. PALMA, G. TALAMINI, M. TAVAN and M. CARENZA, *J. Polmer Sci. (Phys. Ed)* **15** (1977) 1537.
46. A. J. CHOMPF, *Org. Coat. Plast. Chem. Preprints (ACS)* **36** (1976) 529.
47. A. H. WILLBOURN, *Polymer* **17** (1976) 965.
48. L. J. BROUTMAN and F. J. MCGARRY, *J. Appl. Polymer Sci.* **9** (1965) 609.
49. R. GRIFFITHS and D. G. HOLLOWAY, *J. Mater. Sci.* **5** (1970) 302.
50. R. L. PATRICK, W. G. GEHMAN, L. DUNBAR and J. A. BROWN, *J. Adhesion ?* (1971) 165.
51. P. B. BOWDEN and J. A. DUKES, *J. Mater. Sci.* **7** (1972) 52.
52. R. L. PATRICK, "Treatise on Adhesion and Adhesive", Vol. 3, edited by R. L. Patrick (Dekker, New York, 1973) p. 163.
53. R. J. YOUNG and P. W. R. BEAUMONT, *J. Mater. Sci.* **10** (1975) 1343.
54. A. CHRISTIANSEN and J. B. SHORTALL, *ibid.* **11** (1976) 1113.
55. S. MOSTOVOY and E. J. RIPLING, *J. Appl. Polymer Sci.* **10** (1966) 1351.
56. *Idem*, *ibid.* **15** (1971) 611.
57. A. T. DINENNEDETTO and A. D. WAMBACH, *Int. J. Polymer Mater.* **1** (1972) 159.
58. A. D. S. DIGGWA, *Polymer* **15** (1974) 101.
59. A. C. MEEKS, *ibid.* **15** (1974) 675.
60. W. D. BASCOM, R. L. COTTINGTON, R. L. JONES and P. PEYSER, *J. Appl. Polymer Sci.* **19** (1975) 2545.
61. P. G. BABAYEVSKII and Ye. B. TROSTYANSKAYA, *Vysokomol. soyed.* **A17** (1975) 906.
62. R. A. GLEDHILL and A. J. KINLOCH, *J. Mater. Sci.* **10** (1975) 1263.
63. Y. W. MAI and A. G. ATKINS, *ibid.* **10** (1975) 2000.
64. G. PRITCHARD and G. V. RHOADES, *Mater. Sci. Eng.* **26** (1976) 1.
65. D. L. FANTER, *Rev. Sci. Instrum.* **49** (1978) 1005.
66. H. EYRING, *J. Chem. Phys.* **4** (1936) 283.
67. P. B. BOWDEN, "The Physics of Glassy Polymers", edited by R. N. Haward (Wiley, New York, 1973) Ch. 5.
68. J. A. ROELTING, *Polymer* **6** (1965) 311.
69. D. L. HOLT, *J. Appl. Polymer Sci.* **12** (1968) 1653.
70. J. C. BAUWENS, C. BAUWENS-CROWET and G. HOMES, *J. Polymer Sci. A-2* **7** (1969) 1745.
71. R. A. DUCKETT, S. RABINOWITZ and I. M. WARD, *J. Mater. Sci.* **5** (1970) 909.
72. P. B. BOWDEN and S. RAHA, *Phil. Mag.* **22** (1970) 463.
73. T. E. BRADY and G. S. Y. YEH, *J. Appl. Phys.* **42** (1971) 4622.
74. E. J. KRAMER, *J. Polymer Sci. (Phys. Ed.)* **13** (1975) 509.
75. E. PINK and J. D. CAMPBELL, *J. Mater. Sci.* **9** (1974) 665.
76. R. J. MORGAN and J. E. O'NEAL, *Polymer Plast. Tech. Eng.* **10** (1978) 49.
77. J. MURRAY and D. HULL, *Polymer* **10** (1969) 451.
78. S. RABINOWITZ, A. R. KRAUSE and P. BEARDMORE, *J. Mater. Sci.* **8** (1973) 11.
79. P. L. CORNES and R. N. HAWARD, *Polymer* **15** (1974) 149.
80. J. MURRAY and D. HULL, *J. Polymer Sci. A-2* **8** (1970) 1521.
81. P. BEAHAN, M. BEVIS and D. HULL, *J. Mater. Sci.* **8** (1972) 162.
82. M. J. DOYLE, *J. Polymer Sci. (Polymer Phys. Ed.)* **13** (1975) 127.
83. *Idem*, *J. Mater. Sci.* **10** (1975) 300.
84. J. HOARE and D. HULL, *J. Mater. Sci.* **10** (1975) 1861.
85. F. ZANDEMAN, *Publs. Scient. Tech. Minst. Air*, Paris No. 291 (1954) Ch. IV.
86. S. B. NEWMAN and I. WOLOCK, *J. Appl. Phys.* **29** (1958) 49.
87. I. WOLOCK and S. B. NEWMAN, "Fracture Processes

- in Polymeric Solids," edited by B. Rosen (Interscience, New York, (1964) Ch. IIc.
88. R. J. BIRD, J. MANN, G. POGANY and G. ROONEY, *Polymer* **7** (1966) 307.
89. R. P. KUSY and D. F. TURNER, *ibid.* **18** (1977) 391.
90. M. J. OWEN and R. G. ROSE, *J. Mater. Sci.* **10** (1975) 1711.
91. M. J. DOYLE, *ibid.* **10** (1975) 159.
92. H. EL-HAKEEM, G. P. MARSHALL, E. I. ZICHY and L. E. CULVER, *J. Appl. Polymer Sci.* **19** (1975) 3093.
93. D. L. LAINCHBURY and M. BEVIS, *J. Mater. Sci.* **11** (1976) 2222, 2235.
94. M. D. SKIBO, R. W. HERTZBERG and J. A. MANSON, *ibid.* **11** (1976) 479.
95. R. W. TRUSS and G. A. CHADWICK, *ibid.* **12** (1977) 1383.
96. R. P. KAMBOUR, *J. Polymer Sci.* **A3** (1965) 1713.
97. J. B. C. WU and J. C. M. LI, *J. Mater. Sci.* **11** (1976) 434.
98. P. B. BOWDEN and J. A. JUKES, *ibid.* **3** (1968) 183.
99. S. S. STERNSTEIN and L. ONGCHIN, *Polymer Preprints* **10** (1969) 1117.
100. R. N. HAWARD, B. M. MURPHY and E. F. T. WHITE, *J. Polymer Sci. A-2* **9** (1971) 801.
101. R. J. MORGAN and J. E. O'NEAL, *J. Polymer Sci. (Polymer Phys. Ed.)* **14** (1976) 1053.
102. D. HULL, *Acta Met.* **8** (1960) 11.
103. N. J. MILLS, *J. Mater. Sci.* **11** (1976) 363.
104. R. J. MORGAN and J. E. O'NEAL, unpublished data (1978).

Received 11 April and accepted 22 May 1978.

APPENDIX F: The Modes of Deformation and Failure of
Polycarbonate, Polymer 20, 375 (1979)

Modes of deformation and failure of polycarbonate

Roger J. Morgan[†] and James E. O'Neal

McDonnell Douglas Research Laboratories, McDonnell Douglas Corporation, St. Louis, Missouri 63166, USA

(Received 12 June 1978; revised 2 October 1978)

Electron and optical microscopy studies of the modes of deformation and failure of polycarbonate are reported. The high toughness of glassy polycarbonate is controlled by the ease of shear-band deformation and the surface craze characteristics. Such crazes form in tension prior to macroscopic necking and cold-drawing and serve as sites for ultimate fracture. The surface craze characteristics and the role they play in the fracture processes are reported as a function of strain-rate (10^{-2} – 10^{+2} min⁻¹) from scanning electron microscopy studies of the fracture topographies and edges of polycarbonate specimens fractured in tension at room temperature. The mechanism by which surface crazing in polycarbonate is enhanced by handling is also reported. The surface regions that come into contact with islands of finger-grease are plasticized, and fabrication stresses within these regions relax near T_g at a faster rate than in the unplasticized surroundings. Microcracks which are produced at the boundary between the plasticized and unplasticized regions serve as sites for craze initiation and growth. The craze processes in thin polycarbonate films strained directly in the electron microscope are also reported. Undeformable ~ 10 nm sized nodular regions were observed during the craze flow processes in these thin films.

INTRODUCTION

Polycarbonate is a tough thermoplastic with good impact properties. This amorphous but crystallizable glass is, however, susceptible to solvent-crazing^{1–8} and, also, can embrittle on annealing below T_g ^{8–23}. To predict the durability of polycarbonate in a service environment with confidence requires a knowledge of (a) the physical arrangement of the macromolecules in the bulk, (b) the microscopic modes of deformation and failure, (c) the structural parameters that control the modes of deformation and failure, (d) the effect of the modes of deformation and failure on the mechanical response and (e) how these interrelations are modified by fabrication procedures, specimen geometry and environmental and stress exposure.

Precrystalline or crystalline structures do not form in bulk polycarbonate below T_g ($T_g \approx 150^\circ\text{C}$)^{18,20,23–25}. Indeed, annealing polycarbonate below T_g produces only changes in free volume which are reversible for reversible thermal anneal cycles^{18,20,23}. Polycarbonate does, however, crystallize immediately above T_g , which allows precrystalline or crystalline entities to grow below the bulk T_g in thin films and on free surfaces of thick films where mobility restrictions are less severe than in the bulk^{18,20,26–31}. The surface structures consist of aggregates of 5–6 nm diameter nodules, which are the size of ordered molecular domains^{18–20,23,29}. There is, however, no evidence that similar morphological entities form in the bulk above T_g during the initial stage of crystal-

lization. Although these surface morphological entities do not play a direct role in the bulk flow processes of polycarbonate, such structures could affect the failure initiation processes which generally occur at surfaces.

Polycarbonate is a tough, ductile material which deforms by shear yielding, even at cryogenic temperatures, in the absence of flaws of critical geometries⁸. Surface flaws are, however, often produced during the fabrication of polycarbonate specimens by, for example, machining, drilling or sawing. Also, exposure to organic environments, such as handling, together with interaction with fabrication stresses are sufficient to generate critical surface flaws. Polycarbonate, typical of a ductile thermoplastic, is extremely notch sensitive^{22,32}. This glass embrittles as a result of the cessation of shear yielding and reverts to a crazing deformation mode with a corresponding decrease in molecular flow and energy to failure^{12,18,20,23,33}.

In addition to surface flaw characteristics, the embrittlement of polycarbonate is dependent on specimen thickness, molecular weight, thermal history, strain-rate and test temperature. The mechanical response of a polycarbonate specimen containing a critical flaw is sensitive to specimen thickness as a result of plane-strain conditions in the deformation zone because lateral contraction becomes inhibited with increasing thickness^{10,15,17,18,20,21,34–37}. For plane-stress conditions, shear-band deformation is favoured; for plane-strain conditions, crazing and premature fracture is favoured. Indeed, Mills²¹ reports that notched polycarbonate bars > 5 mm thick are always brittle from -196° to 115°C in the impact strain-rate region. Fraser and Ward³⁸ have found that the fracture toughness of notched polycarbonate specimens depends on molecular weight in addition to the notch-tip radii. They suggest that lower-molecular-weight polycarbonates possess lower crazing stresses and, therefore, exhibit more brittle mechanical responses. For polycarbo-

* Research sponsored in part by the McDonnell Douglas Independent Research and Development Program and in part by the Air Force Office of Scientific Research/AFSC, United States Air Force, under Contract No. F44620-76-C-0075. The United States Government is authorized to reproduce and distribute reprints for governmental purposes notwithstanding any copyright notation hereon.

[†] Present address: Lawrence Livermore Laboratory, L-338, University of California, P. O. Box 808, Livermore, CA 94550

nate specimens < 5 mm thick, a transition from ductile to brittle behaviour has been observed with increasing strain-rate and/or decreasing temperature^{15, 18, 20, 22, 33, 34}. This embrittlement is also affected by thermal history because above 80°C, polycarbonate has sufficient molecular mobility to allow decrease in free volume. These liquid-like packing decreases in free volume inhibit molecular flow associated with both shear yielding and crazing and cause the glass to be more sensitive to craze/crack growth^{18, 20, 23}.

Hence, the embrittlement and durability of polycarbonate depend on a complex number of interacting phenomena, not all of which are completely understood.

This study addresses three areas related to the modes of deformation and failure of polycarbonate which are pertinent to its embrittlement and durability:

(1) In previous studies we observed a ductile-brittle transition in tension at a strain-rate of $\sim 10^2$ /min for 1 mm thick, un-notched polycarbonate specimens that had been annealed at 125°C^{18, 20, 23}. At lower strain-rates and greater free volumes (i.e., quenched or 145°C equilibrium-state glasses), shear-band deformation was the predominant mode of deformation, whereas crazing became the predominant mode on embrittlement at higher strain-rates. Kastelic and Baer³⁹ have reported that at room temperature and above, crazes form in polycarbonate prior to shear-band deformation and cold-drawing at strain-rates of $\sim 10^{-2}$ /min. Such crazes appear to be blunted by micro-shear bands and do not readily nucleate fracture. They also noted that subsequent shear-band formation and propagation is unhindered by the presence of these crazes. In earlier studies on polycarbonate, Spurr and Niegisch¹ also reported that crazes are carried through and survive the necking process virtually unchanged in size or shape. However, more recently Cornes, Smith and Haward⁴⁰ reported that such crazes formed at 70°C in polycarbonate develop into diamond-shaped cavities during cold-drawing, and final fracture occurs by the interconnection of adjacent diamond cavities.

In this study scanning electron micrographs of the fracture topographies and edges of 1 mm thick polycarbonate specimens fractured at room temperature as a function of strain-rate from 10^{-2} to 10^2 /min were investigated. Such studies reveal how the modes of deformation and failure, including surface crazes, vary with strain-rate. The characteristics of these surface crazes can control directly the stage of deformation at which fracture occurs and, hence, the mechanical response of polycarbonate.

(2) The initiation and propagation of crazes in polycarbonate are enhanced by exposure to certain organic chemicals¹⁻⁸. Polycarbonate crystallization is enhanced by the presence of plasticizers which allow the greater chain mobility necessary for crystallization^{2, 4, 28, 29, 41-45}. Neki and Geil²⁹ report that even a fingerprint will cause crystallization on the surface of polycarbonate after annealing at 110°C. Miller *et al.*² have suggested that the solvent crazing of polycarbonate is caused by stresses arising from the crystallization process. Certainly surface crystallization can cause sufficiently high surface stresses to produce micro-cracks. We have observed directly surface micro-cracks along the edges of prespherulitic arms on the surface of polycarbonate^{16, 18}. Kambour³ notes, however, that solvent crazing behaviour of polycarbonate is too similar to that of non-crystallizable polymers to involve a separate and distinct mechanism dependent on crystallizability. Caird⁸ has documented that handling the surface of polycarbonate followed by exposure to 130°C under stress causes crazing and seriously deteriorates the mechanical response relative to untouched glasses exposed to the same

temperatures and stresses. In this study we investigated the embrittlement of polycarbonate caused by handling, using optical and scanning electron microscopy to elucidate the primary mechanisms responsible.

(3) Electron microscopy has been used to investigate the microscopic deformation modes of polycarbonate by studying microtomed sections⁴⁶⁻⁴⁸ or replicas of prestrained films^{4, 5, 27, 28, 49}. However, we have found polymer films strained directly in the electron microscope can also generate useful information on the modes of deformation of polymers^{23, 50-52} and, therefore, have conducted similar studies on polycarbonate.

EXPERIMENTAL

Materials and sample preparation

The bisphenol A polycarbonate (poly-4,4'-dioxydiphenyl 2,2-propane carbonate) (Lexan, General Electric Co.) had a viscosity-average molecular weight of 30 000 and contained no significant additives. The polymer in the powdered form and prior to any sample preparation was preheated at 125°C overnight in vacuum to remove moisture.

For the fracture topography specimens, compression-moulded sheets (~ 1.0 mm thick) of polycarbonate were prepared by moulding the dry polymer powder at 180°C for 15 min at ~ 35 MPa and then cooling under pressure to room temperature at 2°C/min. Dogbone-shaped specimens, suitable for tensile fracture, were machined from the sheets, and the edges were polished along the gauge length. These specimens were then vacuum annealed at 160°C for 1 h, which minimized fabrication stresses, and then annealed below T_g at either 145° or 125°C.

Discs, ~ 3 cm in diameter and ~ 1.0 mm thick, to be utilized in the studies of the embrittlement of polycarbonate as a result of handling were prepared in circular moulds under the same conditions as those used for the fracture topography specimens. These specimens, however, were not annealed after moulding.

Polycarbonate films, ~ 1 μ m thick, suitable for straining directly in the electron microscope were prepared by spreading a few drops of a 1% solution of the polymer in methylene chloride onto NaCl crystals. The films and substrates were exposed to vacuum for 12 h at room temperature, and any remaining solvent was evaporated at 160°C for 30 min. under vacuum. The salt crystals were dissolved in water, and the films were washed with distilled water. Specimens, 2 mm square, were cut from the polycarbonate films.

Experimental

For the fracture topography studies, the dogbone-shaped samples were fractured in tension at room temperature in a tensile tester (Instron TM-S-1130) at crosshead speeds of 0.05 to 100 cm/min. A scanning reflection electron microscope (Jeol model JEM-100B) was used to study the fracture topographies and edges of these specimens. For these studies the fracture surfaces and edges were coated with gold while the sample was rotated in vacuum.

To study the effects of handling on the embrittlement of polycarbonate, a single thumbprint was placed on the surface of the polycarbonate disc. This disc was then stressed at ~ 10 MPa (at its maximum cross-section) for 1 h at 130°C. The disc was then examined at room temperature by reflection and transmission optical microscopy, using an optical microscope (Zeiss Ultraphot II), and scanning reflection electron microscopy. The disc was coated with gold prior to the scanning electron microscopy studies.

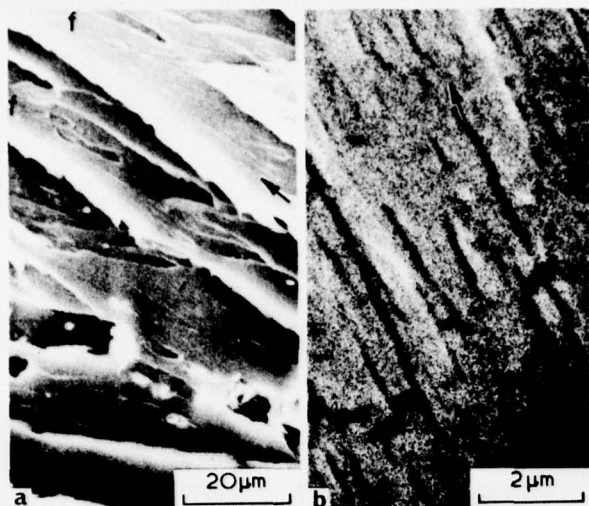


Figure 1 Scanning electron micrographs of fracture surfaces of polycarbonate that deformed and failed under a strain-rate of $\sim 10^{-2} \text{ min}^{-1}$ illustrating (a) parallel planes that intersect at the flaplike structures (f) and (b) microcracks within these planes (arrows indicate direction of crack propagation).

Bright-field transmission electron microscopy was used to monitor the modes of deformation of the $\sim 1 \mu\text{m}$ thick films that were strained directly in the electron microscope. The 2 mm square polycarbonate specimens were fastened to standard cartridge specimen holders with cement (Duco E. I. duPont). The specimen holder was attached to an EM-SEH specimen elongation holder which was introduced into the microscope through the side-entry goniometer. The specimens were deformed in the microscope at a strain-rate of $\sim 10^{-2} \text{ min}^{-1}$.

RESULTS AND DISCUSSION

Variation of modes of deformation and failure with strain-rate

The fracture topographies and edges of the 1 mm thick polycarbonate specimens fractured at room temperature were monitored as functions of strain-rate from $\sim 10^{-2}$ to 10^{+2} min^{-1} . The fracture topographies and edge features of these specimens were similar for both the 125° and 145°C annealed polycarbonates, with the exception that only the 125°C annealed glasses deformed predominantly by crazing in the $\sim 10^{+2} \text{ min}^{-1}$ strain-rate region.

In the 10^{-2} – 1 min^{-1} strain-rate region, polycarbonate deformed predominantly by macroscopic shear-band deformation, and all specimens exhibited necking and cold-drawing prior to fracture by fast crack propagation through the oriented neck. The fractured specimens decreased in width, thus indicating plane stress fracture conditions. The fracture topographies exhibited striations parallel to the direction of crack propagation^{18,21,33,50}. The striations are steps formed by the subdivision of the crack front into segments running on parallel planes as illustrated in Figure 1a. A similar subdivision of the crack front produces river markings in the more brittle polymeric thermosets^{51,53,54}. The flaplike striations [designated by (f) in Figure 1a] that occur at the intersections of the crack planes are a result of tearing and cold-drawing of the polymer and have been observed by Mills²¹ for polycarbonate and Murray and Hull⁵⁵ for polystyrene. The parallel planes shown in Figure 1a exhibit finer striations which are situated parallel or perpendicular to the

direction of crack propagation, as illustrated in Figure 1b. These finer striations appear to be fine cracks which could result from the relaxation of a surface layer of polymer that has been swept onto the fracture surface and oriented in the direction of crack propagation. Elongated fractured fibrils that have been swept down onto the fracture surface have been reported by Doyle^{56,57} and Hoare and Hull⁵⁸ for polystyrene and by the authors for epoxies^{50,59}. Indeed, in certain areas of the polycarbonate surface we observe 100–200 nm diameter fibrils that have been swept onto the fracture surface and aligned in the direction of crack propagation, as illustrated in Figure 2.

Examination of the edges of the polycarbonate specimens that deformed in the 10^{-2} – 1 min^{-1} strain-rate region revealed a network of cavities as illustrated in Figure 3a. These cavities propagated from surface crazes which had developed prior to cold-drawing and had passed into the necked region. The formation during the cold-drawing process of diamond-shaped cavities that initiate from either crazes or surface defects has been reported for a number of polymers, including polycarbonate^{40,60–62}. Such cavities propagate by tearing at the pointed tips of the diamond resulting in a cavity consisting of two straight edges and two pointed extremities^{40,60}. The remnants of such cavities are found in Figures 3a and b. However, many of the surface cavities illustrated in Figure 3a are too irregular to be associated with original diamond-shaped structures. Cornes *et al.*^{40,60} report that the nature of this plastic deformation is controlled by the presence of four shear bands which propagate from each end of the straight edges of the cavity. These cavities grow to thicknesses that are many times that of the original craze. Fracture of the polycarbonate specimens occurs by interconnection of the cavities illustrated in Figure 4a. Cornes, Smith and Haward⁴⁰ have noted that fracture by this process is controlled by the stress concentrations associated with the cavities, which depend on the cavity size and tip radii, the stored elastic energy within the specimen, and the strain-hardening characteristics and crack resistance of the oriented polymer. Cornes and



Figure 2 Scanning electron micrograph of fibrils that have swept onto the fracture surface of polycarbonate that deformed and failed under a strain-rate of $\sim 10^{-2} \text{ min}^{-1}$

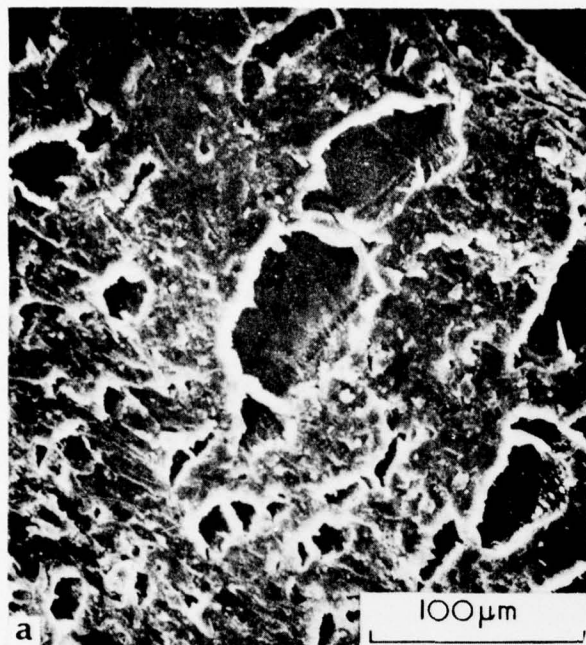


Figure 3 Scanning electron micrographs of the edge of cold drawn polycarbonate that deformed and failed under a strain-rate of $\sim 10^{-2}$ min^{-1} illustrating (a) numerous edge cavities and (b) the topography within a cavity

Haward⁶⁰ associate the smoothness of the cavity walls (Figure 3b) with a slow tearing process. The fractured fibrils on the cavity walls near the specimen surface in Figure 3b originate from the original craze that formed prior to cold-drawing. A distinct boundary is evident in this micrograph between the interior smooth surface associated with the tearing of non-crazed material and the exterior fibrillar, crazed region of the cavity. The latter region has propagated to a depth of 5–10 μm into the specimen prior to the onset of the tearing process.

Hence, polycarbonate specimens that were strained in the 10^{-2} – 1 min^{-1} strain-rate region deform predominantly by shear-band deformation and cold-drawing. However, surface crazes that form prior to macroscopic necking and cold-drawing serve as sites for subsequent plastic tearing and ultimate fracture.

In the 1 to 10^{+2} min^{-1} strain-rate region, polycarbonate still deforms predominantly by macroscopic shear yielding and subsequent cold-drawing. The crazes that form prior to the cold-drawing process are, however, $\geq 100 \mu\text{m}$ in length which is tenfold larger than those that grew in the 10^{-2} to 1 min^{-1} strain-rate region. Such crazes act as sites for crack growth and ultimate failure of the glass.

The fracture topography of an edge craze in the 1 to 10^{+2} min^{-1} strain-rate region is illustrated in Figure 4 in which a curved, cusp separates the edge craze topography from that of the cold-drawn region. In the regions where the craze was thickest, nearer the specimen edge, a patch pattern in the fracture topography is observed as illustrated in Figure 5a. The protruding patches and depressions on one fracture surface match the reverse pattern of protrusions and depressions on the opposite fracture surface. This type of topography is associated with crack propagation along the boundary between the crazed and uncrazed material with the crack jumping irregularly from one boundary to the other^{18,33,63,64}. In previous studies the patches, whose thicknesses are those of the original craze, were generally found to be smooth with no fine structure. In this case, however, the protruding patches exhibit a distinct topography of fractured fibrils interdispersed by voids as illustrated in Figures 5b and c. The depressions on one fracture surface that match the protruding patches on the opposite fracture surface are relatively smooth with the exception of a few fractured fibrils which are perpendicular to the surface (Figure 5a). Similarly situated fibrils have been observed by Doyle⁵⁶ in the fracture surfaces of preoriented polystyrene. The voids on the protruding patches were largest in the regions associated with the thickest portion of the original craze and exhibited a dimple-like structure with dimple diameters of 1–5 μm (Figure 5b). (In metallurgy a dimpled fracture topography is associated with a ductile fracture mode that involves nucleation, growth and coalescence of voids by internal necking^{65–67}.) The dimples in the polycarbonate fracture topography are separated from one another by a single

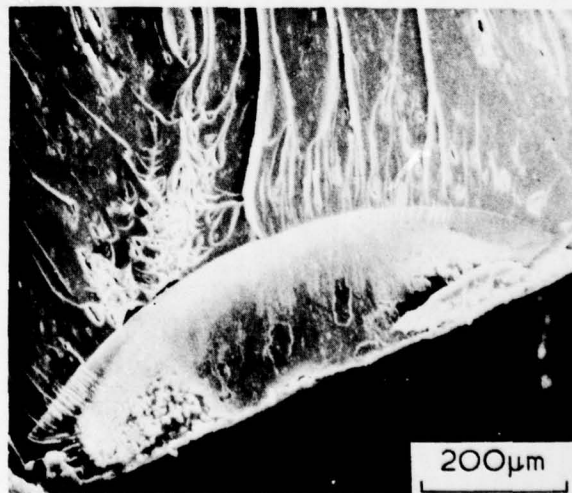


Figure 4 Scanning electron micrograph of the fracture topography of an edge craze in polycarbonate (strain-rate of $\sim 2 \text{ min}^{-1}$)

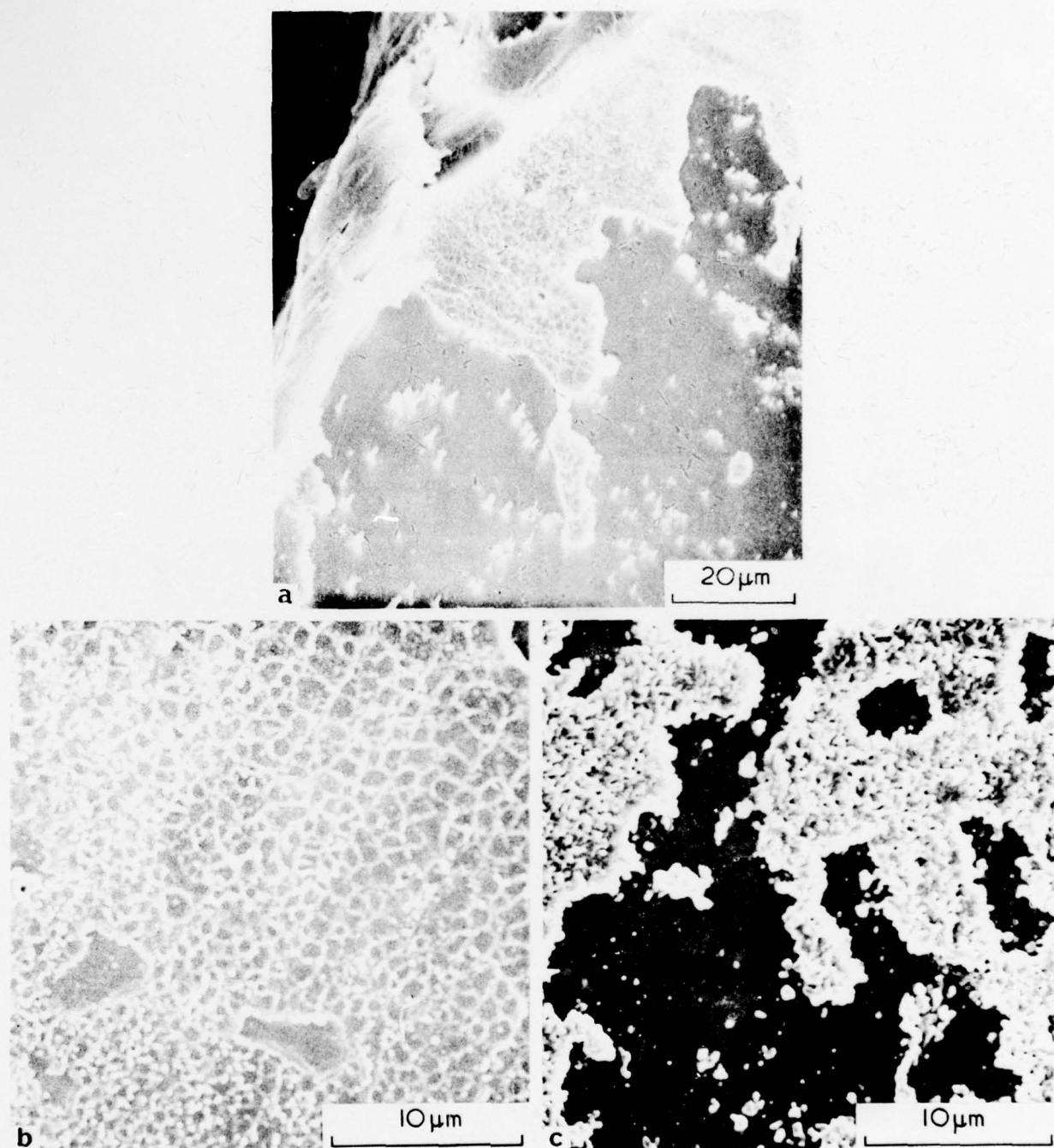


Figure 5 Scanning electron micrographs of the patch-pattern fracture topography of an edge craze in polycarbonate that deformed and failed under a strain-rate of $\sim 2 \text{ min}^{-1}$ illustrating (a) overall, (b) dimpled and (c) fibrillar topographies

boundary of fractured fibrils which are $\leq 500 \text{ nm}$ in diameter. The surfaces of the protruding patches develop a more fractured fibrillar appearance as the voids decrease in size with decreasing thickness of the original craze (Figure 5c).

The overall fracture topography nearer the tip of the craze is shown in Figure 6a. The patch pattern persists in this region, but the patches are much thinner than those nearer the specimen edge because the craze tapers to a thin section. In this region 100–300 nm diameter voids and poorly developed fibrils are evident (Figures 6b and c).

These voids are considerably smaller than those observed in the thicker regions of the original craze. This observation is consistent with other fracture topography studies that also reported a decrease in void size as the craze tip is approached^{68,70}. The voids and poorly formed fibrils taper to a series of fine fingers near the craze tip as illustrated in Figure 6a. These regions are shown in more detail in Figure 7. Highly drawn, thin films of polymer that are perpendicular to the fracture surface and parallel to many of the fine craze fingers are evident in Figure 6a. These highly drawn regions are caused by the crack propagating at a slower rate

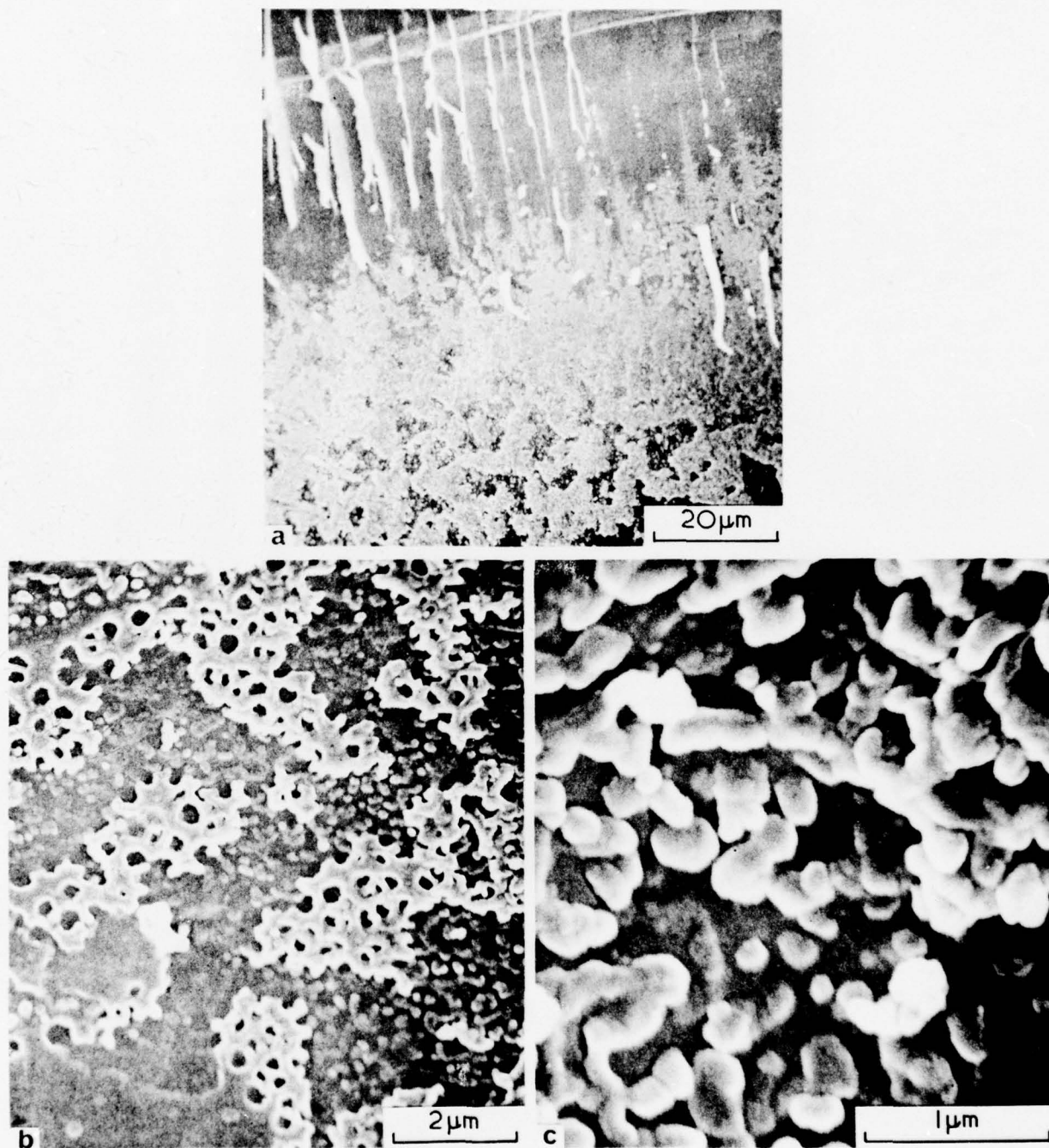


Figure 6 Scanning electron micrographs of craze tip fracture topography of edge craze in polycarbonate that deformed and failed under a strain-rate of $\sim 2 \text{ min}^{-1}$ illustrating (a) overall, (b) microvoid and (c) poorly developed fibrillar topographies of this region

through the crazed fingers and thus lagging-behind the general crack front. No evidence of significant ductile tearing of the craze as a result of cold-drawing was found in the fracture topography crack tip region in Figure 6a.

Crazes normally grow preferentially by areal growth rather than by a thickening mechanism caused by drawing new material across the craze-matrix boundary interface^{3,71}. In the 1 to 10^{+2} min^{-1} strain-rate region, however, after cold-drawing occurs, the oriented material at the craze tip inhibits further areal craze growth in polycarbonate. Crazes do not propagate easily through polymeric material oriented

perpendicular to the craze growth direction^{72,73}. Also, no significant growth of the craze occurs by the ductile tearing process that was observed at lower strain-rates. Therefore, during cold-drawing the craze extends by further internal void growth, coalescence and fibrillation. The strains produced during cold-drawing will be greatest in the thicker regions of the original craze thereby causing larger voids in these regions because of fibrillar fracture and void coalescence.

The distinct porous-fibrillar structure present on the surfaces of the protruding patches in the thicker craze regions

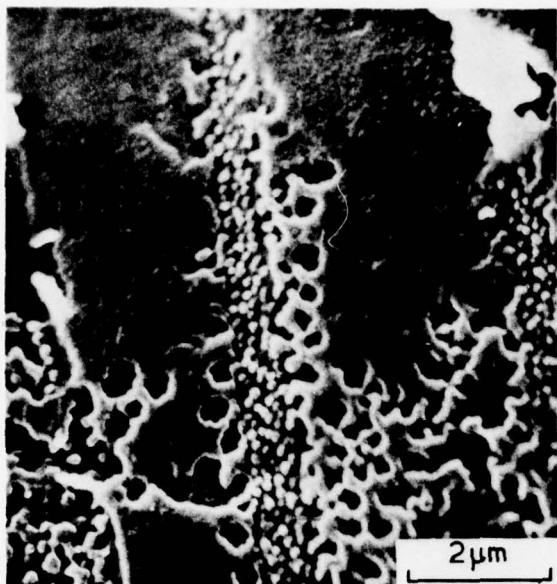


Figure 7 Scanning electron micrograph of fracture topography of craze fingers at tip of edge craze in polycarbonate that deformed and failed under a strain-rate of $\sim 2 \text{ min}^{-1}$

results from crack propagation along the craze-matrix boundary interface. This structure is unusually distinct possibly because of abnormal stresses in the craze, and at the craze-matrix boundary interface during crack propagation caused by the oriented state of the surrounding material. The magnitude and distribution of the stress fields in the vicinity of these crazes during fracture will be different than those that exist in polymers which deform only by crazing.

The fracture topography of the crazes that initiated fracture in polycarbonate in the 1 to 10^{+2} min^{-1} strain-rate region did not exhibit any characteristic slow crack-growth regions on matching fracture surfaces. Initial crack propagation generally proceeds through the median of the craze^{51,54,55,57,59,63,74} producing a fractured fibrillar or rough topography on matching surfaces^{51,54,59}. The absence of a slow crack-growth region suggests that significant crack growth occurred only under the influence of the highly strained surrounding cold-drawn material rather than prior to the onset of cold-drawing.

Hence at room temperature in 1 to 10^{+2} min^{-1} strain-rate region, polycarbonate still deforms predominantly by shear-band deformation and cold-drawing. However, the surface crazes that form prior to cold-drawing and cause ultimate fracture are tenfold larger than those that form in the 10^{-2} to 1 min^{-1} strain-rate region. Also, significant plastic tearing does not occur from these larger crazes prior to catastrophic crack propagation.

In the 10^2 min^{-1} strain-rate region, many 125°C annealed polycarbonate specimens cease to cold-draw and fail by either neck rupturing or crazing. Such specimens are embrittled because of a corresponding decrease in molecular flow and energy to failure.

In neck rupture, failure occurs prior to neck formation but after macroscopic shear zones have propagated to approximately the centre of the specimen. The intersection of the shear bands, which occurs at right-angles, causes a stress concentration^{21,75} sufficient to cause a crack to propagate through the planes of the shear bands. Recently, we have

observed that this fracture mechanism produces microscopic right-angle steps in certain thermoset resins^{23,59,76}.

The specimens that deform and fail by crazing alone exhibit large fracture topography initiation regions which often extend up to $\sim 500 \mu\text{m}$ from the specimen edge. The initiation topography is a porous structure containing 50 – 100 nm diameter fractured fibrils as illustrated in Figure 8. A slow tearing process through the median of the craze produces this topography^{51,54,55,57,59,63,74}. Craze and/or crack growth is not inhibited in these specimens by the presence of any cold-drawn oriented material at the craze tip. The absence of the constraints of oriented material in the craze tip region allows the slow-crack growth process to occur.

An overall view of the faster crack-growth fracture topography region of polycarbonate specimens that deformed and failed by crazing is illustrated in Figure 9a. A distinct patch pattern is observed in the topography immediately adjacent to the initiation region (Figure 9b). This topography is caused by the crack propagating along the craze-matrix boundary interface and jumping irregularly from one boundary to the other^{18,33,63,64,74}. Further removed from the initiation region, the topography consists of alternate bands of smooth valleys and rough hills (Figure 9c). The bands of rough hills consist of the patch topography which is associated with crack propagation through pre-existing crazes. The patches are, however, on a finer scale than those observed nearer the initiation region in Figure 9b. Banded structures have been observed by Jacoby and Cramer⁷⁷, Hull and Owen³³ and Ravetti *et al.*⁷⁸ in previous studies of polycarbonate fracture topographies.

Bands in the fracture topography has been observed in many other polymers and are generally described in terms of rib markings or striations^{33,54,64,77–103}. These bands are



Figure 8 Scanning electron micrograph of fracture topography initiation region of polycarbonate that deformed and failed by crazing under a strain-rate of $\sim 10^2 \text{ min}^{-1}$

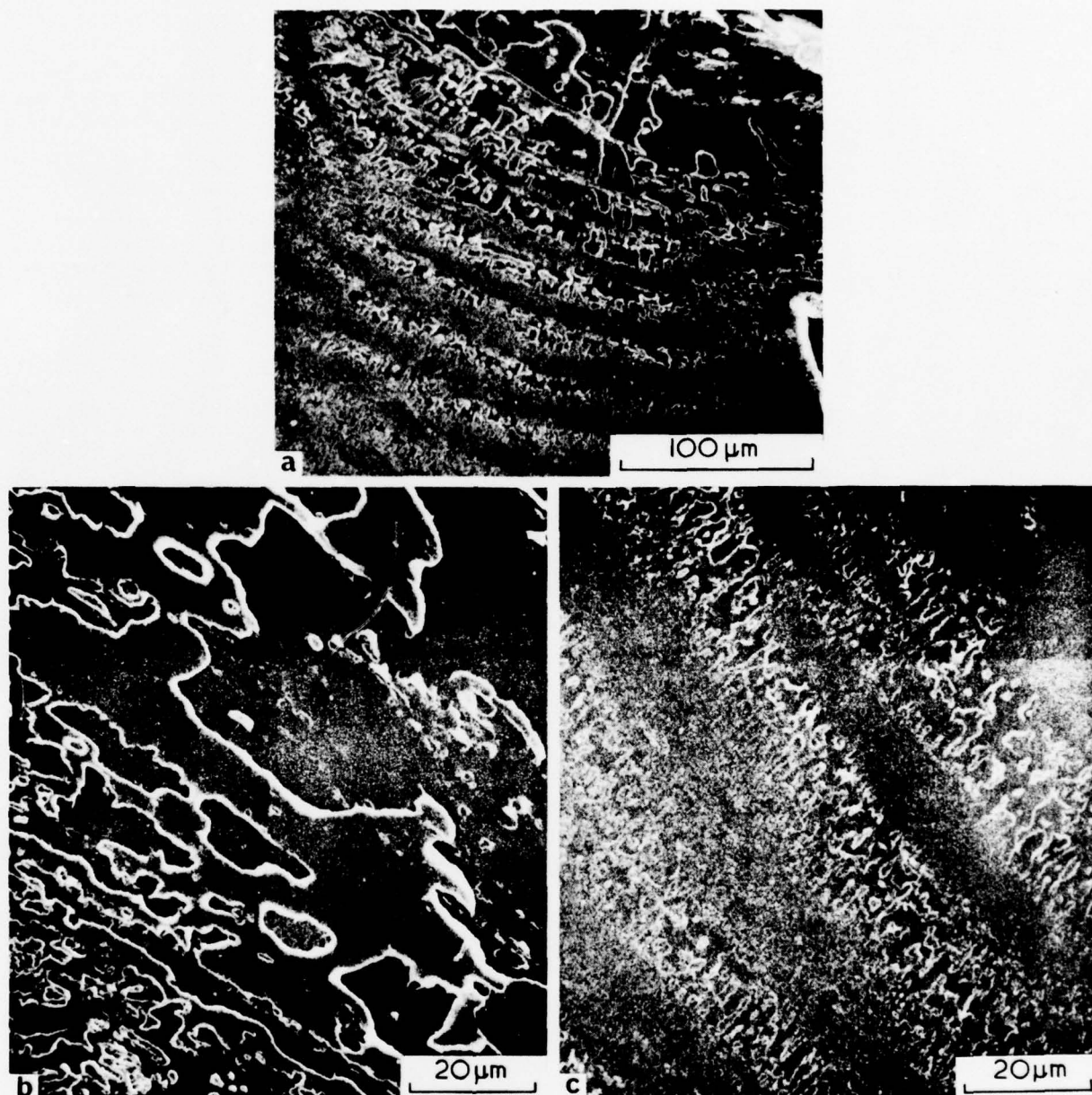
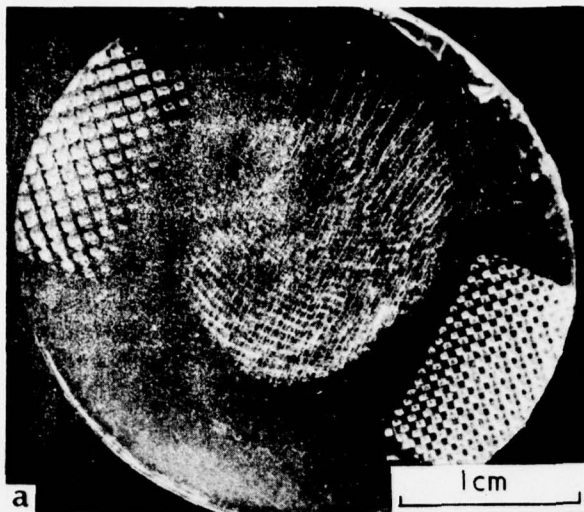


Figure 9 Scanning electron micrographs of the fast crack-growth fracture topography in polycarbonate that deformed and failed by crazing under a strain-rate of $\sim 10^2 \text{ min}^{-1}$ illustrating (a) overall, (b) patch and (c) banded-patch topographies of this region

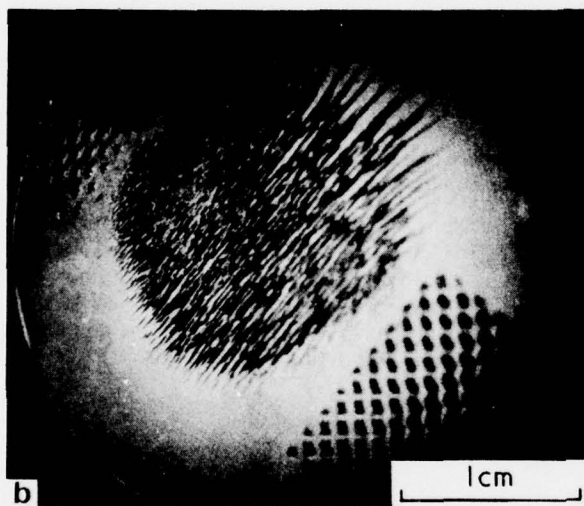
characteristic of relatively brittle fracture and cover a larger area of the fracture surface, with an accompanying decrease in band spacing, when the molecular weight and/or temperature is decreased and/or the strain-rate is increased. Two different mechanisms have been suggested to explain the banded fracture topographies in polymeric materials: (1) Yoffe¹⁰⁴ has theoretically shown that a crack in an elastic material is expected to accelerate to a limiting velocity and then bifurcate. Andrews⁹² notes that branching would be expected to relieve the stress and decelerate the crack. The stress will be restored in a tensile test and, therefore, the processes of crack acceleration followed by bifurcation will be repeated. Craze formation rather than pure crack bifurcation has been suggested to be an intricate part of this slip-stick process in polymers^{33,64,100,102}. (2) The banded topographies could also be Wallner lines which are formed at the loci of the

intersection of the main-crack front with transverse shock waves released during the fracture processes. Such lines were first observed by Wallner¹⁰⁵ in inorganic glasses. This phenomenon is complex in polymers because any perturbation in the stress caused by shock waves can produce changes in both crack and craze growth, and the growth changes in these two processes may not be the same³³. In the case of the banded topographies illustrated in Figure 9, the mechanism involves a crazing process. However, it is not possible to determine whether the banded topographies arise purely from a slip-stick or a Wallner line mechanism. Kusy and Turner¹⁰² have recently noted that both mechanisms could occur in band formation in poly(methyl methacrylate).

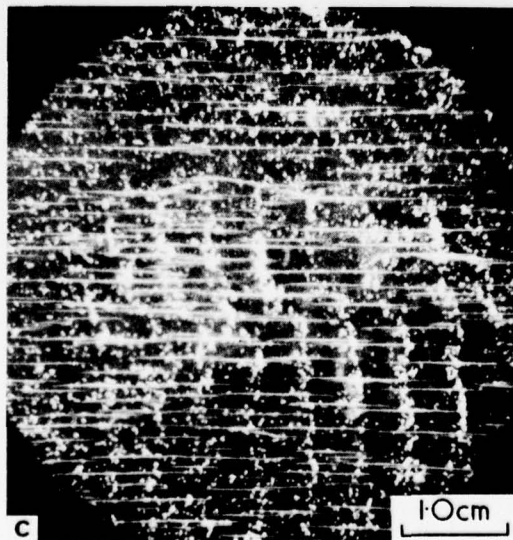
Hence, in the 10^2 min^{-1} strain-rate region, the lower-free-volume, 125°C annealed polycarbonate specimens exhibit evidence of a ductile-brittle transition. These speci-



a



b



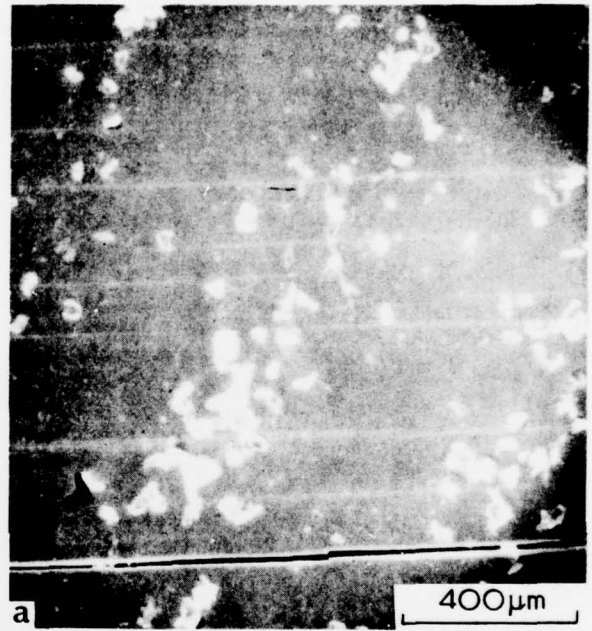
c

Figure 10 Optical micrographs in (a) reflection, (b) transmission and (c) reflection of crazes that initiated from a thumbprint in polycarbonate

mens embrittle as a result of the cessation of cold-drawing with resultant failure by either neck rupture or crazing with a corresponding decrease in molecular flow and energy to failure. The effect of thermal history and free volume on this ductile-brittle transition have been considered in a previous study¹⁸.

Embrittlement mechanism caused by handling

Caird⁸ has documented that handling the surface of polycarbonate followed by exposure to 130°C under stress seriously deteriorates the mechanical properties relative to untouched glasses exposed to the same temperatures and stresses. We investigated the mechanism responsible for this embrittlement by optical and scanning electron microscopy.



a



b

Figure 11 Scanning electron micrographs of crazes in polycarbonate that initiated from islands that had been contacted with finger-grease illustrating (a) overall phenomena and (b) protruding islands

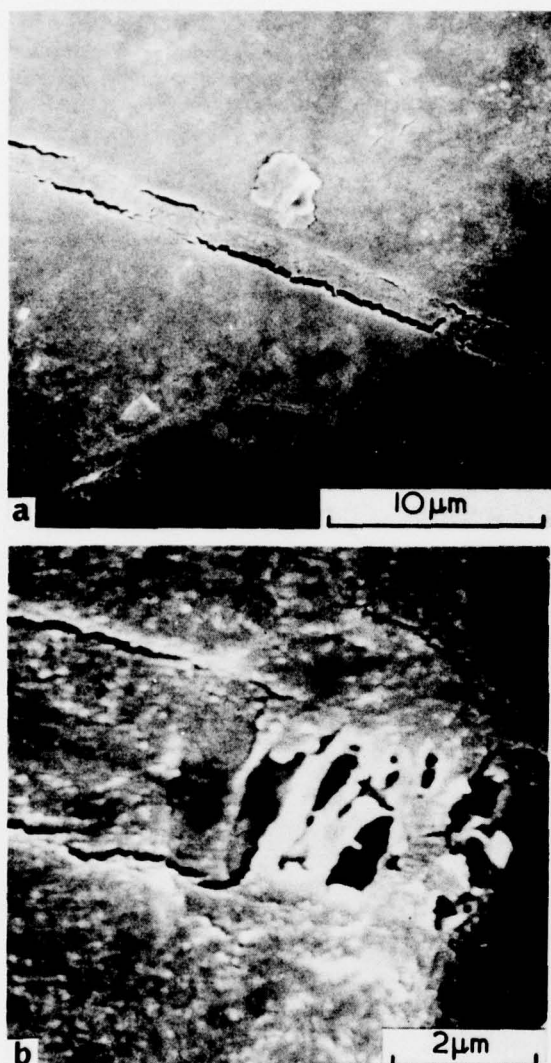


Figure 12 Scanning electron micrographs of surface craze induced by finger-grease in polycarbonate

The optical micrographs in Figure 10 illustrate crazes that have preferentially grown from a thumbprint after the sample was stressed at 10 MPa for 1h at 130°C. Figures 10a and b are reflection and transmission optical micrographs respectively of the crazed region. The reflection optical micrograph in Figure 10c illustrates the lines of the thumbprint and crazes in more detail. In this latter micrograph the thicker, middle portion of each craze generally coincides with a thumbprint line which suggests that crazes initiated at this line. The thumbprint lines, which consist of ~100 μm sized islands of thumb-grease, and associated cracks and/or crazes are illustrated in more detail in the scanning electron micrograph in Figure 11a. Figure 11b illustrates protruding areas where thumb-grease has come into contact with the polymer surface; these areas are separated from the surrounding surface, thereby producing a surface microcrack ~100 μm in length. These cracks act as stress concentrators for craze initiation and growth which leads to premature failure prior to the development of significant flow via shear-band deformation. The parallel lines in Figure 11b are well-developed cracks and/or crazes that have initiated from the ~100 μm microcracks that surround the plasticized islands. The sur-

face crazes often appear as linear surface depressions with parallel cracks along their edges in scanning electron microscopy (Figure 12a). Evidence of the fibrillar craze structure was observed in isolated regions in these micrographs as illustrated in Figure 12b.

From the preceding observations, the following mechanism is suggested by which finger-grease causes surface microcracking. The regions of polycarbonate that have come into contact with finger-grease are plasticized and, therefore, fabrication stresses in such regions relax at a faster rate than those in the unplasticized surroundings. These islands separate from their surroundings and rise above the general surface contour when the fabrication stresses and orientation are parallel to the polymer surface. The inhomogeneous distribution of the plasticizing agent is a significant factor in this particular solvent-crazing mechanism. However, smearing finger-grease to produce a continuous surface grease layer still produces general microcracking, following stress and temperature exposure, as a result of a general relaxation of fabrication stresses. These microcracks which are illustrated in Figure 13 are, however, < 10 μm in length which is a factor of 10 smaller than those produced from the plasticized islands.

These studies produced no evidence that solvent-induced surface crystallization plays any role in the craze initiation and growth processes.

Deformation processes in polycarbonate films strained directly in the electron microscope

Polycarbonate films ~1 μm thick, were strained directly in the electron microscope. These films deformed and failed by crazing as illustrated in the transmission electron micrographs in Figure 14. Crazes initiate as thinned regions in these films rather than by void formation. This thinning process has been previously reported in thin polycarbonate



Figure 13 Scanning electron micrograph of surface microcracks in polycarbonate induced by a layer of finger-grease

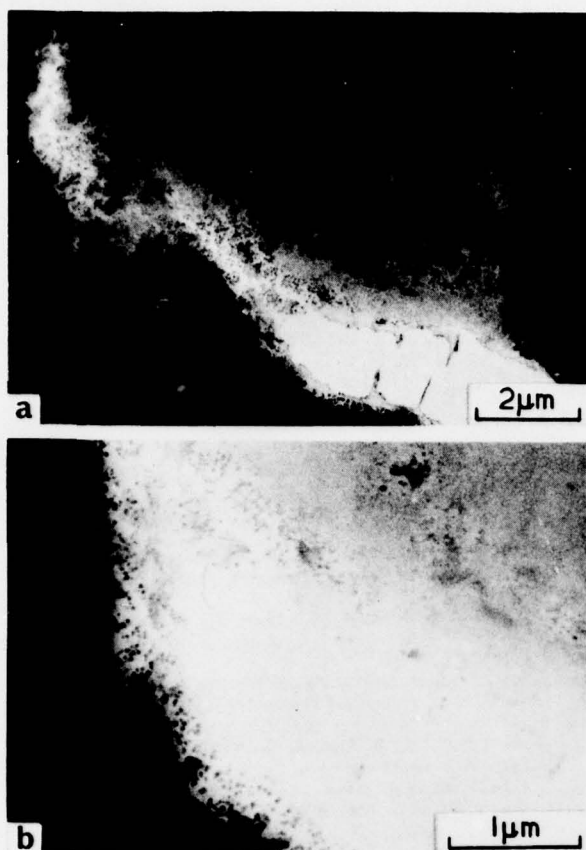


Figure 14 Bright-field transmission electron micrographs of a craze in a strained polycarbonate thin film illustrating (a) overall craze and surroundings and (b) craze structure

films by Wyzgoski and Yeh⁴ and Thomas and Israel⁵ and is attributed to the lateral contraction of the film during deformation. Voids and fibrils develop in the later stages of growth in these regions; the remnants of such fractured fibrils are evident in Figure 14.

In the thinned regions and the craze fibrils in the micrographs in Figure 14, dark, ~ 10 nm sized nodular regions are evident. These regions are evidently less susceptible to deformation and do not break-up and become thinner during the flow processes but simply move past one another. These less-deformable, ~ 10 nm sized nodular regions are illustrated in more detail in the craze-crack tip region in the bright-field transmission electron micrograph in Figure 15. Such nodular regions appear dark in bright-field transmission because they are thicker than their surroundings. It is uncertain whether such regions are (a) precrystalline nodular structures, (b) less-deformable regions produced by electron-beam damage or (c) thicker regions produced during the solvent evaporation processes. Certainly precrystalline and/or crystalline entities can form during film fabrication from solution or grow below the bulk T_g in thin films or on free surfaces where mobility restrictions are less severe than in the bulk¹⁸. Hence, if these less-deformable regions are a consequence of surface crystallization processes in polycarbonate, such regions could also be present on the surfaces of bulk specimens and play a role in the bulk craze initiation processes.

CONCLUSIONS

The flow processes and toughness of glassy polycarbonate in tension are controlled by the ease of shear-band deforma-

tion and the resultant strain-hardening characteristics of the cold-drawn material, together with the characteristics of surface crazes which form prior to macroscopic necking. The geometry and physical structure of the surface crazes together with the crack resistance of the oriented polymer can directly control at what stage of deformation fracture occurs, and, hence, toughness of the polymer. The characteristics of these surface crazes varied as a function of strain-rate in 1 mm thick polycarbonate specimens deformed in tension at room temperature. In the 10^{-2} – 10^{+2} min^{-1} strain-rate region, the polycarbonate specimens deformed predominantly by shear-band deformation and cold drawing. However, surface crazes that form prior to macroscopic necking and cold-drawing serve as sites for ultimate fracture. In the 10^{-2} – 1 min^{-1} strain-rate region, the crazes grow to ~ 5 – 10 μm in length prior to macroscopic shear-band deformation. Subsequent cold-drawing leads to the growth of these craze sites by plastic tearing. In the 1 – 10^2 min^{-1} strain-rate region, larger surface crazes up to ~ 100 μm in length develop prior to macroscopic shear-band deformation. These crazes, however, do not significantly grow in area prior to catastrophic crack propagation through the oriented, cold-drawn material. In the $\sim 10^2$ min^{-1} strain-rate region, specimens with low free-volumes, as a result of annealing at 125°C , ceased to cold-draw and deformed and failed either by crazing or by a neck rupture process. Such specimens are embrittled because of a corresponding decrease in molecular flow and energy to failure.

Surface crazing is enhanced in polycarbonate by environmental factors such as handling. The regions of the polycarbonate surface that have come into contact with finger-grease are plasticized, and fabrication stresses in such regions relax near T_g at a faster rate than those in the unplasticized surroundings. The plasticized, relaxed regions separate from their surroundings producing microcracks which serve as sites for craze initiation and growth, and possible embrittlement of the polymer.

Crazes initiated and propagated in thin polycarbonate films that were deformed directly in the electron microscope. Nodular regions, ~ 10 nm in size, which did not break-up

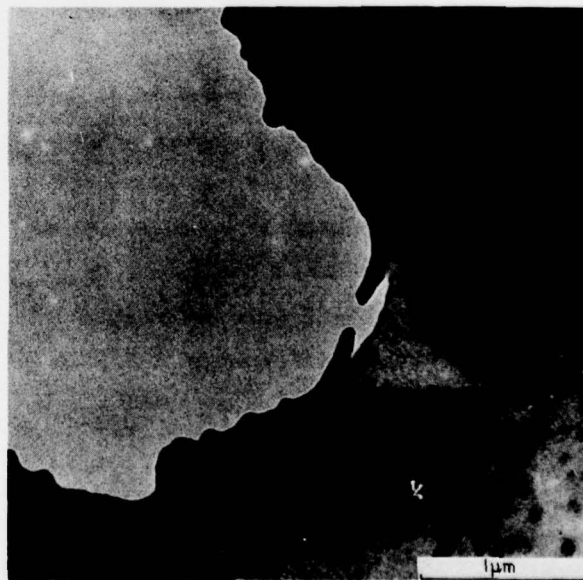


Figure 15 Bright-field transmission electron micrograph of craze-crack tip region in strained polycarbonate thin film

during the craze flow processes were observed in these films.

ACKNOWLEDGEMENTS

The authors wish to acknowledge Lt. Col. Richard Haffner and Dr. Donald Ulrich (AFOSR), and Drs. Donald P. Ames and Clarence J. Wolf (MDRL, St. Louis) for their support and encouragement of this work.

REFERENCES

- 1 Spurr, O. K., Jr. and Neigisch, W. D., *J. Appl. Polym. Sci.* 1962, **6**, 585
- 2 Miller, G. W., Visser, S. A. D., and Morecroft, A. S., *Polym. Eng. Sci.* 1971, **11**, 73
- 3 Kambour, R. P. *Macromol. Rev.* 1973, **7**, 1
- 4 Wyzgoski, M. G. and Yeh, G. S. Y., *J. Macromol. Sci. (B)* 1974, **10(3)**, 441 and 647
- 5 Thomas, F. L. and Israel, S. J., *J. Mater. Sci.* 1975, **10**, 1603
- 6 Brown, N. and Imai, Y., *J. Appl. Phys.* 1975, **46**, 4130
- 7 Ohishi, F., Nakamura, S., Koyama, D., Minabe, K., Fujisawa, Y., and Tsuruga, Y., *J. Appl. Polym. Sci.* 1976, **20**, 79
- 8 Caird, D. W., Proc. of Air Force Conference on Aerospace Transparent Materials and Enclosures, AFML-TR-76-54 (1976) p 367
- 9 Peilstocker, G., *Kunststoffe* 1961, **51**, 509
- 10 Peilstocker, G., *Brit. Plastics* 1962, **35**, 365
- 11 Golden, J. H., Hammant, B. L., and Hazell, E. A. *J. Appl. Polym. Sci.* 1967, **11**, 1571
- 12 LeGrand, D. G., *J. Appl. Polym. Sci.* 1969, **13**, 2129
- 13 LeGrand, D. G., *J. Appl. Polym. Sci.* 1972, **16**, 1367
- 14 Robertson, R. E. and Joynson, C. W., *J. Appl. Polym. Sci.* 1972, **16**, 733
- 15 Allen, G., Morley, D. C. W., and Williams, T., *J. Mater. Sci.* 1973, **8**, 1449
- 16 Morgan, R. J. and O'Neal, J. E., *Polym. Plast. Tech. and Eng.* 1975, **5(2)**, 173
- 17 Adam, G. A., Cross, A., and Haward, R. N., *J. Mater. Sci.* 1975, **10**, 1582
- 18 Morgan, R. J. and O'Neal, J. E., *J. Polym. Sci. (Polym. Phys. Edn)* 1976, **14**, 1053
- 19 Morgan, R. J. and O'Neal, J. E. in *Toughness and Brittleness of Plastics, Advances in Chemistry Series 154*, Eds. Deanin, R. D. and Grignola, A. M., (ACS, Washington, D. C., 1976) Ch 2
- 20 Morgan, R. J., Proc. of Air Force Conference on Aerospace Transparent Materials and Enclosures, AFML-TR-76-54 (1976) p 349
- 21 Mills, N. J. *J. Mater. Sci.* 1976, **11**, 363
- 22 Yee, A. F., *J. Mater. Sci.* 1977, **12**, 757
- 23 Morgan, R. J. and O'Neal, J. E., *Org. Plast. Coat. Preprints (ACS)* 1977, **37(2)**, 480
- 24 Renninger, A. L., Wicks, G. G., and Uhlmann, D. R., *J. Polym. Sci. (Polym. Phys. Edn)* 1975, **13**, 1247
- 25 Wignall, G. D. and Longman, G. W. *J. Macromol. Sci. (B)* 1976, **12(1)**, 99
- 26 Frank, W., Goddar, H., and Stuart, H. A. *J. Polym. Sci. (B)* 1967, **5**, 711
- 27 Carr, S. H., Geil, P. H. and Baer, E., *J. Macromol. Sci. (B)* 1968, **2(1)**, 13
- 28 Siegmann, A. and Geil, P. H. *J. Macromol. Sci. (B)* 1970, **4(2)**, 239 and 273
- 29 Neki, K. and Geil, P. H. *J. Macromol. Sci. (B)* 1973, **8(1-2)**, 295
- 30 Wyzgoski, M. G. and Yeh, G. S. Y., *Int. J. Polymeric. Mater.* 1974, **3**, 149
- 31 Geil, P. H., *J. Macromol. Sci. (B)* 1976, **12(2)**, 173
- 32 Takano, M. and Nielson, L. E. *J. Appl. Polym. Sci.* 1976, **20**, 2193
- 33 Hull, D. and Owen, T. W., *J. Polym. Sci. (Polym. Phys. Edn)* 1973, **11**, 2039
- 34 Parvin, M. and Williams, J. G., *J. Mater. Sci.* 1975, **10**, 1833
- 35 Kambour, R. P. and Miller, S., *J. Mater. Sci.* 1976, **11**, 823
- 36 Ishikawa, M., Narisawa, I., and Ogawa, H., *J. Polym. Sci. (Polym. Phys. Edn.)* 1977, **15**, 1791
- 37 Kambour, R. P. and Miller, S., *J. Mater. Sci.* 1977, **12**, 2281
- 38 Fraser, R. A. W. and Ward, I. M., *J. Mater. Sci.* 1977, **12**, 459
- 39 Kastelic, J. R. and Baer, E., *J. Macromol. Sci. (B)* 1973, **7(4)**, 679
- 40 Cornes, P. L., Smith, K., and Haward, R. N. *J. Polym. Sci. (Polym. Phys. Edn)* 1977, **15**, 955
- 41 Moore, W. R. and Sheldon, R. P. *Polymer* 1961, **2**, 315
- 42 Kambour, R. P., Karasz, F. E., and Duane, J. M. *J. Polym. Sci. (A)*, 1966, **2**, 4, 327
- 43 Mercier, J. P., Groeninckx, G., and Lesne, M., *J. Polym. Sci. C*, 1967, **16**, 2059
- 44 Titow, W. V., Braden, M., Currell, B. R. and Loneragan, R. J. *J. Appl. Polym. Sci.* 1974, **18**, 867
- 45 Gallez, F., Legras, R., and Mercier, J. P. *J. Polym. Sci. (Polym. Phys. Edn.)* 1976, **14**, 1367
- 46 Kambour, R. P., *Polymer* 1964, **5**, 143
- 47 Kambour, R. P. and Holik, A. S., *J. Polym. Sci. (A)* 1969, **2**, 7, 1393
- 48 Kambour, R. P. and Russell, R. R., *Polymer* 1971, **12**, 237
- 49 Klement, J. J. and Geil, P. H. *J. Macromol. Sci. (B)*, 1972, **6(1)**, 31
- 50 Morgan, R. J. and O'Neal, J. E., *J. Mater. Sci.* 1977, **12**, 1338
- 51 Morgan, R. J. and O'Neal, J. E., *J. Mater. Sci.* 1977, **12**, 1966
- 52 Morgan, R. J. and O'Neal, J. E., in *Chemistry and Properties of Crosslinked Polymers*, E. Labana, S. S. (Academic Press, 1977) p 289
- 53 Owen, M. J. and Rose, R. G. *J. Mater. Sci.* 1975, **10**, 1711
- 54 Morgan, R. J. and O'Neal, J. E., *J. Macromol. Sci. (B)*, 1978, **15(1)**, 139
- 55 Murray, J. and Hull, D., *J. Polym. Sci. (A)*, 1970, **2**, 8, 1521
- 56 Doyle, M. J., *J. Polym. Sci. (Polym. Phys. Edn.)* 1975, **13**, 127
- 57 Doyle, M. J., *J. Mater. Sci.* 1975, **10**, 300
- 58 Hoare, J. and Hull, D., *J. Mater. Sci.* 1975, **10**, 1861
- 59 Morgan, R. J. and O'Neal, J. E., *Polym. Plast. Tech. and Eng.* 1978, **10(1)**, 49
- 60 Cornes, P. L. and Haward, R. N. *Polymer* 1974, **15**, 149
- 61 Tormala, P., Lehtinen, S., and Lindberg, J. J. *J. Mater. Sci.* 1976, **11**, 1764
- 62 Smith, K. and Haward, R. N. *Polymer* 1977, **18**, 746
- 63 Murray, J. and Hull, D., *Polymer* 1969, **10**, 451
- 64 Murray, J. and Hull, D., *J. Polym. Sci. A-2*, 1970, **8**, 583
- 65 Cottrell, A. H., in *Fracture*, Eds. Averbach, B. L., Felbeck, D. K., Hahn, G. T. and Thomas, D. A. (Wiley, 1959) p 20
- 66 Rogers, H., *Trans. Met. Soc. AIME* 1960, **218**, 498
- 67 Low Jun, J. R., *Eng. Fract. Mech.* 1968, **1**, 47
- 68 Hertzberg, R. W. and Manson, J. A. *J. Mater. Sci.* 1973, **8**, 1554
- 69 Skibo, M. D., Hertzberg, R. W. and Manson, J. A. *J. Mater. Sci.* 1976, **11**, 479
- 70 Skibo, M. D., Hertzberg, R. W., Manson, J. A., and Kim, S. L. *J. Mater. Sci.* 1977, **12**, 531
- 71 Rabinowitz, S. and Beardmore, P., in *Critical Reviews in Macromolecular Science* (Chem. Rubber Company, Cleveland, 1972), Vol. 1, p 1
- 72 Rehage, G. and Goldbach, G., *Angew. Macromol. Chem.* 1967, **1**, 125
- 73 Haward, R. N., Murphy, B. M., and White, E. F. T., *Fracture*, Proc. 2nd Int. Conf. Fracture, Brighton (Chapman and Hall, London, 1969), p 579
- 74 Beahan, P., Bevis, M., and Hull, D., *J. Mater. Sci.* 1972, **8**, 162
- 75 Hull, D., *Acta Met.* 1960, **8**, 11
- 76 Morgan, R. J., O'Neal, J. E. and Miller, D. B. *J. Mater. Sci.* (in press)
- 77 Jacoby, G. and Cramer, C., *Rheol. Acta*, 1968, **7**, 23
- 78 Ravetti, R., Gerberich, W. W., and Hutchinson, T. E. *J. Mater. Sci.* 1975, **10**, 1441
- 79 Rexer, E., *Z. Tech. Phys.* 1939, **20**, 97
- 80 Kies, J. A., Sullivan, A. M., and Irwin, G. R., *J. Appl. Phys.* 1950, **21**, 716
- 81 Hsiao, C. C. and Sauer, J. A., *J. Appl. Phys.* 1950, **21**, 1071
- 82 Cheatham, R. G. and Dietz, A. G. H. *Mod. Plast.* 1951, **29**, No. 1, 113
- 83 Zanderman, F., *Publ. Scient. Tech. Minist. Air, Paris*, No. 291 (1954) Ch. IV
- 84 Leeuwrik, J. and Schwarzl, F., *Plastica* 1955, **8**, 474
- 85 Smith, D. C., *Nature* 1958, **182**, 132
- 86 Newman, S. B. and Wolock, I., *J. Appl. Phys.* 1958, **29**, 49
- 87 Andrews, E. H., *J. Appl. Phys.* 1959, **30**, 740
- 88 Benbow, J. *J. Proc. Phys. Soc.* 1961, **78**, 970

- 89 Wolock, I. and Newman, S. B., in *Fracture Processes in Polymeric Solids*. Ed. Rosen, B. (Interscience, 1964) Ch. IIc
- 90 Broutman, L. J. and McGarry, F. J., *J. Appl. Polym. Sci.* 1965, **9**, 589
- 91 Cottrell, B., *Appl. Mater. Res.* 1965, **4**, 227
- 92 Andrews, F. H., *Fracture in Polymers* (Elsevier, New York, 1968)
- 93 Murray, J. and Hull, D., *J. Polym. Sci. (B)* 1970, **8**, 159
- 94 Hull, D., *J. Mater. Sci.* 1970, **5**, 357
- 95 Doyle, M. J., Maranci, A., Orowan, E., and Stork, S. T. *Proc. Roy. Soc. (London)* 1972, **A239**, 137
- 96 Moskowitz, H. D. and Turner, D. T. *J. Mater. Sci.* 1974, **9**, 861
- 97 Doyle, M. J., *J. Mater. Sci.* 1975, **10**, 159
- 98 Doll, W., *J. Mater. Sci.* 1975, **10**, 935
- 99 Kusy, R. P., *J. Mater. Sci.* 1976, **11**, 1381
- 100 Kusy, R. P., Lee, H. B. and Turner, D. T. *J. Mater. Sci.* 1976, **11**, 118
- 101 Friederich, K., *J. Mater. Sci.* 1977, **12**, 640
- 102 Kusy, R. P. and Turner, D. T. *Polymer* 1977, **18**, 391
- 103 Kusy, R. P., Lee, H. B. and Turner, D. T. *J. Mater. Sci.* 1977, **12**, 1694
- 104 Yoffe, E. H. *Phil. Mag.* 1951, **42**, 739
- 105 Wallner, H., *Z. Phys.* 1939, **114**, 368

APPENDIX G: The Effect of Thermal History and Strain-Rate on
the Mechanical Properties of Diethylene Triamine-
Cured Bisphenol-A-Diglycidyl Ether Epoxies,
J. Appl. Polym. Sci. 23, 2711 (1979)

The Effect of Thermal History and Strain Rate on the Mechanical Properties of Diethylenetriamine-Cured Bisphenol-A-Diglycidyl Ether Epoxies

ROGER J. MORGAN,* *McDonnell Douglas Research Laboratories,
McDonnell Douglas Corporation, St. Louis, Missouri 63166*

Synopsis

The tensile mechanical properties of diethylenetriamine (DETA)-cured bisphenol-A-diglycidyl ether (DGEBA) epoxies prepared from 9, 11 and 13 phr DETA are reported as a function of thermal history, strain-rate and test temperature. These epoxies exhibit macroscopic yield stresses and >10% ultimate elongations. The mechanical properties of these epoxies exhibit a free-volume dependence as a function of thermal history. Annealing below T_g causes an increase in the macroscopic yield stress and a decrease in the ultimate elongation, whereas quenching from above T_g lowers the yield stress and increases the elongation. These mechanical property modifications are shown to be reversible with reversible thermal-anneal cycles. The activation volumes associated with Eyring's theory for stress-activated viscous flow for the DGEBA-DETA epoxies are within the range of values (9–12 nm³) reported for noncrosslinked polymers. These observations suggest that the DGEBA-DETA epoxies are not as highly crosslinked as would be expected from normal addition reactions of epoxide groups with primary and secondary amines. The formation of lower crosslink density networks is discussed in terms of potential chemical reactions.

INTRODUCTION

The increasing use of epoxies as adhesives and composite matrices has led to a need to predict the durability of these materials in service environments. The durability of epoxies can be predicted with confidence only if their basic structure-property relations are understood.

The structure of epoxies can be complex. The chemical and physical structures depend on specific cure conditions because more than one reaction can occur and the kinetics of each reaction exhibits different temperature dependences. In addition, the structure is affected by such factors as steric and diffusional restrictions of the reactants during cure,¹⁻⁶ the presence of impurities which can act as catalysts,⁷ the reactivity of the epoxide and curing agent,⁸ isomerization of epoxide groups,⁹⁻¹¹ inhomogeneous mixing of the reactants,¹² and cyclic polymerization of the growing chains.⁸ These factors can lead to physically and chemically heterogeneous network structures.

Amine-cured epoxides are one of the most common epoxy systems. In these systems, networks are generally assumed to result from addition reactions of epoxide groups with primary and secondary amines. For epoxides and amines with functionalities ≥ 3 , highly crosslinked network structures can be formed. However, recent electron and optical microscopy studies of strained films and fracture topographies of diethylenetriamine (DETA)-cured bisphenol-A-dig-

* Present address: Lawrence Livermore Laboratory, L-338, University of California, P.O. Box 808, Livermore, California 94550.

lycidyl ether (DGEBA) epoxies indicated that these epoxies deform and fail by a crazing process.¹³ This crazing process involves significant microscopic flow, which is not expected for a highly crosslinked epoxy network structure.

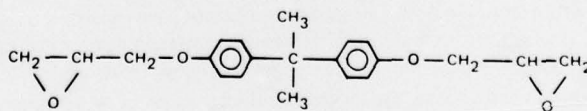
The chemical structures of the DETA and DGEBA molecules are illustrated in Figure 1. The DGEBA epoxide is difunctional, whereas the DETA amine is pentafunctional if all the amine hydrogens react. Hence if all amine hydrogens react with epoxide groups in the absence of side reactions, a highly crosslinked network structure should be produced.

The purpose of this paper is to further illustrate that the DGEBA-DETA epoxies are not highly crosslinked glasses, as indicated by their tensile mechanical properties and the effect of thermal history and strain rate on these properties.

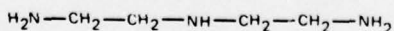
EXPERIMENTAL

DER 332 (Dow) pure DGEBA monomer and DETA (Eastman) were used in this study. Prior to mixing, both the DGEBA and DETA monomers were exposed to vacuum to remove absorbed moisture. The DGEBA epoxy monomer was also heated to 60°C to melt any crystals present¹² and was then immediately mixed with the DETA at room temperature. Epoxies with three different epoxy:amine ratios were prepared: 9, 11, and 13 parts per hundred by weight (phr) DETA. (The stoichiometric mixture for the DGEBA-DETA system contains ~11 phr DETA.¹⁴ This composition was determined by assuming that all amine hydrogens react with epoxide groups in absence of side reactions.) Sheets, 0.75 mm thick, of each epoxy mixture were prepared between glass plates separated by Teflon spacers. A release agent (Crown 3070) was used to facilitate the removal of the epoxy sheets from the glass plates. The epoxy sheets were cured at room temperature for 24 hr in vacuum, then removed from the glass plates, and postcured at 150°C for 24 hr in vacuum. The glasses were cooled slowly at 2°C/min to room temperature to minimize any stresses caused by thermal gradients.

Dogbone-shaped specimens, suitable for tensile mechanical property studies, were machined to a 2.5-cm gauge length and a width of 0.3 cm within the gauge length from the cured sheets; the edges were polished along the gauge length. For T_g measurements a portion of the epoxy sheets were filed to produce a powder suitable for DSC measurements.



bisphenol-A diglycidyl ether epoxy
DGEBA



diethylene triamine
DETA

Fig. 1. The DGEBA-DETA epoxy system.

Some of the dogbone-shaped specimens were exposed to various thermal histories by annealing in a preheated tube furnace in He. These specimens were quenched in ice water when removed from the furnace.

For the room-temperature tensile mechanical property studies, dogbone-shaped specimens were fractured in tension in a tensile tester (Instron TM-S-1130) at crosshead speeds of 0.05–5.0 cm/min. DSC analyses to determine the T_g 's of the epoxy specimens were performed with a differential scanning calorimeter (Rigaku model M 8075) using a heating rate of 5°C/min.

RESULTS AND DISCUSSION

The T_g 's of the DGEBA-DETA epoxy systems are shown in Table I. The T_g exhibits a maximum at the stoichiometric composition. Maxima in T_g as a function of composition have been previously reported for a number of epoxy systems.^{6,15–20} For amine-epoxide addition reactions in the absence of side reactions, Bell¹⁶ has theoretically shown that excess amine increases the molecular weight between crosslinks, which lowers the T_g relative to an epoxy prepared from the stoichiometric mixture. Bell also noted that excess epoxy systems would possess approximately a similar molecular weight between crosslinks. However, unreacted epoxide groups could plasticize the system. Also, excess of one component in the system enhances the possibility of unreacted molecules which act as plasticizers. Furthermore, steric and diffusional restrictions can limit the chemical reactions, which further accentuates the number of unreacted species.

The effect of thermal history on the tensile room-temperature mechanical properties of DGEBA-DETA epoxies are illustrated in Table II. These epoxies exhibit macroscopic yield stresses and >10% ultimate elongations. Lee and Neville²¹ report higher ultimate elongations for these DGEBA-DETA epoxy systems. These types of mechanical responses suggest that these glasses are not highly crosslinked.

Furthermore, the mechanical properties of these epoxies exhibit a free-volume dependence as a function of thermal history, which indicates that these glasses consist of regions of lightly or noncrosslinked material. A typical volume-temperature plot for a polymer is illustrated in Figure 2. Changes in free volume, or local order, in the glassy state can occur as a result of the extension to temperatures below T_g of packing changes associated with the liquid state. The liquid-volume temperature plot extrapolated to below T_g in Figure 2 represents the lower free-volume, equilibrium state of the glass. The time necessary to achieve the equilibrium state at a given temperature below T_g depends on the glassy-state mobility. Below a specific temperature, the glassy-state mobility is too small to allow any changes in free volume. A decrease in free volume that

TABLE I
 T_g 's of DGEBA-DETA Epoxies

Composition	T_g , °C
DGEBA-DETA (9 phr DETA) epoxy	116
DGEBA-DETA (11 phr DETA) epoxy	130
DGEBA-DETA (13 phr DETA) epoxy	107

TABLE II
Effect of Thermal History on the Tensile Room-Temperature Mechanical Properties (Strain Rate $\sim 10^{-2} \text{ min}^{-1}$) of DGEBA-DETA Epoxies

Thermal history	Yield (Y) or fracture (F) stress, ^a MPa ± 1	Ultimate elongation, ^a % ± 1
DGEBA-DETA (9 phr DETA) epoxy		
Unannealed	(Y) 84	11
111°C, 1 day	(Y) 87	11
111°C, 2 days	(Y) 88	11
111°C, 4 days	(F) 77	9
Quenched in ice water from 171°C after 10 min	(Y) 77	14
DGEBA-DETA (11 DETA) epoxy		
Unannealed	(Y) 76	13
125°C, 1 day	(Y) 80	11
Quenched in ice water from 185°C after 10 min	(Y) 75	15
DGEBA-DETA (13 phr DETA) epoxy		
Unannealed	(Y) 81	14
102°C, 1 day	(Y) 84	14
102°C, 3 days	(Y) 84	13
102°C, 6 days	(Y) 84	12
102°C, 17 days	(Y) 86	11
Quenched in ice water from 162°C after 10 min	(Y) 75	15
A-1: 102°C, 1 day	(Y) 84	14
A-2: quenched in ice water from 162°C after 10 min	(Y) 74	17
A-3: 102°C, 1 day	(Y) 84	14

^a Average values for five specimens measured at each specific thermal history.

occurs in the glassy state results in inhibition of the flow processes that occur during deformation and a more brittle mechanical response. Rapid cooling from above T_g , however, produces a glass with a larger free volume.

For each DGEBA-DETA epoxy in Table II, annealing 5°C below T_g causes an increase in the macroscopic yield stress and a decrease in the ultimate extension as the equilibrium states of these glasses are approached. Quenching from 55°C above T_g for each epoxy composition produces lower macroscopic yield stresses because of the high free volume frozen into these glasses. Prior to deformation, DGEBA-DETA (13 phr DETA) epoxy specimens designated A-1, A-2, and A-3 in Table II were exposed to the same thermal history as the preceding samples in this series. After initially annealing at 102°C for 1 day (A-1), quenching from 55°C above T_g (A-2) produces a lower macroscopic yield stress. Subsequent annealing of the quenched specimen in the glassy state 5°C below T_g (102°C) (A-3) produces essentially reversible changes in the macroscopic yield stress and ultimate elongation. These reversible changes in the mechanical properties suggest that little change occurs in the crosslink density in the regions controlling the flow processes as a result of the annealing conditions. Furthermore, the modifications of the macroscopic yield stress and ultimate elongation with thermal history indicate that the flow processes in DGEBA-DETA epoxies are controlled free-volume-dependent regions. Such regions must consist of lightly or noncrosslinked material.

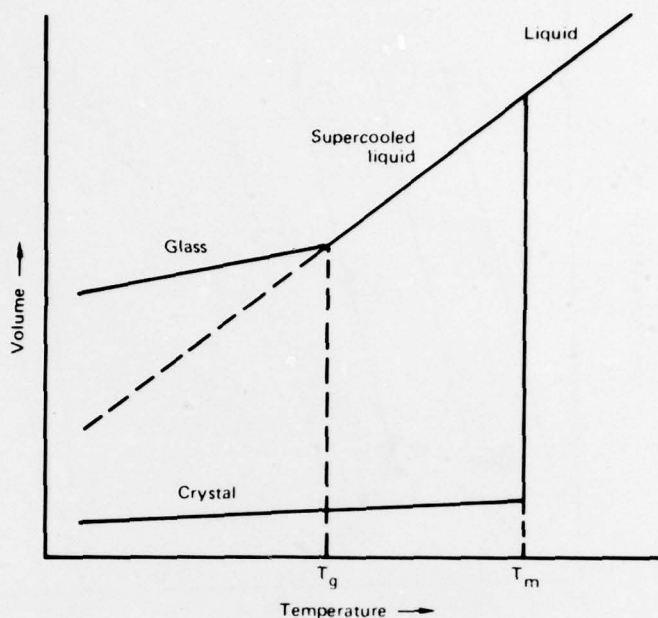


Fig. 2. A schematic volume-temperature plot for a polymer.

Figure 3 illustrates the effect of annealing [5°C below T_g (125°C)] on the temperature and strain-rate dependence of the macroscopic yield stress of DGEBA-DETA (11 phr DETA) epoxy relative to the unannealed epoxy. The general increase in the yield stress at all temperatures and strain rates on annealing below T_g further illustrates the free-volume dependence of these epoxies.

Each of the DGEBA-DETA epoxy systems exhibited a linear dependence of the yield stress (σ_y) with the logarithm of the strain rate ($\dot{\epsilon}$) at constant temperature. These data are consistent with Eyring's theory of stress-activated viscous flow for polymers.²² This theory predicts²³ that the yield stress is a linear function of the logarithm of the strain rate at constant temperature T , i.e.,

$$\frac{d\sigma_y}{d \ln \dot{\epsilon}} = \frac{2kT}{v} \quad (1)$$

where k is Boltzmann's constant and v is the activation volume, which is associated with that volume displaced when a chain segment jumps when acted on by an applied stress. The values of the activation volumes for each DGEBA-DETA epoxy system in the room-temperature- ($T_g - 30^{\circ}\text{C}$) range are $9\text{--}12 \text{ nm}^3$. These values are within the range of those reported for noncrosslinked polymers²⁴⁻³⁰ and two epoxy systems.^{6,31} These observations suggest that either regions of low and/or noncrosslink density control the flow processes of the DGEBA-DETA epoxies and/or the rupturing of crosslinks does not significantly affect the values of the activation volumes.

Hence the effects of thermal history and strain rate on the mechanical response of DGEBA-DETA epoxies indicate that regions of low or noncrosslink density

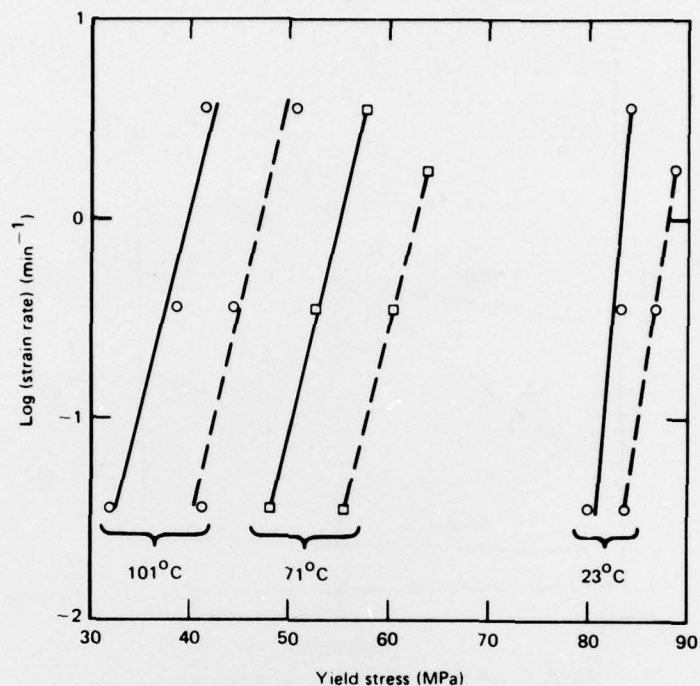


Fig. 3. Yield stress vs $\log(\text{strain rate})$ of a DGEBA-DETA (11 phr DETA) epoxy as a function of temperature and thermal history for (---) annealed 24 hr at 125°C and (—) unannealed samples.

control the flow processes that occur under the influence of stress in these glasses. Such observations are consistent with the reported microscopic deformation and failure processes of these systems and their morphology.¹³ (From straining DGEBA-DETA epoxy films directly in the electron microscope, these epoxies were found to consist of crosslinked molecular domains embedded in a lower crosslinked density matrix, with the latter controlling the flow processes.¹³) These observations suggest that chemically either (1) few epoxide secondary-amine reactions occur in DGEBA-DETA epoxies, thus limiting the number of crosslinks and/or (2) polyether linkages are formed by trans etherification through a ring-opening homopolymerization of the epoxide.^{7,10,14,32} The epoxide-amine reactions are controlled by the presence of H-bond donors such as OH groups, which are necessary to open the epoxide rings.^{2,3,7} The trans etherification reaction requires a tertiary amine as a catalyst and a H-bond donor as a cocatalyst.^{7,10,32} For the DGEBA-DETA system, sufficient quantities of tertiary amines are only formed above 120°C.¹⁰ Hence the final chemical structure of the DGEBA-DETA epoxy system can be complex, because it will depend on such parameters as (1) the relative rates of the chemical reactions at room temperature and the final postcure temperature, (2) the concentrations of catalysts such as sorbed moisture in the system, and (3) the steric restrictions inhibiting reactions at secondary amine sites.

The authors wish to acknowledge Lt. Col. Richard Haffner and Dr. Donald Ulrich (AFOSR) and Drs. Donald P. Ames and Clarence J. Wolf (MDRL, St. Louis) for their support and encouragement.

of this work. This research was sponsored by the Air Force Office of Scientific Research/AFSC, United States Air Force, under Contract No. F44620-76-0075.

References

1. D. M. French, R. A. H. Strecker, and A. S. Tompa, *J. Appl. Polym. Sci.*, **14**, 599 (1970).
2. K. Horie, H. Hiura, M. Sawada, I. Mita, and H. Kambe, *J. Polym. Sci., Part A-1*, **8**, 1357 (1970).
3. M. A. Acitelli, R. B. Prime, and E. Sacher, *Polymer*, **12**, 335 (1971).
4. R. B. Prime and E. Sacher, *Polymer*, **13**, 455 (1972).
5. R. J. Morgan and J. E. O'Neal, *Polym. Plast. Tech. Eng.*, **10**(1), 49 (1978).
6. R. J. Morgan and J. E. O'Neal, *J. Mater. Sci.*, **14**, 109 (1979).
7. D. A. Whiting and D. E. Kline, *J. Appl. Polym. Sci.*, **18**, 1043 (1974).
8. H. Lee and K. Neville, *Handbook of Epoxy Resins*, McGraw-Hill, New York, 1967, Chap. 4.
9. H. Lee and K. Neville, *Handbook of Epoxy Resins*, McGraw-Hill, New York, 1967, Chap. 6.
10. P. V. Sidiyakin, *Vysokomol. Soyedin., Ser. A*, **14**, 979 (1972).
11. J. P. Bell and W. T. McCarvill, *J. Appl. Polym. Sci.*, **18**, 2243 (1974).
12. R. J. Morgan and J. E. O'Neal, *J. Macromol. Sci., Phys.*, **15**, 139 (1978).
13. R. J. Morgan and J. E. O'Neal, *J. Mater. Sci.*, **12**, 1966 (1977).
14. H. Lee and K. Neville, *Handbook of Epoxy Resins*, McGraw-Hill, New York, 1967, Chap. 5.
15. R. P. Krehling and D. E. Kline, *J. Appl. Polym. Sci.*, **13**, 2411 (1969).
16. J. P. Bell, *J. Polym. Sci., Part A-2*, **8**, 417 (1970).
17. T. Murayama and J. P. Bell, *J. Polym. Sci., Part A-2*, **8**, 437 (1970).
18. K. Selby and L. E. Miller, *J. Mater. Sci.*, **10**, 12 (1975).
19. E. H. Andrews and N. E. King, *J. Mater. Sci.*, **11**, 2004 (1976).
20. S. L. Kim, M. D. Skibo, J. A. Manson, R. W. Hertzberg, and J. Janiszewski, *Polym. Eng. Sci.*, **18**, 1093 (1978).
21. H. Lee and K. Neville, *Handbook of Epoxy Resins*, McGraw-Hill, New York, 1967, Chap. 7.
22. H. Eyring, *J. Chem. Phys.*, **4**, 283 (1936).
23. P. B. Bowden, in *The Physics of Glassy Polymers*, R. N. Haward, Ed., Wiley, New York, 1973, Chap. 5.
24. J. A. Roelting, *Polymer*, **6**, 311 (1965).
25. D. L. Holt, *J. Appl. Polym. Sci.*, **12**, 1653 (1968).
26. J. C. Bauwens, C. Bauwens-Crowet, and G. Holmes, *J. Polym. Sci., Part A-2*, **7**, 1745 (1969).
27. R. A. Duckett, S. Rabinowitz, and I. M. Ward, *J. Mater. Sci.*, **5**, 909 (1970).
28. P. B. Bowden and S. Raha, *Phil. Mag.*, **22**, 463 (1970).
29. T. E. Brady and G. S. Y. Yeh, *J. Appl. Phys.*, **42**, 4622 (1971).
30. E. J. Kramer, *J. Polym. Sci. Polym. Phys. Ed.*, **13**, 509 (1975).
31. E. Pink and J. D. Campbell, *J. Mater. Sci.*, **9**, 665 (1974).
32. E. Narracott, *Br. Plast.*, **26**, 120 (1953).

Received May 31, 1978

Revised July 21, 1978

DISTRIBUTION LIST

Donald F. Adams
Mechanical Engineering Department
University of Wyoming
Laramie, Wyoming 82071

Donald L. Ball
Directorate of Chemical Sciences
Air Force Office of Scientific
Research (AFSC)
Bolling Air Force Base
Building 410
Washington, DC 20332

Willard D. Bascom
Polymeric Materials Branch
Naval Research Laboratory
Washington, DC 20375

Charles F. Bersch
Non-Metals Section (Air-52032)
Naval Air Systems Command
Washington, DC 20361

John O. Brittain
Materials Research Center
Northwestern University
Evanston, IL 60201

Lawrence J. Broutman
IIT Research Institute
10 West 35th Street
Chicago, IL 60616

Charles F. Browning
Structural Composites (MBC)
Air Force Materials Laboratory
Wright-Patterson Air Force Base,
Ohio 45433

T. T. Chiao
University of California
Lawrence Livermore Laboratory
P.O. Box 808
Livermore, CA 94550

John Emerson
Engineering Research Center
Western Electric
P.O. Box 900
Princeton, NJ 08540

John K. Gillham
Department of Chemical Engineering
Princeton University
Princeton, NJ 08540

Ivan J. Goldfarb
Air Force Materials Laboratory
Nonmetallic Materials Division
Polymer Branch
Wright-Patterson Air Force Base,
Ohio 45433

John C. Halpin
Advanced Composite Technology (FB)
Air Force Flight Dynamics Laboratory
Wright-Patterson Air Force Base,
Ohio 45433

Thomas V. Hinkle
McDonnell Aircraft Co.
Dept 234, Building 32, Level 2
St. Louis, MO 63166

John Hurt
U.S. Army Research Office
P.O. Box 12211
Research Triangle Park, NC 27709

Raymond J. Juergens
McDonnell Aircraft Co.
Dept. 247, Building 32, Level 2
St. Louis, MO 63166

David H. Kaeble
Rockwell International Science Center
1049 Camino Dos Rios
Thousand Oaks, CA 91360

Frank E. Karasz
Polymer Science and Engineering
Materials Research Laboratory
Office of the Director
University of Massachusetts
Amherst, MA 01003

John L. Kardos
Materials Research Laboratories
Chemical Engineering Dept.
Washington University
Box 1087
St. Louis, MO 63130

A. J. Kinloch
Ministry of Defense (P.E.)
Propellants, Explosives and
Rocket Motor Establishment
Waltham Abbey, Essex, England

James A. Koutsky
Department of Chemical Engineering
University of Wisconsin
Madison, WI 53706

John A. Manson
Materials Research Center
Lehigh University
Bethlehem, PA 18015

Clayton May
Lockheed Missiles and Space Co.
P.O. Box 504
Sunnyvale, CA 94088

George Mayer
Metallurgy and Materials Sciences
U.S. Army Research Office
P.O. Box 12211
Research Triangle Park, NC 27709

Larry Peebles
Office of Naval Research
495 Summer Street
Boston, MA 02210

Dusan C. Prevorsek
Central Research Laboratory
Allied Chemical Corporation
Morristown, NJ 07960

Richard A. Pride
Composites Section
NASA-Langley Research Center
Hampton, VA 23665

Brian Quinn
Director-Aerospace Sciences (NA)
Air Force Office of Scientific
Research
Bolling Air Force Base
Washington, DC 20332

Theodore J. Reinhart
Plastics Branch
Air Force Materials Laboratory
Wright-Patterson Air Force Base,
Ohio 45433

N. S. Schneider
Polymer and Chemistry Division
Army Materials and Mechanics Research
Ctr
Watertown, MA 02172

Simon Strauss
Headquarters, AFSC/DL
Andrews AFB, DC 20334

George R. Thomas
DRXMR-R, Organic Materials Laboratory
Army Materials/Mechanics Research
Center
Watertown, MA 02172

Kevin W. Thomson
Department of Materials Engineering
Monash University
Victoria, 3168, Australia

Charles Tiffany
Aeronautical Systems Division (ASD-EN)
Wright-Patterson Air Force Base,
OH 45433

Hank M. Toellner
Dept. 253, Location C1
Mail-Code 1-18
Douglas Aircraft Co.
3855 Lakewood Blvd.
Long Beach, CA 90846

Stephen Tsai
Mechanics and Surface Interaction
Branch (MBM)
Air Force Materials Laboratory
Wright-Patterson Air Force Base,
OH 45433

Donald R. Uhlmann
Department of Materials Science and
Engineering
MIT, Cambridge
Massachusetts 02139

R. L. Van Deusen
Polymer Branch
Nonmetallic Materials Division
Air Force Materials Laboratory
Wright-Patterson Air Force Base,
OH 45433

William J. Walker
Air Force Office of Scientific
Research
Bldg. 410
Bolling Air Force Base
Washington, DC 20332

Garth L. Wilkes
Department of Chemical Engineering
Virginia Polytechnic Institute
and State University
Blacksburg, VA 24061

Richard J. Wilkins
General Dynamics
P.O. Box 748
Fort Worth, TX 76101

Kenneth Wynne
Office of Naval Research
800 N. Quincy Street
Arlington, VA 22217

R. J. Young
Department of Materials
Queen Mary College
University of London
Mile End Road,
London E1 4NS, England

Defense Documentation Center 2 Cys
Cameron Station
Alexandria, VA 22314